Contribution à l'étude de la stabilité des systèmes électriques distributés autour d'un bus commun d'alimentation

Ahmed-Bilal Awan

NANCY Université - Institut National Polytechnique de Lorraine

Ecole Doctorale « Informatique - Automatique - Electrotechnique - Electronique - Mathématiques »
Département de Formation Doctorale « Electrotechnique - Electronique »

THESE

Présentée à

L'Institut National Polytechnique de Lorraine

En vue de l'obtention du titre de

DOCTEUR de l'INPL
Spécialité : Génie Electrique

par

Ahmed-Bilal AWAN

Contribution à l'étude de la stabilité des systèmes électriques distribués autour d'un bus commun d'alimentation

Soutenue publiquement le 2 décembre 2011 devant la commission d'examen

Membres du Jury :

Président :		
Rapporteurs :	Hubert Piquet	
	Mohamed-Fouad Benkhoris	
Examinateurs :	Benoit Robyns	
	Serge Pierfederici	directeur de thèse
	Babak Nahid-Mobarakeh	co-directeur de thèse

Thèse préparée au Groupe de Recherche en Electrotechnique et Electronique de Nancy

NANCY University - Institut National Polytechnique de Lorraine

Ecole Doctorale « Informatique - Automatique - Electrotechnique - Electronique - Mathématiques »
Département de Formation Doctorale « Electrotechnique - Electronique »

DOCTORAL THESIS

Presented at

The Institut National Polytechnique de Lorraine

In fulfillment of the requirements for the degree of

DOCTOR of INPL
Speciality: Electrical Engineering

by

Ahmed-Bilal Awan

Contribution to the Stability Investigation of Distributed Power Systems

Defended on 2 December 2011 in front of the following Jury

Members of Jury:

President:		
Reviewers:	Hubert Piquet	
	Mohamed-Fuad Benkhoris	
Examiners:	Benoit Robyns	
	Serge Pierfederici	Thesis Director
	Babak Nahid-Mobarakeh	Thesis Co-director

Thesis prepared at Groupe de Recherche en Electrotechnique et Electronique de Nancy

TABLE OF CONTENTS

Table of Contents

Résumé de thèse

Résumé de thèse

Chapitre 1

Introduction :

Les filtres d'entrée sont des composants nécessaires mais impopulaires dans les systèmes d'alimentation électrique. Ils sont en général volumineux, lourds et coûteux. Ils permettre de résoudre certains problèmes de qualité du réseau, mais en génèrent d'autres. Pourtant, en raison des exigences d'émission et de susceptibilité pour le contrôle des interférences électromagnétiques ils sont absolument nécessaires. La question n'est pas de savoir si oui ou non il est nécessaire d'utiliser des filtres d'entrée mais plutôt comment minimiser leur taille, leur poids, leur coût et leur impact sur les performances globale du réseau électrique.

Dans le chapitre 1, nous allons discuter de la fonction principale des filtres d'entrée et les problèmes de stabilité liés à leur utilisation dans les dispositifs électriques asservis. La dernière partie du chapitre traite des méthodes existantes pour résoudre les problèmes d'instabilité lors d'interactions entre les filtres et les dispositifs qu'ils alimentent.

Objectif Principal des filtres d'interconnexion:

Afin de lutter contre les perturbations électromagnétiques, un filtre LC est habituellement utilisée entre le convertisseur et sa source d'énergie qui est en général non régulée. Une part substantielle du coût de fabrication des convertisseurs de puissance dans les applications critiques est due aux éléments de filtrage qui doivent permettre au dispositif électrique de se conformer aux normes d'anti pollution en vigueur. Cependant, même un filtre bien conçu permettant de se conformer aux normes d'anti pollution peut, lorsqu'il est interconnecté avec une dispositif électrique muni d'asservissements internes, provoquer une dégradation significative des performances [Mi 76], telle que l'instabilité.

Si l'amortissement du filtre est insuffisant, la fonction de transfert en tension du filtre présente alors un pic au voisinage de sa fréquence de coupure. Ce pic provoque une amplification du bruit d'entrée à la fréquence de résonance, de sorte que la tension de bruit à l'entrée du filtre est amplifiée quand elle atteint les bornes d'entrée de l'alimentation.

En plus de cette amplification, les filtres faiblement amortis peuvent avoir un impact significatif sur les performances des boucles d'asservissement des dispositifs qu'ils alimentent. Il y a une forte variation du gain et de la phase à la fréquence de résonance du filtre. Dans les cas extrêmes, ces variations peuvent engendrer des oscillations dans le système. En effet au voisinage de la fréquence de résonnance du filtre, le module de l'impédance de sortie du filtre augmente significativement, sa phase diminuant fortement. Parallèlement, un hacheur DC/DC contrôlé en tension ou un actionneur régulé en couple ou en vitesse peuvent être assimilés vue de leurs bornes d'alimentation, à des dispositifs présentant une impédance différentielle d'entrée négative ce qui peut conduire à une instabilité de l'ensemble du système [Mi 76], [Mi 78], [04 Sad]. Si le

module de l'impédance de sortie du filtre d'entrée est supérieur au module de l'impédance d'entrée du convertisseur ou de l'actionneur dans un certain domaine fréquentiel, alors le système peut entrer en oscillation.

Les systèmes électriques fonctionnant à puissance constante :

Les convertisseurs d'électronique de puissance et les onduleurs souvent présents dans les systèmes d'entraînement électrique, quand ils sont munis de régulateurs à large bande passante, se comportent comme des charges à puissance constant (CPL). Un exemple d'un tel système électrique est indiqué sur la Figure 1.1 où le convertisseur DC-AC alimentant le moteur est relié au réseau d'alimentation via un convertisseur DC-DC.

Le moteur électrique est supposé contrôlé en couple ou en vitesse. Lors d'une variation de la tension d'alimentation de l'actionneur, la charge mécanique ne change pas. La vitesse mécanique et le couple de charge ne changent donc pas. La puissance mécanique reste donc constante. Si on néglige les pertes dans la structure de conversion, la puissance électrique à l'entrée du système sera constante.

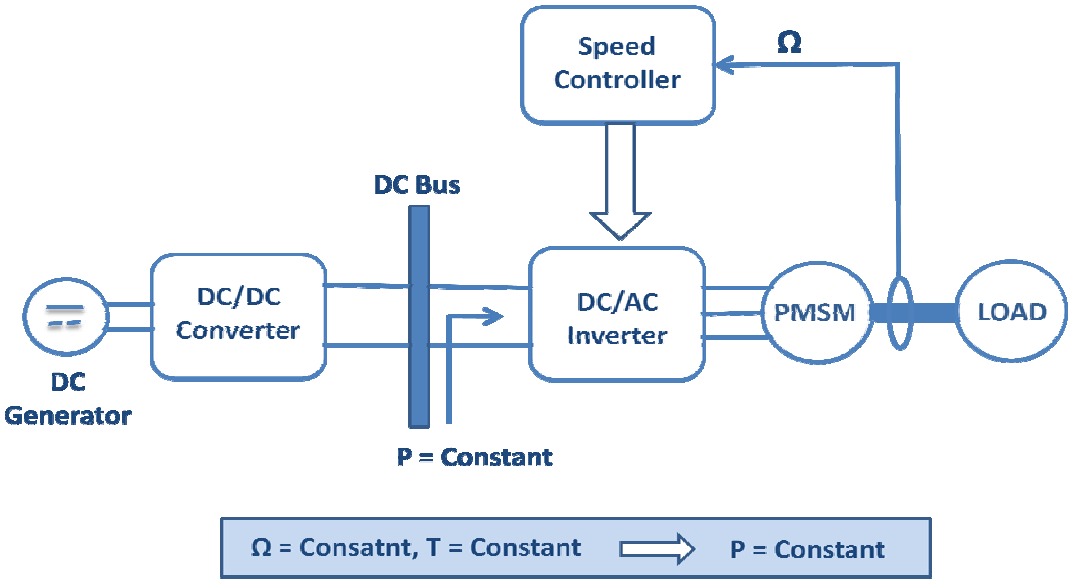

Figure 1.1: DC-AC Onduleur Moteur qui présente des caractéristiques de charge à puissance constante

Système électrique distribué interconnectant des charges à puissance constante (CPL):

Un développement exponentiel des technologies dans le domaine de l'électronique de puissance et les systèmes de contrôle de ces dernières années nous ont conduit à de nouvelles architectures électriques dans l'automobile et dans l'industrie aéronautique. Ces nouvelles architectures électriques sont appelées "systèmes à puissance distribuées" (DPS). Dans ce type de systèmes électriques, différentes charges sont reliés à un bus continu ou alternatif commun qui est alimenté en énergie par des sources multiples. Les charges se composent généralement

d'actionneurs, de convertisseurs DC-DC ou DC-AC. Ce type de DPS est présenté sur la figure 1.2.

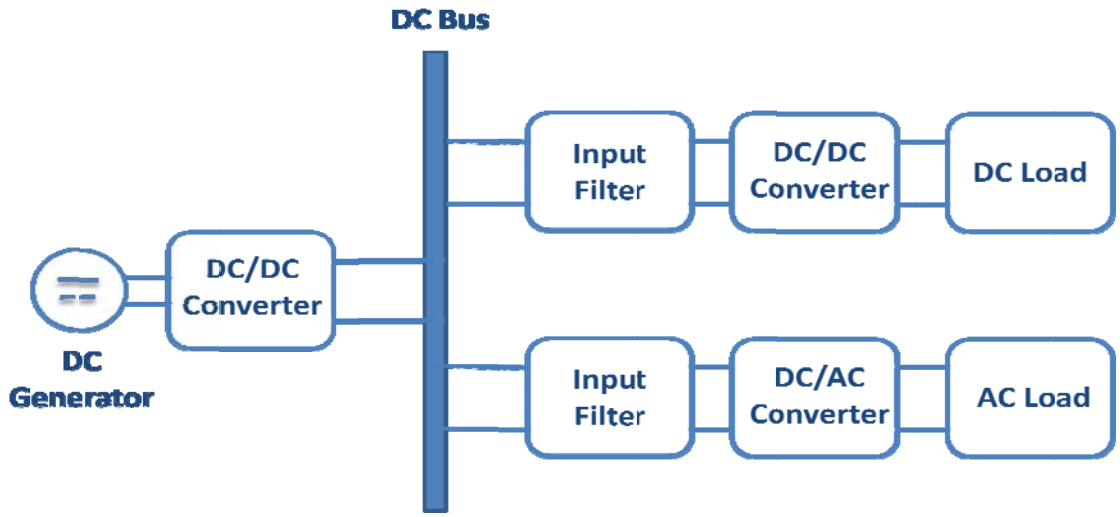

Figure 1.2: Système à Puissance Distribué (SPD)

Instabilité engendrée par les dispositifs fonctionant à puissance constante:

Le comportement d'une CPL est illustré sur la figure 1.3. Comme le montre cette figure, si la tension d'alimentation augmente (respectivement diminue), le courant consommé va diminuer (respectivement augmenter) pour assurer un fonctionnement à puissance constante. Cette propriété est à l'origine du problème de stabilité engendré par les CPL [Gri 98], [Bel 95], [98 Glo], [98 Cie], [Ema 00], [Cho 99]. Une charge consommant une puissance constante P, connectée en série à une inductance L et alimentée par une source de tension V , est présentée sur la figure 1.4. Le point d'équilibre A du circuit correspond au point d'intersection de la caractéristique de source avec celle de la charge comme présenté sur la Figure 1.5.

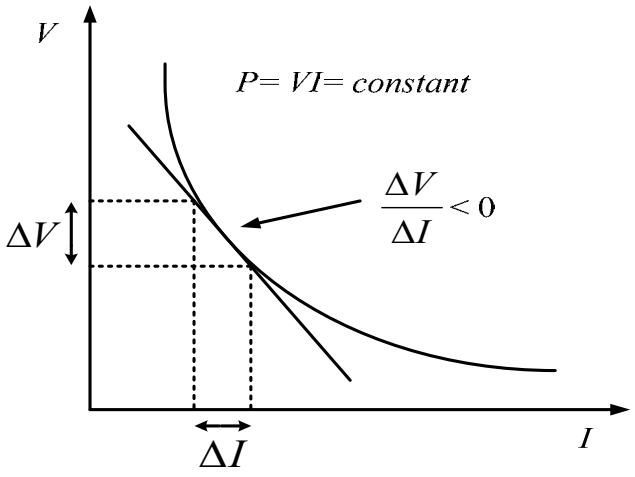

Figure 1.3: Caractéristique statique V-I d'un dispositif électrique fonctionnant à puissance constante

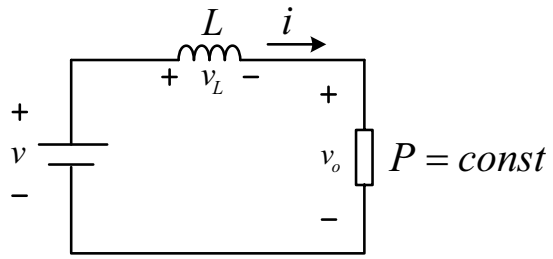

Figure 1.4: CPL en série avec une source de tension et son filtre inductif

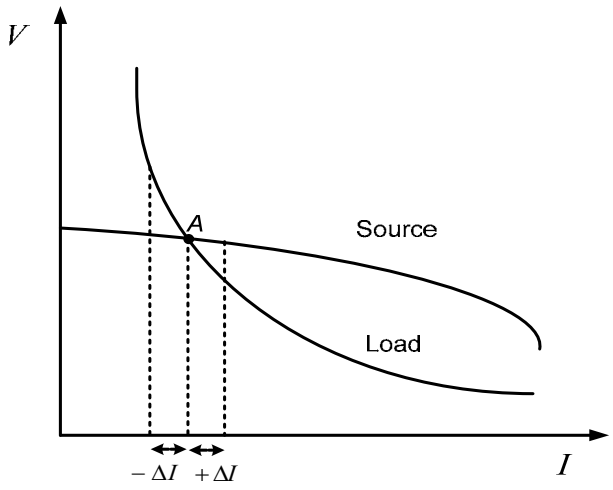

Figure 1.5: caractéristique statique V-I d'une source et d'une CPL

Le point d'équilibre est considéré comme stable quand le système retourne à sa position d'équilibre suite une petite perturbation. Examinons la stabilité du point de l'état d'équilibre A de la Figure 1.5. Supposons qu'une petite perturbation entraîne une réduction du courant de charge de Δi. La tension de source augmente alors ce qui entraine alors une nouvelle diminution du courant de source. Le point de fonctionnement s'écarte donc de plus en plus du point d'équilibre. De même, une augmentation du courant va se traduire par une diminution de la tension de source qui va à son tour provoquer une augmentation du courant de charge. Le point de focntionnement A correspond donc à un état d'équilibre instable [Ema 03], [Ema 99].

Méthode d'analyse de la stabilité des DPS:

Le problème de la stabilité des systèmes électriques avec des filtres d'entrée a été identifié et étudié à partir des années soixante-dix. Les documents sur ce sujet remontent à aussi loin que 1971 [Yu 71]. L'analyse détaillée de ce problème pour un convertisseur abaisseur avec un filtre d'entrée a d'abord été donnée par RD Middlebrook dans [Mi 76] et [Mi 78].

Critère de Middlebrook:

Pour l'étude de la stabilité petit signal du système, le concept de critère d'impédance a été établi par Middlebrook en 1976 [Mi 76]. Middlebrook a démontré que la stabilité pouvait être garantie à partir du moment ou le module de l'impédance d'entrée reste, quelque soit la fréquence, supérieur au module d'impédance de sortie.

$$|Z_s(s)| \ll |Z_I(s)|$$

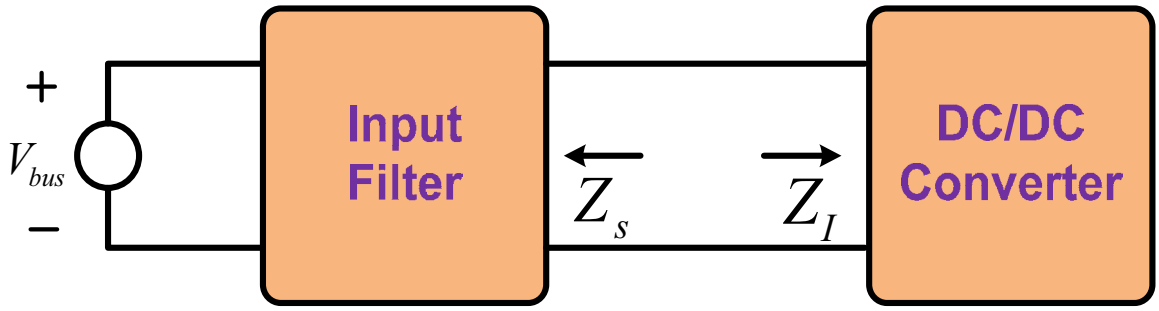

Figure 1.6 : Mise en cascade de deux dispositifs électriques

Critère de la marge de gain et de phase (GMPM):

Dans les systèmes distribués autour d'un bus continu (DPS), il est très difficile de vérifier le critère de Middlebrook sur toutes les gammes de fréquence, car cela rendrait la conception assez conservatrice et coûteuse [Wil 92], [95 Wil], [Fen 02]. Un critère moins conservatif, connu sous le nom de critère de Marge de Gain et de Phase (GMPM) est proposé dans [Wil 92], [95 Wil], [99 Fen], [Fen 02].

On pose : $T_m(s) = Z_o(s)/\, Z_{in}(s)$ et on impose à cette fonction de transfert de vérifier :

soit $|T_m(s)| < \frac{1}{\mathrm{GM_{min}}}$

soit $\mathrm{PM} > \mathrm{PM_{min}}$ si $|T_m(s)| < \frac{1}{\mathrm{GM_{min}}}$

On peut par exemple se fixer comme cela est présenté sur la figure 1.7, une marge de phase de 60 degrés et une marge de gain de 6 dB et assurer la stabilité du système avec les marges de robustesse choisies si le tracé de Nyquist de T_m n'entre pas dans la partie grisée de la figure 1.7.

Cette méthode permet aussi de définir une spécification d'impédance de charge, lorsqu'on se donne l'impédance de sortie.

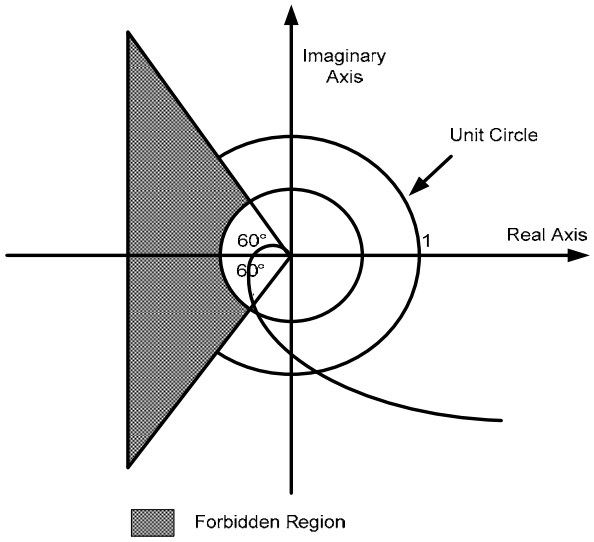

Figure 1.7: Région interdite par la méthode GMPM

Analyse des valeurs propres:

Pour les DPS de grande taille, l'utilisation de critères d'impédance (méthodes Middelbrook ou GMPM) est trop conservatrice. Afin d'analyser la stabilité d'un tel réseau par des méthodes basées sur des spécifications d'impédance, il est nécessaire dans une première étape, de prouver la stabilité de chaque composant de réseau séparément. Puis dans une seconde étape, on analyse la stabilité de l'ensemble du réseau en tenant compte de l'impédance d'entrée de chacun des composants du réseau et de l'impédance de source de l'alimentation au point de connexion. Une autre méthode pour l'analyse de la stabilité locale d'un tel DPS consiste à étudier les valeurs propres du système autour d'un point de fonctionnement.

A titre d'exemple, le DPS représenté sur la figure 1.8 peut être mis sous la forme d'état suivante pour étudier sa stabilité :

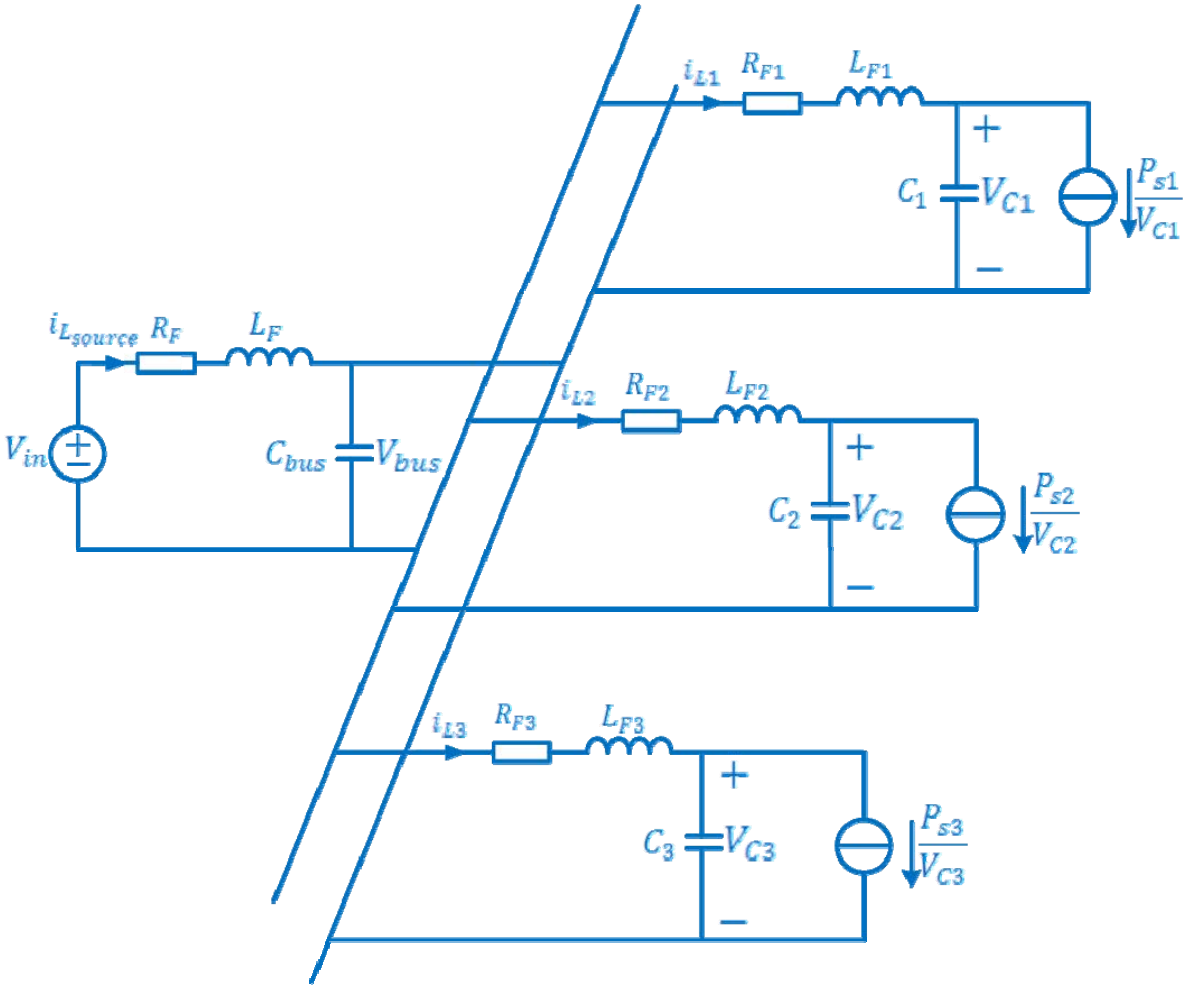

Figure 1.8: DPS with three CPLs

$$\frac{di_{L_{source}}}{dt} = -\frac{R_F}{L_F} i_{L_{source}} - \frac{V_{bus}}{L_F} + \frac{V_{in}}{L_F}$$

$$\frac{di_{L1}}{dt} = -\frac{R_{F1}}{L_{F1}} i_{L1} - \frac{V_{C1}}{L_{F1}} + \frac{V_{bus}}{L_{F1}}$$

$$\frac{di_{L2}}{dt} = -\frac{R_{F2}}{L_{F2}} i_{L2} - \frac{V_{C2}}{L_{F2}} + \frac{V_{bus}}{L_{F2}}$$

$$\frac{di_{L3}}{dt} = -\frac{R_{F3}}{L_{F3}} i_{L3} - \frac{V_{C3}}{L_{F3}} + \frac{V_{bus}}{L_{F3}}$$

$$\frac{dV_{C1}}{dt} = \frac{i_{L1}}{C_1} - \frac{i_{Load1}}{C_1} = \frac{i_{L1}}{C_1} - \frac{P_{s1}}{C_1 V_{C1}}$$

$$\frac{dV_{C2}}{dt} = \frac{i_{L2}}{C_2} - \frac{i_{Load2}}{C_2} = \frac{i_{L2}}{C_2} - \frac{P_{s2}}{C_2 V_{C2}}$$

$$\frac{dV_{C3}}{dt} = \frac{i_{L3}}{C_3} - \frac{i_{Load3}}{C_3} = \frac{i_{L3}}{C_3} - \frac{P_{s3}}{C_3 V_{C3}}$$

$$\frac{dV_{bus}}{dt} = \frac{i_{L_{source}}}{C_1} - \frac{(i_{L1} + i_{L2} + i_{L3})}{C_1}$$

Le modèle ci-dessus est non linéaire. L'analyse de sa stabilité locale repose sur l'étude des valeurs propres de sa matrice de Jacobi évaluées autour d'un point de fonctionnement. Cette méthode revient donc à analyser les valeurs propres du modèle linéarisé au premier ordre :

$$\frac{d\tilde{\imath}_{L_{source}}}{dt} = -\frac{R_F}{L_F}\tilde{\imath}_{L_{source}} - \frac{\tilde{v}_{bus}}{L_F} \qquad \frac{d\tilde{\imath}_{L1}}{dt} = -\frac{R_{F1}}{L_{F1}}\tilde{\imath}_{L1} - \frac{\tilde{v}_{C1}}{L_{F1}} + \frac{\tilde{v}_{bus}}{L_{F1}}$$

$$\frac{d\tilde{\imath}_{L2}}{dt} = -\frac{R_{F2}}{L_{F2}}\tilde{\imath}_{L2} - \frac{\tilde{v}_{C2}}{L_{F2}} + \frac{\tilde{v}_{bus}}{L_{F2}} \qquad \frac{d\tilde{\imath}_{L3}}{dt} = -\frac{R_{F3}}{L_{F3}}\tilde{\imath}_{L3} - \frac{\tilde{v}_{C3}}{L_{F3}} + \frac{\tilde{v}_{bus}}{L_{F3}}$$

$$\frac{d\tilde{v}_{C1}}{dt} = \frac{\tilde{\imath}_{L1}}{C_1} - \frac{\tilde{\imath}_{Load1}}{C_1} = \frac{\tilde{\imath}_{L1}}{C_1} + \frac{P_{s10}}{C_1 {V_{C10}}^2}\,\tilde{v}_{C1}$$

$$\frac{d\tilde{v}_{C2}}{dt} = \frac{\tilde{\imath}_{L2}}{C_2} - \frac{\tilde{\imath}_{Load2}}{C_2} = \frac{\tilde{\imath}_{L2}}{C_2} + \frac{P_{s20}}{C_2 {V_{C20}}^2}\,\tilde{v}_{C2}$$

$$\frac{d\tilde{v}_{C3}}{dt} = \frac{\tilde{\imath}_{L3}}{C_3} - \frac{\tilde{\imath}_{Load3}}{C_3} = \frac{\tilde{\imath}_{L3}}{C_3} + \frac{P_{s30}}{C_3 {V_{C30}}^2}\,\tilde{v}_{C3}$$

$$\frac{d\tilde{v}_{bus}}{dt} = \frac{\tilde{\imath}_{L_{source}}}{C_1} - \frac{\tilde{\imath}_o}{C_1} = \frac{\tilde{\imath}_{L_{source}}}{C_1} - \frac{(\tilde{\imath}_{L1} + \tilde{\imath}_{L2} + \tilde{\imath}_{L3})}{C_1}$$

qui se réécrit sous la forme matricielle suivante :

$$\dot{X} = AX + U$$

$$\frac{d}{dt}\begin{bmatrix} \tilde{\imath}_{L_{source}} \\ \tilde{\imath}_{L1} \\ \tilde{\imath}_{L2} \\ \tilde{\imath}_{L3} \\ \tilde{v}_{C1} \\ \tilde{v}_{C2} \\ \tilde{v}_{C3} \\ \tilde{v}_{Cbus} \end{bmatrix} = \begin{bmatrix} -\frac{R_F}{L_F} & 0 & 0 & 0 & 0 & 0 & 0 & -\frac{1}{L_F} \\ 0 & -\frac{R_{F1}}{L_{F1}} & 0 & 0 & -\frac{1}{L_{F1}} & 0 & 0 & \frac{1}{L_{F1}} \\ 0 & 0 & -\frac{R_{F2}}{L_{F2}} & 0 & 0 & -\frac{1}{L_{F2}} & 0 & \frac{1}{L_{F2}} \\ 0 & 0 & 0 & -\frac{R_{F3}}{L_{F3}} & 0 & 0 & -\frac{1}{L_{F3}} & \frac{1}{L_{F3}} \\ 0 & \frac{1}{C_1} & 0 & 0 & \frac{P_{s10}}{C_1 V_{C10}} & 0 & 0 & 0 \\ 0 & 0 & \frac{1}{C_2} & 0 & 0 & \frac{P_{s20}}{C_2 V_{C20}} & 0 & 0 \\ 0 & 0 & 0 & \frac{1}{C_3} & 0 & 0 & \frac{P_{s30}}{C_3 V_{C30}} & 0 \\ \frac{1}{C} & -\frac{1}{C} & -\frac{1}{C} & -\frac{1}{C} & 0 & 0 & 0 & 0 \end{bmatrix} \cdot \begin{bmatrix} \tilde{\imath}_{L_{source}} \\ \tilde{\imath}_{L1} \\ \tilde{\imath}_{L2} \\ \tilde{\imath}_{L3} \\ \tilde{v}_{C1} \\ \tilde{v}_{C2} \\ \tilde{v}_{C3} \\ \tilde{v}_{Cbus} \end{bmatrix} \quad (1.12)$$

les valeurs propres λ de la matrice *A* sont solutions des équations suivantes :

$$A \cdot \varphi = \lambda \cdot \varphi \qquad \Rightarrow \qquad (A - \lambda \cdot I) = 0$$

ou encore :

$$A \cdot \boldsymbol{\psi}^T = \lambda \cdot \boldsymbol{\psi}^T \qquad \Rightarrow \qquad (A - \lambda \cdot I) = 0$$

Où φ et $\boldsymbol{\psi}$ sont respectivement les vecteurs propres non nuls à droite et à gauche de A. Le système sera dit localement asymptotiquement stable si la condition suivante est respectée :

$$Real\ (\lambda(A)) < 0$$

Les différentes configurations de filtre avec réglage passif de l'amortissement

Une approche possible pour régler l'amortissement d'un filtre est d'ajouter une résistance d'amortissement Rd en parallèle avec le condensateur CF, comme le montre la figure1.9 (a). Malheureusement, cette configuration implique une dissipation par effet joule dans Rd et donc une diminution du rendement de l'installation électrique.

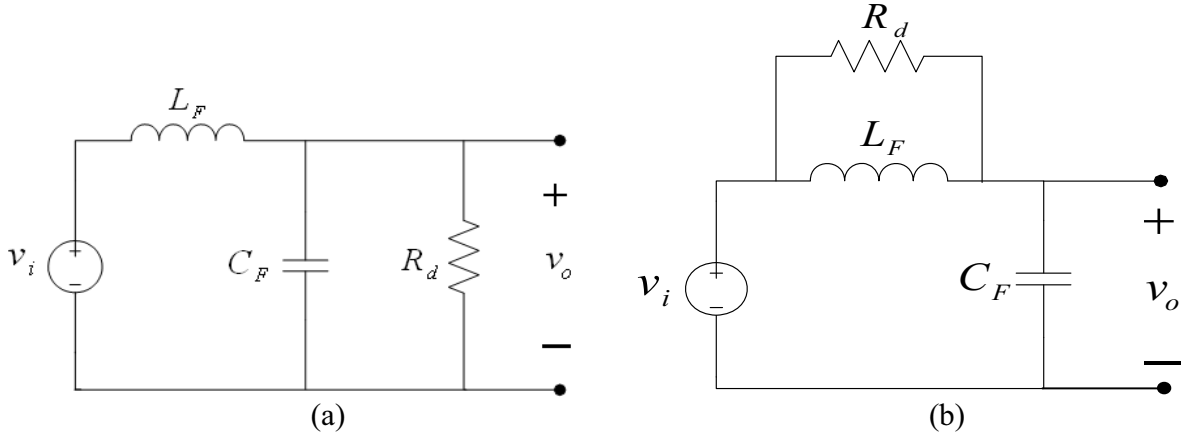

Figure 1.9: (a): résistance d'amortissement en parallèle sur la capacité C_F; (b): en parallèle sur l'inductance L_F.

Une solution au problème de la dissipation de puissance est de placer la résistance d'amortissement en parallèle avec l'inductance LF comme illustré sur la Figure 1.9 (b). Comme la valeur moyenne de tension aux bornes de l'inductance LF est nulle en régime établi, les pertes par effet joule dans R_d sont alors réduites. Néanmoins, le principal problème avec ce circuit est que sa fonction de transfert contient un zéro à haute fréquence. L'ajout de Rd dégrade la pente de l'asymptote haute fréquence [Eri 01].

Une solution pratique pour régler l'amortissement du filtre d'entrée est illustré dans Figure 1.10. Un condensateur de blocage est ajoutée en série avec la résistance R_d. Comme aucun courant

continu ne peut passer à travers Rd en régime permanent, les pertes par effet joule dans R_d sont une fois encore réduites.
La valeur du condensateur de blocage C_d est choisie bien plus grande que celle de C_F de sorte qu'à la fréquence de résonance du filtre, l'impédance de la branche R_d-C_d soit dominée par la résistance R_d.

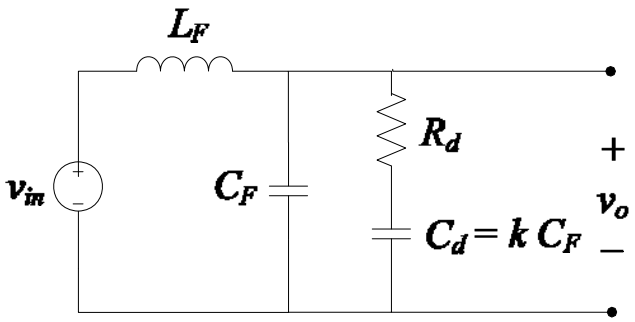

Figure 1.10: méthode pratique pour régler l'amortissement du filtre d'entrée

Cependant cette méthode n'est pas utilisable dans les réseaux AC car l'utilisation de valeur de condensateur C_d élevée peut provoquer une dissipation excessive à la fréquence de ligne à cause du courant alternatif qui circule dans la branche d'amortissement. Pour de telles applications, les structures de filtre présentées sur la figure 1.11 avec l'utilisation d'un circuit Rd-Ld série ou parallèle peut conduire à une meilleure conception. Cette méthode élimine la dissipation excessive dans la résistance et est largement utilisée dans les filtres alternatifs d'interconnexion avec les convertisseur de puissance. La conception et l'optimisation de ces filtres sont discutées dans [Phe 79] et [Eri 99].

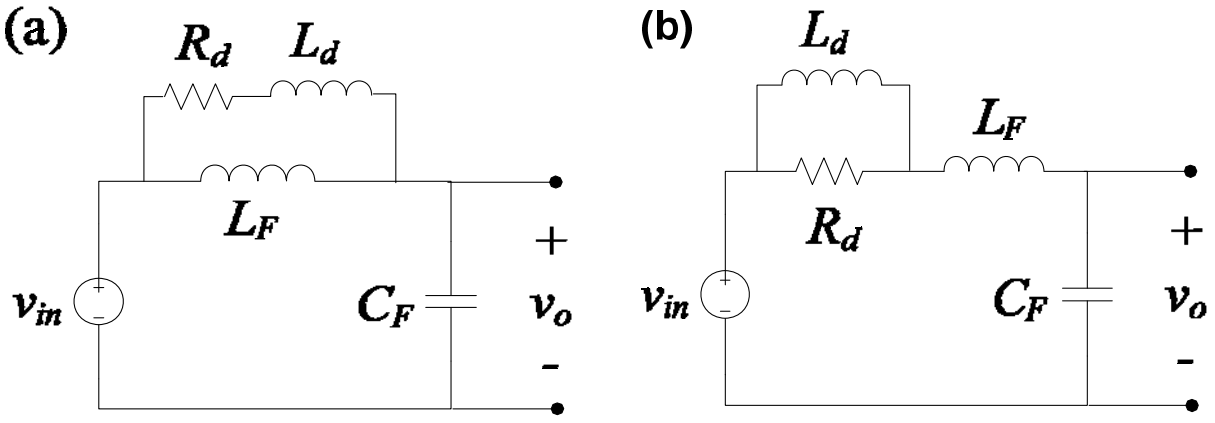

Figure 1.11: méthode pratique pour régler l'amortissement du filtre d'entrée sur les réseaux alternatifs; (a): circuit $R_d - L_d$ en série; (b): circuit $R_d - L_d$ parallèle.

Conclusion:

Le travail présenté ici traite des méthodes permettant l'étude de la stabilité des systèmes électriques interconnectés. Dans un premier temps, nous avons expliqué l'origine des instabilités lorsqu'on connecte une alimentation munie de son filtre de sortie à un dispositif électrique fonctionnant à puissance constante. Nous avons ensuite détaillé les méthodes d'étude permettant de prouver la stabilité des systèmes interconnectés. A l'aide de l'impédance de sortie de la source et de l'impédance d'entrée de la charge, nous avons montré qu'il était possible de définir des critères d'impédance permettant d'assurer la stabilité de la mise en cascade de deux dispositifs électriques tout en respectant des marges de robustesses pour le système. Nous avons ensuite étudié différentes structures de filtre permettant d'ajuster de manière passive l'amortissement du système de filtrage et de garantir ainsi la stabilité de la mise en cascade.

Chapter 2

Introduction :

Les dispositifs d'électroniques de puissance tels que les convertisseurs et les actionneurs, quand étroitement réglementé, se comportent comme des charges de puissance constante et ont une résistance d'entrée négative dans la bande passante des boucles de régulation du système. Ces dispositifs lorsqu'ils sont connectés à l'alimentation via filtre LC d'entrée, peut conduire à des problèmes de stabilité. Ce phénomène est plus en plus rencontré puis que les moteurs électriques sont de plus en plus utilisés au lieu et place des traditionnelles machines hydrauliques et pneumatiques, en particulier dans les applications aéronautiques. Les principaux avantages de l'utilisation de moteurs électriques plus tôt que des machines hydrauliques ou pneumatiques sont : la maintenance, la flexibilité et de la précision accru de la commande.

Dans ce chapitre, nous présentons une méthode analytique qui permet d'étudier la stabilité locale d'un ensemble onduleur-machine-commande alimenté par une source de puissance continue imparfaite. La méthode peut être appliquée lorsque moteurs synchrones à aimants permanents (MSAP) ou les moteurs à induction sont utilisés. Nous supposons que les régulateurs utilisés dans l'ensemble onduleur-machine-commande, sont linéaires. Ensuite, une technique d de compensation 'oscillation est utilisée pour améliorer la marge de stabilité du système et de réduire la taille de la capacité du bus-DC sans modifier la forme du couple ou de boucles de courant. L'amélioration de tension bus-DC dépend des exigences de conception, l'écart de tension maximale et son temps de réponse pour une perturbation puissance de charge donnée et l'impact de la stabilisation de la tension sur la commande dynamique. Lors de la conception du bloc de compensation d'oscillation, un bon designer sait que bus de tension continu plus stable, conduit généralement à une dynamique d'entraînement de couple pire. Pour trouver un bon compromis, le concepteur a besoin d'outils simples, généralement linéaires, tels que les diagrammes de Bode et de Nyquist, et un modèle suffisamment représentatif de l'ensemble du système. Puis, il ou elle peut atteindre les exigences de conception en ajustant les paramètres du bloc de compensation d'oscillation. Dans ce chapitre, un exemple de conception complet est donné ; de la modélisation à la conception et la mise en œuvre expérimentale d'un bloc de stabilisation linéaire appliquée à un ensemble onduleur-machine-commande alimenté par une source de puissance continue imparfaite.

Etude de la stabilité d'un ensemble onduleur -moteur avec filtre d'entrée:

Le système étudié est celui de la figure 2.1. Le système est constitué d'une source de tension continue imparfaite fournissant de l'énergie à un ensemble onduleur-machine-convertisseur. La source de courant continu comporte trois niveaux: la source alternative de puissance, le redresseur et le filtre LC. Sa sortie de tension continu, appelée tension continue de bus-DC (v_s), est utilisée pour alimenter onduleur de tension commande par MLI. Cet onduleur transfère la puissance électrique au moteur. Nous supposons que cette dernière est une MSAP.

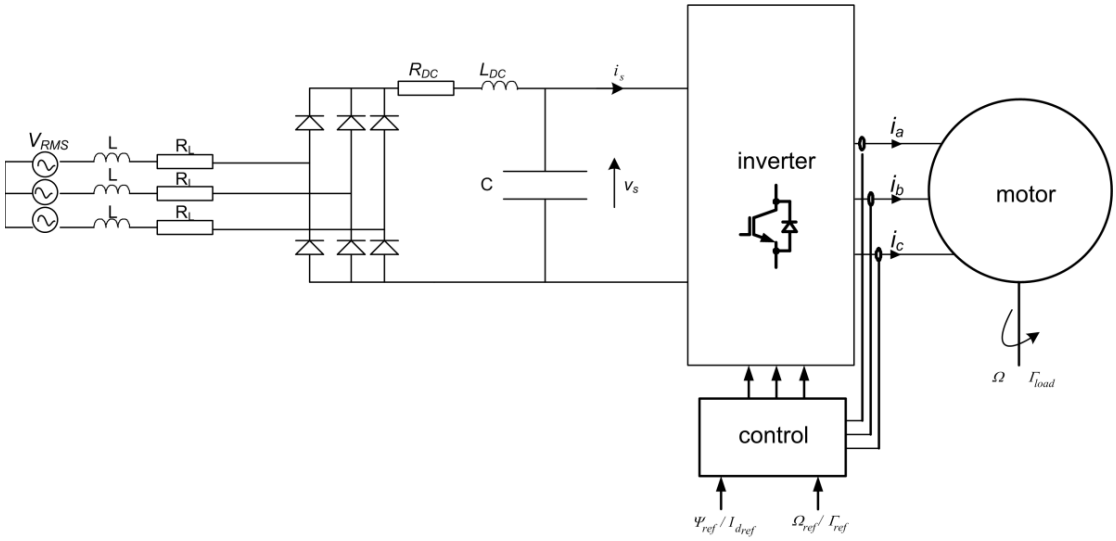

Fig. 2.1-Architecture typique des actionneurs électriques

To simplify the model, the ac voltage source – rectifier are replaced by an equivalent DC source. As explained in [Har 05] and [Rou 07], a six-pulse rectifier can be modeled with reasonably good accuracy as a DC grid as shown in Fig. 2.2.

Pour simplifier le modèle, la source de tension alternative et le redresseur sont remplacés par une source de courant continu équivalent. Comme expliqué dans [Har 05] et [Rou 07], un redresseur à six bras peut être modélisé avec une assez précision bonne comme une grille DC comme le montre la Fig. 2.2.

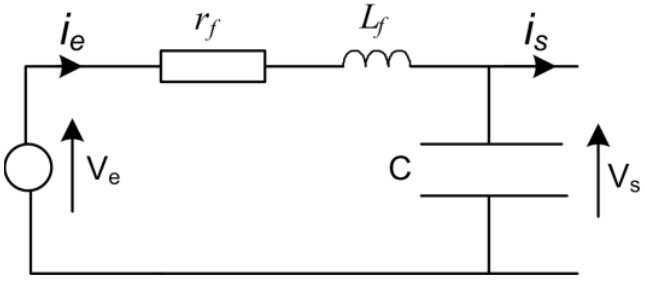

Fig. 2.2- Modèle de la source de tension continu.

La tension continue V_e, l'inductance équivalente série L_f et la résistance r_f sont définis par les relations suivantes:

$$V_e = \frac{3\sqrt{2}}{\pi} V_{RMS} \tag{2.1}$$

$$L_f = 2L + L_{DC} \tag{2.2}$$

$$r_f = 2R_L + R_{DC} + \frac{3}{\pi} L\omega \tag{2.3}$$

Où V_{RMS} est la valeur efficace de la tension de ligne; L et R_L sont respectivement l'inductance ligne et la résistance série de l'alimentation triphasée; L_{DC} et R_{DC} représentent respectivement l'inductance équivalente du bus-DC et la résistance et le terme $3L\omega/\pi$ est empiétement. Ce modèle permet de définir facilement l'impédance de sortie de la source de tension. Pour les petites variations de signaux, nous avons:

$$Z_o(s) = -\left(\frac{\tilde{v}_s}{\tilde{\imath}_s}\right)_{\tilde{v}_e=0} = \frac{L_f s + r_f}{L_f C_f s^2 + r_f C_f s + 1} \tag{2.4}$$

Où $\tilde{x}$ représente la variation de la variable x autour de sa valeur en régime permanent.

Stabilisation de la tension du bus continu :

La stabilité des systèmes en cascade a été largement étudiée dans la littérature en particulier pour les convertisseurs DC / DC. Lorsque la puissance de la charge est supposée constante, la condition de stabilité asymptotique suivante est souvent proposée:

$$p_s < p_{smax} = \frac{r_f C}{L_f} V_e^2 \tag{2.5}$$

Où p_s est la puissance de la charge.

Dans les applications aéronautiques, l'objectif est de réduire la taille de la capacité du bus-DC. Dans ces cas, un tel contrôle n'est pas adapté car il conduit à de grandes valeurs de la capacité capacité du bus-DC, sinon le bus continu sera instable conformément à (2,5). Par conséquent, une technique de stabilisation bus continu est nécessaire pour maintenir la tension du bus continu stable tout en réduisant la capacité du fil conducteur et en maintenant les performances de contrôle de l'actionneur.

Il est prouvé que la stabilité locale autour d'un point de fonctionnement de deux convertisseurs en cascade dépend des pôles de la fonction de transfert $1/(1 + Z_o(s)/Z_{in}(s))$, où $Z_o(s)$ est l'impédance de sortie du premier convertisseur et $Z_{in}(s)$ est l'impédance d'entrée de la charge du convertisseur. Il peut être facilement démontré que pour un ensemble onduleur-machine-commande ayant une source de tension défectueuse, le même résultat peut être obtenu grâce à l'utilisation de la modélisation petits signaux autour du point de fonctionnement étudié. Les variations des grandeurs de sortie du système sont liées aux variations des grandeurs d'entrées par la relation suivante.

$$\begin{bmatrix}\tilde{v}_s(s)\\ \tilde{\imath}_e(s)\end{bmatrix} = \begin{bmatrix}T_v(s) & Z_o(s)\\ 1/Z_{in}(s) & -T_c(s)\end{bmatrix}\begin{bmatrix}\tilde{v}_e(s)\\ -\tilde{\imath}_s(s)\end{bmatrix} \quad (2.6)$$

Où

$T_v(s)$ représente la fonction de transfert stable illustrant la fonction de transfert de tension du filtre LC lorsque $\tilde{\imath}_s = 0$.

$T_c(s)$ représente la fonction de transfert stable illustrant la fonction de transfert en cours ;

$Z_{in}(s)$ Est l'impédance d'entrée.

$Z_o(s)$ Est l'impédance de sortie.

En effet, les petites variations de la tension du bus continu peuvent être décrites par la relation :

$$\tilde{v}_s(s) = \frac{T_v(s)}{1 + \frac{Z_o(s)}{Z_{in}(s)}}\tilde{v}_e(s) \quad (2.7)$$

Où $Z_{in}(s)$ est l'impédance d'entrée de l'ensemble onduleur-machine-commande et peut être calculée comme suit:

$$Z_{in}(s) = \left(\frac{\tilde{v}_s}{\tilde{\imath}_s}\right)_{\substack{\tilde{\Omega}=0 \text{ or } \tilde{\Gamma}_{ref}=0 \\ \tilde{\Psi}_{dref}=0 \text{ or } \tilde{\imath}_{dref}=0}} \quad (2.8)$$

Calcul de l'impédance d'entrée:

De l'équation (2.7), il est évident que la stabilité locale du système dépend du rapport $Z_o(s)/Z_{in}(s)$, où $Z_{in}(s)$ est déterminé en utilisant (2.8). Pour calculer cette impédance, certains auteurs ont utilisé un modèle linéaire de mesures, pour obtenir un modèle linéaire bien adapté [32]. Une approche consiste à simplifier le modèle physique de l'ensemble du schéma de commande de la figure 2.3. Dans cette figure, les régulateurs de courants dq statoriques sont désignés par $C_d(s)$ et $C_q(s)$.la commande à partir de ces régulateurs doit est découplée grâce au bloque $A(s)$ présenté plus haut. Les fonctions de transfert $C_\Phi(s)$ et $C_v(s)$ représentent les régulateurs de flux et de vitesse s'ils existent. Un bloque supplémentaire modélisé par la fonction de transfert $h_v(s)$, est introduit pour compenser les oscillations de la tension d'entrée. Pour simplifier l'étude, les effets de saturation et d'échantillonnage ne sont pas pris en compte. Par ailleurs, les pertes par commutation sont aussi négligées. Ainsi les bilans de puissance au voisinage du point de fonctionnement du bus continus, et autour du point de fonctionnement conduisent à l'équation :

$$\tilde{v}_s(s)\cdot I_s + V_s\cdot\tilde{\imath}_s(s) = \tilde{v}_d(s)\cdot I_d + V_d\cdot\tilde{\imath}_d(s) + \tilde{v}_q(s)\cdot I_q + V_q\cdot\tilde{\imath}_q(s) \quad (2.9)$$

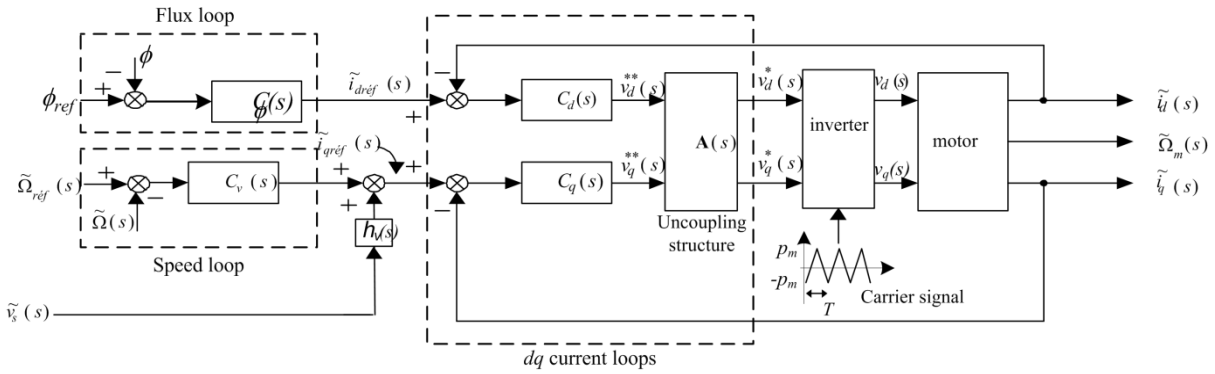

Fig. 2.3- Schéma de commande de l'onduleur-moteur avec un bloc de compensation d'oscillation. .

Pour un fonctionnement à basse fréquence, Nous modélisons l'onduleur comme étant un gain multiplié par la tension de bus dc.

$$G_{VSI} = \alpha \cdot v_s \tag{2.10}$$

Avec: $\alpha = 1/2p_m$ (Fig. 2.3) est une constante. Cette modélisation nous permet d'écrire :

$$\begin{bmatrix}\tilde{v}_d(s)\\ \tilde{v}_q(s)\end{bmatrix} = \alpha \cdot \tilde{v}_s(s) \cdot \begin{bmatrix}V_d^*\\ V_q^*\end{bmatrix} + \alpha \cdot V_s \cdot \begin{bmatrix}\tilde{v}_d^*(s)\\ \tilde{v}_q^*(s)\end{bmatrix} \tag{2.11}$$

En utilisant le formalisme petit signal pour la modélisation de moteur, il est possible d'exprimer les variations en tension *dq* en fonction des variations des courants *dq*.

$$\begin{bmatrix}\tilde{v}_d(s)\\ \tilde{v}_q(s)\end{bmatrix} = Z(s) \cdot \begin{bmatrix}\tilde{\imath}_d(s)\\ \tilde{\imath}_q(s)\end{bmatrix} \tag{2.12}$$

Où, la matrice $Z(s)$ représente d'impédance de moteur (2.13).

$$Z(s) = \begin{bmatrix}z_{11}(s) & z_{12}(s)\\ z_{21}(s) & z_{22}(s)\end{bmatrix} \tag{2.13}$$

Ainsi, la combinaison des relations (2.9), (2.12) et (2.13) nous permette d'écrire:

$$\tilde{v}_s(s) \cdot I_s + V_s \cdot \tilde{\imath}_s(s) = V_1(s) \cdot \tilde{\imath}_d(s) + V_2(s) \cdot \tilde{\imath}_q(s) \tag{2.14}$$

Avec :

$$\begin{cases}V_1(s) = V_d + I_d \cdot z_{11}(s) + I_q \cdot z_{21}(s)\\ V_2(s) = V_q + I_d \cdot z_{12}(s) + I_q \cdot z_{22}(s)\end{cases} \tag{2.15}$$

Les variations des courants *dq* fonction des tensions d'entrées ainsi que les variations en tensions de contrôle peuvent être exprimées comme suit :

$$\begin{bmatrix}\tilde{\imath}_d(s)\\ \tilde{\imath}_q(s)\end{bmatrix} = Y(s)\cdot\left(\alpha\cdot\tilde{v}_s(s)\cdot\begin{bmatrix}V_d^*\\ V_q^*\end{bmatrix} + \alpha\cdot V_s\cdot\begin{bmatrix}\tilde{v}_d^*(s)\\ \tilde{v}_q^*(s)\end{bmatrix}\right) \tag{2.16}$$

Ici, le bloc de découplage est modélisé par la matrice $A(s)$:

$$\begin{bmatrix}\tilde{v}_d^*(s)\\ \tilde{v}_q^*(s)\end{bmatrix} = A(s)\cdot\begin{bmatrix}\tilde{v}_d^{**}(s)\\ \tilde{v}_q^{**}(s)\end{bmatrix} \tag{2.17}$$

Avec $\tilde{v}_d^{**}$ et $\tilde{v}_q^{**}$ sont les sorties *dq*- des contrôleurs de courants. Trois cas peuvent être considérés [33]:

1- Sans structure de decouplage, la matrice $A(s)$ est égale à la matrice unité I_2 dans R^{2x2};
2- Une structure de découplage à base feedforward: $A(s)$ est une matrice complète (remplie) dans R^{2x2}. Ainsi, grâce au découplage, le produit $Y(s)\cdot A(s)$ est une matrice diagonale, qui est égale à l'admittance du système sans termes de couplage.
3- Une structure de découplage à base de retour d'états: $A(s)$ est égale à la matrice unité *(I_2)*. De plus, l'effet de la structure de découplage sera considéré en prenant la matrice correspondant à l'admittance diagonale.

En se référant à la Fig. 2.3.

$$\begin{bmatrix}\tilde{v}_d^*(s)\\ \tilde{v}_q^*(s)\end{bmatrix} = \left(A(s)\cdot\begin{bmatrix}C_d(s) & 0\\ 0 & C_q(s)\end{bmatrix}\cdot\begin{bmatrix}\tilde{\imath}_{dref}(s)-\tilde{\imath}_d(s)\\ \tilde{\imath}_{qref}(s)-\tilde{\imath}_q(s)\end{bmatrix}\right) \tag{2.18}$$

En remplaçant (2.16) dans (2.30) :

$$\begin{bmatrix}\tilde{\imath}_d(s)\\ \tilde{\imath}_q(s)\end{bmatrix} = Y(s)\cdot\left(\begin{matrix}\alpha\cdot\tilde{v}_s(s)\cdot\begin{bmatrix}V_d^*\\ V_q^*\end{bmatrix}\\ +\alpha\cdot V_s\cdot A(s)\cdot\begin{bmatrix}C_d(s) & 0\\ 0 & C_q(s)\end{bmatrix}\cdot\begin{bmatrix}\tilde{\imath}_{dref}(s)-\tilde{\imath}_d(s)\\ \tilde{\imath}_{qref}(s)-\tilde{\imath}_q(s)\end{bmatrix}\end{matrix}\right) \tag{2.19}$$

Les courant *dq* de références (i_{dref} et i_{qref}) sont obtenus par la boucles de régulation des flux et de la vitesse (si ces deux régulateurs existes). Pour évaluer l'impédance d'entrée de convertisseur dédié au contrôle de moteur, les références en flux ou en vitesse sont supposées constantes (i.e. leurs variations sont supposées nulle). Maintenant, si on suppose que la dynamique de ces deux contrôleurs sont très faibles comparée à celle de la boucle interne (courants), leurs influences sur l'impédance d'entrée peut être exprimé comme suit :

$$\begin{aligned}\begin{bmatrix}\tilde{\imath}_{dref}(s)\\ \tilde{\imath}_{qref}(s)\end{bmatrix} &= \begin{bmatrix}h_{d1}(s) & h_{d2}(s)\\ h_{q1}(s) & h_{q2}(s)\end{bmatrix}\cdot\begin{bmatrix}\tilde{\imath}_d(s)\\ \tilde{\imath}_q(s)\end{bmatrix} + \begin{bmatrix}0\\ h_v(s)\end{bmatrix}\cdot\tilde{v}_s(s)\\ &= H(s)\cdot\begin{bmatrix}\tilde{\imath}_d(s)\\ \tilde{\imath}_q(s)\end{bmatrix} + S(s)\cdot\tilde{v}_s(s)\end{aligned} \tag{2.20}$$

À partir de (2.19) et (2.20), les variations en courants *dq* devienne :

$$\begin{bmatrix}\tilde{\imath}_d(s)\\ \tilde{\imath}_q(s)\end{bmatrix} = Y(s)\cdot\left(\begin{array}{c}\alpha\cdot\tilde{v}_s(s)\cdot\begin{bmatrix}V_d^*\\ V_q^*\end{bmatrix}\\ +\alpha\cdot V_s\cdot A(s)\cdot\begin{bmatrix}C_d(s) & 0\\ 0 & C_q(s)\end{bmatrix}\cdot\left(H(s)\cdot\begin{bmatrix}\tilde{\imath}_d(s)\\ \tilde{\imath}_q(s)\end{bmatrix}+S(s)\cdot\tilde{v}_s(s)\right)-\\ \alpha\cdot V_s\cdot A(s)\cdot\begin{bmatrix}C_d(s) & 0\\ 0 & C_q(s)\end{bmatrix}\cdot\begin{bmatrix}\tilde{\imath}_d(s)\\ \tilde{\imath}_q(s)\end{bmatrix}\end{array}\right)$$

$$\begin{bmatrix}\tilde{\imath}_d(s)\\ \tilde{\imath}_q(s)\end{bmatrix} = D^{-1}(s)\cdot\left(\begin{array}{c}\alpha\cdot Y(s)\cdot\begin{bmatrix}V_d^*\\ V_q^*\end{bmatrix}\\ +\alpha\cdot V_s\cdot Y(s)\cdot A(s)\cdot\begin{bmatrix}C_d(s) & 0\\ 0 & C_q(s)\end{bmatrix}\cdot S(s)\end{array}\right)\cdot\tilde{v}_s(s) \qquad (2.21)$$

Avec :

$$D(s) = I_2 - \alpha\cdot V_s\cdot Y(s)\cdot A(s)\cdot\begin{bmatrix}C_d(s) & 0\\ 0 & C_q(s)\end{bmatrix}\cdot(H(s)-I_2) \qquad (2.22)$$

En posant,

$$\begin{cases}\tilde{\imath}_{ds}(s) = Y_d(s)\cdot\tilde{v}_s(s)\\ \tilde{\imath}_{qs}(s) = Y_q(s)\cdot\tilde{v}_s(s)\end{cases} \qquad (2.23)$$

Sachant que $Y_d(s)$ et $Y_q(s)$ peuvent être identifies par l'utilisation de (2.23) et (2.24).

Et, en utilisant (2.14) et (2.23), nous pouvons écrire:

$$\left(I_s - V_1(s)\cdot Y_d(s) - V_2(s)\cdot Y_q(s)\right)\cdot\tilde{v}_s(s) = -V_s\cdot\tilde{\imath}_s(s) \qquad (2.24)$$

Ainsi, l'expression analytique de l'impédance d'entrée est comme suit :

$$Z_{in}(s) = -\frac{V_s}{I_s - V_1(s)\cdot Y_d(s) - V_2(s)\cdot Y_q(s)} \qquad (2.25)$$

Bloc de stabilisation proposé :

Le bloc de stabilisation proposé ici est un compensateur proportionnel suivi d'un filtre passe-bande. Ce filtre permet de préserver le comportement du système aux très basses fréquences (dynamique de la vitesse) et de rejeter les mesures du bruit. De plus, comme il a déjà été dit dans [Mos 07], [Liu 08a], [Mos 05], un filtrage passe-bande est la meilleure solution pour stabiliser un

bus de tension DC. On obtient la fonction de transfert suivante pour le bloc de stabilisation $h_v(s)$:

$$h_v(s) = K\frac{2\xi\omega_f s}{s^2 + 2\xi\omega_f s + \omega_f^2} \tag{2.26}$$

avec ω_f la fréquence centrale du filtre et K le gain proportionnel à définir. Il est évident d'après (2.21) que ce bloc modifie l'impédance d'entrée de la commande Z_{in} en permettant de stabiliser le bus de tension DC.

Exemple pratique d'analyse de stabilité :

Afin d'analyser la stabilité du bus de tension DC en utilisant (2.4) et (2.25) dans un cas pratique, la stabilité de la tension de bus DC d'une commande AC construite pour des applications aéronautiques est étudiée dans cette section. Les paramètres du système sont donnés dans le tableau 2.I. Ils correspondent à notre banc d'essai.

TABLEAU 2.I
PARAMETRES DU SYSTEME EXPERIMENTAL

Tension de bus DC (V_e)	200 *V*
Inductance du bus DC (L_f)	39.5 *mH*
Résistance du bus DC (r_f)	1.1 Ω
Fréquence de découpage	10 *kHz*
no. de paires de pôles (P)	4
Résistance statorique (R_s)	0.5 Ω
Inductance statorique (L_s)	3.1 *mH*
Flux magnétique (Ψ_f)	124×10^{-3} *Nm/A*
Constante de frottement (f)	24×10^{-3} $Kg.m^2/s$
Moment d'inertie (J)	3.1×10^{-3} $Kg.m^2$

La figure 2.4 montre trois diagrammes de Bode obtenus pour trois capacités DC différentes, tous les autres paramètres étant maintenus constants. L'impédance d'entrée de la commande (Z_{in}) est calculée à partir de (2.25) sans compensateur ($h_v = 0$) pour Ω=1500*rpm*, p_s=620*W*. Evidemment, il y a plus d'interactions entre Z_o and Z_{in} sur le diagramme de Bode quand la capacité DC diminue. Ceci est potentiellement indésirable puisque les marges de stabilité peuvent diminuer. Pour vérifier cela, le diagramme de Nyquist est tracé sur la Fig. 2.5 où on peut voir que, pour un même point de fonctionnement, la tension DC est stable pour C=1000μF, mais est instable pour C=500μF and C=200μF. Les paramètres du système sont donnés dans Tableau 2,I.

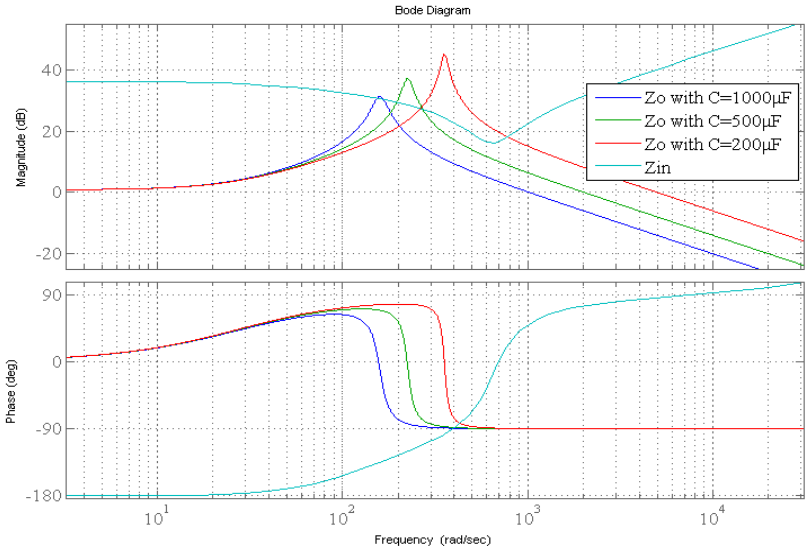

Fig. 2.4 - Influence de la capacité DC sur la stabilité : Bode diagram (K=0).

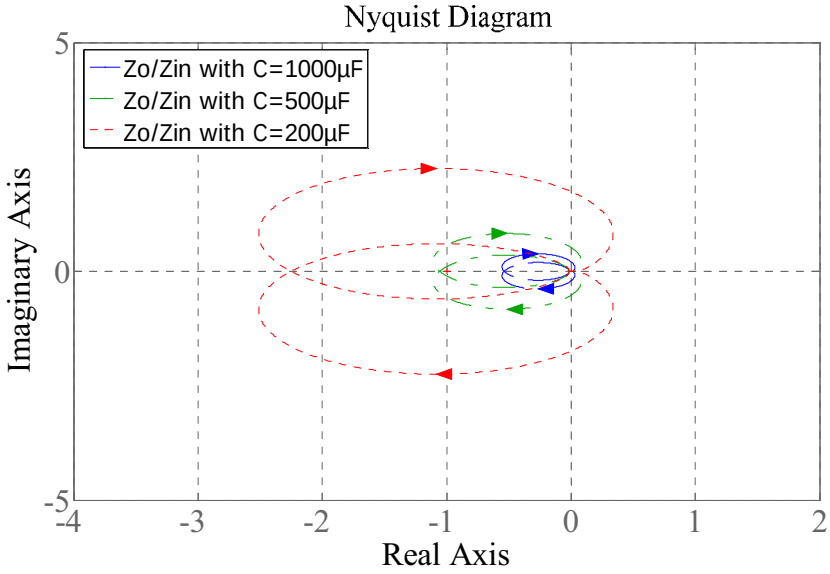

Fig. 2.5- Influence de la capacité DC sur la stabilité : Nyquist diagram (K=0).

Comme montré dans (2.26), le bloc de compensation est composé d'un filtre passe-bas et d'un correcteur proportionnel. Le choix du filtre passe-bas permet d'affecter i_{qref} uniquement dans une bande de fréquences limitée afin d'améliorer la robustesse vis à vis des bruits de mesure du bus DC sans modifier la valeur du régime permanent. La coupure des fréquences doit être fixée en fonction de la zone d'interaction entre Z_o et Z_{in} du diagramme de Bode pour un jeu de paramètres donné. Par exemple, si on choisit C=500μF, la zone d'interaction se situe de 190 *rad/s* à 270 *rad/s* d'après le diagramme de bode (Fig. 2.4). C'est pourquoi un choix approprié pour couvrir la zone d'interaction est ω_{c1}=100 *rad/s* and ω_{c2}=400 *rad/s*. Le troisième et dernier paramètre du compensateur est K. D'après l'application étudiée, la meilleur solution doit

satisfaire des marges de stabilité suffisantes et une bonne dynamique du couple. Figs. 2.6 montre les diagrammes de Nyquist correspondants à différentes valeur de K pour le même point de fonctionnement que Fig. 5 (Ω=1500 *rpm*, p_s=620 *W*).

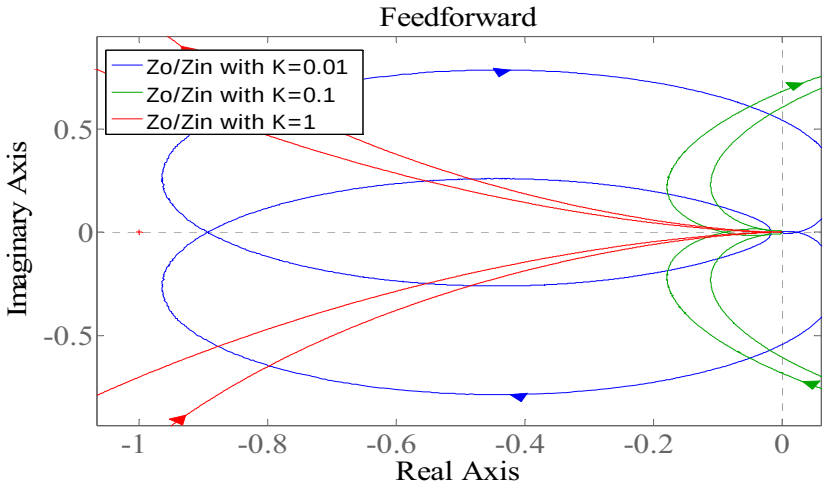

Fig. 2.6- Influence du paramètre de stabilisation (K) sur les marges de stabilité : diagramme de Nyquist (zoom)

Validation de l'analyse de stabilité :

L'analyse de stabilité présentée dans la section précédente par les diagrammes de Bode et de Nyquist sont validés par les résultats de simulation et expérimentaux. Pour cela, un modèle Simulink correspondant au système étudié (onduleur-moteur-commande avec une source DC et un filtre LC) est développé. Les paramètres du système contrôlé et des paramètres de contrôle sont donnés respectivement dans Tableau 2.I and Tableau 2.II.

TABLEAU 2.II
PARAMETRES DU SYSTEME EXPERIMENTAL

Gain proportionnel du contrôle de vitesse (K_{pv})	0.02
Constante de temps du contrôle intégral de vitesse (τ_{iv})	0.2 *s*
Gain proportionnel du contrôle de courant ($K_{pd} = K_{pq}$)	10
Constante de temps du contrôle intégrale du courant ($\tau_{id} = \tau_{iq}$)	$2ms$
Fréquence de coupure inférieure du bloc de stabilisation (f_{c1})	$16Hz$
Fréquence de coupure supérieure du bloc de stabilisation (f_{c2})	$64Hz$

La Fig. 2.7 montre les résultats du modèle de simulation pour (C=500μF, K=0). Selon le diagramme de Nyquist Fig. 2.5, la tension du bus DC devrait osciller. Les résultats de simulation, montrés Fig. 2.11, confirment l'analyse donnée : les variations de la tension du bus DC ($\tilde{v}_s$) et les

courants d'entrée du bus DC (i_e) sont instables quand un échelon sur le courant q est appliqué. Il faut noter que cet échelon est équivalent à un changement de la puissance de charge pour le filtre d'entrée.

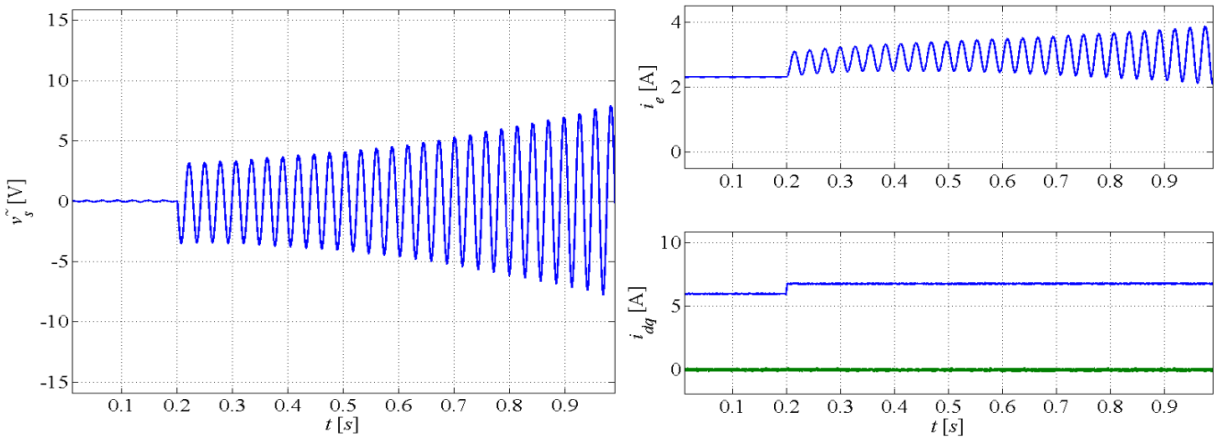

Fig. 2.7- Instabilité des variation de tension du bus DC ($\tilde{v}_s$) et du courant du bus DC (i_e) après un échelon de puissance (C=500µF, K=0)

Le même test sous les mêmes conditions a été réalisé sur le banc expérimental. La Fig. 2.8 illustre les résultats expérimentaux qui sont proches de ceux des variables de la Fig. 2.7 et confirment l'analyse de stabilité donnée dans la section précédente.

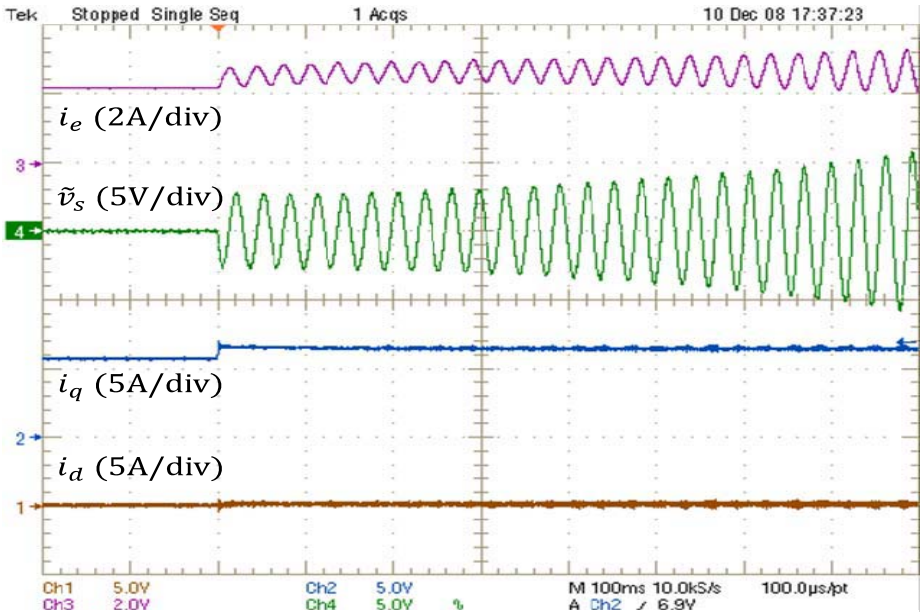

Fig. 2.8- Courants statoriques, variations de la tension du bus DC ($\tilde{v}_s$) et courants du bus DC (i_e) après un échelon de puissance sans compensation(C=500µF, K=0).

Conclusion :

Une charge à puissance constante connectée à une source de tension DC peut conduire à des instabilités sur les variables du bus DC. Dans ce chapitre, la stabilité locale des variables du bus DC a été étudiée en utilisant le tracé de Nyquist de Z_o/Z_{in} (impédance de sortie du filyre de la source/impédance d'entrée de la source). Ensuite, une méthode générale donnant l'expression analytique de l'impédance d'entrée d'un système de l'onduleur et MSAP a été présenté. Cette modélisation est évidemment basée sur les variations petit-signal à cause de la nature locale de cette étude. Quoi qu'il en soit, toutes les dynamiques sont prises en compte excepté celles de l'onduleur seulement qui peuvent souvent être négligées dans les applications pratiques. Un bloc de stabilisation, composé d'un filtre passe-bande et d'un compensateur proportionnel, ont été proposés et ajoutés à la structure de contrôle usuelle du système. Cela permet de stabilisé la tension du bus DC quand des petites capacités DC sont utilisées. C'est pourquoi ce bloc de stabilisation est utile dans les applications aéronautiques quand les capacités du bus DC doivent être petites à cause des contraintes mécaniques. Les résultats de simulation et expérimentaux confirment la validité et l'efficacité de l'approche proposée.

Chapter 3:

Introduction:

Dans ce chapitre, nous présentons deux techniques de stabilisation non linéaires pour un système électrique composé d'une alimentation DC, un filtre LC et un actionneur (Onduleur - Moteur synchrone à aimant permanent ou Moteur à induction). Dans le chapitre précédent, la stabilité locale de ce système électrique a été étudié. Bien que les modèles linéaires peuvent être employés avec succès pour décrire le comportement au niveau local d'un système physique, ils omettent souvent de fournir une caractérisation globale satisfaisante [Nij 90]. Dans ce chapitre, nous tenons compte de la non linéarité du système étudié et présentons deux méthodes pour l'étude de la stabilité globale du système électrique ci-dessus. Nous allons d'abord étudier la stabilité globale de ce système en utilisant le critère du cercle. Ensuite, une approche basée sur la réalisation d'une résistance virtuelle sera présentée. Les simulations et expérimentations confirmeront les techniques proposées.

Modèle réduit du système étudié :

Le système électrique étudié est composé d'une alimentation DC, un filtre LC et une charge à puissance constante. Cette charge est réalisée avec un ensemble onduleur-moteur synchrone à aimants permanents (MSAP). Ici, nous supposons que les performances de la commande de la charge sont satisfaisantes. En particulier, il est supposé que la dynamique des courants statoriques en boucle fermée est suffisamment élevée. Si nous supposons que la fréquence de commutation est très élevée, alors l'actionneur peut être modélisé avec une charge à puissance constante. Dans ce cas, le modèle moyen du système est le suivant (voir Fig. 3.1):

$$\begin{cases} L_f \frac{d}{dt} i_e = -r_f i_e - v_s + V_e \\ C_f \frac{d}{dt} v_s = i_e - i_s \end{cases} \tag{3.1}$$

avec:

$$i_s = {p_s}/{v_s} \tag{3.2}$$

où p_s est la puissance absorbée par l'actionneur.

Pour étudier la stabilité du modèle (3.1) autour de son point de fonctionnement $(\boldsymbol{i_{e0}, v_{s0}})$, il est fréquent de déplacer ce point de fonctionnement à l'origine par le changement de variable suivant:

$$\begin{cases} \tilde{\boldsymbol{i}}_{\boldsymbol{e}} = \boldsymbol{i_e} - \boldsymbol{i_{e0}} \\ \tilde{\boldsymbol{v}}_{\boldsymbol{s}} = \boldsymbol{v_s} - \boldsymbol{v_{s0}} \end{cases} \tag{3.3}$$

avec :

$$\begin{cases} i_{e0} = \dfrac{V_e - v_{s0}}{r_f} = \dfrac{p_{s0}}{v_{s0}} \\ v_{s0} = \dfrac{V_e + \sqrt{V_e^2 - 4 p_{s0} r_f}}{2} \end{cases} \tag{3.4}$$

où $\boldsymbol{p_{s0}}$ est la puissance absorbée par la charge au point de fonctionnement ($\boldsymbol{p_{s0} = v_{s0} \cdot i_{e0}}$). Puis, à partir de (3.1) et (3.4), le modèle du système peut être écrit comme suit :

$$\begin{cases} \frac{d}{dt}\tilde{i}_e = \dfrac{-r_f}{L_f} \cdot \tilde{i}_e - \dfrac{1}{L_f} \cdot \tilde{v}_s \\ \frac{d}{dt}\tilde{v}_s = \dfrac{1}{C_f} \cdot \tilde{i}_e + \dfrac{p_{s0}}{C_f v_{s0}} \cdot \dfrac{\tilde{v}_s}{\tilde{v}_s + v_{s0}} - \dfrac{1}{C_f} \cdot \dfrac{\tilde{p}}{\tilde{v}_s + v_{s0}} \end{cases} \tag{3.5}$$

Dans ce modèle, la puissance de charge $\boldsymbol{p_s}$ a été remplacée par la relation suivante :

$$\boldsymbol{p_s = p_{s0} + \tilde{p}} \tag{3.6}$$

où $\tilde{p}$ est la puissance stabilisante venant du bloc de stabilisation.

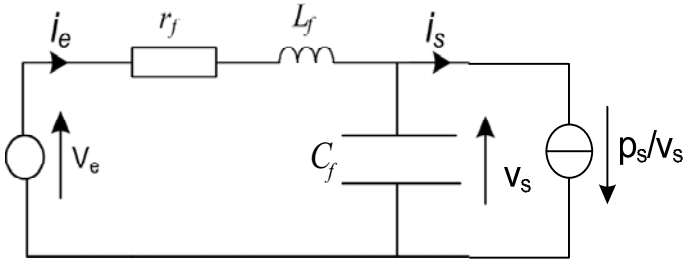

Fig. 3.1- Modèle réduit du système étudié.

Dans ce qui suit, nous présentons deux méthodes pour déterminer cette puissance stabilisante.

Première Méthode de Stabilisation :

Dans cette section, une méthode pour étudier la stabilité globale d'un système électrique composé d'une alimentation DC, un filtre LC et une charge à puissance constante est présentée. Le critère du cercle est utilisé pour réaliser cette étude. Afin de stabiliser ce système, une structure de stabilisation non linéaire est également présentée. Dans l'approche proposée, la structure de contrôle du système électrique doit être légèrement modifié pour mettre en œuvre la structure de stabilisation non linéaire pour améliorer la stabilité large signal du système et permet donc de réduire la valeur de la capacité du filtre LC. L'efficacité de la structure de stabilisation non linéaire proposée est évaluée par expérimentation sur un bus DC alimentant une charge de type moteur synchrone à aimants permanents (MSAP) via un onduleur de tension.

Le modèle réduit du système illustré sur la figure 3.1 peut être mis sous la forme d'un système bouclé composé d'un système dynamique linéaire invariant dans le temps subissant un retour statique non linéaire tel illustré sur la figure 3.2. Cette représentation nous permet d'analyser la stabilité absolue de l'ensemble du système en utilisant le critère du cercle.

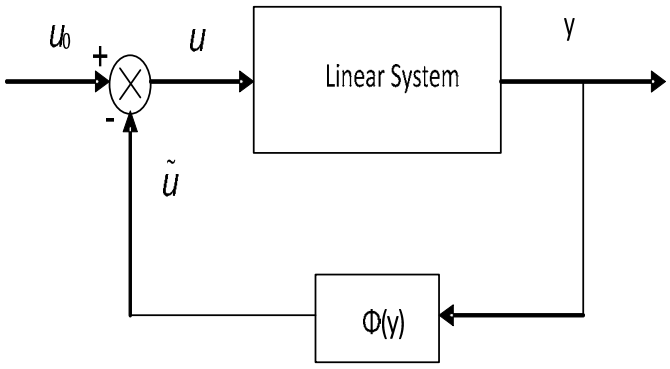

Fig.3.2- Représentation du modèle sous une forme adaptée pour l'étude de la stabilité.

Le modèle d'état du système linéaire est le suivant:

$$\frac{d}{dt}\tilde{\imath}_e = -\frac{r_f}{L_f}\tilde{\imath} - \frac{1}{L_f}\tilde{\boldsymbol{v}}_s \qquad (3.7)$$

$$\frac{d}{dt}\tilde{\boldsymbol{v}}_s = -\frac{1}{C_f}\tilde{\imath}_e + \frac{1}{C_f}u \qquad (3.8)$$

$$\frac{d}{dt}x_1 = \omega_{p2}\tilde{\boldsymbol{v}}_s - \omega_{p2}x_1 \qquad (3.9)$$

$$\frac{d}{dt}x_2 = \omega_{p1}x_1 - \omega_{p1}x_2 \qquad (3.10)$$

$$y = x_1 - x_2 \qquad (3.11)$$

avec:

$$\tilde{v}_s = v_s - v_{s0} \qquad \tilde{\imath}_e = i_e - i_{e0} \qquad (3.12)$$

où z_0 correspond à la valeur de *z* sur le point d'équilibre, et ω_{p1} et ω_{p2} sont des fréquences de coupure du filtre passe-bande. Sans perte de la généralité, la valeur deu_0 est fixée à 0. Le stabilisateur proposé consiste en la conception d'une fonction non linéaire $\psi(y)$ de telle sorte que le système linéaire de la figure 3.2 avec la loi de commande $u = -\psi(y)$ soit "absolument stable". Ensuite, grâce à cette loi de commande, il est possible de déduire la puissance stabilisante $\tilde{p}$ supplémentaire que la charge doit consommer pour stabiliser la tension du bus DC. En effet, cette puissance stabilisante vérifie la relation suivante:

$$u = i_{e0} - \frac{P_0 + \tilde{p}}{v_{s0} + \tilde{v}_s} = -\psi(y)$$
$$\Rightarrow \tilde{p} = v_s . i_{e0} - P_0 + v_s . \psi(y) \qquad (3.13)$$

Pour que le système présenté sur la Fig. 3.2 soit "absolument stable", il faut satisfaire les deux conditions suivantes :

I. *La non linéarité $\psi(y)$ appartient au secteur [α , β].*

II. *L'une des conditions suivantes est vraie :*

- *0 < α < β, le diagramme de Nyquist du système linéaire n'entre pas dans le cercle D(α , β).*
- *0 = α < β, le diagramme de Nyquist du système linéaire reste dans le demi plan (droite) Re(s) > -1/β.*
- *α < 0 < β, le diagramme de Nyquist du système linéaire reste à l'intérieur du cercle D(α , β).*

La non linéarité $\psi(y)$ appartient au secteur *[α , β]* si elle satisfait la condition suivante :

$$(\psi(y) - \alpha . y) . (\psi(y) - \beta . y) \leq 0 \qquad (3.14)$$

Cette condition implique que la fonction non linéaire $\psi(y)$ se situe entre deux droites *αy* et *βy*. Les pentes *α* et *β* doivent donc être choisies de manière à ce que $\psi(y)$ reste entre ces droites pour un intervalle *[y_{min} , y_{max}]* donné. Ici, nous proposons l'équation suivante pour $\psi(y)$:

$$\psi(y) = \begin{cases} K \cdot \left(1 - \frac{\delta}{y}\right) \; if \; y > \delta \\ 0 \; if \; |y| \leq \delta \\ K \cdot \left(-1 - \frac{\delta}{y}\right) \; if \; y > -\delta \end{cases} \qquad (3.15)$$

Il est évident que le choix de cette fonction affecte la puissance stabilisante $\tilde{p}$ générée par le stabilisateur (3.13).

Bloc de Stabilisation :

La figure 3.3 illustre le schéma de la technique de stabilisation proposée (voir l'équation (3.13)).

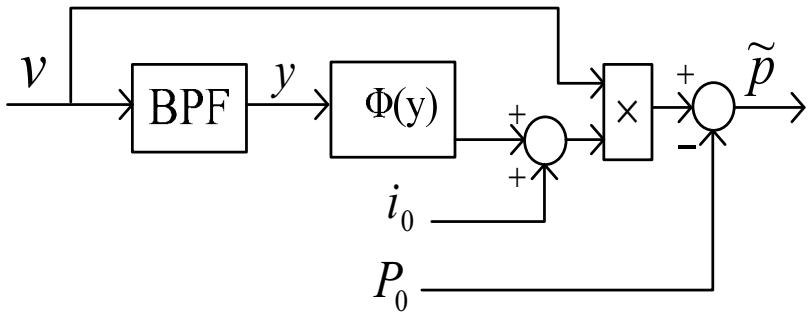

Fig. 3.3- Bloc de stabilisation.

La puissance absorbée par la charge (P_0) est calculée à partir des grandeurs disponibles (courants *dq* (i_d and i_q) et tensions de commande (v_d and v_q) pour un moteur électrique). Le courant du bus DC au point de fonctionnement est le suivant :

$$i_0 = \frac{P_0}{v_0} \qquad (3.16)$$

Et enfin, la tension du bus DC au point de fonctionnement (v_0) est obtenue par le filtrage passe-bas de la tension v. Ensuite, pour réaliser la puissance stabilisante ($\tilde{p}$) dans le cas d'un actionneur, nous la transformons en une référence de couple qui sera superposée sur la référence du couple moteur (sortie du régulateur de vitesse ou le régulateur de couple) pour obtenir la référence totale du couple moteur. Cela nous permet de bien modifier la puissance absorbée et de stabiliser le bus DC. Cette technique de stabilisation améliore la stabilité du système et permet donc de diminuer la taille de la capacité du bus DC.

Resultats de Simulation:

L'impact de cette technique de stabilisation peut être vérifiée par simulation. En choisissant *K* le gain optimal pour la fonction non linéaire $\psi(y)$, le système de stabilisation donne la marge maximale de la stabilité ou réduit la taille de la capacité du bus DC. Un modèle Simulink, basé sur (3.7)-(3.11) et (3.15), est développé. Ses paramètres sont donnés dans la Table 3.I.

TABLE 3.I. PARAMETRES DU SYSTEME ETUDIE

Tension du bus DC	$200\ V$
inductance du bus DC	$39.5\ mH$
résistance du bus DC	$1.1\ \Omega$
capacité du bus DC	$500\ \mu F$
Fréquence de commutation	$10\ kHz$
Nb. de paires de pôles	4
résistance statorique	$0.5\ \Omega$
inductance statorique	$3.1\ mH$
Coefficient du couple	$124 \times 10^{-3}\ Nm/A$
Coefficient de frottement	$24 \times 10^{-3}\ Kg.m^2/s$
Moment d'inertie	$3.1 \times 10^{-3}\ Kg.m^2$

Les résultats de simulation, illustrés sur la Fig. 3.4, sont obtenus sans stabilisation. Les variations de la tension du bus DC ($\tilde{v}$) ne sont pas stables suite à un échelon de puissance de charge de $0.9 \times P_n$ à $1.1 \times P_n$.

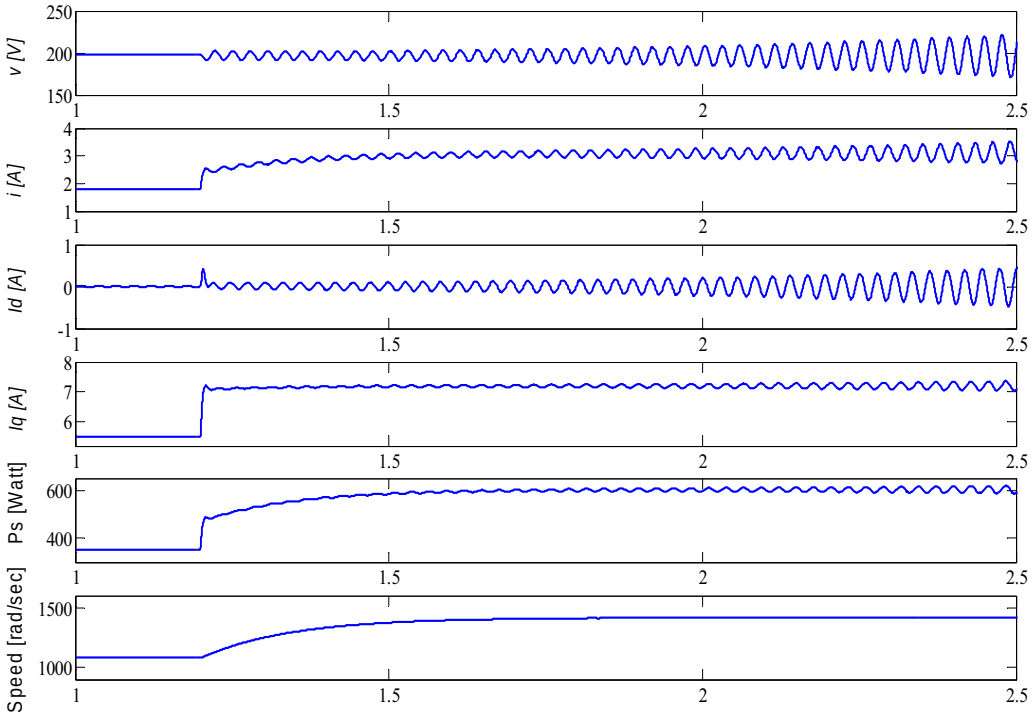

Fig. 3.4- Instabilité sur le bus DC après un échelon de charge (sans stabilisation).

Fig. 3.5 montre les résultats de simulation dans les mêmes conditions que dans l'essai précédent, mais après l'activation de la structure de stabilisation non linéaire (voir Fig. 3.3). Les résultats

confirment l'efficacité de notre technique de stabilisation. En effet, on remarque sur cette figure que les variations de la tension du bus DC ($\tilde{v}$) ne sont pas plus instables lorsque le même échelon de puissance de charge est appliqué.

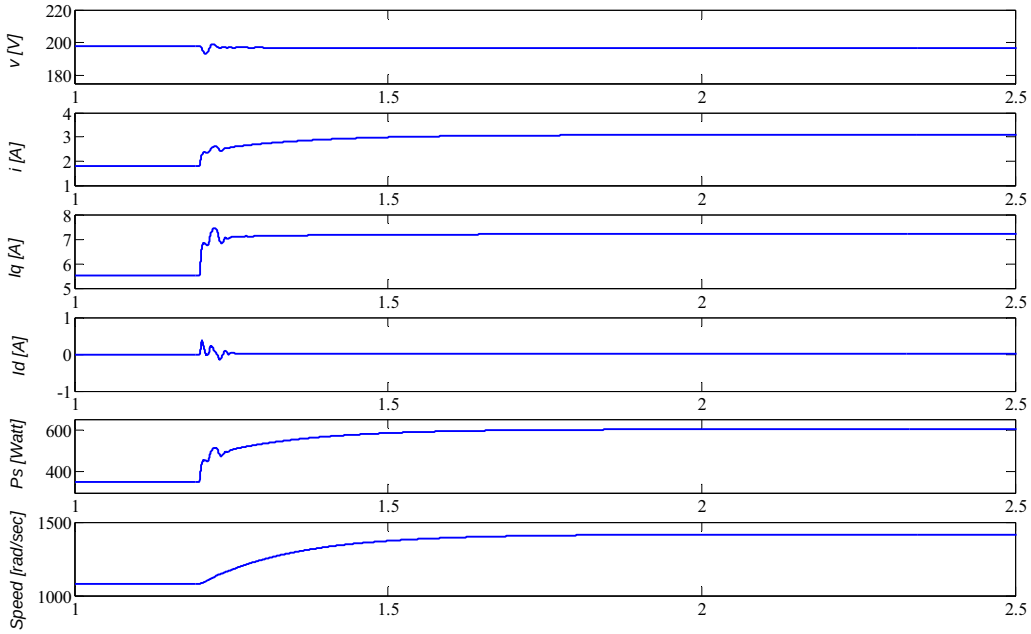

Fig. 3.5- Stabilisation du bus DC avec la méthode proposée (K=1).

Validation Experimentale :

Les performances et l'efficacité du bloc de stabilisation ont été validées par différents tests effectués sur un banc expérimental. Dans le premier test, la puissance stabilisante est forcée à zéro (pas de stabilisation) et un échelon de puissance de charge est réalisé grâce au courant i_q. Les résultats sont présentés sur la Fig. 3.6 qui montre que les variations de la tension du bus DC et celles du courant d'entrée ne sont pas stables. Dans le second test (Fig. 3.7), le bloc de stabilisation a été activé avec K = 0,1 et $\omega_{p1} = 100 rad/s$ et $\omega_{p2} = 600 rad/s$. Les résultats illustrés sur la Fig. 3.7 montrent que les variations de la tension du bus DC et celles du courant d'entrée ne sont plus instables suite à l'application du même échelon de puissance de charge.

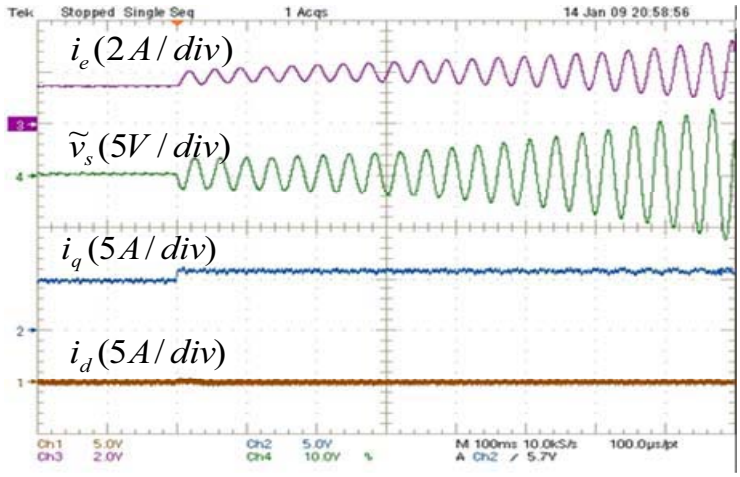

Fig. 3.6- Courant statoriques (Ch1 and Ch2), courant du bus DC (Ch3) et variations de la tension du bus DC (Ch4) après un échelon de puissance de charge (pas de stabilisation, K=0).

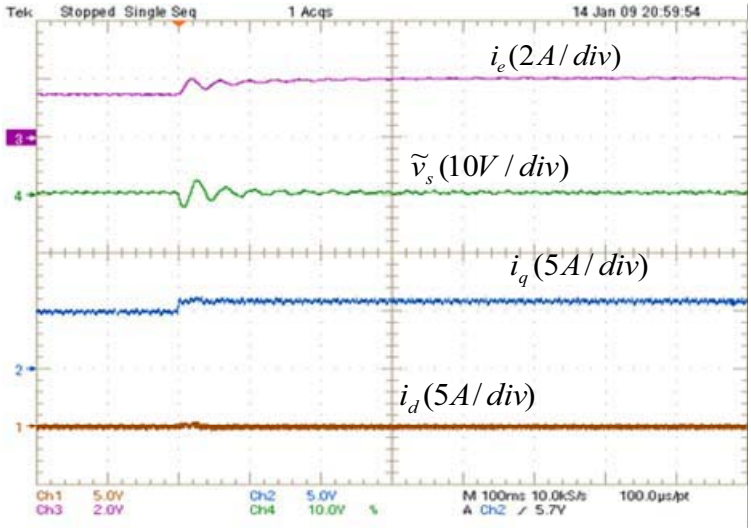

Fig. 3.7- Courant statoriques (Ch1 and Ch2), courant du bus DC (Ch3) et variations de la tension du bus DC (Ch4) après un échelon de puissance de charge (avec la stabilisation, K=0.1).

Seconde Methode de Stabilisation :

Dans cette **section**, nous présentons une méthode de stabilisation basée sur une conductance virtuelle en parallèle avec la capacité du bus DC. La réalisation de cette conductance consiste à modifier la puissance absorbée par la charge de manière à superposer la puissance absorbée par cette conductance sur la puissance de charge habituelle. Il est à noter que cette conductance doit être nulle pour la composante continue de la tension du bus DC. Par conséquent, nous proposons la loi de stabilisation suivante :

$$\boldsymbol{U = K \cdot v_s^2} \qquad (\mathbf{3.17})$$

dans laquelle *K* est le paramètre de la conception à définir pour stabiliser le système (3.5). En effet, cette loi de stabilisation injecte de l'amortissement dans le système et fait disparaître les oscillations non amorties. *K* est en fait la conductance virtuelle souhaitée. Le schéma bloc de cette approche est illustré sur la Fig. 3.8. $\boldsymbol{K \cdot v_s^2}$ correspond à une puissance dissipatives. Sachant que cet amortissement est inutile pour la composante continue, il devrait être suivi par un filtre passe-haut pour enlever sa composante continue due à la tension du bus DC. En pratique, il est préférable de mettre un filtre passe-bande pour rejeter les bruits haute fréquence. Cela conduit à:

$$\begin{cases} \frac{d}{dt}x_1 = 2Kv_{s0}\omega_1 \cdot \tilde{v}_s - \omega_1 \cdot\ x_1 + K\omega_1 \cdot {\tilde{v}_s}^2 \\ \tilde{p} = 2Kv_{s0} \cdot \tilde{v}_s - x_1 + K \cdot {\tilde{v}_s}^2 \end{cases} \tag{3.18}$$

pour un filtre passe-haut premier ordre et à :

$$\begin{cases} \frac{d}{dt}x_1 = 2Kv_{s0}\omega_1 \cdot \tilde{v}_s - \omega_1 \cdot\ x_1 + K\omega_1 \cdot {\tilde{v}_s}^2 \\ \frac{d}{dt}x_2 = 2Kv_{s0}\omega_2 \cdot \tilde{v}_s - \omega_2 \cdot\ x_1 - \omega_2 \cdot\ x_2 + K\omega_2 \cdot {\tilde{v}_s}^2 \\ \tilde{p} = x_2 \end{cases} \tag{3.19}$$

pour un filtre passe-bande.

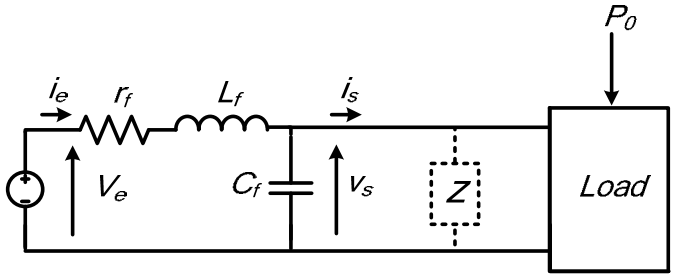

Fig. 3.8: Introduction d'une conductance virtuelle sur le bus DC.

Le bloc de stabilisation proposé est illustré sur la Fig. 3.9.

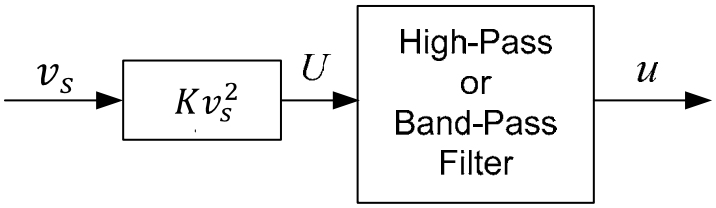

Fig. 3.9- Stabilisation basée sur la conductance virtuelle.

Pour évaluer l'efficacité du stabilisateur proposé, nous supposons que la puissance de charge ne respecte pas la condition de stabilité (point de fonctionnement instable sans le stabilisateur) :

$$p_{s0} > p_{smax} = \frac{r_f C_f}{L_f} v_{s0}^2 \tag{3.20}$$

Pour illustrer cette instabilité, la Fig. 3.10 montre le plan de phase du système (3.5) sans compensation ($\tilde{\boldsymbol{p}} = \mathbf{0}$). Les paramètres du système sont les mêmes que ceux du banc expérimental et donnée dans la Table 3.I. L'état initial est proche du point de fonctionnement fixé comme suit :

$$\begin{cases} i_{e0} = 4.1\ A \\ v_{s0} = 195.5\ V \end{cases} \tag{3.21}$$

Ce qui donne :

$$p_{s0} = 800\ W > p_{smax} \cong 540\ W$$

On peut constater sur la Fig. 3.10 que les trajectoires du système ne convergent pas vers le point de fonctionnement, ce qui signifie que le système non compensé est instable.

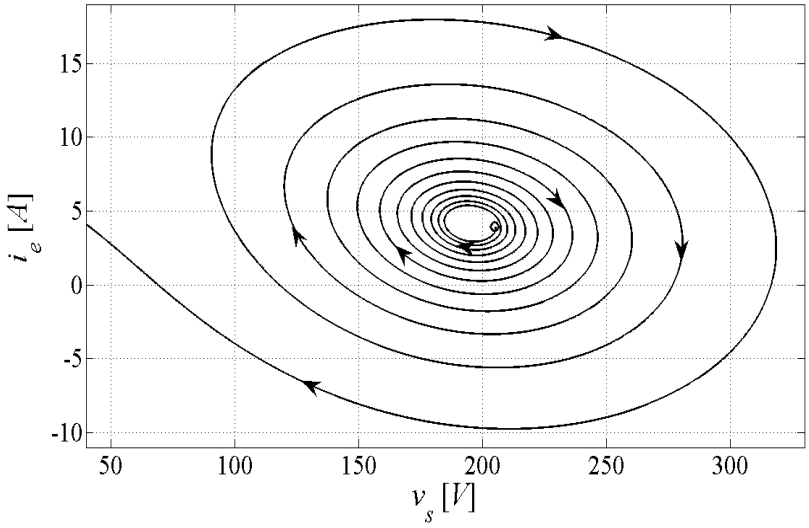

Fig. 3.10- Plan de phase du système (3.17) sans compensation ($\tilde{\boldsymbol{p}} = \mathbf{0}$).

Pour déterminer le gain *K* du stabilisateur, une analyse de stabilité basée sur le théorème de Lyapunov est faite. Le modèle du système en boucle fermée (modèle (3.5) + stabilisateur (3.18)) peut se mettre sous la forme suivante :

$$\frac{d}{dt}x = A_c \cdot x + f(x) \tag{3.22a}$$

avec :

$$A_c = \begin{bmatrix} \frac{-r_f}{L_f} & \frac{-1}{L_f} & 0 \\ \frac{1}{C} & \frac{-K}{C} & 0 \\ 0 & 2Kv_{s0}\omega_1 & -\omega_1 \end{bmatrix} \tag{3.22b}$$

$$f(x) = \begin{bmatrix} 0 \\ \dfrac{p_{s0} - K v_{s0}^2}{C_f v_{s0}} \cdot \dfrac{x_2}{x_2 + v_{s0}} + \dfrac{1}{C_f} \cdot \dfrac{x_3}{x_2 + v_{s0}} \\ K\omega_1 \cdot x_2^2 \end{bmatrix} \qquad (3.22c)$$

Cette analyse, détaillée dans l'Annexe II, montre que l'origine ($\boldsymbol{x_1 = x_2 = x_3 = 0}$) du système (3.22) est globalement asymptotiquement stable si la fréquence de coupure du filtre passe-haut est choisie telle que $\boldsymbol{\omega_1 \ll \omega_0 = \frac{1}{\sqrt{L_f C_f}}}$ et :

$$\boldsymbol{K > K_{min}} > 0 \qquad (23)$$

La preuve mathématique de la stabilité et l'expression de K_{min} sont donnés en Annexe II. Fig. 3.11 illustre les trajectoires du système dans le plan sur $v_s - i_e$ avec :

$$K = 0.1 > K_{min} \cong 0.023$$

Cette figure montre que toutes les trajectoires d'état convergent asymptotiquement vers le point de fonctionnement souhaité et confirme la stabilité large signal du système.

Chapter 4:

Introduction:

Dans ce chapitre, une nouvelle méthode basée sur les spécifications dynamiques est proposé d'étudier la stabilité d'un système en cascade électrique. Pour appliquer cette méthode, une nouvelle modélisation basée sur des variables énergétiques est introduit pour étudier la stabilité des systèmes en cascade. Contrairement à l'approche classique pour lequel les tensions et courants sont les variables d'état, nous proposons d'utiliser les énergies électrostatiques et puissances comme les variables d'état. Nous allons prouver que cette approche de l'étude de stabilité, en considérant certaines hypothèses, peut être moins dépend du point de fonctionnement. Ainsi la stabilité du système distribué à grande échelle peut être simplifiée si tous les composants du système vérifient telles propriétés.

Modèle d'un dispositif électrique:

Le modèle d'un système électrique avec une nouvelle modélisation basée sur des variables dynamiques telles que l'énergie électrostatique et la puissance est présenté dans Fig.4.1. Les indices *i* et *o* sont associés respectivement aux variables d'entrée et sortie du système. *Pi* et *Po* représentent respectivement la puissance d'entrée et sortie du système; *yi* et *yo* correspondent aux énergies électrostatiques stockées dans capacitances d'entrée et sortie.

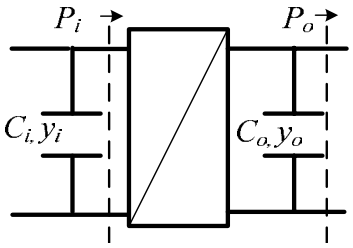

Figure 4.1: présentation des notations utilisées pour la modélisation d'un dispositif électrique

Maintenant, afin de prouver la stabilité autour d'un point de fonctionnement, nous prenons de petites variations de l'énergie électrostatique et la puissance autour d'un point de fonctionnement donné X_0. Les variations des variables sorties du système (y_o, P_i) sont liées aux variations des entrées (y_i, P_o) selon la relation suivante:

$$\begin{bmatrix} \tilde{y}_o \\ \tilde{P}_i \end{bmatrix} = \begin{bmatrix} H_y(s) & T(s) \\ Y(s) & -H_p(s) \end{bmatrix}_{X_0} \cdot \begin{bmatrix} \tilde{y}_i \\ -\tilde{P}_o \end{bmatrix} \qquad (4.1)$$

Où

Hy représente la fonction de transfert de l'énergie électrostatique,

HP représente la fonction de transfert de puissance,

T représente l'impédance de sortie énergique,

Y représente l'admittance d'entrée énergique.

L'admittance d'entrée énergique et l'impédance de sortie du système électrique sont définies par la relation suivante :

$$Y(s) = \left(\frac{\tilde{P}_i}{\tilde{y}_i}\right)_{\substack{\tilde{P}_{load}=0 \\ \tilde{y}_{oref}=0}} \qquad et \qquad T(s) = \left(\frac{\tilde{y}_o}{-\tilde{P}_{load}}\right)_{\substack{\tilde{y}_i=0 \\ \tilde{y}_{oref}=0}}$$

Le système en cascade est présenté dans la Fig.4.2.

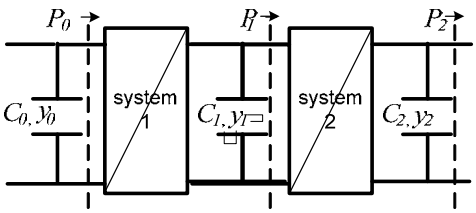

Figure 4.2: Deux dispositifs électriques connectés en cascade.

Ainsi, une relation entre les variations de l'énergie électrostatique peut être obtenue. Il vient:

$$\left(\frac{\tilde{y}_2}{\tilde{y}_0}\right)_{\tilde{P}_2=0} = \frac{H_{y1}(s)\cdot H_{y2}(s)}{1+T_1(s)\cdot Y_2(s)} \qquad \left(\frac{\tilde{y}_1}{\tilde{y}_0}\right)_{\tilde{P}_2=0} = \frac{H_{y1}(s}{1+T_1(s)\cdot Y_2(s)} \qquad (4.2)$$

Si les fonctions de transfert H_{y1} et H_{y2} sont supposés stables pour tout point de fonctionnement, puis la stabilité du système en cascade dépend de la fonction de transfert $T_1(s).\ Y_2(s)$ et une condition suffisante pour parvenir à la stabilité du système en cascade, c'est que le diagramme de Nyquist de la fonction de transfert $T_1(s).\ Y_2\ (s)$ n'encerclent le point (-1,0). Dans la section suivante, nous proposons de modifier la stratégie de contrôle d'actionneurs ou convertisseurs DC - DC qui sont connectés au bus DC de telle manière que les fonctions de transfert qui apparaissent dans (4.2) est moins dépendante du mode de fonctionnement.

Stratégie de contrôle proposée pour convertisseurs DC / DC:

La stratégie de contrôle que nous proposons d'utiliser pour le convertisseur DC-DC est montrée dans la Fig.4.4. Cette stratégie utilise deux boucles de contrôle. La boucle interne est une boucle de bande passante à haute puissance. On suppose que la puissance contrôlée suit parfaitement sa référence P_{ref} qui conduit à l'utilisation de n'importe quel contrôleur dynamique élevée (par exemple contrôleur en mode glissant ou plat peut être utilisée [Sha 10a], [Payer 08]). Comme le montre la Fig.4.4, la référence de puissance P_{ref} est composé de deux éléments $P_{yo,ref}$ et $P_{yi,ref}$ Le premier est généré par le contrôleur d'énergie qui assure que l'énergie électrostatique stockée dans la capacité de sortie y_o suit sa référence y_{oref}. La planification de trajectoire de transfert de la fonction de $H_{yo}(s)$ permet de définir les propriétés dynamiques du convertisseur pour des perturbations de charge.

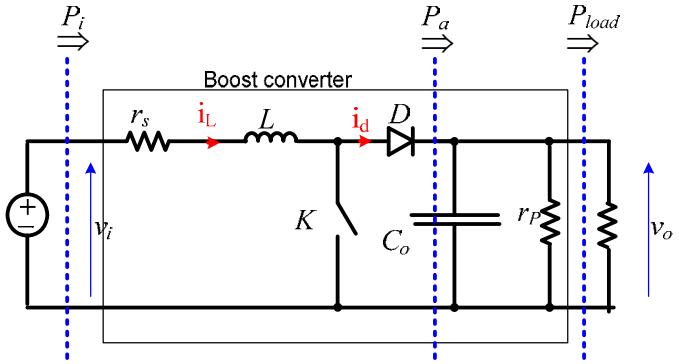

Figure 4.3. Modèle équivalent d'un convertisseur élévateur.

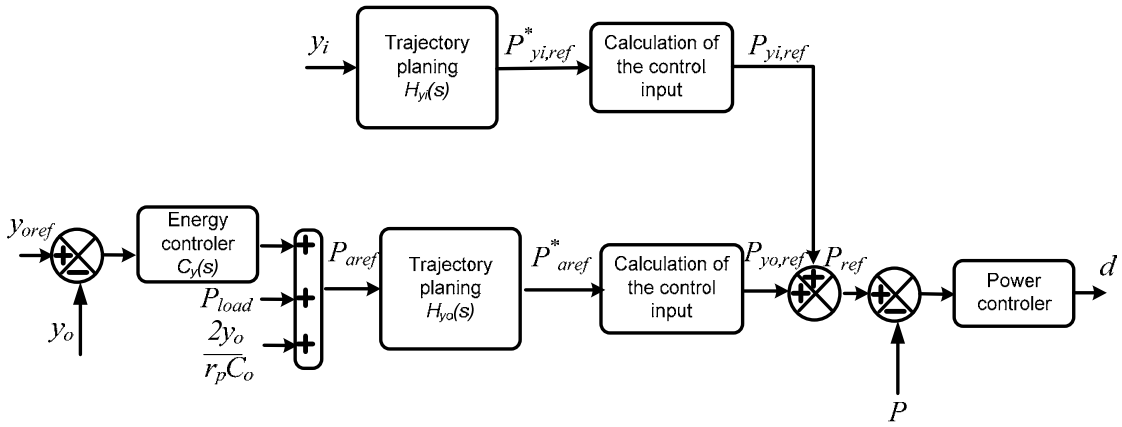

Figure 4.4: stratégie de contrôle proposée de convertisseur DC-DC utilisé pour SPD

La trajectoire définie par la fonction de transfert $H_{yi}(s)$ permet de dimensionner le comportement dynamique du convertisseur pour les variations d'énergie du condensateur d'entrée. Avec l'aide de cette stratégie de contrôle, nous pouvons ainsi supprimer ces variations de l'énergie électrostatique, ce qui assurere la stabilité du système. Les deux autres blocs nommés *calcul du contrôle d'entrée* permettent de calculer la puissance de référence P_{ref} qui est effectivement contrôlée dans le convertisseur. Cette puissance doit être un signal continu pour en assurer le contrôle. Dans le cas d'un convertisseur Boost, elle correspond à la puissance d'entrée P_i. Pour un convertisseur Buck, il s'agit de la puissance fournie à la capacité de sortie. Ici, nous supposons que la puissance ajoutée due aux variations de l'énergie magnétique dans l'inducteur est faible par rapport à celle fournie à la charge. $P_{yo,ref}$ et $P_{yi,ref}$ peuvent être calculées comme suit:

$$P_{y_{o,ref}} = 2\frac{v_i^2}{4 \cdot r_s} \cdot \left(1 - \sqrt{1 - \frac{P^*_{aref}}{\frac{v_i^2}{4 \cdot r_s}}} \right) \tag{4.3}$$

$$P_{y_{i,ref}} = P^*_{y_{i,ref}} \tag{4.4}$$

Modèle petit signal d'un convertisseur Boost contrôlé avec l'approche proposée:

Pour analyser la stabilité de deux systèmes en interaction, les quatre fonctions de transfert de la matrice données par (4.1) doivent être déterminées. Pour cette étude, nous supposons que la puissance contrôlée suit parfaitement sa référence. Pour n'importe quelle structure de convertisseur, il est toujours possible d'écrire des relations entre les puissances d'entrée et de sortie du convertisseur. Dans le cas du convertisseur Boost contrôlé par la méthode décrite en Fig. 4.4, nous avons:

$$P_a = P_i - \frac{r_s \cdot C_i}{2} \cdot \frac{P_i^2}{y_i} - \frac{LP_i}{\sqrt{2y_i/C_i}} \cdot \frac{d}{dt}\left(\frac{P_i}{\sqrt{2y_i/C_i}} \right) = \Psi_{P_a}\left(P_i, \frac{dP_i}{dt}, y_i, \frac{dy_i}{dt}, y_o \right) \tag{4.5}$$

$$P_i = P_{ref} = P_{yo,ref} + P_{yi,ref} = \frac{y_i}{r_s \cdot C_i} \cdot \left(1 - \sqrt{1 - \frac{P^*_{aref}}{\frac{y_i}{2 \cdot r_s \cdot C_i}}}\right) + P^*_{yi,ref}$$

$$= \Psi_{P_i}\left(P^*_{aref}, y_i, P^*_{yi,ref}\right) \quad (4.6)$$

Fonctions de transfert$H_y(s)$ *et* $Y(s)$*:*

$$H_y(s) = \left(\frac{\tilde{y}_o}{\tilde{y}_i}\right)_{\substack{\tilde{P}_{load}=0 \\ \tilde{y}_{oref}=0}}$$

$$= \frac{\left(\frac{\partial \Psi_{P_a}}{\partial y_i}\right)_{X_o} + \left(\frac{\partial \Psi_{P_a}}{\partial \frac{dy_i}{dt}}\right)_{X_o} s + \left(\left(\frac{\partial \Psi_{P_a}}{\partial P_i}\right)_{X_o} + \left(\frac{\partial \Psi_{P_a}}{\partial \frac{dP_i}{dt}}\right)_{X_o} s\right) \cdot \left[\left(\frac{\partial \Psi_{P_i}}{\partial y_i}\right)_{X_o} + \left(\frac{\partial \Psi_{P_i}}{\partial P^*_{yi,ref}}\right)_{X_o} \cdot H_{yi}(s)\right]}{s + \left(\left(\frac{\partial \Psi_{P_a}}{\partial P_i}\right)_{X_o} + \left(\frac{\partial \Psi_{P_a}}{\partial \frac{dP_i}{dt}}\right)_{X_o} s\right) \cdot \left(\frac{\partial \Psi_{P_i}}{\partial P^*_{aref}}\right)_{X_o} \cdot H_{yo}(s) \cdot \left(C_y(s) - \frac{2}{r_P \cdot C_o}\right) - \left(\frac{\partial \Psi_{P_a}}{\partial y_o}\right)_{X_o} + \frac{2}{r_P \cdot C_o}}$$

(4.7)

$$Y(s) = \left(\frac{\tilde{P}_i}{\tilde{y}_i}\right)_{\substack{\tilde{P}_{load}=0 \\ \tilde{y}_{oref}=0}} = \left(\frac{\partial \Psi_{P_i}}{\partial P^*_{aref}}\right)_{X_o} \cdot H_{yo}(s) \cdot \left(-C_y(s) + \frac{2}{r_P \cdot C_o}\right) \cdot H_y(s) + \left(\frac{\partial \Psi_{P_i}}{\partial y_i}\right)_{X_o}$$

$$+ \left(\frac{\partial \Psi_{P_i}}{\partial P^*_{yi,ref}}\right)_{X_o} \cdot H_{yi}(s) \quad (4.8)$$

Fonctions de transfert$\mathbf{T(s)}$ and $\mathbf{H_p(s)}$:

$$T(s) = \left(\frac{\tilde{y}_o}{-\tilde{P}_{load}}\right)_{\substack{\tilde{y}_i=0 \\ \tilde{y}_{oref}=0}}$$

$$= \frac{1}{s + \left(\left(\frac{\partial \Psi_{P_a}}{\partial P_i}\right)_{X_o} + \left(\frac{\partial \Psi_{P_a}}{\partial \frac{dP_i}{dt}}\right)_{X_o} s\right) \cdot \left(\frac{\partial \Psi_{P_i}}{\partial P^*_{aref}}\right)_{X_o} \cdot H_{yo}(s) \cdot \left(C_y(s) - \frac{2}{r_P \cdot C_o}\right) - \left(\frac{\partial \Psi_{P_a}}{\partial y_o}\right)_{X_o} + \frac{2}{r_P \cdot C_o}}$$

(4.9)

$$H_p(s) = \left(\frac{\tilde{P}_i}{-\tilde{P}_{load}}\right)_{\substack{\tilde{y}_i=0 \\ \tilde{y}_{oref}=0}} = \left(\frac{\partial \Psi_{P_i}}{\partial P^*_{aref}}\right)_{X_o} \cdot H_{yo}(s) \cdot \left(-C_y(s) + \frac{2}{r_P \cdot C_o}\right) \cdot T(s) \qquad (4.10)$$

Un dimensionnement correct des régulateurs du convertisseur mènent à des fonctions de transfert $H_p(s)$ et $H_y(s)$ stables pour n'importe quel point de fonctionnement. Ainsi, les fonctions de transfert $Y(s)$ et $T(s)$ permettent d'étudier la stabilité des systèmes mis en cascade.

Contrôle des actionneurs à aimants permanents :

Il est possible d'étendre cette stratégie pour le contrôle d'actionneurs. La figure 4.5 décrit la stratégie de contrôle d'un actionneurs à aimants permanents. Le modèle équivalent de l'actionneur est donné sur la figure 4.5a. Les pertes sont modélisées par 2 résistances. La première, notée r_s, est connectée en série avec les trois phases de la machines tandis que la seconde, notée R_p, est connectée en parallèle de la capacité d'entrée C_i. La puissance mécanique est notée P_{load}. La figure 4.5b donne la stratégie de contrôle utilisée. y_c et y_{cref} représentent respectivement l'énergie cinétique et sa référence, P_{aref} la puissance mécanique de réference et comme pour le convertisseur DC/DC, $P_{yi,ref}$ est la puissance mécanique stabilisatrice généreé par les variations d'entrée de l'énergie électrostatique. 2 possibilités existent pour le choix du contrôle de la puissance: on peut choisir la puissance mécanique ou électrique. Dans ce chapitre, nous décidons d'utiliser la puissance mécanique et donc P_{aref} sera vue comme la puissance mécanique de référence.

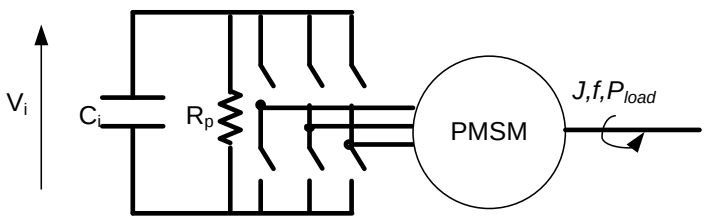

Figure 4.5a. Modèle équivalent d'un actionneur à aimants permanents.

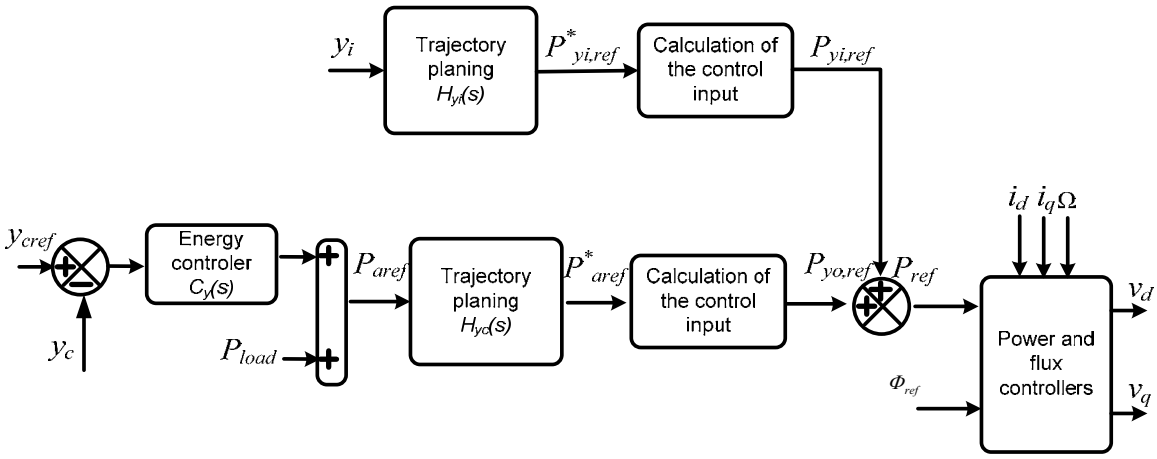

Figure 4.5b. Stratégie de contrôle proposée pour les actionneurs aimants permanents.

Modèle "petit signal" de l'actionneur à aimants permanents:

On suppose que la puissance mécanique et le flux suivent leurs références respectives. En ce qui concerne les charges mécaniques, seule la fonction de transfert *Y(s)* doit être connue pour étudier la stabilité du système en cascade Les équation 4.5 et 4.6 dans le cas d'un actionneur à aimants permanents contrôlé via la puissance mécanique P_a peuvent se réécrire comme il suit:

$$P_i = \frac{2 \cdot y_i}{R_p \cdot C_i} + P_a + r_s \cdot \left(\left(\frac{\Phi_{ref} - \Psi_f}{L_d} \right)^2 + \left(\frac{P_a}{p \cdot \Psi_f \cdot \Omega} \right)^2 \right) + L_q \cdot \left(\frac{P_a}{\left(p \cdot \Psi_f \right)^2 \cdot \sqrt{2 \cdot y_c / J}} \right) \cdot \frac{d}{dt} \left(\frac{P_a}{\sqrt{2 \cdot y_c / J}} \right)$$

$$= \Psi_{Pi} \left(y_i, P_a, \Phi_{ref}, \frac{dP_a}{dt}, y_c, \frac{dy_c}{dt} \right) \quad (4.11)$$

$$P_a = P_{yo,ref} + P_{yi,ref} = P^*_{aref} + F\left(P^*_{aref}, P^*_{yi,ref}\right) = \Psi_{Pa}\left(P^*_{aref}, P^*_{yi,ref}, y_c\right) \quad (4.12)$$

Avec la fonction F, qui régle de la loi de commande et choisi égal à:

$$F\left(P^*_{aref}, P^*_{yi,ref}\right) = \frac{\left(p \cdot \Psi_f \cdot \Omega\right)^2}{2 \cdot r_s} \cdot \left(-\left(1 + 2 \cdot r_s \cdot \frac{P^*_{aref}}{\left(p \cdot \Psi_f \cdot \Omega\right)^2} \right) + \sqrt{\left(1 + 2 \cdot r_s \cdot \frac{P^*_{aref}}{\left(p \cdot \Psi_f \cdot \Omega\right)^2} \right)^2 + 4 \cdot r_s \cdot \frac{P^*_{yi,ref}}{\left(p \cdot \Psi_f \cdot \Omega\right)^2}} \right) \quad (4.13)$$

Fonctions de transfert $H_y(s)$ *and* $Y(s)$*:*

$$H_y(s) = \left(\frac{\tilde{y}_c}{\tilde{y}_i}\right)_{\substack{\tilde{P}_{load}=0 \\ \tilde{y}_{cref}=0 \\ \tilde{\Phi}_{ref}=0}} = \frac{\left(\frac{\partial \Psi_{P_a}}{\partial P^*_{yi,ref}}\right)_{X_o} \cdot H_{yi}(s)}{s + \frac{2 \cdot f}{J} + \left(\frac{\partial \Psi_{P_a}}{\partial P^*_{aref}}\right)_{X_o} \cdot H_{yo}(s) \cdot C_y(s) - \left(\frac{\partial \Psi_{P_a}}{\partial y_c}\right)_{X_o}} \tag{4.14}$$

$$\begin{aligned} Y(s) = \left(\frac{\tilde{P}_i}{\tilde{y}_i}\right)_{\substack{\tilde{P}_{load}=0 \\ \tilde{y}_{cref}=0 \\ \tilde{\Phi}_{ref}=0}} &= \left(\left(\frac{\partial \Psi_{P_i}}{\partial P_a}\right)_{X_o} + \left(\frac{\partial \Psi_{P_i}}{\partial \frac{dP_a}{dt}}\right)_{X_o} \cdot s \right) \\ &\cdot \left[\left(\frac{\partial \Psi_{P_a}}{\partial P^*_{aref}}\right)_{X_o} \cdot H_{yo}(s) \cdot \left(-C_y(s)\right) \cdot H_y(s) + \left(\frac{\partial \Psi_{P_a}}{\partial P^*_{yi,ref}}\right)_{X_o} \cdot H_{yi}(s) \right. \\ &\left. + \left(\frac{\partial \Psi_{P_a}}{\partial y_c}\right)_{X_o} \cdot H_y(s) \right] + \left(\left(\frac{\partial \Psi_{P_i}}{\partial y_c}\right)_{X_o} + \left(\frac{\partial \Psi_{P_i}}{\partial \frac{dy_c}{dt}}\right)_{X_o} \cdot s \right) \cdot H_y(s) + \frac{2}{R_p \cdot C_i} \end{aligned} \tag{4.15}$$

Conclusion:

Comparé aux approches classiques utilisant les variables courant/tensions, nous proposons une nouvelle approche basée sur les variables énergie/puissance pour étudier la stabilité de systèmes en cascade. Tout comme pour les approches classiques basées sur les impédances d'entrées et de sorties, l'utilisation de la méthode proposée et des impédances énergétiques permet d'analyser la puissance de système en cascade ou de système ou la puissance est distribuée. Néanmoins contrairement à certaines approches ou l'analyse de la stabilité dépend du point de fonctionnement, nous avons montré qu'il est possible de trouver, dans le cas de charges électriques, des structures de contrôle mettant en jeu des impédances énergétiques moins dépendantes du point de fonctionnement. Cette avancée permet de simplifier l'analyse "petit signal" de la stabilité de systèmes en cascade et à plus large échelle de systèmes de distribution de la puissance électrique. Pour certaines architectures de puissance, l'approche conduit à une analyse "petit signal" de la stabilité qui est indépendante du point de fonctionnement. Cette propriété est liée au fait que nous connaissons les paramètres du système. Dans le cas d'une machine à aimants permanents, nous avons montré qu'une bonne connaissance de l'inductance d'axe q est nécessaire pour obtenir des impédances énergétique d'entrée peu dépendante du point de fonctionnement.

GENERAL INTRODUCTION

Stability is the first and very important factor in all modes of operation for a Distributed Power System (DPS). In the DPS containing various subsystems connected to one common DC-bus, possible subsystem interactions complicate the behavior of the whole system. In DPS, loads are connected to the DC-bus through an input LC filter. Change of the load in one subsystem may lead a stable system into instability. Subsystems may be connected or disconnected at any time, thus causing a change in the overall configuration of the system.

Most of the loads in DPS of aircraft present a constant power load characteristic within a domain of operation in which they are tightly controlled. A constant power load absorbs a constant power whatever the DC-bus voltage is. This characteristic is strongly related to the load controllers capability on rejecting the DC-bus voltage disturbances. Thus, the load draws a constant power from the bus. Such loads are very common in aerospace applications.

An example of CPL is a DC/AC inverter, which drives a Permanent Magnet Synchronous Motor (PMSM) or Induction Motor (IM) and tightly regulates the speed. For an ideal switching regulator, the average input power remains constant. If the input voltage increases by some factor, the PWM closed-loop control circuitry cuts back the duty cycle of the controlled switch to maintain a constant output average voltage. This, in turn, causes the input current to decrease by the same proportion. In incremental term, a positive incremental change in the input voltage results in a negative incremental change in the input current and vice versa, causing the converter to look like a negative differential resistance at the input terminal which might lead a stable system into instability.

One possible solution to decrease the risk of instability is to increase the size of the capacitor of input LC filter. But this solution results in increase of volume, weight and cost of the system which is undesirable. In aerospace applications, volume and weight of the system are of utmost importance; therefore, this solution is not practical. The other solution is to add damping to the circuit. An easy method to mitigate the instability problem is to simply introduce an adequate resistance into the input filter to counteract the negative input impedance. However, it is not practical to add a damping resistance arbitrarily to the filter circuit, because a damping resistor in series with the inductor would decrease converter efficiency since it must pass all of the input current. While a damping resistor in series with the capacitor would seriously degrade its attenuation characteristic as well as the efficiency since it must essentially pass entire ac input current component.

Another solution consists in modifying the control of the converters or inverter-motor drive system connected to the DC-bus. This solution permits to stabilize the system even with a smaller size of capacitor. In this thesis, we apply this approach to an inverter-motor drive and will present three different techniques to stabilize the system.

In the first chapter, we discuss the stability issues of electrical systems with input filter and DPSs where different loads are connected to common DC-bus through a LC filter. Then, various existing stability study methods are discussed.

In the second chapter, a linear method is presented which allows investigating local stability of an inverter-motor-drive system connected to the grid through an LC filter and a rectifier. This

method can be applied when Permanent Magnet Synchronous Motor (PMSM) or Induction Motor (IM) are used. An oscillation compensation technique is used to improve the stability margin of the system and the size of the dc-link capacitance without modifying structure of the torque or current loops. This technique consists in superposing a stabilizing power on the absorbed power by the drive. For motor drive systems, this stabilizing power is realized by a stabilizing torque reference. By merely a small signal study, impedance criterion and Nyquist plot are used to evaluate the stability margins with and without the oscillation compensation block.

Although linear models can be successfully employed to locally describe the behavior of a physical system, they often fail to provide a satisfactory large signal characterization. In the third chapter, two methods for the large signal stabilization of an electrical system containing a DC power supply, an LC Filter and a constant power load is presented. In order to analyze the stability of the electrical system, nonlinear tools like the circle criterion and the Lyapunov theorem are applied. Two stabilization structures are presented and their impact on the large signal stability is studied. The first approach is based on the circle criterion. The idea is to use a proper nonlinear function in the stabilizer in such a way that the closed-loop system satisfies the absolute stability requirements. In the second approach, a proper damping is added to the DC-bus system by a virtual impedance. Then, a Lyapunov function is proposed to prove the large signal stability of the system. In both cases, the load is considered as a CPL and its internal dynamics are neglected.

In the last chapter, a new method, based on dynamic specifications, is proposed to study the stability of a cascaded electric system. To apply this method, a new modeling, based on energetic variables, is introduced to investigate the stability of the cascaded system. Contrary to classical approach for which voltages and currents are the state variables, we propose to use electrostatic energies and powers as state variables. This approach allows applying impedance criterion for studying the large signal stability of the system without neglecting internal dynamics.

CHAPTER 1

STATE OF ART IN THE STABILITY ANALYSIS OF DISTRIBUTED POWER SYSTEM

Chapter 1

1.1 INTRODUCTION :

The trend in next generation DC-DC and DC-AC converters is to achieve smaller size and lighter weight. This trend naturally pushes to increase the switching frequency because at higher operating frequencies not only the size and weight of the passive components are dramatically reduced but the relevant operational costs are also lessened. However, besides providing compact high-density converters (DC-DC or DC-AC), the high-frequency switching operation also raises electromagnetic interaction (EMI) issues. Switched-mode power converters are typically considered sources of electromagnetic noise as their high-frequency switching of voltage and current generates higher order harmonics that have a potential to cause interference with system operation [Jos 98],[Wil 98]. The problematic conducted input EMI noise generally comprises of reflected ripples in the input current of a switch-mode power converter which interacts with the source impedance of the raw supply voltage [Art 01],[Cho 95]. Combined with any radiated noise, the resultant disturbance can significantly pollute the power-mains and can also cause degradation in systems wherein multiple converter modules are fed by a common power bus as in case of distributed power systems [Art 01],[Flo 96]

Input filters are a necessary but unpopular component of electrical power systems. They are large, heavy, and expensive. They solve some problems, but create others [Kel 84]. Yet because of Electromagnetic Emission and Susceptibility Requirements for the Control of Electromagnetic Interference, they are absolutely necessary. The choice is not whether or not to use an input filter, but how to minimize the size, weight, cost, and adverse impact on performance. In [Gir 09] an analytical method for the design of input filter in DC distributed power systems is presented. The authors have taken the stability and quality criteria into account. The system stability conditions are firstly assessed on the analytical linearized model of the system with the help of Routh Hurwitz criterion. Then, filtering and damping conditions are introduces.

In this chapter we will discuss the purpose of input filter and the stability problems related to the electrical systems with input filter. The last part of the chapter talks about the existing methods to resolve this problem of instability.

1.2 PURPOSE OF THE INPUT FILTER:

Today almost all converters have an input L-C filter. This filter serves two primary purposes; from the system designer's point of view, the filter attenuates AC signal generated inside the converters and prevent them from being conducted back into the source (EMI/EMC control).

From a user's point of view, the filter prevents high frequency AC voltage on the power bus from passing through to the outputs of the power supply and on to the downstream load. From the system design point of view the input filter attenuates the AC voltage superimposed on the DC power bus so that only a small portion of it reaches the converter input terminals. The filter functions as a forward voltage filter attenuating input noise. The sizing of the filter depends on the required attenuation from the applicable standard but the presence of this filter impairs all the other properties of the regulator, in extreme cases to the point of causing instability.

1.2.1 Typical Filter Characteristics:

A plot of the transfer function or "gain" of the simple LC filter (Fig. 1.1) is shown in Fig. 1.2.

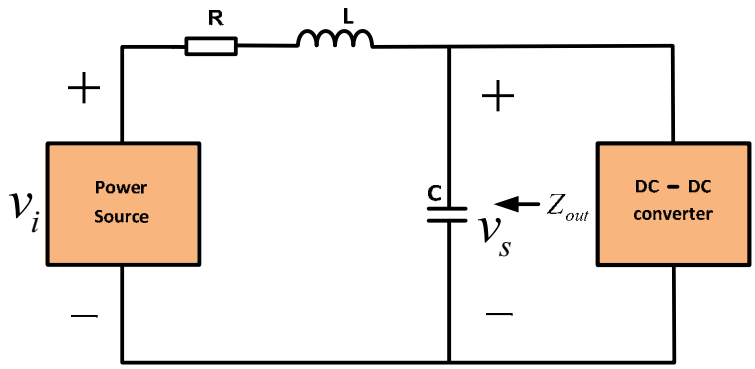

Figure 1.1: Simple input LC Filter

Below the LC resonant frequency, voltage passes through the filter without significant attenuation. Above the LC resonant frequency, voltages are attenuated and the attenuation increases at a 40-dB/decade slope.

At the resonant frequency, there is normally a peak where the output voltage of the filter is actually higher than the input voltage. The amount of this peak is determined by the series and parallel losses associated with various elements and the source and load. The effect of these losses is normally consolidated into a damping factor.

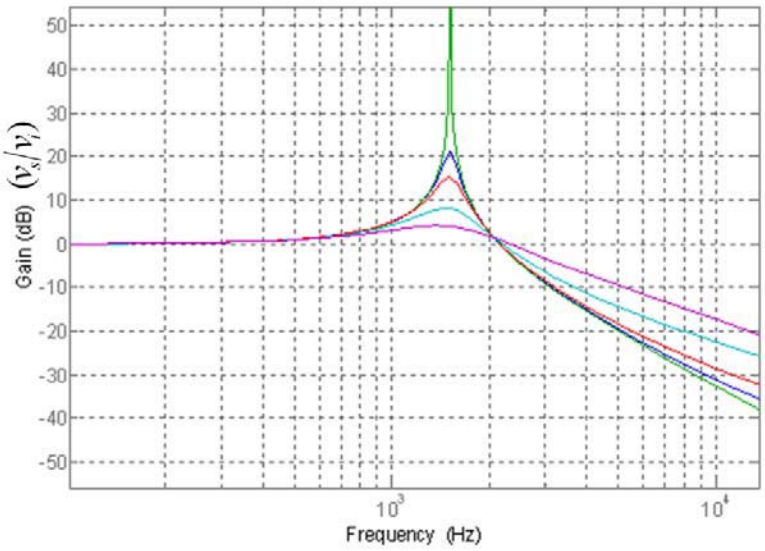

Figure 1.2 : Transfer Function Plot of L-C Filter

With a damping factor of 1, there is no peak. For smaller values of damping, there is a peaking. The curves for various damping factor are shown in Figure 1.2, with the highest peak occurring for undamped filter.

Figure 1.3 is a plot of the output impedance of the filter as a function of frequency and damping factor, for different values of damping. The highest peak in impedance occurs for zero damping. The output impedance of the filter is low at low frequency because the inductor impedance is low and the power bus is essentially a short circuit. At high frequency, the output impedance of the filter is again low because of the low impedance of the capacitor at high frequency. At resonance, the impedance of the filter can be significant, especially if there is little damping.

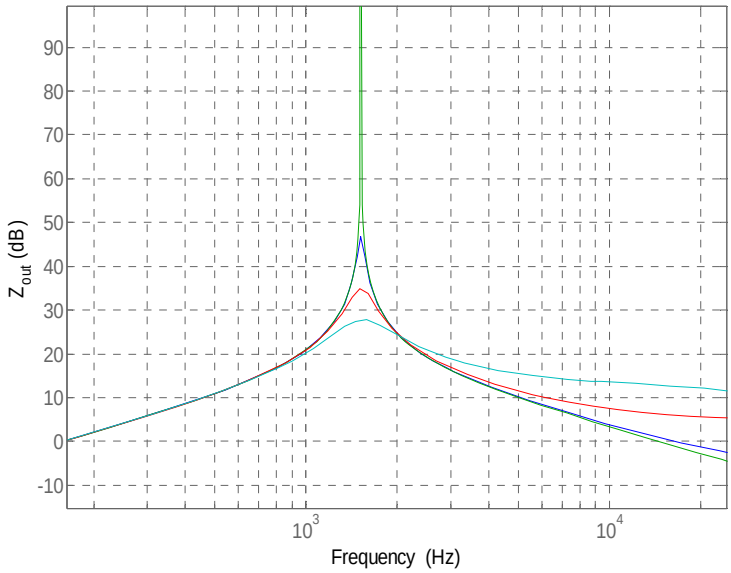

Figure 1.3 : Output Impedance of L-C Filter

1.3 PROBLEM STATEMENT:

In order to combat EMI, an LC filter is usually employed between a converter and its unregulated power source. A substantial part of manufacturing cost for power converters in critical applications involves designing filters to conform to the varying EMI/EMC norms. However, a presumably well-designed input filter, satisfying aforementioned requirements of EMI/EMC, when combined with a switching converter, can often cause significant performance degradation [Mid 76], [Eri 92], [Fay 99], [Kos 04], [Lou 04] such as reduction in loop gain, output impedance and instability.

If there is insufficient damping then transfer function (gain) of the filter peaks near its resonant frequency (Figure 1.2). This peak causes amplification of input noise at the resonant frequency, so that noise voltage applied at the input of the filter is actually larger in amplitude when it reaches the input terminals of the power supply. If this condition happens at a frequency which is above or not far below the bandwidth of the feedback control loop, the power supply will not be able to reject the disturbance and the specification for allowable AC voltage on the outputs of the power supply may be exceeded.

In addition to amplification, poorly damped filters have a significant impact on the transfer function of the feedback control loop. There is a dip in both gain and phase at the resonant frequency of the filter. In moderate cases, this results in power supply output transient response that occurs at the input filter resonance, even though the true control loop crossover frequency may have ample gain and phase margins. In more extreme cases, the input filter can cause the control loop to oscillate.

The output impedance of the input filter peaks at resonance. One characteristic of a simple LC filter is that, if perfect L's and C's could be constructed, the output impedance of the filter approaches infinity at resonance of the filter (Figure 1.3).

Excessive peak of output impedance at the resonant frequency (Figure 1.3) of the filter can interact with the regulator control-loop [mid78]. The cause of this complex interaction is diagnosed to be the negative dynamic resistance characteristic exhibited by converters and Inverter Motor Drive system at their input terminals, which may lead to possible instability of the system [Mid 76], [Mid 78], [Sad 04]. If the peak of the input filter output impedance exceeds the input impedance of the converter or Inverter Motor Drive system at that frequency, the dc-link voltage could oscillate.

Thus on one hand, input filters serve to suppress the EMI, but on the other hand the control-loop design must take into account this input filter in order to assure stability. As a consequent, the control-loop design process becomes more complicated than in the case when no input filter is present, and additional challenges and constraints are imposed on the control system to assure stability.

Middlebrook pointed out that oscillation could be positively prevented by assuring that the magnitude of the output impedance of the source (filter) remained lower than the magnitude of the input impedance of the electrical system (measured beyond the filter).

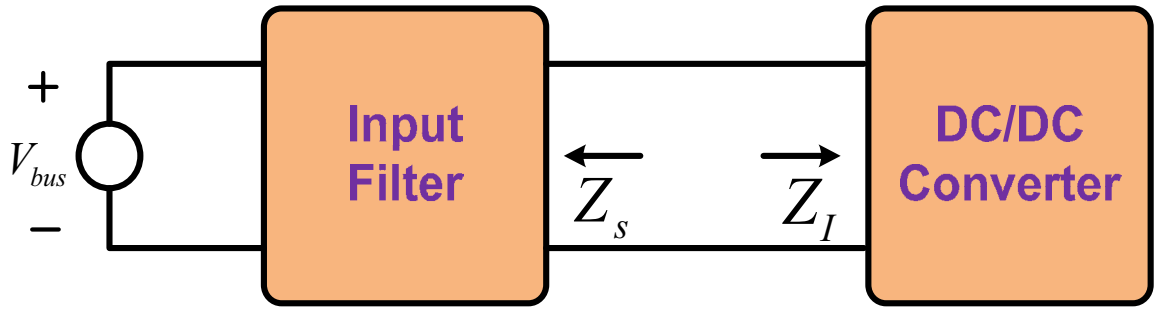

Figure 1.4 : Source impedance and the converter input impedance.

Switching- mode regulators and inverter motor drive systems when tightly regulated behave as constant power loads and have a negative input impedance at low frequencies, and can become unstable by addition of line input filters [Tsu 00], [scl], [Jan 92], [Koh 92]. Preferably, a suitable input filter should be incorporated in original regulator design.

1.3.1 Filter Design Goals:

Minimize Peaking:

There are several improvements that can be made to the simple LC filter to enhance its effectiveness. One is to minimize peaking by adding additional damping. Different methods of implementing damping are discussed later in this chapter.

Minimizing the peaking reduces the gain required in the switching regulator feedback control loop to attenuate input noise to the specified level. It lowers the AC voltage input that the regulation loop must reject [Ven].

In addition to lowering voltage peaking, more damping also lowers the peak value of the output impedance of the filter. This reduces the effect of the filter on the transfer function of the feedback control loop. As mentioned earlier, extreme cases of peaking can actually cause oscillation in the dc-link voltage.

Maximize Attenuation:

The second goal in designing an effective input filter is to maximize attenuation. Since the voltage transfer function in the forward direction is identical to the current transfer function in the reverse direction, maximizing the forward voltage attenuation automatically maximizes the reverse current attenuation. Unfortunately, this goal is in conflict with the first, and an engineering tradeoff is usually required to balance peaking and attenuation.

Single section filter gain falls off at a 40-dB/decade rate. Dual section filters should fall off at an 80-dB/decade rate, but because of damping requirements they actually fall off at a 60 dB/decade rate.

Parasitic components like the capacitance of the inductor and the equivalent series resistance (ESR) and equivalent series inductance (ESL) of the capacitor have a significant effect on attenuation at high frequencies. These effects should be considered in the selection of a filter topology [Ven].

Minimize Output Impedance:

Output impedance is affected by filter topology. Filters, which have nearly the same gain, can have substantially different output impedance. Usually the process, which minimizes peaking, also minimizes the peak value of the output impedance for a given topology of filter.

Minimize Size, Weight, and Cost:

These three considerations are always present, but should not overshadow the design performance requirements. The three tend to move together, with the possible exception of more expensive core materials that may produce smaller and lighter inductors.

1.4 WHY A CONSTANT POWER LOAD WITH INPUT FILTER CAN CAUSE INSTABILITY:

LC filter is connected at the input of DC-DC converter or an Inverter-Motor drive system can degrade the performance of electrical system and consequently may lead to the instability of the system. By their nature, DC-DC converters are classified as constant power loads and same is the case with Inverter-Motor drive system. As the speed has slow dynamic properties, the power delivered by the inverter to the motor can be considered as constant.

Let us take the case of a LC filter connected at the input of a Buck converter (Figure 1.5). For an ideal switching regulator, with no losses, the average input power remains constant in steady state. If the input voltage increases by some factor, the PWM closed-loop control circuitry cuts back the duty cycle of the controlled switch to maintain a constant output voltage. This, in turn, causes the input current to decrease by the same proportion. In incremental terms, a positive incremental change in the input voltage results in a negative incremental change in the input current and vice versa, causing the converter to look like a negative differential resistance at its input terminals.

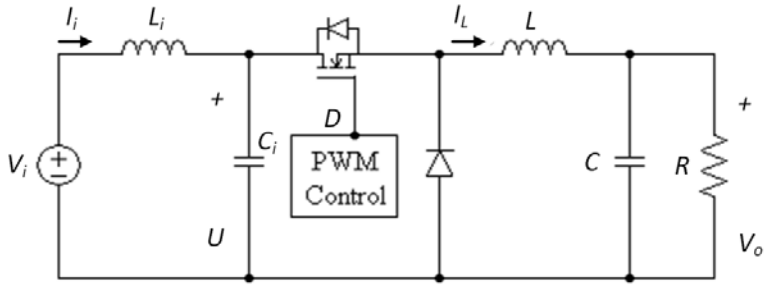

Figure 1. 1: Buck dc-dc converter with input and output filter

The value of this negative resistance depends on the operating point of the converter according to:

$$R_{in} = -\frac{\Delta v_s}{\Delta i_s} \tag{1.1}$$

Where R_{in} is the input resistance, and Δv_s and Δi_s are the incremental changes in the input voltage and input current to the dc-dc converter. To analyze the behavior of the converter and its interaction with the rest of the system, a simplified model of the system is necessary. A simple LC filter, combined with a negative dynamic resistance (Fig. 1.6) allows modeling the interactions between the filter and the switching power supply for low frequency variations.

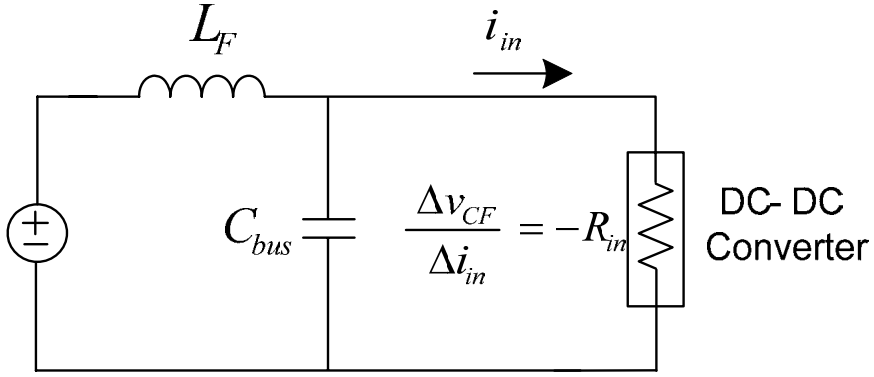

Figure 1.6: LC filter combined with negative dynamic resistance which models a DC-DC converter.

In the vicinity of a given operating point, where R_{in} can be considered constant and the system can therefore be considered linear, the characteristic polynomial of this circuit is:

$$s^2 - \frac{s}{R_{in}C_f} + \frac{1}{L_f C_f} = 0 \tag{1.2}$$

The negative term in this characteristic polynomial transforms to a positive exponential in the time domain, representing an unbounded, hence unstable system. Thus an undamped or lightly damped input filter connected to the regulator input port, can interact with the negative resistance characteristics of the regulator to form a negative-resistance oscillator. This further explains why addition of an input filter tends to lead to instability.

However, despite the theoretical arguments presented above, it is still possible that in some practical applications a DC-DC converter with a simple LC input filter do not exhibit instability. There are several possible reasons why a switching regulator combined with an input filter might not oscillate in practice:

1. The LC filter components or even the power line itself may include enough parasitic resistance to provide sufficient damping.
2. The input filter is designed such that its resonant frequency is well above the switching regulator bandwidth.

Under any one of these conditions it is fairly possible that a DC-DC or DC-AC converter may not oscillate even in presence of an input filter. However, a comprehensive understanding of the problem is important from practical point of view because most of the designers realize a converter design in two distinct steps. First the converter itself is designed according to its given performance specifications, and then in the second step a low-pass filter having sufficient attenuation, to alleviate various noise problems, is added at the input of the converter "black box". There arises a new complication from the fact that the presence of an input filter affects the dynamics of the converter, which otherwise performed well. Apparently it seems that an added input filter is outside the converter feedback loop. However, this is not true, because the input filter is, in fact, not "outside" the feedback loop but interacts with it. It was shown that the input filter actually affects all transfer functions of the converter, including the control-to-output transfer function, the line-to-output transfer function as well as the output impedance of the converter [Mid 76], [Mid 78]. As a consequence, additional criteria need to be established in order to avoid this harmful influence of an input filter upon the regulator terminal properties. The choice is not whether or not to use an input filter but to find an optimum way of minimizing its adverse impact on overall system performance.

1.4.1 Electrical Systems with Constant Power Loads:

Power electronics converters and inverter motor drive systems, when they are tightly regulated, behave as constant power loads (CPL). In fact, loads of multi converter systems also have a tendency to be constant power loads. Loads like actuators, motors, and converters have to be controlled in such a way that constant power is maintained for them. If losses are neglected, which means we suppose 100% efficiency of the electrical system, then output power is equal to input power. As the output power is constant therefore, the input power is constant. As a result these loads present characteristics of the constant power loads [Ema 03], [Ema 99].

An example of electrical system with CPL is shown in Figure 1.7 where a DC-AC inverter motor drive system is connected to the grid through a DC-DC converter. A DC-DC converter connects the common DC bus to the grid and a DC-AC inverter drives an electric motor which is tightly regulated $i.e.$ the speed and torque remains constant. As the speed and torque are constant so the power is constant. If we assume a constant efficiency of the drive system, considering the constant power of the rotating load, the input power of the inverter motor drive system will be constant.

1.4.1.1 DC-DC converters connected in cascade:

Figure 1.8 presents another example of constant power load, where a DC-DC converter connects the grid to the common DC bus and the second DC-DC converter feeds an electric load and tightly regulates the output voltage when the electric load has one-to-one voltage-current characteristic [Mic 99], [Ema 06], [Riv 06], [Nav 91], [Kel 83], [Kel 84], [Dal 85], [Kis 83]. A simplest example of these loads is a resistive load which has a linear relation between voltage and current.

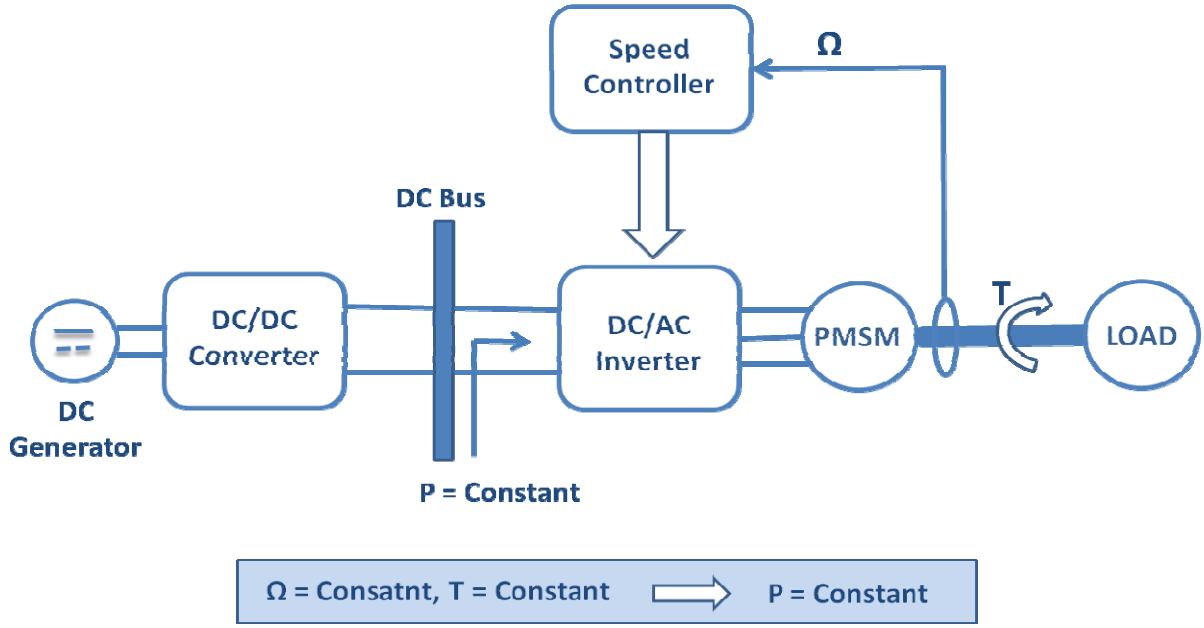

Figure 1.7: DC-AC inverter motor drive system that presents a constant power load characteristics.

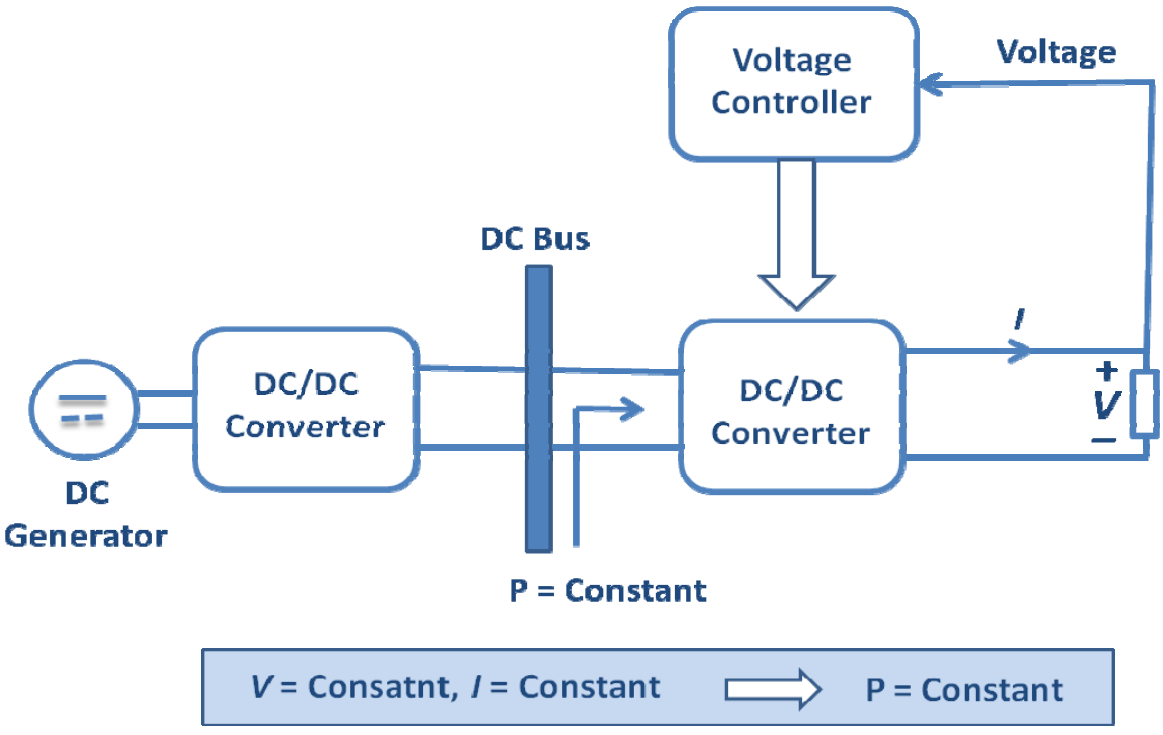

Figure 1.8: DC-DC converter that presents a constant power load characteristics.

When the output voltage of the input filter is increased /decreased, the control of the converter will change the current, absorbed by the converter with an opposite sign, in order to maintain constant power. So for constant power loads, although the instantaneous value of the impedance

is positive($V/I > 0$) , the low frequency input impedance is always negative($dV/dI < 0$). In fact CPLs have negative impedance characteristics which might affect the power quality and stability of the electrical system.

1.4.1.2 Distributed Power Systems with Constant Power Loads (CPLs):

An exponential development of technology in the field of power electronics and control systems in recent years have lead us to a new electrical architecture in automobile and aeronautical industry. This new electrical architecture is called Distributed Power System (DPS). In this type of electrical system, different loads are connected to one common DC or AC bus which is supplied by the multiple sources. The loads generally consist of actuators or other DC-DC or DC-AC converters. This type of DPS is shown in Figure 1.9. These DPS can be classified in to two different categories. The first one consists of a common DC-bus supplying power to different loads connected to that common bus. This system is called DC-DPS. The second category of DPS uses a common AC-bus in order to supply power to interconnected subsystems. In most of the DPSs in industry different sources and loads are connected to a common DC distribution bus with the help of DC-DC, DC-AC or AC- DC converters.

In DPS, possible subsystem interactions complicate the issue. Changes of the load may lead a stable system into instability [Hen 04]. It is expected that 75% of the total load in the DPS of a future aircraft will be presented by constant power load [Ema 06]. Constant power load is usually a load connected to the DC-bus including a voltage regulator or a torque/speed controller.

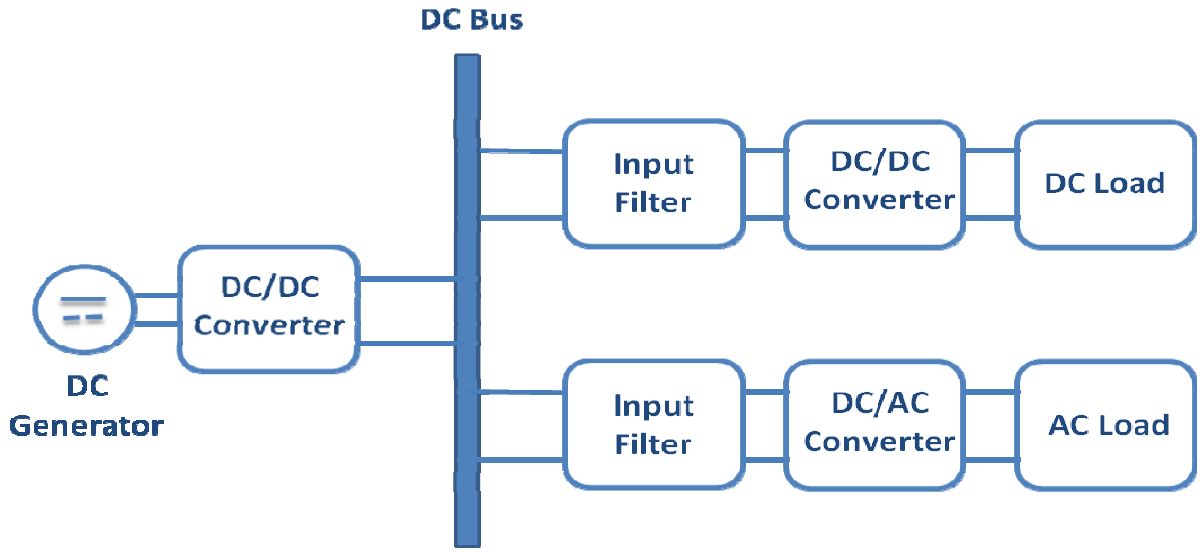

Figure 1.9: Distributed Power System (DPS)

1.5 INSTABILITY OF CONSTANT POWER LOAD SYSTEMS DUE TO NEGATIVE INPUT IMPEDANCE:

Negative impedance behaviour of CPLs is shown in Figure 1.10. As shown in figure 1.10, if the voltage across a CPL increases/decreases, the current through it decreases/increases. This

property of the CPL causes the stability problem for the system that the CPL is connected to [Gri 98], [Bel 95], [Glo 98], [Cie 98], [Ema 00], [Cho 99]. A constant power load with power P, connected in series to an inductor *L* and voltage source *v,* is shown in Figure 1.11. In steady state the circuit will operate at the equiblibrium point which is obtained when source voltage is equal to the CPL voltage.The stability of the system may be assessed from the steady state voltage-current curves of the source and load. Figure 1.12 presents the voltage-current characteristics of typical voltage sources and CPLs.

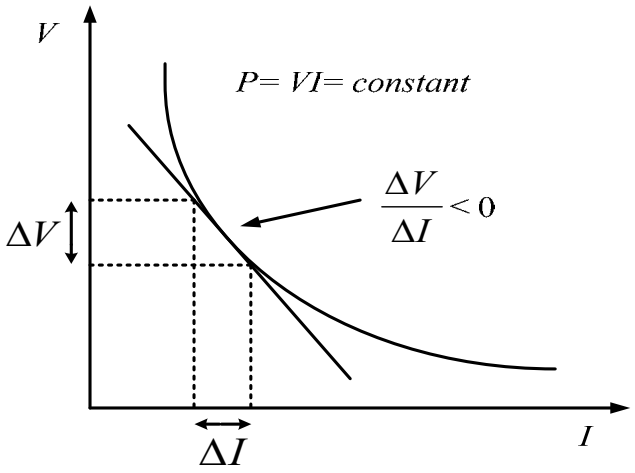

Figure 1.10: V-I characteristics of constant power load (Negative impedance behavior)

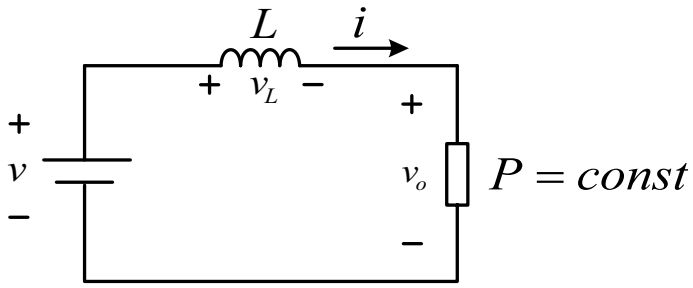

Figure 1.11: CPL in series with an inductor

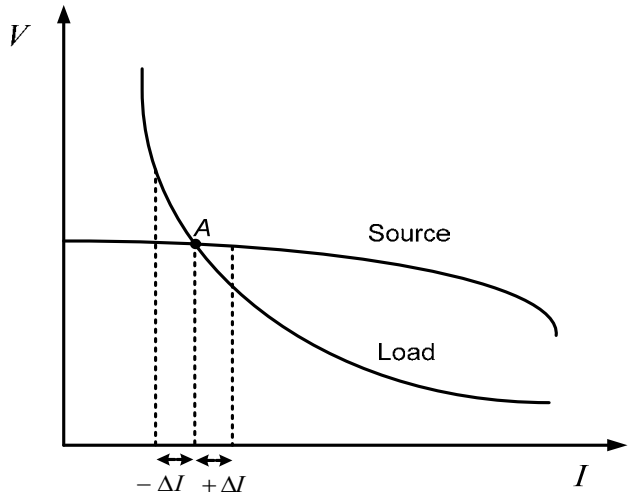

Figure 1.12: V-I characteristics of typical voltage sources and CPLs

The equiblibrium point is considered as asymptotically stable when the operation is restored after a small perturbation due to a disturbance in the source voltage. Let us examine the steady state stability of equiblibrium point *A* in Figure 1.12. Suppose a small perturbation causes a reduction of current Δi. At the new current, the source voltage is less than load voltage; consequently, the current decreases again and the operating pont moves away from *A*. In fact the circuit acts like positive feedback. Finally, current goes to zero and the voltage goes to infinity. Similarly, an increase of current Δi will cause the load voltage to become less than source voltage which will again increase the current. Consequently, the operating point moves away from *A*. Thus, *A* is an unstable point of equiblibrium [Ema 03], [Ema 99].

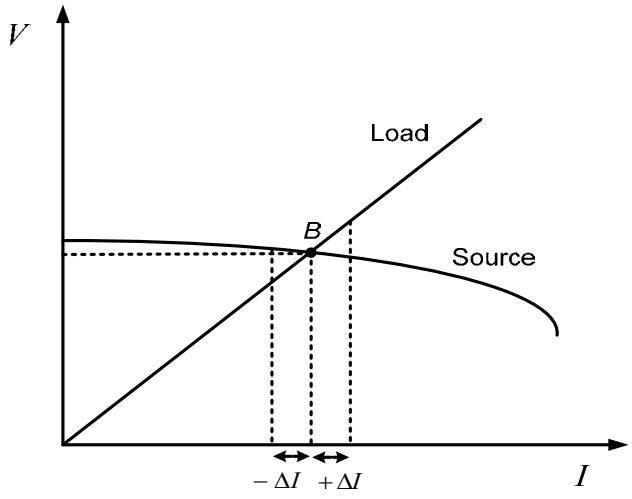

Figure 1.13: V-I characteristics of typical voltage sources and resistive load

The nature of the operating point changes when the nature of the load is different. By example let consider a voltage-current characteristic of typical voltage sources loaded by a resistive load as shown in Figure 1.13. Let us examin the steady state stability of equiblibrium point *B* in Figure

1.13. The resistive load of Figure 1.13 has positive incremental resistance characteristics instead of negative incremental characteristics of CPLs. An increase of current Δi, due to a disturbance, will cause the source voltage to become less than the load voltage; consequently, v_L becomes negative and current decreases. As a result, the operating point will converge to *B.* Similarly, a reduction in current Δi will cause the source voltage to become greater than the load voltage, as a result the voltage v_L becomes positive, and therefore, the current increases and the operating point is restored to *B.* In fact, the circuit acts like negative feedback [Ema 03], [Ema 99].

1.6 STABILITY STUDY METHODS FOR DPS:

The problem of stability of electrical systems with input filters was first identified and brought into spotlight in the early seventies. The papers on this subject extend back to as early as 1971 [Yu 71]. The detailed treatment of this problem for a buck converter with an input filter was first given by Dr. R. D. Middlebrook in [Mid 76] and [Mid 78], the former of which has now become a classic in the field. In [Mid 76] input-filter design criteria were established leading to some impedance inequalities which not only ensured stability, but also specified qualitative impairment of the performance properties caused by this interaction.

The method of stability analysis was extended for the study of other electrical systems interconnected via a common DC-bus by [Pie 04]. In [Gir 09a], input admittance model of an electric drive constituted of inverter-PMSM is developed for the stability analysis purpose. Both time-domain and frequency domain analytical models are presented in [Gir 09a].

In order to study the stability of electrical system we have different methods, like Middlebrook, Gain Margin and Phase Margin (GMPM), Study of Eigenvalues.

1.6.1 Impedance Based Stability:

For the stability analysis based on impedance criteria, the equivalent model of an electrical system consisted of two systems connected in cascade is shown in figure 1.14. $Z_{in}(s)$ and $i_{load}(s)$ represents respectively the input impedance and the thevenin equivalent current of the linearized load subsystem.

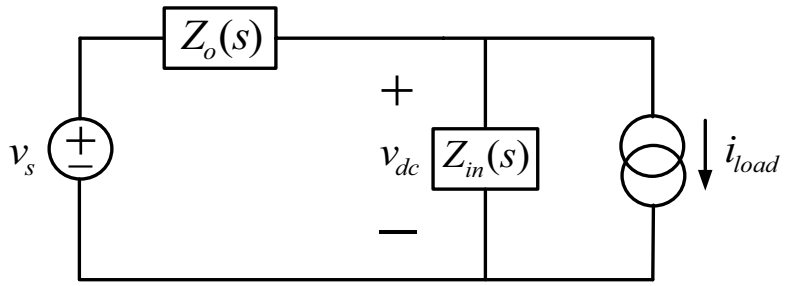

Figure 1.14: Equivalent model of electrical system with two subsystems connected in cascade.

The Thevenin equivalent voltage and the output impedance of the linearized source subsystem are noted respectively $v_s(s)$and $Z_o(s)$. From Figure 1.14 the voltage $v_{dc}(s)$ is given as:

$$v_{dc}(s) = \frac{Z_{in}(s)}{Z_o(s) + Z_{in}(s)} \cdot v_s(s) - \frac{Z_{in}(s) \cdot Z_o(s)}{Z_o(s) + Z_{in}(s)} \cdot i_{load}(s) \tag{1.3}$$

We can define $Z_{in}(s)$ and $Z_o(s)$ as:

$$Z_{in}(s) = \frac{Num_{in}(s)}{Den_{in}(s)} \tag{1.4}$$

$$Z_o(s) = \frac{Num_o(s)}{Den_o(s)} \tag{1.5}$$

Substituting equations (1.4) and (1.5) in (1.3):

$$v_{dc}(s) = \frac{Num_{in}(s)Den_o(s)v_s(s) - Num_o(s)Num_{in}(s)i_{load}(s)}{Num_{in}(s)Den_o(s) + Num_o(s)Den_{in}(s)} \tag{1.6}$$

Supposing that the load is stable if supplied from an ideal source ($Z_o(s) = 0 \Longrightarrow Num_o(s) = 0$), the calculation of the source current variations involves that $Num_{in}(s)$ will not have any zeros in the right half plane. Similarly, assuming that the source can operate in stable fashion if supplying an ideal load (for an ideal load $Z_{in}(s) \to \infty \Longrightarrow Den_{in}(s) \approx 0$), the calculation of the common voltage variations v_{dc} involves that $Den_o(s)$ will not have any zeros in the right half plane. Equation (1.6) can be rewritten as:

$$v_{dc}(s) = \frac{Num_{in}(s)Den_o(s)v_s(s) - Num_o(s)Num_{in}(s)i_{load}(s)}{Num_{in}(s)Den_o(s)(1 + Z_o(s)Y_{in}(s))} \tag{1.7}$$

Where

$$Y_{in}(s) = \frac{1}{Z_{in}(s)}$$

Since both $Num_{in}(s)$ and $Den_o(s)$ do not have any zeros in the right half plane, it means the interconnected system is stable provided that $1 + Z_o(s)Y_{in}(s)$ does not have any zeros in the right half plane. A sufficient stability condition is that the Nyquist plot of $Z_o(s)Y_{in}(s)$ does not encircle the point (-1, 0).

1.6.2 Middlebrook Method:

For the control design of interconnected electrical systems, there are several methods to ensure that Nyquist plot of $Z_o(s)Y_{in}(s)$ does not encircle the point (-1, 0), thereby providing a guarantee of the stability of the electrical system. The first of the methods is Middlebrook criterion [Mid 76] for the study of small signal system stability, the concept of impedance criterion was established by Middlebrook in 1976 [Mid 76]. In order to study the stability of DPS, the

Middlebrook criterion is presented in Figure 1.15. It consists of a circle of radius $1/\mathrm{GM}$ where GM denotes the gain margin. If the Nyquist plot of $Z_o(s)Y_{in}(s)$ is always within the circle then encirclement of the point (-1,0) cannot occur. In order to satisfy Middlebrook criterion the gain margin must be greater than 1. This constraint has an advantage in terms of design criterion, for a given output impedance of the source subsystem $Z_o(s)$ the range of the allowable input admittance of the load subsystem is readily established. It gives:

$$|Y_{in}(s)| < \frac{1}{|Z_o(s)|\mathrm{GM}} \qquad (1.8)$$

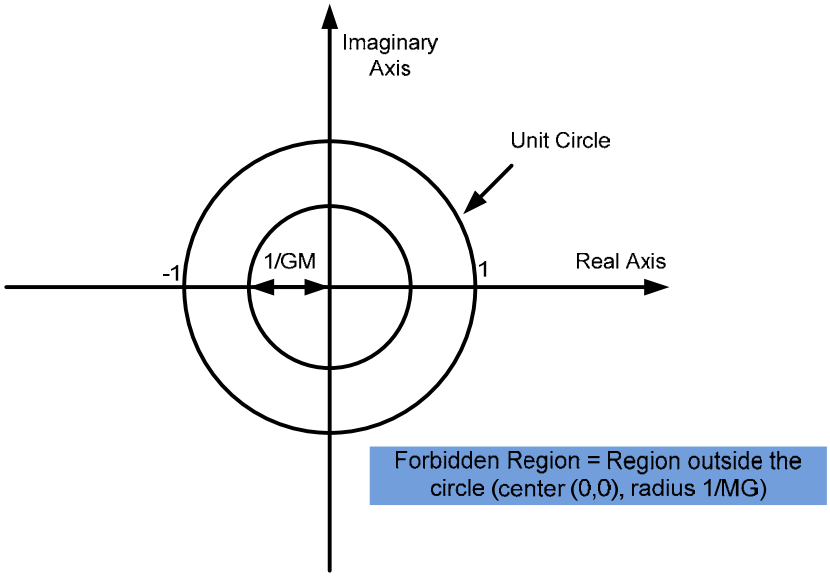

Figure 1.15: Middlebrook criterion for stability

Although convenient for design and readily visualized, the Middlebrook method tends to force artificially conservative designs due to the demand for infinite phase margin. For this reason several other stability approaches have been proposed. One alternate approach is Gain margin and Phase margin method.

1.6.3 Gain Margin and Phase Margin Method (GMPM):

To prevent the interaction between a converter and its input filter, Middlebrook proposed that the output impedance of the filter $Z_o(s)$ should be much smaller than the input impedance of the converter $Z_{in}(s)$ within all frequency ranges:

$$Z_o(s) \ll Z_{in}(s)$$

However, in many DC distributed power systems (DPS), it is impractical to have $Z_o(s) \ll Z_{in}(s)$ in all frequency ranges because this would make the design quite conservative and costly

[Wil 95], [Fen 02], [Wil 93]. A less conservative criterion of Gain margin and phase margin (GMPM) is proposed in [Wil 95], [Fen 02], [Fen 99], [Wil 93].

The asymptotic stability is ensured if the following conditions are satisfied:

$$|T_m(s)| < \frac{1}{\mathrm{GM_{min}}} \text{ or}$$

$$|T_m(s)| > \frac{1}{\mathrm{GM_{min}}} \qquad \text{with} \qquad \mathrm{PM} > \mathrm{PM_{min}}$$

Where

$$T_m(s) = |Z_o(s)Y_{in}(s)|$$

As a conservative design approach, a phase margin of 60 degrees can be applied for most practical applications. The relationship between the phase margin and the performance of the integrated system is discussed in detail in [Fen 02], [Wil 93]. This method allows us to define the load impedance specification, for a given impedance of the source subsystem, to ensure the desired stability margins.

1.6.3.1 Forbidden Region:

We use the polar plot of $T_m(s)$ to verify the stability of DPS. Assuming a desired phase margin of 60 degrees and a gain margin of 6 dB, the corresponding forbidden region is shown on the Figure 1.16. If the plot of $T_m(s)$ does not enter the forbidden region then it is not possible for the Nyquist plot of $Z_o(s)Y_{in}(s)$ to encircle the point (-1, 0), which means the system is stable. Every time the plot of $T_m(s)$ crosses the circle of radius $1/\mathrm{GM}$, the phase margin of $T_m(s)$ will always be at least 60 degrees. Furthermore, each time the plot of $T_m(s)$ crosses the negative real axis, the magnitude of $T_m(s)$ will be less than 0.5 ensuring at least 6 dB of gain margin.

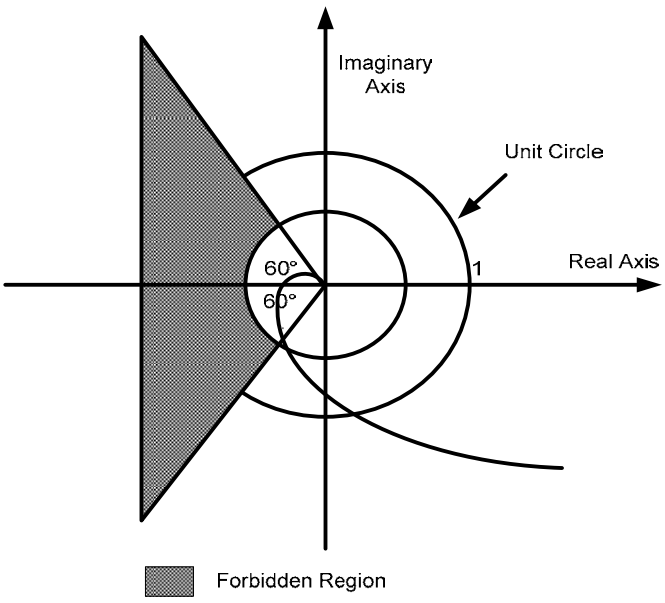

Figure 1.16: Forbidden region for GMPM Method

If we suppose that the output impedance of the source subsystem is known then the forbidden region defined previously can be transformed into two conditions on the input impedance $Z_{in}(s)$.

$$|Z_{in}(s)|_{dB} - |Z_o(s)|_{dB} > GM_{dB} \tag{1.9}$$

$$180^o - PM \quad < \angle Z_o(s) - \angle Z_{in}(s) < 180^o + PM \tag{1.10}$$

From (1.9), we can define the gain limit of the input impedance of the load subsystem for a given output impedance of the source subsystem.

$$|Z_{in}(s)|_{LimitdB} = |Z_o(s)|_{dB} + GM_{dB} \tag{1.11}$$

When $Z_{in}(s)$ falls below the gain limit for some frequency, the polar plot of $T(s)$ could enter the forbidden region. In this case, the phase of the input impedance of the load subsystem should be tested. Figure 1.17a presents the $|Z_o(s)|_{dB}$ and gain limit for 6 dB of gain margin.

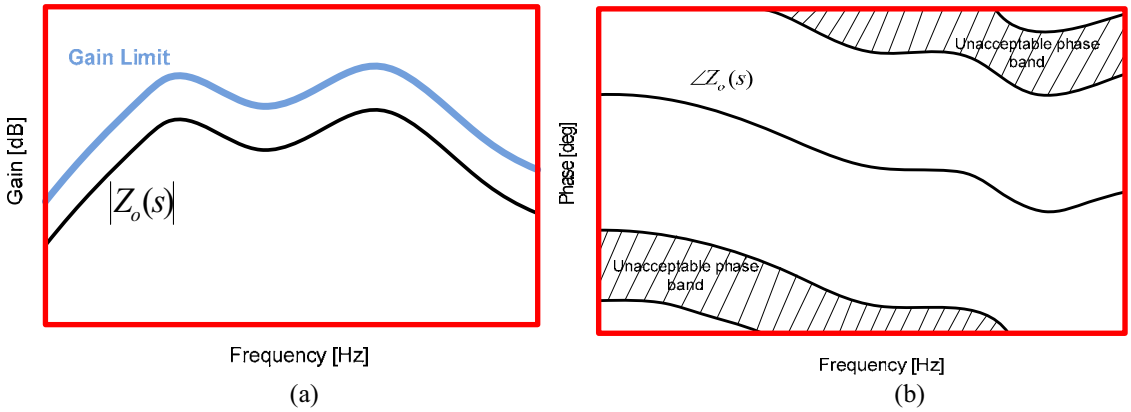

Figure 1.17: Load Impedance specification. (a) gain specification. (b) phase specification.

Unacceptable phase band:

The unacceptable phase band is the region where $\angle Z_{in}(s)$ should not enter to ensure the desired phase margin. For a given $\angle Z_o(s)$ and desired phase margin, the unacceptable phase band can be easily obtained using (1.10). Figure 1.17b shows the $\angle Z_o(s)$ and two unacceptable phase bands. In order to avoid the forbidden region, $\angle Z_{in}(s)$ should not enter the unacceptable phase band for all frequencies where $|Z_{in}(s)|$ is lower than the gain limit of the input impedance.

1.6.4 Study of Eigen Values:

In large scale DPS, the use of impedance criteria (Middelbrook or GMPM methods) is too conservative. In order to analyse stability of such a network, in the first step, the stability of each network components has to be done. The second step consists in analysing the stability of the whole network by considering the input impedance of each network components. Another method for local stability analysis of DPS consists in studying the system Eigen-Values

evaluated around an operating point. Two models can be used to analyse the asymptotic stability. In the first one, the loads are modelled by constant power load. Contrary to methods based the dynamical impedance, the load internal dynamic are not taken into account in the stability analysis. This approximation can leads to conservative results. For the second one, all the differential equations of loads are taken into account in the stability analysis. Nevertheless, it involves a perfect knowledge of all the loads which is practically very difficult to ensure. As example, the Electrical DPS based on the first approach can be represented by the following model for studying the stability of the dc-link variables (Fig. 1.18).

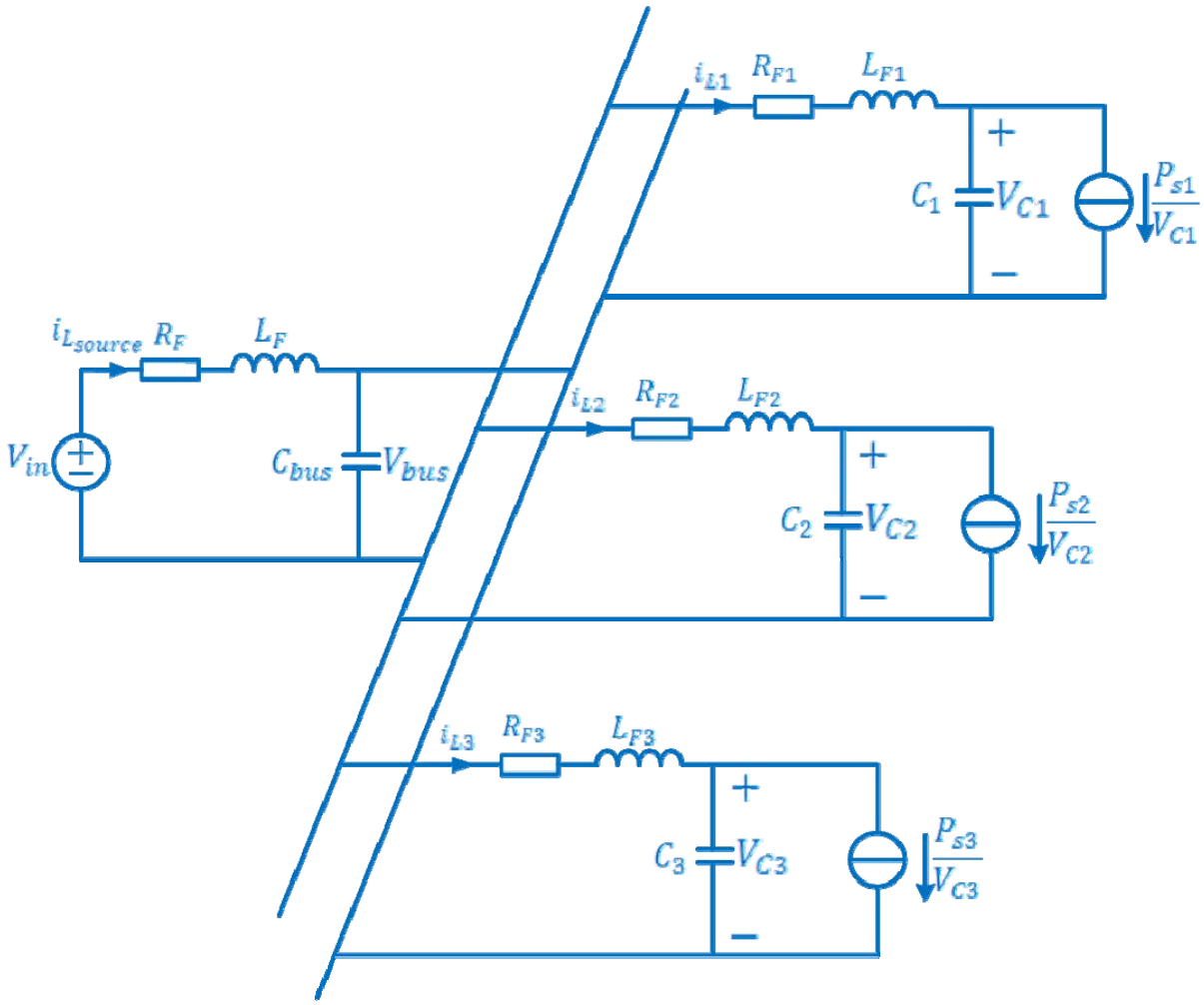

Figure 1.18: DPS with three CPLs

$$\frac{di_{L_{source}}}{dt} = -\frac{R_F}{L_F} i_{L_{source}} - \frac{V_{bus}}{L_F} + \frac{V_{in}}{L_F} \qquad \frac{di_{L1}}{dt} = -\frac{R_{F1}}{L_{F1}} i_{L1} - \frac{V_{C1}}{L_{F1}} + \frac{V_{bus}}{L_{F1}}$$

$$\frac{di_{L2}}{dt} = -\frac{R_{F2}}{L_{F2}} i_{L2} - \frac{V_{C2}}{L_{F2}} + \frac{V_{bus}}{L_{F2}} \qquad \frac{di_{L3}}{dt} = -\frac{R_{F3}}{L_{F3}} i_{L3} - \frac{V_{C3}}{L_{F3}} + \frac{V_{bus}}{L_{F3}}$$

$$\frac{dV_{C1}}{dt} = \frac{i_{L1}}{C_1} - \frac{i_{Load1}}{C_1} = \frac{i_{L1}}{C_1} - \frac{P_{s1}}{C_1 V_{C1}} \qquad \frac{dV_{C2}}{dt} = \frac{i_{L2}}{C_2} - \frac{i_{Load2}}{C_2} = \frac{i_{L2}}{C_2} - \frac{P_{s2}}{C_2 V_{C2}}$$

$$\frac{dV_{C3}}{dt} = \frac{i_{L3}}{C_3} - \frac{i_{Load3}}{C_3} = \frac{i_{L3}}{C_3} - \frac{P_{s3}}{C_3 V_{C3}} \qquad \frac{dV_{bus}}{dt} = \frac{i_{L_{source}}}{C_1} - \frac{(i_{L1} + i_{L2} + i_{L3})}{C_1}$$

The above model is a nonlinear model and for the small signal analysis, the system must be linearized around an operating point. The linearization of this model around an operating point leads to the following linear model of the DPS.

$$\frac{d\tilde{\imath}_{L_{source}}}{dt} = -\frac{R_F}{L_F}\tilde{\imath}_{L_{source}} - \frac{\tilde{v}_{bus}}{L_F} \qquad \frac{d\tilde{\imath}_{L1}}{dt} = -\frac{R_{F1}}{L_{F1}}\tilde{\imath}_{L1} - \frac{\tilde{v}_{C1}}{L_{F1}} + \frac{\tilde{v}_{bus}}{L_{F1}}$$

$$\frac{d\tilde{\imath}_{L2}}{dt} = -\frac{R_{F2}}{L_{F2}}\tilde{\imath}_{L2} - \frac{\tilde{v}_{C2}}{L_{F2}} + \frac{\tilde{v}_{bus}}{L_{F2}} \qquad \frac{d\tilde{\imath}_{L3}}{dt} = -\frac{R_{F3}}{L_{F3}}\tilde{\imath}_{L3} - \frac{\tilde{v}_{C3}}{L_{F3}} + \frac{\tilde{v}_{bus}}{L_{F3}}$$

$$\frac{d\tilde{v}_{C1}}{dt} = \frac{\tilde{\imath}_{L1}}{C_1} - \frac{\tilde{\imath}_{Load1}}{C_1} = \frac{\tilde{\imath}_{L1}}{C_1} + \frac{P_{s10}}{C_1 {V_{C10}}^2}\,\tilde{v}_{C1}$$

$$\frac{d\tilde{v}_{C2}}{dt} = \frac{\tilde{\imath}_{L2}}{C_2} - \frac{\tilde{\imath}_{Load2}}{C_2} = \frac{\tilde{\imath}_{L2}}{C_2} + \frac{P_{s20}}{C_2 {V_{C20}}^2}\,\tilde{v}_{C2}$$

$$\frac{d\tilde{v}_{C3}}{dt} = \frac{\tilde{\imath}_{L3}}{C_3} - \frac{\tilde{\imath}_{Load3}}{C_3} = \frac{\tilde{\imath}_{L3}}{C_3} + \frac{P_{s30}}{C_3 {V_{C30}}^2}\,\tilde{v}_{C3}$$

$$\frac{d\tilde{v}_{bus}}{dt} = \frac{\tilde{\imath}_{L_{source}}}{C_1} - \frac{\tilde{\imath}_o}{C_1} = \frac{\tilde{\imath}_{L_{source}}}{C_1} - \frac{(\tilde{\imath}_{L1} + \tilde{\imath}_{L2} + \tilde{\imath}_{L3})}{C_1}$$

In matrix form the above model leads to:

$$\dot{X} = AX + U$$

$$\frac{d}{dt}\begin{bmatrix}\tilde{\imath}_{L_{source}}\\ \tilde{\imath}_{L1}\\ \tilde{\imath}_{L2}\\ \tilde{\imath}_{L3}\\ \tilde{v}_{C1}\\ \tilde{v}_{C2}\\ \tilde{v}_{C3}\\ \tilde{v}_{Cbus}\end{bmatrix} = \begin{bmatrix} -\frac{R_F}{L_F} & 0 & 0 & 0 & 0 & 0 & 0 & -\frac{1}{L_F} \\ 0 & -\frac{R_{F1}}{L_{F1}} & 0 & 0 & -\frac{1}{L_{F1}} & 0 & 0 & \frac{1}{L_{F1}} \\ 0 & 0 & -\frac{R_{F2}}{L_{F2}} & 0 & 0 & -\frac{1}{L_{F2}} & 0 & \frac{1}{L_{F2}} \\ 0 & 0 & 0 & -\frac{R_{F3}}{L_{F3}} & 0 & 0 & -\frac{1}{L_{F3}} & \frac{1}{L_{F3}} \\ 0 & \frac{1}{C_1} & 0 & 0 & \frac{P_{s10}}{C_1 V_{C10}} & 0 & 0 & 0 \\ 0 & 0 & \frac{1}{C_2} & 0 & 0 & \frac{P_{s20}}{C_2 V_{C20}} & 0 & 0 \\ 0 & 0 & 0 & \frac{1}{C_3} & 0 & 0 & \frac{P_{s30}}{C_3 V_{C30}} & 0 \\ \frac{1}{C} & -\frac{1}{C} & -\frac{1}{C} & -\frac{1}{C} & 0 & 0 & 0 & 0 \end{bmatrix} \cdot \begin{bmatrix}\tilde{\imath}_{L_{source}}\\ \tilde{\imath}_{L1}\\ \tilde{\imath}_{L2}\\ \tilde{\imath}_{L3}\\ \tilde{v}_{C1}\\ \tilde{v}_{C2}\\ \tilde{v}_{C3}\\ \tilde{v}_{Cbus}\end{bmatrix} \quad (1.12)$$

The eigenvalues λ of the state matrix A of a system are defined as the solution of the following equations:

$$A \cdot \varphi = \lambda \cdot \varphi \qquad \Rightarrow \qquad (A - \lambda \cdot I) = 0$$

Or

$$A \cdot \boldsymbol{\psi}^T = \lambda \cdot \boldsymbol{\psi}^T \qquad \Rightarrow \qquad (A - \lambda \cdot I) = 0$$

Where φ and $\boldsymbol{\psi}$ are respectively the right and left eigenvectors of A and not equal to 0. So the non trivial solution is for $\det(A - \lambda \cdot I) = 0$. In order to stabilize the linearized DPS the eigenvalues of the matrix A must strictly be in the left half complex plane $i.e. Real\ (\lambda(A)) < 0$. When this condition is true then the electrical system is asymptotically locally stable.

Note on the parameters sensitivity: For the dynamical impedance methods, the parameters sensitivity is taken into account for the desired phase or gain margins. When the stability of DPS is realised by an eigenvalue analysis, the modal approach or the use of sensitivity equations can be used to study the effect of parameters variations on the stability.

Modal Analysis approach:

The sensitivity of the eigenvalue λ_i of a system to the element a_{kl} of the state matrix A is defined as:

$$\frac{\partial \lambda_i}{\partial a_{kl}} = \varphi_{ki} \cdot \boldsymbol{\psi}_{li} \quad (1.13)$$

It is possible to determine which elements of matrix A have most influence on each eigenvalue.

The comparison of modal analysis approach with the Middlebrook criterion is presented in [Bar 05] for buck converter. The stability is observed with the Middlebrook criterion by looking at the Nyquist diagram and transfer function locus around critical point (-1,0). It is concluded in [Bar 05] that the modal approach has a clear advantage as compared to Middlebrook criterion in terms of design conception. The modal approach identifies the dominant eigenvalues which are close to marginal stability and the sensitive parameters linked to these eigenvalues. On the other hand, the Nyquist diagram provides the only information on stability margin.

Sensitivity equations approach:

Suppose that $f(x,\beta)$ is continuous in (x,β) and has continuous first partial derivatives with respect to x and β. Let β_0 be the nominal value of β. The sensitivity equation is given as under [Khalil]:

$$\dot{S}(t) = A(t,\beta_0)S(t) + B(t,\beta_0), \qquad S(t_0) = 0 \tag{1.14}$$

Where the function $S(t)$ is called the sensitivity function and is defined by $S(t) = \frac{\partial x}{\partial \beta}$. Sensitivity functions provide first order estimates of the effect of the parameters variations on solutions. They can be used to approximate the solutions when β is sufficiently close to its nominal value β_0. The procedure for calculating the sensitivity function $S(t)$ consists of two steps. In the first step, we solve the nominal state equations and in the second step we evaluate the two Jacobian matrices

$$A(t,\beta_0) = \left.\frac{\partial f(x,\beta_0)}{\partial x}\right|_{x=x(\beta_0),\beta=\beta_0}, \qquad B(t,\beta_0) = \left.\frac{\partial f(x,\beta_0)}{\partial \beta}\right|$$

The parameters sensitivity study using sensitivity equations approach involves very complicated mathematical solution. Except for some trivial cases, we are forced to solve these equations numerically.

1.6.5 Passive Damping Techniques to stabilize the electrical systems with input filter:

Instabilities in power converters with input filters were discussed in [Tsu 01] for railway vehicle applications. Three different damping methods were analyzed for input filters, but the need for further study on damping networks was emphasized. A different technique for input-filter damping design was suggested in [Cal 02] based on the zero dynamics analysis. However, the results yielded by this method were equivalent to those obtained using the classical approach [Mid 78] based on minimizing the filter output impedance.

In [Kar 03], [Usm 06], [Usm 07], a different and more practical approach was presented to design input-filter damping solely based on the open-loop control-to-output transfer function. It was highlighted that a second order input filter causes two Right Hand Plane(RHP) zeros in the open-loop transfer function of the converter, and these zeros are

the source of instability in the closed-loop. A design criterion was proposed to shift these zeros to the Left Hand Plane (LHP) by adding R-C parallel damping to the filter circuit. In [Usm 06], [Usm 07], it was found that not only there exist a minimum value of damping resistance required for stability but there also exists an upper limit on this resistance value. These lower and upper limits on damping resistance were determined accurately in these papers. Thus they permit to define a stable operating region in the damping-circuit parameters space. The required stability conditions, for which all zeros of the transfer-function remain on the LHP, were intuitively obtained by application of Routh- Hurwitz criterion to the numerator polynomial of the transfer function. In this section we focus on passive damping solution.

1.6.5.1 *Various Passive Damping Configurations:*

An easy method to mitigate the instability problem is to simply introduce an adequate resistance into the input filter to counteract the negative input resistance of the dc-dc converter. As a result, the detrimental effect of input filter on converter transfer functions becomes negligible. However, it is not practical to add a damping resistance arbitrarily to the filter circuit, because a damping resistor in series with L_F would decrease converter efficiency since it must pass all of the input current. While a damping resistor in series with C_F would seriously degrade its attenuation characteristic as well as the efficiency since it must essentially pass entire ac input current component.

One possible approach of damping the filter is to add a damping resistance R_d in parallel with capacitor C_F, as shown in Figure 1.19(a). Unfortunately, this configuration also suffers from power dissipation problem in R_d.

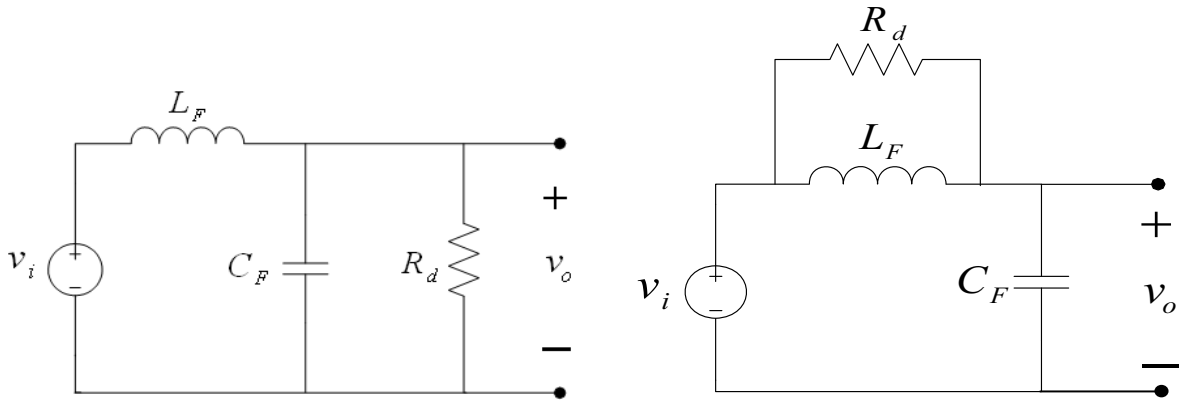

Figure 1.19: (a): Addition of damping resistance aross C_F; (b): Addition of damping resistance in parallel with L_F.

One solution to solve power dissipation problem is to place R_d in parallel with L_F as illustrated in Figure 1.19(b). Since the DC voltage across inductor L_F is ideally zero, there is now low DC power loss in resistor R_d. Nevertheless, the main problem with this circuit is that its transfer function contains a high-frequency zero. Addition of R_d degrades the slope of the high-frequency asymptote from -40dB/decade to -20dB/decade [Eri 01]. Hence this circuit effectively behaves as a single-pole R-C low-pass filter with no attenuation provided by inductor L_F.

One practical solution for damping the input filter is illustrated in Figure 1.20. A DC blocking capacitor is added in series with resistance R_d. Since no DC current can flow through R_d, its DC power loss is reduced [Eri 99]. The value of the blocking capacitor C_d can be expressed as $C_d = kC_F$ and is chosen to be very large as compared to C_F so that at filter resonant frequency f_F, the impedance of R_d-C_d branch is dominated by resistor R_d.

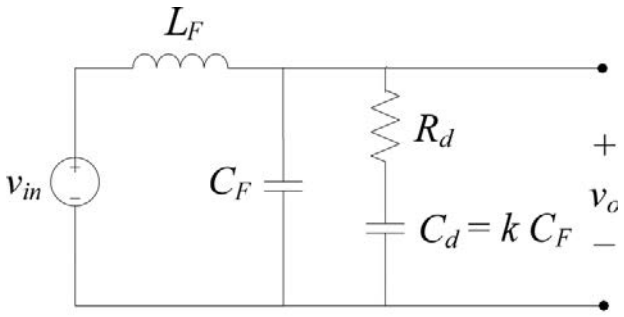

Figure 1.20: Practical method of damping, including resistance R_d and DC blocking capacitor C_d .

The R_d-C_d parallel damping approach, as shown in Figure 1.20 finds significant application in DC- DC converters. Since a resistor is to be placed in series with C_d, this capacitor can be realized using capacitor types having substantial equivalent series resistance (ESR), such as electrolytic and tantalum types. However this method is not desirable in AC power converters as large capacitor C_d can cause excessive dissipation at line frequency because of the AC current flowing through the damping branch. In such applications, the parallel and series R_d-L_d approaches presented in Figure 1.21 can lead to smaller designs. This method eliminates the excessive dissipation in resistor and is, therefore, widely used in AC power converter filters. The design and optimization of these damping networks is discussed in [Phe 79] and [Eri 99].

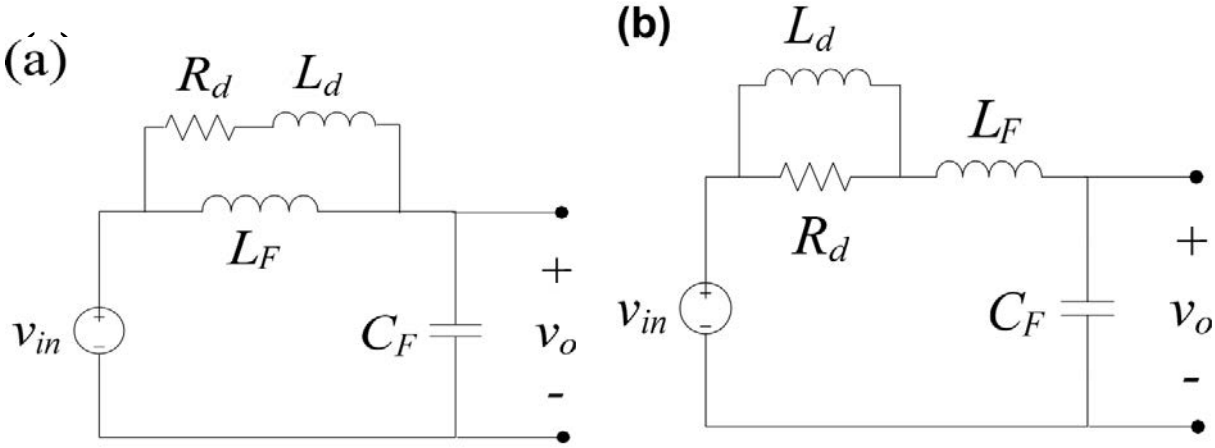

Figure 1.21: Practical methods of damping in AC power converters; (a): $R_d - L_d$ parallel damping; (b): $R_d - L_d$ series damping.

Effect of R_d–C_d Parallel Damping on Filter Characteristics:

Being the most practical damping approach for DC-DC converter applications [Mid 78], we detail only the R_d-C_d parallel damping in this section. The input-to-output transfer function and the output impedance of an L-C filter with R_d-C_d shunt damping (as shown in Figure 1.20) can be expressed as below:

Input-to-output transfer function:

$$G_F(s) = \frac{v_o(s)}{v_{in}(s)} = \frac{s(R_dC_d) + 1}{s^3(L_FC_FC_dR_d) + s^2[L_F(C_F + C_d)] + s(R_dC_d) + 1} \tag{1.11}$$

Output impedance:

$$Z_{out}(s) = \frac{sL_F[s(R_dC_d) + 1]}{s^3(L_FC_FC_dR_d) + s^2[L_F(C_F + C_d)] + s(R_dC_d) + 1} \tag{1.12}$$

Plot of the filter transfer function and output impedance are shown in Figure 1.22, for various values of damping resistance R_d while keeping other parameters constant. Below the resonant frequency of the filter ($f_F = 1/2\pi\sqrt{L_FC_F}$), the input voltage passes through the filter without significant attenuation. Above this resonant frequency, voltages are attenuated and the attenuation increases at a slop of 40dB/decade. At the resonant frequency, there is a peak in gain where the output voltage of the filter is actually higher than the input voltage (Figure 1.22a). The amount of this peak is determined by the series and parallel losses of the system. The effect of these losses is normally consolidated into a damping factor. With a damping factor of 1, there is no peak whereas the highest peak occurs for zero damping.

The output impedance of the filter is low at low frequency because the inductor impedance is low and the power bus is essentially a short circuit. At high frequencies, the output impedance of the filter is again low because of the low impedance of the capacitor at high frequency. However, at resonance, the impedance of the filter can be significantly high, especially if there is little damping.

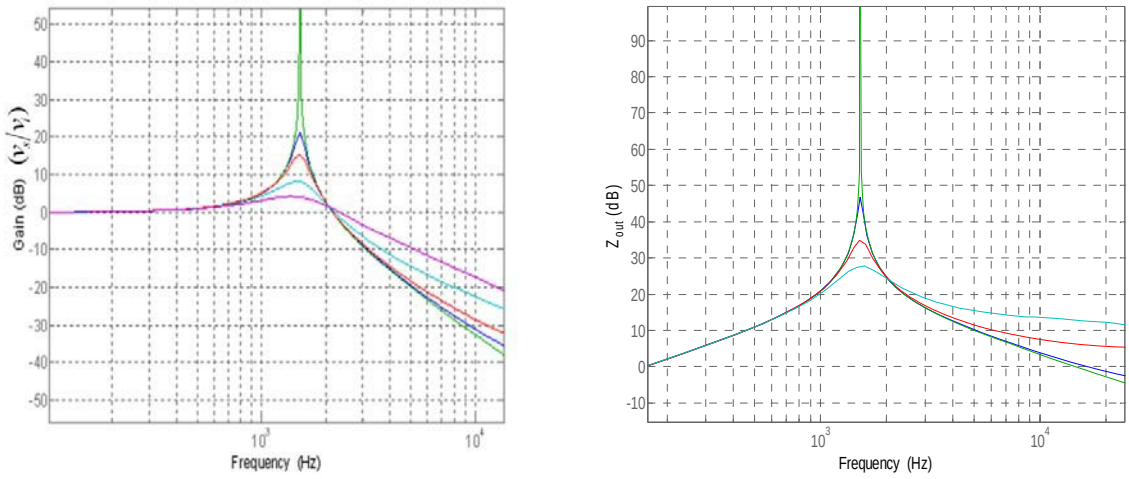

Figure 1.22: (a): Plot of filter transfer function. (b) Output impedance plot of input filter.

1.7 CONCLUSION:

In this chapter, the stability issues of electrical systems with input filter and constant power load connected to a common DC bus are addressed. This chapter discusses that an inverter-motor-drive system connected to the grid through a LC filter and rectifier, when tightly regulated, behaves as constant power load. An increase/decrease of input voltage results in a decrease/increase of input current, causing the inverter motor-drive-system to look like negative impedance at the input terminal. This negative impedance behavior may lead to the instability of the system. Similarly the problem of instability arises in Distributed Power System (DPS) where multiple sources and loads are connected to a common bus. We have discussed different stability criteria and various existing damping techniques and stability analysis methods were analyzed. Impedance based stability criterion is the most practical one. So for this criterion we only need to study the output impedance of the source subsystems and input impedance of the load subsystems to study the stability of the DPS.

CHAPTER 2

LINEAR STABILZATION OF DC-BUS SUPPLYING A CONSTANT POWER LOAD

Chapter 2

2.1 INTRODUCTION:

Today, almost all converters have input LC filter. Input filters serve two primary purposes. From a system designer's standpoint, the input LC filter prevents electromagnetic interface or noise which is generated in all switching power sources from reaching the power bus and affecting other equipments. In this case, the purpose of the filter is to attenuate the AC portion of the power supply input current so that only a small portion of it reaches the power bus. The filter functions as a reverse current filter.

From a user's standpoint, the input LC filter prevents high frequency AC voltage on the power bus from passing through to the output of the power supply and on to the using equipment. In this case, the purpose of the input LC filter is to attenuate the AC voltage superimposed on the DC power bus so that only a small portion of it reaches the power supply input terminals. The LC filter functions as a forward voltage filter, attenuating input noise.

Power electronic devices such as converters and motor devices, when tightly regulated, behave as constant power loads and have a negative input resistance within the bandwidth of system control loops. These devices when connected with the supply via an input LC filter may case stability problem. This phenomenon is becoming more and more important as electric motor drives are increasingly used instead of traditional hydraulic and pneumatic devices, particularly in aerospace applications. The main benefits of using electric motors to replace conventional hydraulic and pneumatic devices are health-monitoring, maintenance flexibility and increased control precision.

When a DC load is connected to power bus through an LC filter, the risk of instability of the dc-link voltage increases when reducing the dc-link capacitance of the filter [Har 05], [Mos 03], [Rou 07], [Wan 07]. Indeed the problem of interaction between two electrical systems in cascade is well known and a lot of work has already been published to explain this phenomenon but essentially in the case of DC/DC converter in cascade with their input filter [Mid 76], [Mid 78], [Ema 99], [Jan 92], [Eri 92], [Al-f 99]. For the stand-alone DC/DC converter, and in distributed systems, design requirements that guarantee stability have been previously advanced and extensively used in the design and specification of these systems. However design-oriented stability criteria have not been developed for distributed AC systems with constant power loads. Concerning the interaction between the power supply stage and inverter-motor drive system, some work has already been published for DC/AC applications [Sud 98], [Mos 07], [Che 06], [Liu 07]. In [Sud 98], a nonlinear compensation structure is proposed to ensure the dc-link stabilization. In [Mos 03] and [Mos 07], the authors take into account the torque dynamic thanks to a simplified dynamic model and propose a modification of the torque control loop to stabilize the dc-link voltage. Even if this solution allows stabilizing the dc-link voltage, it decreases the

dynamic performance of the torque loop especially as regard to disturbance rejection. In [Liu 07]. another approach for drives based on Brushless DC motors (BLDC) is proposed. The authors give a simplified expression for the system input impedance and propose a frequency high-pass stabilization block without discussing about the robustness with respect to the measurement noise.

In this chapter, an analytical method is presented which allows investigating local stability of an inverter-motor-drive system supplied by an imperfect DC power supply. The method can be applied when Permanent Magnet Synchronous Motors (PMSM) or Induction Motors (IM) are used. Only linear controllers are supposed to be used for the inverter-motor-drive system. Then, an oscillation compensation technique is used to improve the stability margin of the system and reduce the size of the dc-link capacitance without modifying the structure of the torque or current loops. The dc-link voltage improvement depends on the design requirements, maximum voltage deviation and its response time for a given load power disturbance and the impact of the voltage stabilization on the drive dynamic. When designing the oscillation compensation block, a good designer knows that more stable dc-link voltage leads generally to worse drive torque dynamic. To find a good trade-off, the designer needs simple tools, usually linear ones like as Bode and Nyquist plots, and a sufficiently representative model of the whole system. Then, he/she can achieve the design requirements by adjusting the oscillation compensation block parameters. In this chapter, a complete design example is given from modelling to design and experimental implementation of a linear stabilization block applied to an inverter-motor-drive system supplied by an imperfect DC power supply.

2.2 STABILITY STUDY OF INVERTER MOTOR DRIVE SYSTEM WITH INPUT FILTER:

2.2.1 Studied Inverter Motor Drive System:

The studied system is shown in figure 1. The system is constituted of an imperfect DC voltage source providing energy to an inverter-motor-drive system. The DC source has three stages: AC power source, rectifier and LC filter. Its output DC voltage, called dc-link voltage (v_s), is used to supply a PWM controlled Voltage Source Inverter (VSI). This inverter transfers electrical power to the motor. We suppose that this latter is a PMSM without loss of the generality.

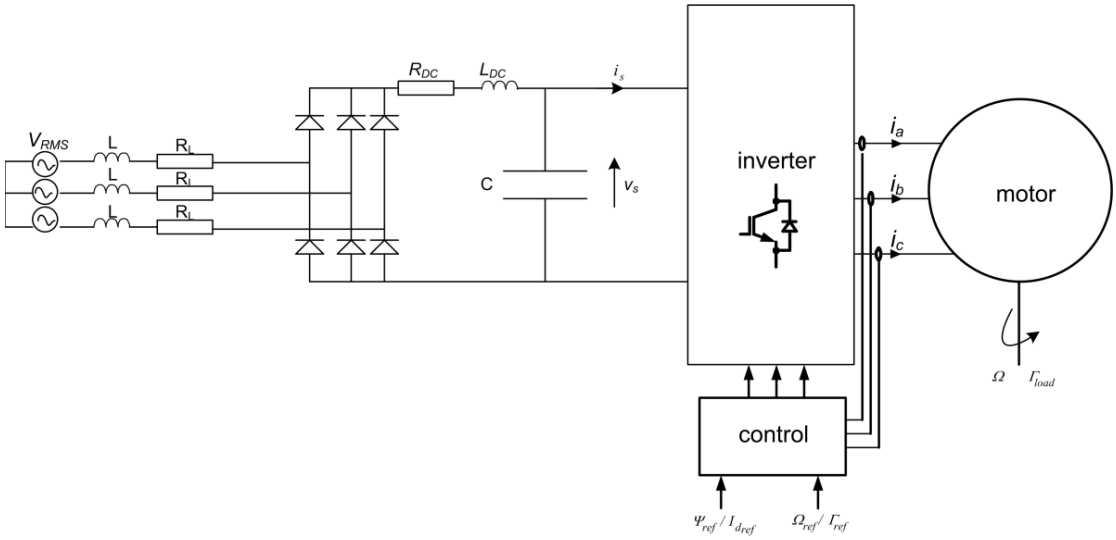

Fig. 1- Typical electrical architecture of actuators

For such an application, the inverter-motor-drive system owns four inputs: input dc-link voltage noted v_s, the load torque of the motor noted Γ_{load}, the flux reference or the d-current reference noted respectively Ψ_{ref} and I_{dref}, and the mechanical speed reference or the motor torque reference noted respectively Ω_{ref} and Γ_{ref}. The system outputs are the mechanical angular speed (Ω) and the stator dq-currents noted i_d and i_q. These outputs are controlled by proper controllers and the whole system is stable if all reference values are achieved and the dc-link voltage and current (v_s and i_s) are not oscillating.

2.2.2 DC Power Supply Model of AC Voltage Source and Rectifier:

To simplify the model, the ac voltage source – rectifier are replaced by an equivalent DC source. As explained in [Har 05] and [Rou 07], a six-pulse rectifier can be modeled with reasonably good accuracy as a DC grid as shown in Fig. 2.

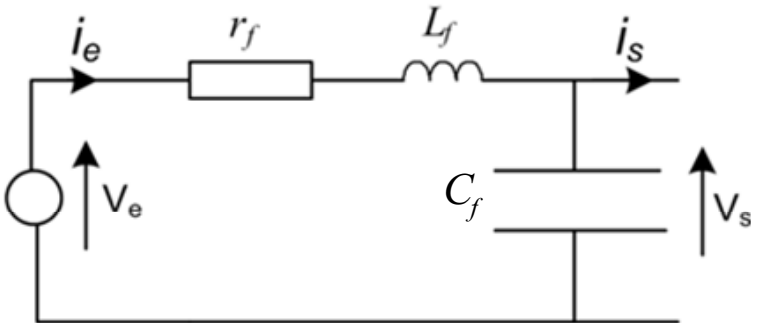

Fig. 2- DC model of the voltage source.

The DC voltage V_e, the equivalent serial inductance L_f and the resistance r_f are defined by the following relations:

$$V_e = \frac{3\sqrt{2}}{\pi} V_{RMS} \tag{2.1}$$

$$L_f = 2L + L_{DC} \tag{2.2}$$

$$r_f = 2R_L + R_{DC} + \frac{3}{\pi} L\omega \tag{2.3}$$

Where V_{RMS} represents the *rms* value of the line voltage; L and R_L are respectively the line inductance and serial resistance of the three phase power supply; L_{DC} and R_{DC} represent respectively the dc-link equivalent inductance and resistance and the term $3L\omega/\pi$ is due to the commutation voltage drop. This model allows defining easily the output impedance of the voltage source. For small signal variations, it comes:

$$Z_o(s) = -\left(\frac{\tilde{v}_s}{\tilde{\imath}_s}\right)_{\tilde{v}_e=0} = \frac{L_f s + r_f}{L_f C_f s^2 + r_f C_f s + 1} \tag{2.4}$$

Where $\tilde{x}$ denotes the variation of the variable x around its steady state value X.

2.2.3 DC-Link Voltage Stabilization:

The stability analysis of cascaded system has been widely studied in the literature especially for DC/DC converters [Wil 95], [Fen 02], [Fen 99], [Sud 00], [Sud 00a].In [Liu 04], [Liu 08], [Liu 08a], [Mar 08], [Luc 06], [Kun 07], [Liu 08b], [Abu 04], [Las 04], [Wai 05], when the load is an actuator, the stability of the system is studied when the motor variables are tightly controlled; *i.e.* robust controllers with high dynamic properties are used to drive the motor. Using this kind of controllers, the current and then the torque remain almost unchanged even if the dc-link voltage varies. Therefore, while the machine is controllable, the speed and so the absorbed power by the drive are not significantly affected by the dc-link voltage variations. In this case, the power delivered by the inverter to the motor can be considered as constant. When the load is supposed to be a constant power load, the following asymptotic local stability condition is often proposed [Mos 07], [Dél 95], [Bae 01]:

$$p_s < p_{smax} = \frac{r_f C_f}{L_f} V_e^2 \tag{2.5}$$

Where p_s denotes the load power.

According to this condition, the dc-link capacitance C_f should be increased for improving the stability condition. Meanwhile, in some cases like as aerospace applications, the objective is to reduce the size of the dc-link capacitance. In these cases, a dc-bus stabilization technique is required to keep the dc-link voltage stable while reducing the dc-link capacitance and maintaining the actuator control performances.

It is proved that local stability around an operating point of two converters in cascade depends on poles of the transfer function $1/(1 + Z_o(s)/Z_{in}(s))$ where $Z_o(s)$ is the output impedance of the first converter and $Z_{in}(s)$ is the input impedance of the load converter [Liu 08a]. It can be easily shown that for inverter-motor-drive systems with imperfect voltage source, the same result can

be obtained thanks to the use of small signal modeling around the studied operating point. The variations of the system output variables are bounded to the variations of the inputs according to the following relationship:

$$\begin{bmatrix} \tilde{v}_s(s) \\ \tilde{\imath}_e(s) \end{bmatrix} = \begin{bmatrix} T_v(s) & Z_o(s) \\ 1/Z_{in}(s) & -T_c(s) \end{bmatrix} \begin{bmatrix} \tilde{v}_e(s) \\ -\tilde{\imath}_s(s) \end{bmatrix} \tag{2.6}$$

where

$T_v(s)$ represents stable transfer function illustrating the voltage transfer function of the LC filter when $\tilde{\imath}_s = 0$.

$T_c(s)$ represents the stable transfer function illustrating the current transfer function.

$Z_{in}(s)$ represents the input impedance.

$Z_o(s)$ represents the output impedance.

Indeed, small signal variations of the dc-link voltage can be described by the following relation:

$$\tilde{v}_s(s) = \frac{T_v(s)}{1 + \dfrac{Z_o(s)}{Z_{in}(s)}} \tilde{v}_e(s) \tag{2.7}$$

where $Z_{in}(s)$ is the inverter-motor-drive input impedance and can be calculated as follows:

$$Z_{in}(s) = \left(\frac{\tilde{v}_s}{\tilde{\imath}_s}\right)_{\substack{\tilde{\Omega}=0 \text{ or } \tilde{\Gamma}_{ref}=0 \\ \tilde{\Psi}_{dref}=0 \text{ or } \tilde{\imath}_{dref}=0}} \tag{2.8}$$

At the following, we will study local stability of the system by examining the Nyquist plot of $Z_o(s)/Z_{in}(s)$ [Liu 10]. For the studied system, $Z_o(s)$ is given in (2.4) and $Z_{in}(s)$ should be determined by taking into account the dynamic of all control loops. The expression for $Z_{in}(s)$ is developed in the next paragraph for a PMSM.

2.2.3.1 Calculation of Input Impedance:

From (2.7), it is obvious that the local stability of the system depends on the ratio $Z_o(s)/Z_{in}(s)$ in which $Z_{in}(s)$ should be determined using (2.8). To calculate this impedance, either we can adapt a linear model of measurements [Mos 03a] or we develop a closed expression for Z_{in} by using the physical model of the system [Liu 10]. Here, the second approach is employed. It consists in developing the average model of the whole drive control whose scheme is shown in Fig. 2.3. In this figure, the stator *dq*-current controllers are called $C_d(s)$ and $C_q(s)$. The control commands from these controllers may pass through a decoupling block $A(s)$ presented later. The transfer functions $C_\Phi(s)$ and $C_v(s)$ represent the flux and the speed controllers if they exist. An additional block modeled by the transfer function $h_v(s)$ has been introduced to compensate the

input voltage oscillation. To simplify the study, the saturation effects and the sampling effects are not taken into account. Moreover, the inverter losses are neglected. Thus, a power balance equation and a first-order development around the dc-link operating point (V_s, I_s) and the motor operating point (V_d, I_d, V_q, I_q) lead to the following:

$$\tilde{v}_s(s) \cdot I_s + V_s \cdot \tilde{\imath}_s(s) = \tilde{v}_d(s) \cdot I_d + V_d \cdot \tilde{\imath}_d(s) + \tilde{v}_q(s) \cdot I_q + V_q \cdot \tilde{\imath}_q(s) \tag{2.9}$$

As usual, the VSI is modeled at low frequencies by a simple gain proportional to the dc-link voltage:

$$G_{VSI} = \alpha \cdot v_s \tag{2.10}$$

where $\alpha = 1/2p_m$ (Fig. 2.3) is constant. The control voltages v_d^* and v_q^* are often normalized by multiplying them with V_s/v_{sf} where v_{sf} is the low pass filtered value of v_s:

$$v_{sf} = F_s(s) \cdot v_s \tag{2.11}$$

where $F_s(s)$ is the transfer function of the low-pass filter. So, we have

$$\begin{bmatrix} v_d(s) \\ v_q(s) \end{bmatrix} = \alpha \cdot V_s \cdot \frac{v_s}{v_{sf}} \cdot \begin{bmatrix} v_d^*(s) \\ v_q^*(s) \end{bmatrix} \tag{2.12}$$

Then, neglecting higher order small variation terms, it yields from (2.12)

$$\begin{bmatrix} \tilde{v}_d(s) \\ \tilde{v}_q(s) \end{bmatrix} = \alpha \cdot \tilde{v}_s(s) \cdot \begin{bmatrix} V_d^* \\ V_q^* \end{bmatrix} - \alpha \cdot \tilde{v}_{sf}(s) \cdot \begin{bmatrix} V_d^* \\ V_q^* \end{bmatrix} + \alpha \cdot V_s \cdot \begin{bmatrix} \tilde{v}_d^*(s) \\ \tilde{v}_q^*(s) \end{bmatrix} \tag{2.13}$$

Now, thanks to the small signal model of the motor, it is possible to express the variations of *dq*-voltages as a function of the variations of the *dq*-currents:

$$\begin{bmatrix} \tilde{v}_d(s) \\ \tilde{v}_q(s) \end{bmatrix} = Z(s) \cdot \begin{bmatrix} \tilde{\imath}_d(s) \\ \tilde{\imath}_q(s) \end{bmatrix} \tag{2.14}$$

where $Z(s)$ is the impedance matrix of the motor defined as:

$$Z(s) = \begin{bmatrix} z_{11}(s) & z_{12}(s) \\ z_{21}(s) & z_{22}(s) \end{bmatrix} \tag{2.15}$$

Relations (2.9), (2.14) and (2.15) lead to:

$$\tilde{v}_s(s) \cdot I_s + V_s \cdot \tilde{\imath}_s(s) = V_1(s) \cdot \tilde{\imath}_d(s) + V_2(s) \cdot \tilde{\imath}_q(s) \tag{2.16}$$

with:

$$\begin{cases} V_1(s) = V_d + I_d \cdot z_{11}(s) + I_q \cdot z_{21}(s) \\ V_2(s) = V_q + I_d \cdot z_{12}(s) + I_q \cdot z_{22}(s) \end{cases} \tag{2.17}$$

The variations of the *dq*-currents as a function of the input voltage and the control voltage variations are given by equations (2.13) and (2.14):

$$\begin{bmatrix} \tilde{\imath}_d(s) \\ \tilde{\imath}_q(s) \end{bmatrix} = Y(s) \cdot \left(\alpha \cdot \tilde{v}_s(s) \cdot \begin{bmatrix} V_d^* \\ V_q^* \end{bmatrix} - \alpha \cdot \tilde{v}_{sf}(s) \cdot \begin{bmatrix} V_d^* \\ V_q^* \end{bmatrix} + \alpha \cdot V_s \cdot \begin{bmatrix} \tilde{v}_d^*(s) \\ \tilde{v}_q^*(s) \end{bmatrix} \right) \tag{2.18}$$

with

$$Y(s) = Z^{-1}(s) \tag{2.19}$$

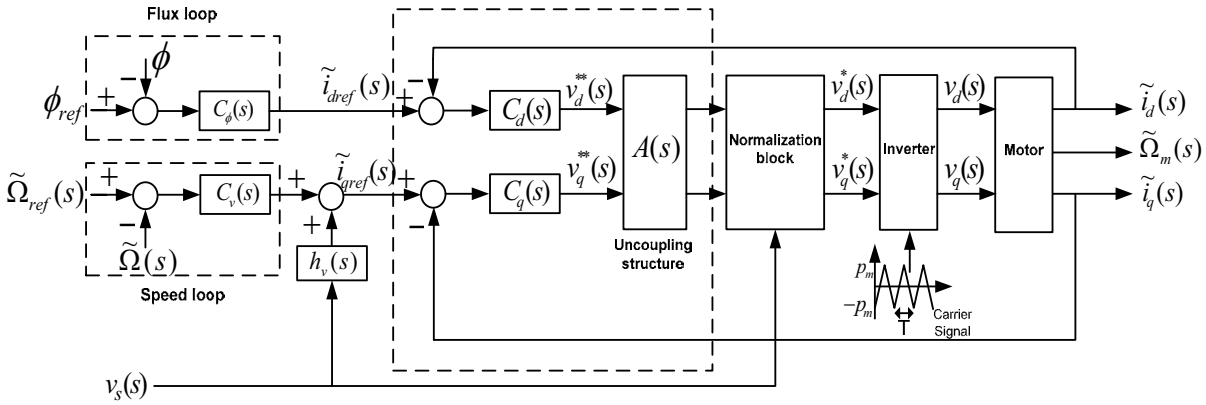

Fig. 2.3- Typical field oriented controlled inverter-motor-drive system with oscillation compensation block.

The decoupling block which is used in the current control loops is shown in Fig. 2.3. This block permits to decouple the control of the stator *dq*-currents. It is frequently employed in the control of ac drives for improving the control performances [Nah 01]. Here, the decoupling block is modeled by a matrix $A(s)$ defined as follows:

$$\begin{bmatrix} \tilde{v}_d^*(s) \\ \tilde{v}_q^*(s) \end{bmatrix} = A(s) \cdot \begin{bmatrix} \tilde{v}_d^{**}(s) \\ \tilde{v}_q^{**}(s) \end{bmatrix} \tag{2.20}$$

where $\tilde{v}_d^{**}$ and $\tilde{v}_q^{**}$ are the *dq*-current controllers output. Three cases can be considered [Glo 98]:

1- No decoupling structure is used: the matrix $A(s)$ is equal to the unity matrix I_2 of R^{2x2};
2- A feedforward decoupling structure is used: $A(s)$ is a full matrix of R^{2x2}. But thanks to the decoupling, the product $Y(s) \cdot A(s)$ is a diagonal matrix equal to the admittance of the system without coupling terms;
3- A feedback decoupling structure is used: $A(s)$ is equal to the unity matrix I_2 and the effect of the decoupling structure is considered by taking a diagonal admittance (and so impedance) matrix.

From Fig. 2.3, it yields

$$\begin{bmatrix}\tilde{v}_d^*(s)\\ \tilde{v}_q^*(s)\end{bmatrix} = \left(A(s) \cdot \begin{bmatrix} C_d(s) & 0 \\ 0 & C_q(s)\end{bmatrix} \cdot \begin{bmatrix}\tilde{\imath}_{dref}(s) - \tilde{\imath}_d(s)\\ \tilde{\imath}_{qref}(s) - \tilde{\imath}_q(s)\end{bmatrix}\right) \tag{2.21}$$

Now relation (2.18) changes to:

$$\begin{bmatrix}\tilde{\imath}_d(s)\\ \tilde{\imath}_q(s)\end{bmatrix} = Y(s) \cdot \left(\begin{array}{c} \alpha \cdot \tilde{v}_s(s) \cdot \begin{bmatrix}V_d^*\\ V_q^*\end{bmatrix} - \alpha \cdot \tilde{v}_{sf}(s) \cdot \begin{bmatrix}V_d^*\\ V_q^*\end{bmatrix} \\ +\alpha \cdot V_s \cdot A(s) \cdot \begin{bmatrix} C_d(s) & 0 \\ 0 & C_q(s)\end{bmatrix} \cdot \begin{bmatrix}\tilde{\imath}_{dref}(s) - \tilde{\imath}_d(s)\\ \tilde{\imath}_{qref}(s) - \tilde{\imath}_q(s)\end{bmatrix} \end{array} \right) \tag{2.22}$$

The current references (i_{dref} and i_{qref}) come usually from the flux control loop and the speed control loop (if they exist). To evaluate the input impedance of an inverter-motor-drive system, the speed or flux references are supposed to be constant (i.e. their variations are supposed to be equal to zero). If we suppose that the dynamic of these two control loops are much slower than that of the current loops, then their influence on the input impedance can be taken into account as follows:

$$\begin{aligned}\begin{bmatrix}\tilde{\imath}_{dref}(s)\\ \tilde{\imath}_{qref}(s)\end{bmatrix} &= \begin{bmatrix} h_{d1}(s) & h_{d2}(s)\\ h_{q1}(s) & h_{q2}(s)\end{bmatrix} \cdot \begin{bmatrix}\tilde{\imath}_d(s)\\ \tilde{\imath}_q(s)\end{bmatrix} + \begin{bmatrix}0\\ h_v(s)\end{bmatrix} \cdot \tilde{v}_s(s)\\ &= H(s) \cdot \begin{bmatrix}\tilde{\imath}_d(s)\\ \tilde{\imath}_q(s)\end{bmatrix} + S(s) \cdot \tilde{v}_s(s)\end{aligned} \tag{2.23}$$

From equations (2.22) and (2.23), we obtain the following relation for *dq*-currents variations:

$$\begin{bmatrix}\tilde{\imath}_d(s)\\ \tilde{\imath}_q(s)\end{bmatrix} = Y(s) \cdot \left(\begin{array}{c} \alpha \cdot \tilde{v}_s(s) \cdot \begin{bmatrix}V_d^*\\ V_q^*\end{bmatrix} - \alpha \cdot \tilde{v}_{sf}(s) \cdot \begin{bmatrix}V_d^*\\ V_q^*\end{bmatrix} \\ +\alpha \cdot V_s \cdot A(s) \cdot \begin{bmatrix} C_d(s) & 0 \\ 0 & C_q(s)\end{bmatrix} \cdot \left(H(s) \cdot \begin{bmatrix}\tilde{\imath}_d(s)\\ \tilde{\imath}_q(s)\end{bmatrix} + S(s) \cdot \tilde{v}_s(s) \right) - \\ \alpha \cdot V_s \cdot A(s) \cdot \begin{bmatrix} C_d(s) & 0 \\ 0 & C_q(s)\end{bmatrix} \cdot \begin{bmatrix}\tilde{\imath}_d(s)\\ \tilde{\imath}_q(s)\end{bmatrix} \end{array} \right)$$

$$\begin{bmatrix}\tilde{\imath}_d(s)\\ \tilde{\imath}_q(s)\end{bmatrix} = D^{-1}(s) \cdot \left(\begin{array}{c} \alpha \cdot Y(s) \cdot \begin{bmatrix}V_d^*\\ V_q^*\end{bmatrix} \\ +\alpha \cdot V_s \cdot Y(s) \cdot A(s) \cdot \begin{bmatrix} C_d(s) & 0 \\ 0 & C_q(s)\end{bmatrix} \cdot S(s) \end{array} \right) \cdot \tilde{v}_s(s)$$

$$-D^{-1}(s)\cdot\ Y(s)\cdot\left(\alpha\cdot\tilde{v}_{sf}(s)\cdot\begin{bmatrix}V_d^*\\V_q^*\end{bmatrix}\right) \tag{2.24}$$

with

$$D(s)=I_2-\alpha\cdot V_s\cdot Y(s)\cdot A(s)\cdot\begin{bmatrix}C_d(s) & 0\\0 & C_q(s)\end{bmatrix}\cdot(H(s)-I_2) \tag{2.25}$$

From equations (2.24) and (2.25), it is possible to give the following expressions for the *dq*-currents variations as a function of the input voltage variation:

$$\begin{bmatrix}\tilde{\imath}_d(s)\\\tilde{\imath}_q(s)\end{bmatrix}=D^{-1}\cdot\left(\alpha\cdot Y(s)\cdot\begin{bmatrix}V_d^*\\V_q^*\end{bmatrix}+\alpha\cdot V_s\cdot Y(s)\cdot A(s)\cdot\begin{bmatrix}C_d(s) & 0\\0 & C_q(s)\end{bmatrix}\cdot S(s)-\alpha\cdot Y(s)\cdot F_s(s)\cdot\begin{bmatrix}V_d^*\\V_q^*\end{bmatrix}\right)\cdot\tilde{v}_s(s) \tag{2.26}$$

Then, we set:

$$\begin{cases}\tilde{\imath}_d(s)=Y_d(s)\cdot\tilde{v}_s(s)\\\tilde{\imath}_q(s)=Y_q(s)\cdot\tilde{v}_s(s)\end{cases} \tag{2.27}$$

Where $Y_d(s)$ and $Y_q(s)$ can be identified using (2.25) and (2.26). Then, from relations (2.16) and (2.27), we have:

$$\left(I_s-V_1(s)\cdot Y_d(s)-V_2(s)\cdot Y_q(s)\right)\cdot\tilde{v}_s(s)=-V_s\cdot\tilde{\imath}_s(s) \tag{2.28}$$

So, the analytical expression of the input impedance is the following:

$$Z_{in}(s)=-\frac{V_s}{I_s-V_1(s)\cdot Y_d(s)-V_2(s)\cdot Y_q(s)} \tag{2.29}$$

Note- In [Liu 10], the case where the control voltages are not normalized by V_s/v_{sf} is studied. In this case, we have:

$$\begin{bmatrix}\tilde{\imath}_d(s)\\\tilde{\imath}_q(s)\end{bmatrix}=Y(s)\cdot\left(\alpha\cdot\tilde{v}_s(s)\cdot\begin{bmatrix}V_d^*\\V_q^*\end{bmatrix}+\alpha\cdot V_s\cdot\begin{bmatrix}\tilde{v}_d^*(s)\\\tilde{v}_q^*(s)\end{bmatrix}\right) \tag{2.30}$$

This leads to the following relation:

$$\begin{bmatrix}\tilde{\imath}_d(s)\\ \tilde{\imath}_q(s)\end{bmatrix} = Y(s)\cdot\left(\begin{array}{c}\alpha\cdot\tilde{v}_s(s)\cdot\begin{bmatrix}V_d^*\\ V_q^*\end{bmatrix}\\ +\alpha\cdot V_s\cdot A(s)\cdot\begin{bmatrix}C_d(s) & 0\\ 0 & C_q(s)\end{bmatrix}\cdot\left(H(s)\cdot\begin{bmatrix}\tilde{\imath}_d(s)\\ \tilde{\imath}_q(s)\end{bmatrix}+S(s)\cdot\tilde{v}_s(s)\right)-\\ \alpha\cdot V_s\cdot A(s)\cdot\begin{bmatrix}C_d(s) & 0\\ 0 & C_q(s)\end{bmatrix}\cdot\begin{bmatrix}\tilde{\imath}_d(s)\\ \tilde{\imath}_q(s)\end{bmatrix}\end{array}\right)$$

$$\begin{bmatrix}\tilde{\imath}_d(s)\\ \tilde{\imath}_q(s)\end{bmatrix} = D^{-1}(s)\cdot\left(\begin{array}{c}\alpha\cdot Y(s)\cdot\begin{bmatrix}V_d^*\\ V_q^*\end{bmatrix}\\ +\alpha\cdot V_s\cdot Y(s)\cdot A(s)\cdot\begin{bmatrix}C_d(s) & 0\\ 0 & C_q(s)\end{bmatrix}\cdot S(s)\end{array}\right)\cdot\tilde{v}_s(s) \qquad (2.31)$$

Then from (2.29) and (2.31) we can calculate the input impedance.

2.2.3.2 Proposed stabilization block:

The proposed stabilization block here is a proportional compensator followed by a band-pass filter. This filter permits to preserve the system behavior at very low frequencies (speed dynamic) and to reject measurement noise. In addition, as it has been already reported in [Mos 07], [Liu 08a], [Mos 05], a band-pass filtering is the best choice for stabilizing the dc-link voltage. This leads to the following transfer function for stabilization block $h_v(s)$:

$$h_v(s) = K\frac{2\xi\omega_f s}{s^2+2\xi\omega_f s+\omega_f^2} \qquad (2.32)$$

with ω_f as the central frequency of the filter and K as the proportional gain to be defined. It is obvious from (2.31) and (2.26) that this block modifies the drive input impedance (Z_{in}) allowing the stabilization of the dc-link voltage.

2.2.4 Practical Example of Stability Analysis:

In order to analyze the stability of the dc-link voltage using (2.4) and (2.29) for a practical case, the dc-link voltage stability of an ac drive designed for aerospace applications is studied in this section. Then, for reducing the dc-link capacitance without losing the stability, a proper stabilization block will be designed and later in the next section, this stabilization approach will be tested by simulations and experimentations.

Let's consider a Permanent Magnet Synchronous Motor (PMSM) with a speed control loop. Thus, we set $C_\Phi(s)=0$ (i.e. $h_{d1}(s)=h_{d2}(s)=0$) and $i_{dref}=0$. Only linear controllers are supposed to be used for the system. In this section, no normalization is considered. The effect of the normalization of the control voltages by V_s/v_{sf} will be studied in the next section. The PI controllers used for the speed and the stator currents are:

$$\begin{cases} C_v(s) = K_{pv}\dfrac{1+\tau_{iv}s}{\tau_{iv}s} \\ C_d(s) = K_{pd}\dfrac{1+\tau_{id}s}{\tau_{id}s} \\ C_q(s) = K_{pq}\dfrac{1+\tau_{iq}s}{\tau_{iq}s} \end{cases} \tag{2.33}$$

Then, the different matrices and polynomial expressions given in the previous section can be obtained easily. We begin by the impedance matrix of the motor given in (2.15):

$$Z(s) = \begin{bmatrix} R_s + L_d s & -L_q\omega_0 \\ L_d\omega_0 & R_s + L_q s \end{bmatrix} \tag{2.34}$$

where $\omega_0 = P\Omega_0$ is the electrical pulsation at the operating point. Then, from (2.17) we have:

$$V_1(s) = V_d + (R_s + L_d s)\cdot I_d + \omega_0 L_d I_q \tag{2.35}$$

$$V_2(s) = V_q + (R_s + L_d s)\cdot I_q - \omega_0 L_q I_d \tag{2.36}$$

For decoupling the control of the dq-currents, a feedforward decoupling technique is used. Thus, we have:

$$Y(s)\cdot A(s) = \begin{bmatrix} \dfrac{1}{R_s + L_d s} & 0 \\ 0 & \dfrac{1}{R_s + L_q s} \end{bmatrix} \tag{2.37}$$

And finally, $H(s)$ and $S(s)$ in (2.23) are given by:

$$H(s) = \begin{bmatrix} 0 & 0 \\ 0 & -C_v(s)\cdot\dfrac{P\Psi_f}{f + Js} \end{bmatrix} \tag{2.38}$$

$$S(s) = \begin{bmatrix} 0 \\ h_v(s) \end{bmatrix} \tag{2.39}$$

Replacing (2.33) and (2.37)-(2.39) in (2.25), (2.27) and (2.28), we obtain the expression of $Y_d(s)$ and $Y_q(s)$. Then, these latter together with (2.35) and (2.36) give the input impedance of the drive ($Z_{in}(s)$) around the dc-link operating point (V_s, I_s) according to (2.29).

Now, we study at first the stability of the uncompensated system for different values of the dc-link capacitance. To do that, Bode and Nyquist diagrams are applied to the transfer function $Z_o(s)/Z_{in}(s)$ for evaluating the system stability margins. Then, the oscillation compensator $h_v(s)$ (2.32) will be added to the system and its effect on the stability will be studied. This study

permits to make in evidence the influence of the compensator parameters on the stability and then on the design of the dc-link capacitance.

Fig. 2.4 presents three Bode diagrams obtained for three different dc-link capacitances, all other parameters are kept constant. The drive input impedance (Z_{in}) is calculated according to (2.29) without any compensator ($h_v = 0$) at Ω=1500rpm, p_s=620W. Obviously, there is more interaction between Z_o and Z_{in} Bode plots when the dc-link capacitance decreases. It is potentially undesirable because stability margins may decrease. To verify it, corresponding Nyquist diagrams are plotted in Fig. 2.5 where it can be seen that, for the same operating point, the dc-link voltage is stable with C=1000μF, but it is unstable with C=500μF and C=200μF. The parameters of the system are given in Table I. They correspond to our experimental test bench.

TABLE I
Experimental system parameters

DC-link input voltage (V_e)	200 V
DC-link inductance (L_f)	39.5 mH
DC-link resistance (r_f)	1.1 Ω
Switching frequency	10 kHz
no. of pole pairs (P)	4
Stator resistance (R_s)	0.5 Ω
Stator inductance (L_s)	3.1 mH
Magnet flux linkage (Ψ_f)	124×10^{-3} Nm/A
Friction constant (f)	24×10^{-3} $Kg.m^2/s$
Inertia constant (J)	3.1×10^{-3} $Kg.m^2$

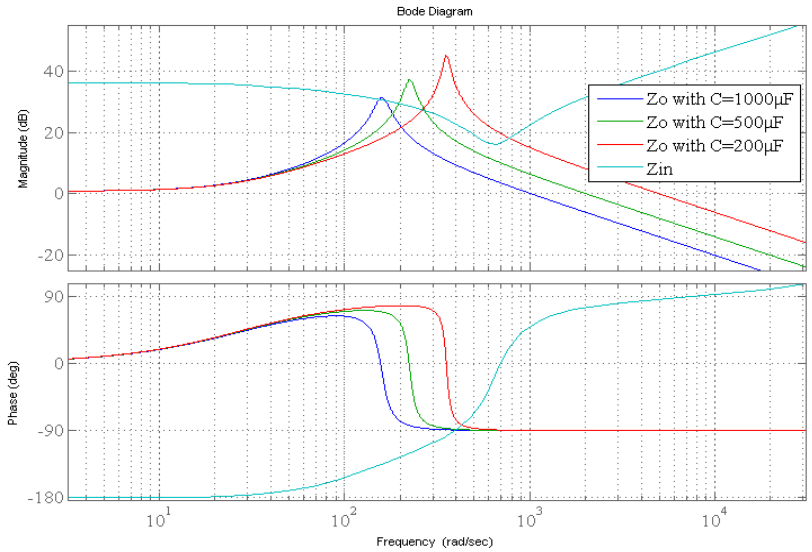

Fig. 2.4 - Influence of the dc-link capacitance on the stability: Bode diagram (K=0).

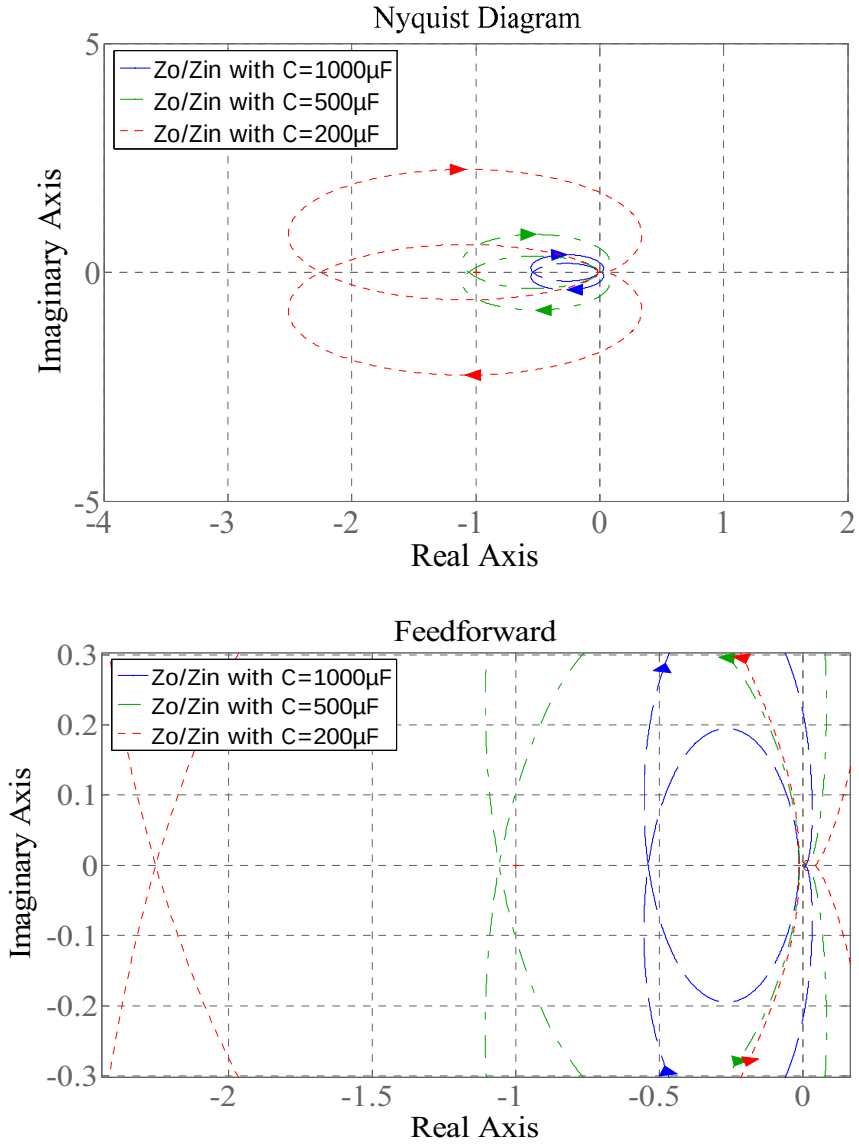

Fig. 2.5- Influence of the dc-link capacitance on the stability: Nyquist diagram (above) and its zoom (below) (K=0).

As given in (2.32), the oscillation compensation block is composed of a band-pass filter and a proportional corrector. The choice of the band-pass filter allows affecting i_{qref} only within a limited frequency band in order to improve the robustness with respect to the dc-bus voltage measurement noise without modifying its steady state value. The cut-off frequencies should be fixed according to the interaction zone between Z_o and Z_{in} Bode plots for a given set of parameters. For example, if we choose C=500μF, the interaction zone lies from 190 *rad/s* to 270 *rad/s* according to Bode diagrams (Fig. 2.4). Therefore, an appropriate choice for covering the interaction zone is ω_{c1}=100 *rad/s* and ω_{c2}=400 *rad/s*. The third and last parameter of the compensator is K. Its best choice should satisfy, according to the studied application, the design requirements like as good stability margins and good torque dynamic.

Fig. 2.6 shows Nyquist plots corresponding to different values of K for the same operating point as in Fig. 2.5 (Ω=1500 *rpm*, p_s=620 *W*). It can be seen that:

1- The system is no more unstable for C_f=500μF (compare Figs. 2.5 and 2.6);
2- A growing K does not lead to more robustness: stability margins for K=1 are smaller than those for K=0.1.

Therefore, K should be sufficiently high to stabilize the system, but not too much high because of robustness cares. There is an optimum value for K which depends on the system parameters, the control gains and particularly the design requirements. A designer may maximize the phase margin while another one may prefer the best module margin and a third one prefers to find a trade-off between the dc-link voltage stabilization and the drive torque disturbance rejection in a torque control scheme.

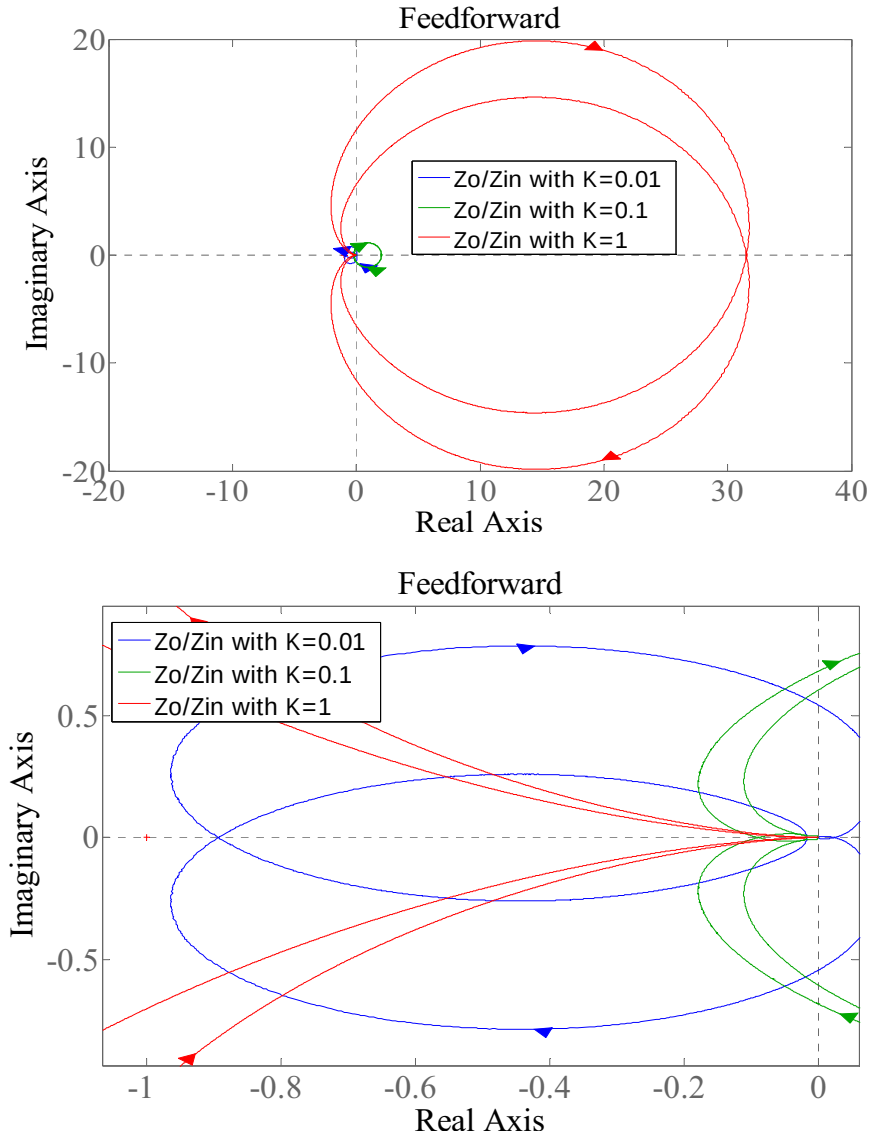

Fig. 2.6- Influence of the stabilization parameter (K) on the stability margins: Nyquist diagram (above) and its zoom (below) (C_f =500μF).

The influence of the speed control loop dynamic on the dc-link voltage stabilization is shown in Fig. 2.7. For many applications, the frequency range where interactions between Z_o and Z_{in} exist, is far from the speed loop frequency bandwidth. Thus, it is expected that the influence of the speed controller on the oscillation compensation is limited. Fig. 2.7 illustrates Nyquist plots obtained for three different values of the speed time constant in closed-loop (t_v) at the same operating point as in Figs. 2.5 and 2.6 (Ω=1500 *rpm*, p_s=620 *W*). We remark that the inverter-motor-drive input impedance is not very sensitive to t_v. Indeed, it is obvious from this figure that the speed dynamic has a negligible impact on the stability properties of the system as it was expected.

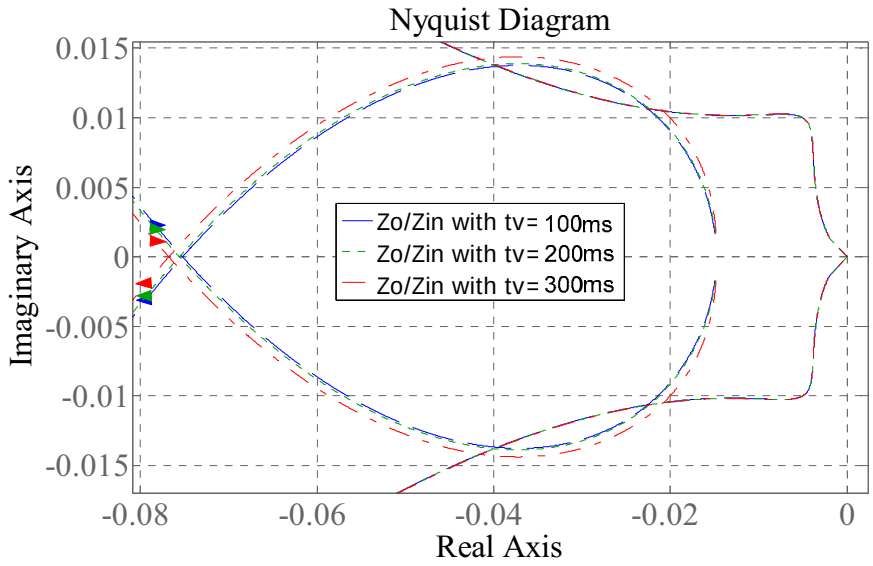

Fig. 2.7- Influence of the speed loop dynamic on the stability of the dc-link voltage: Nyquist diagram zoom (C_f =500µF, K=0.1).

2.2.5 *Effect of Normalization on stability and torque disturbance rejection:*

In this section we will study the effect of normalization of dc-link voltage with low pass filtered dc-link voltage v_{sf} on stability of dc-link variables of electrical system. The advantage of normalization is that it helps in dc-link voltage disturbances rejection. But, as we will see, when the control voltages are normalized, the system risks to become unstable or its stability margins may reduce. To study that, a first-order low-pass filter is used here:

$$\tilde{v}_{sf} = F_s(s) \cdot \tilde{v}_s = \frac{\omega_s}{s + \omega_s} \cdot \tilde{v}_s \tag{2.40}$$

The cut-off frequency is fixed to $\omega_s = 600$. Fig. 2.8 shows the Nyquist plot for Z_o/Z_{in} impedence with and without normalization at Ω=1500*rpm*, p_s=620*W*. It can be seen in this figure that the system is stable without normalization, but it becomes unstable when we normalize. Fig. 2.8b shows the Nyquist plot for Z_o/Z_{in} impedence for oscillation compensation block gain K =

0.01 with and without normalization. It can be seen in this figure that the stability margins decreases in case of normalization.

We test the effect of the normalization on the stability of the dc-link variables in Figs. 2.9 and 2.10. A simulation proram was developed for this purpose, with the perameters given in Table I and Table II. Fig. 2.9 shows the simulation results without normalization and it can be observed in this figure that the dc-link voltage and current tend to become stable when a *q-current* step is applied. But results in Fig. 2.10 (with normalization) indicate that the dc-link variables become unstable after the same *q-current* step as in Fig. 2.9. In this case, some ripples are quite visible on the dc-link variables which is an evident that the normalization degrades the stability margins of the system.

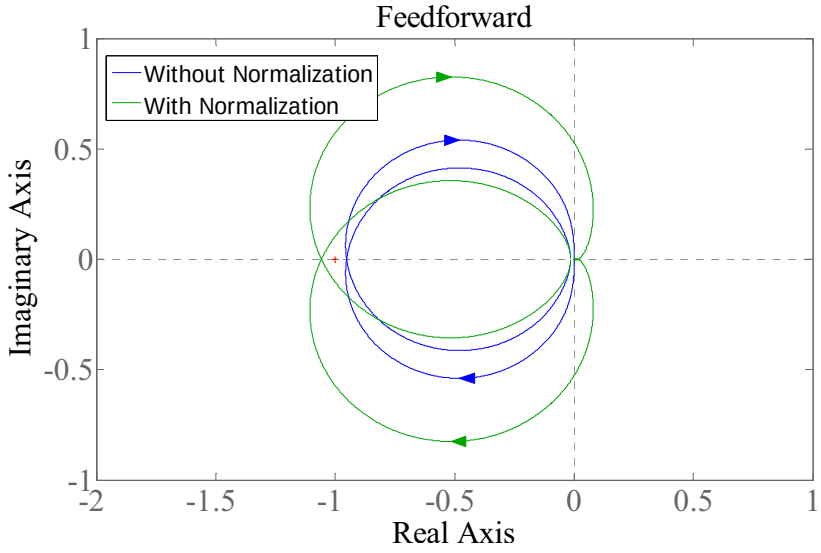

Fig. 2.8a - Nyquist plot with and without normalization of control voltages and C_f =500μF, K=0.

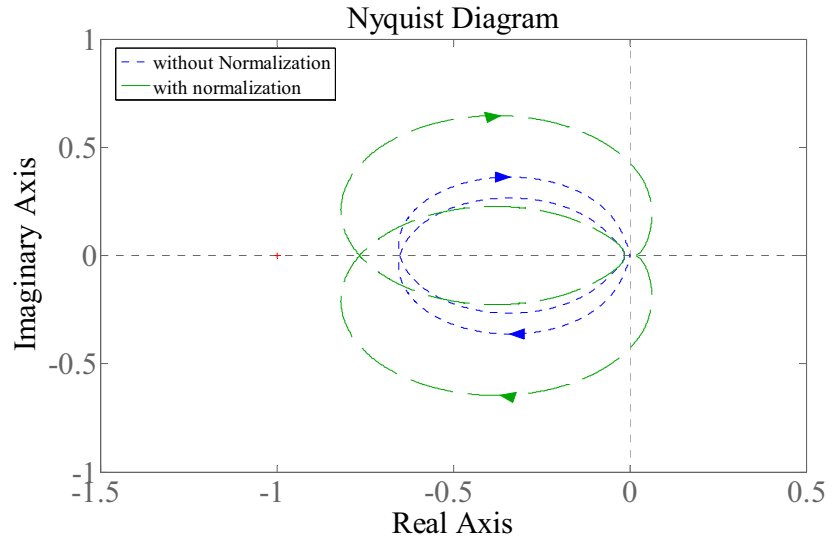

Fig. 2.8b - Nyquist plot with and without normalization of control voltages and C_f =500μF, K=0.01.

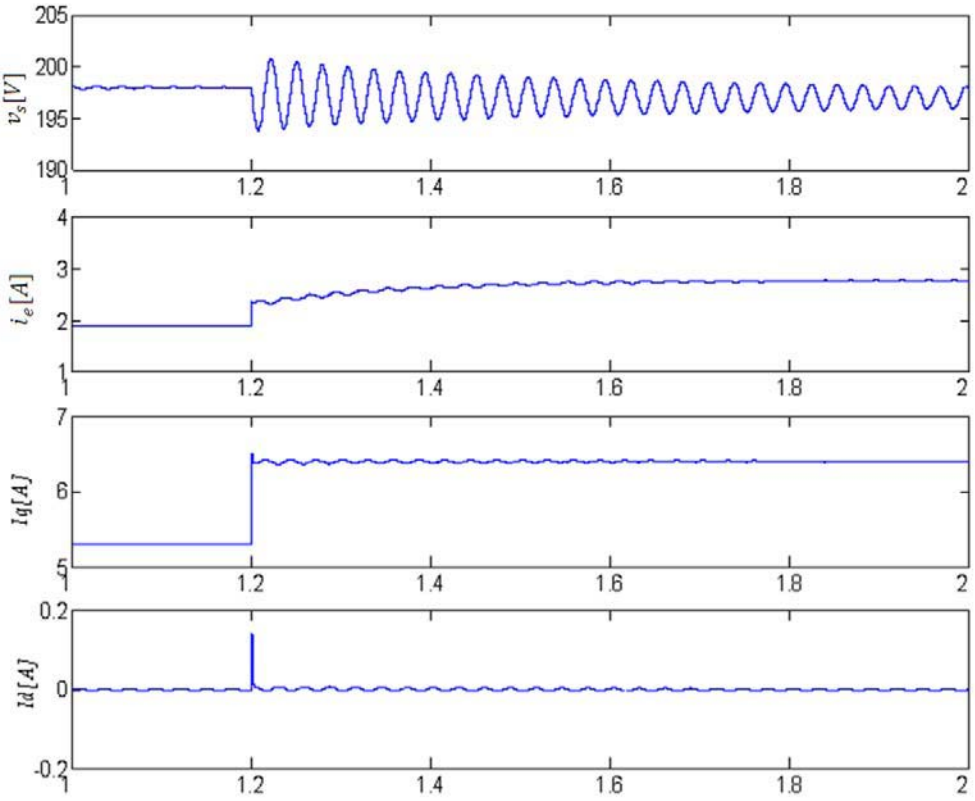

Fig. 2.9 – dc-link voltage and current after an Iq step with K=0(without normalization)

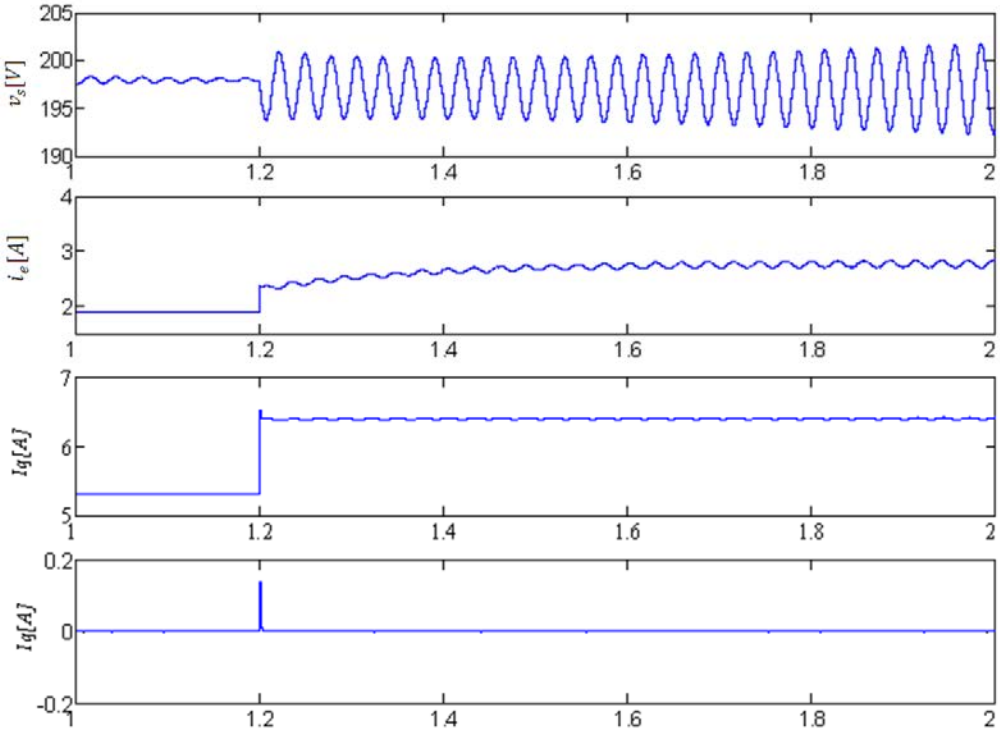

Fig. 2.10 – dc-link voltage and current after an Iq step with K=0(with normalization)

2.2.6 Validation of Stability Analysis:

The stability analysis presented in the previous section by Nyquist and Bode plots are validated in this section by simulations and experimental results. For this purpose a Simulink model, corresponding to the studied system (an inverter-motor-drive with its DC supply and its LC filter), is developed. The parameters of the controlled system and the controllers are given respectively in Table 2.I and Table 2.II.

TABLE 2.II
Experimental System Parameters

Speed controller proportional gain (K_{pv})	0.02
Speed controller integral time constant (τ_{iv})	0.2 s
Current controller proportional gain ($K_{pd} = K_{pq}$)	10
Current controller integral time constant ($\tau_{id} = \tau_{iq}$)	$2ms$
Stabilization block low cut-off frequency (f_{c1})	$16Hz$
Stabilization block high cut-off frequency (f_{c2})	$64Hz$

Fig. 2.11 shows the results of the simulation model for (C_f =500μF, K=0), according to Nyquist plot in Fig. 2.5, the dc-link voltage should oscillate. Simulation results, shown in Fig. 2.11, confirm the given analysis: the dc-link voltage variations ($\tilde{v}_s$) and the dc-link input current (i_e) are not stable when a q-current step is applied. It should be noted that this step is equivalent to an instantaneous change of the load power seen by the input filter.

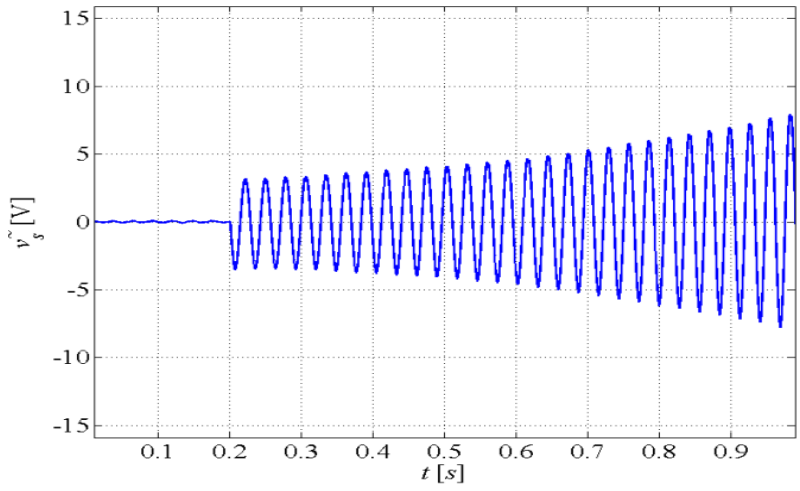

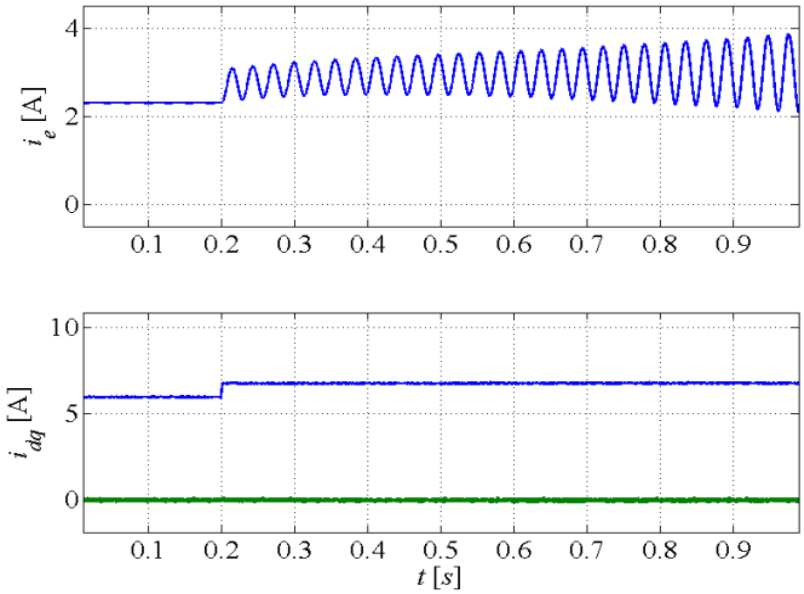

Fig. 2.11- Instability of dc-link voltage variations ($\tilde{v}_s$) and dc-link current (i_e) after a load power step (C_f =500µF, K=0)

The same test under the same conditions was performed on the experimental bench. Fig. 2.12 illustrates the experimental results which are close to variables shown in Fig. 2.11 and confirm the stability analysis given in the previous section.

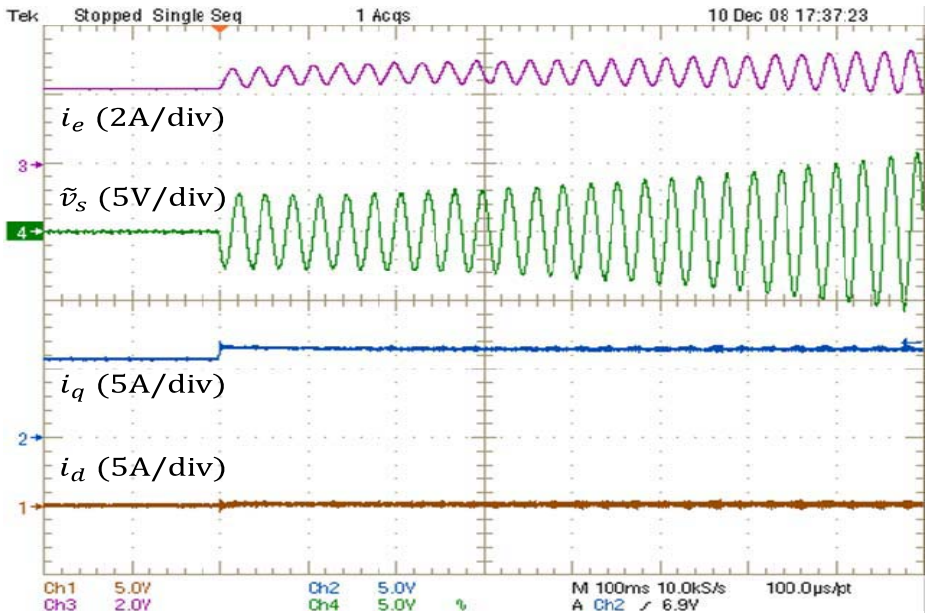

Fig. 2.12- Stator currents, dc-link voltage variations ($\tilde{v}_s$) and dc-link current (i_e) after a load power step without compensation (C_f =500µF, K=0).

Different tests were performed with the help of Simulink model of our system and on the experimental bench for different values of gain K to prove the effectiveness of the oscillation compensation block. The second test consists in activating the stabilization block with the gain

K=0.1. The stabilization block cut-off frequencies are fixed to ω_{c1}=100 *rad/s* and ω_{c2}=400 *rad/s*. Other parameters are kept constant (C_f =*500µF*). Fig. 2.13 shows simulation results where the dc-link voltage variations ($\tilde{v}_s$) and the dc-link input current (i_e) are no more unstable when the load power step is applied. Let's focus on how the stator *q*-current, and so the load power, is modified by the stabilization block. This modification has a negligible effect on the speed dynamic. Fig. 2.14 depicts corresponding experimental results and confirms the validity and the efficiency of the proposed approach.

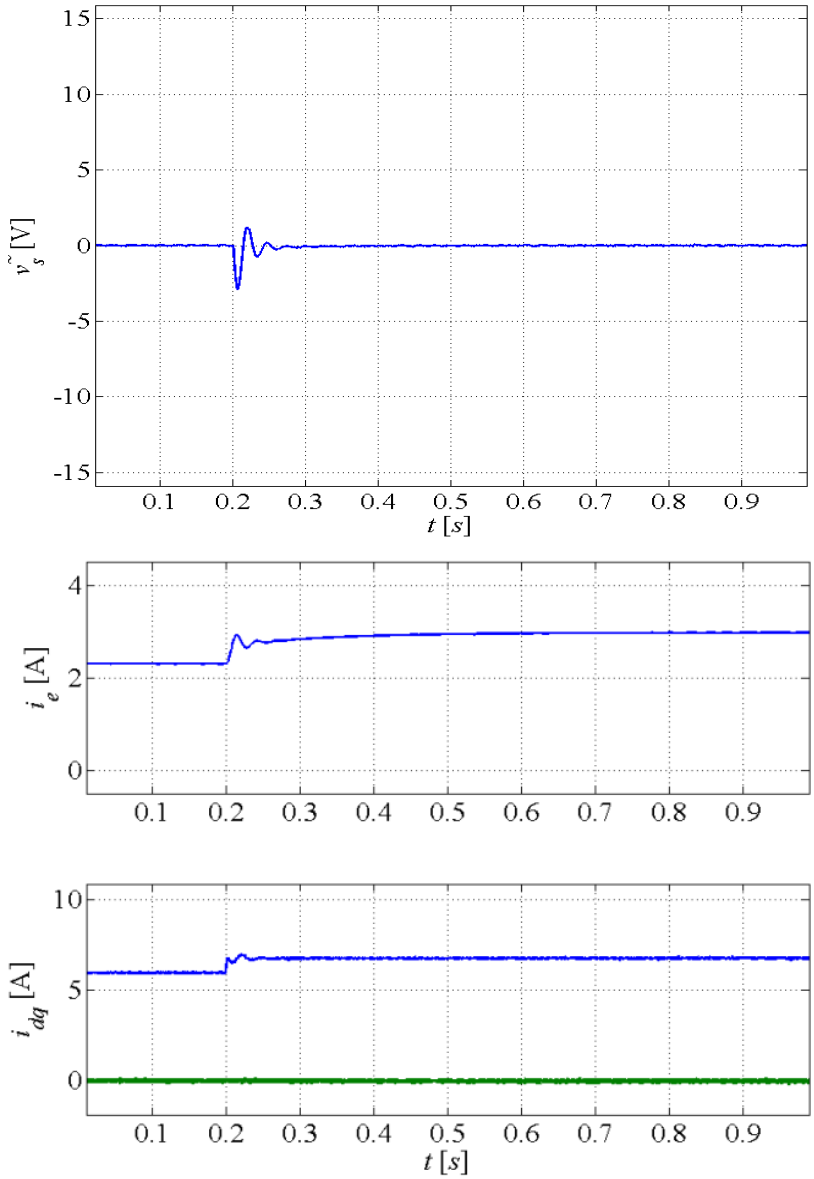

Fig. 2.13- Stabilization of dc-link voltage variations ($\tilde{v}_s$) and dc-link current (i_e) (C_f =500µF, K=0.1).

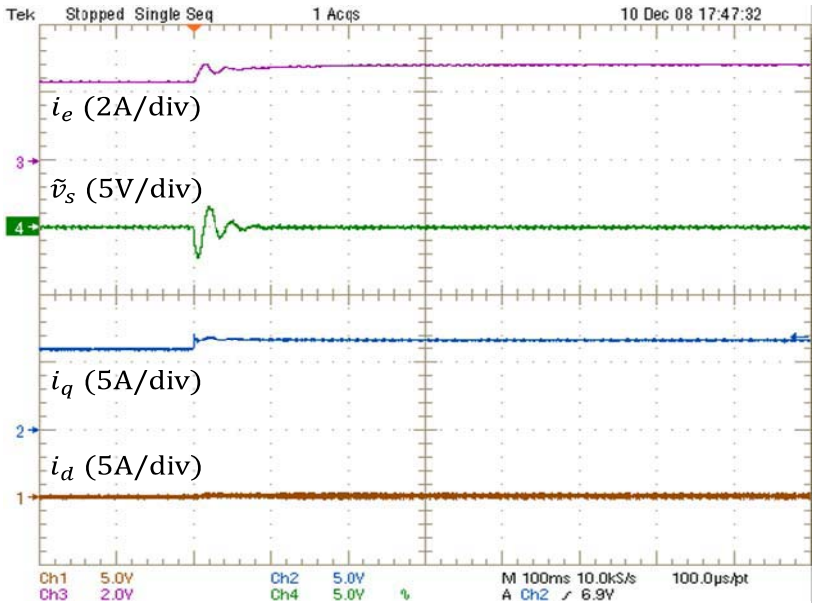

Fig. 2.14- Stabilization of dc-link voltage variations ($\tilde{v}_s$) and dc-link current (i_e) (C_f =500µF, K=0.1) (measurements)

Two other tests are performed with two other gains (a small and a high) in the stabilization block. Figs. 2.15 and 2.16 show the obtained results for K=0.01 and Figs. 2.17 and 2.18 illustrate those for K=1. In both cases, the dc-link variables are stable. But, they are under-damped for K=0.01 and over-damped for K=1. In addition, it can be seen in Fig. 2.18 that a high stabilization gain affects the mechanical dynamic and may excite non-modeled nonlinearities leading to undamped stable oscillations.

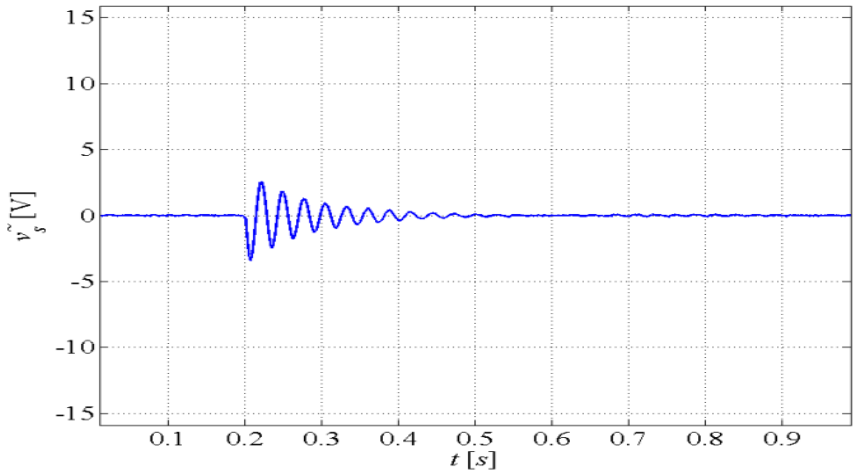

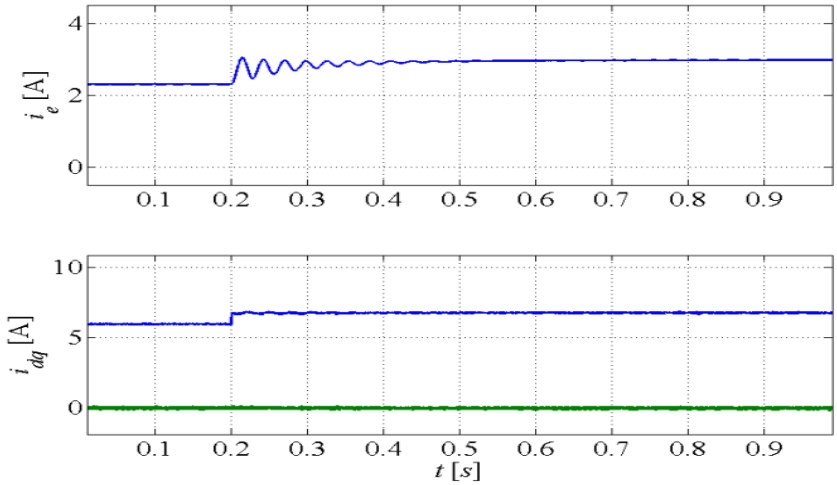

Fig. 2.15- Stabilization of dc-link voltage variations ($\tilde{v}_s$) and dc-link current (i_e) (C_f =500µF, K=0.01).

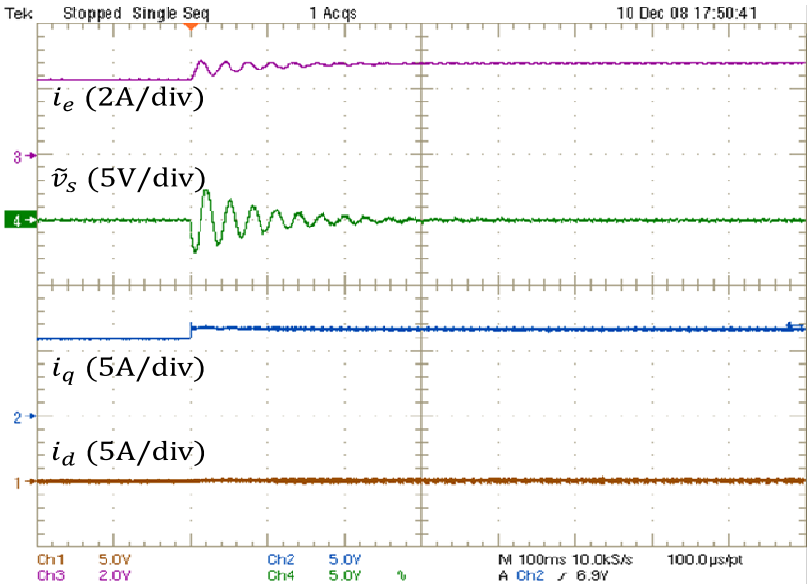

Fig. 2.16- Stabilization of dc-link voltage variations ($\tilde{v}_s$) and dc-link current (i_e) (C_f =500µF, K=0.01) (measurements).

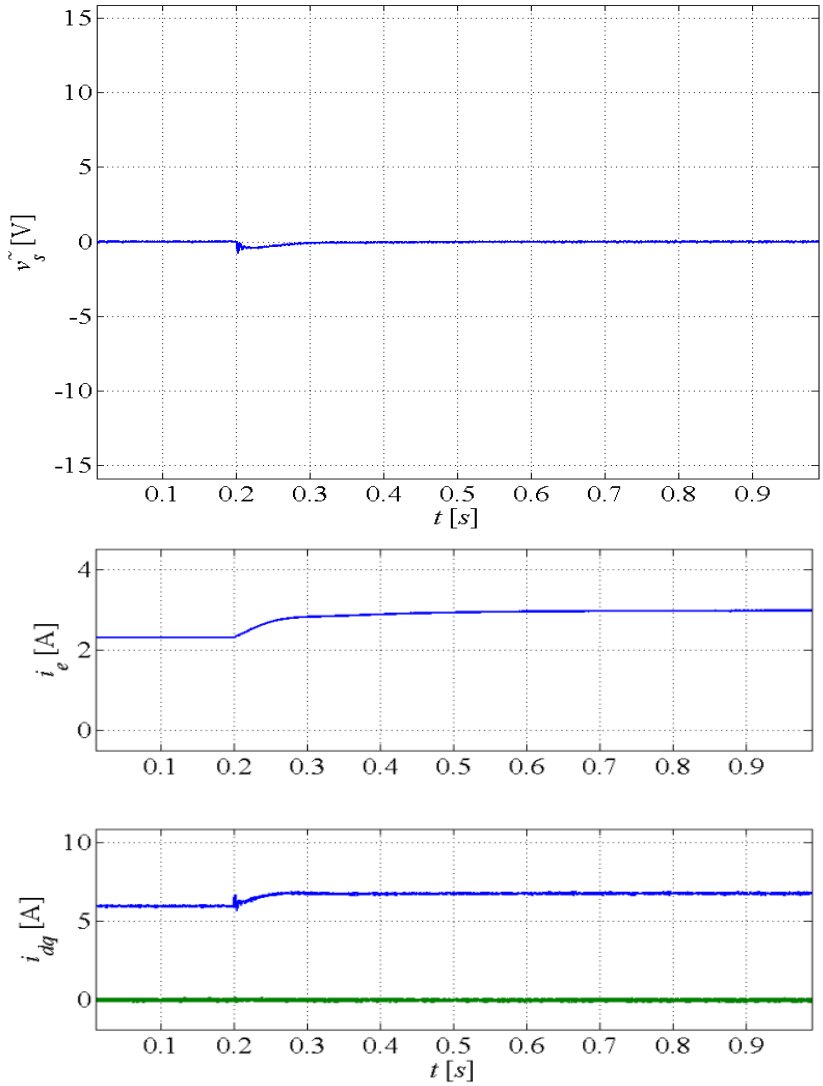

Fig. 2.17- Stabilization of dc-link voltage variations ($\tilde{v}_s$) and dc-link current (i_e) (C_f =500µF, K=1)

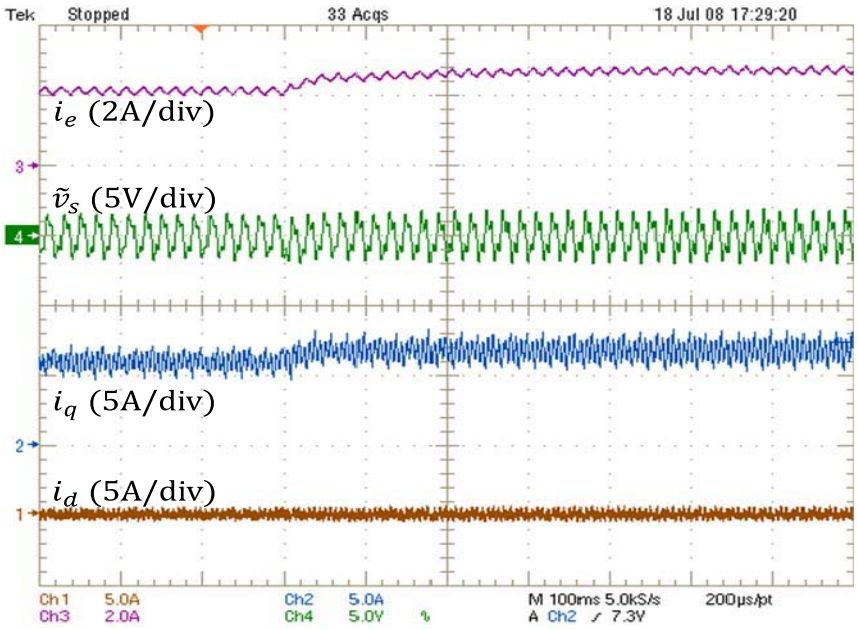

Fig. 2.18- Stabilization of dc-link voltage variations ($\tilde{v}_s$) and dc-link current (i_e) (C_f =500µF, K=1) (measurements).

2.3 CONCLUSION

It is well known that a tightly controlled load connected to a DC power supply may lead to instability on the dc-link variables. In this chapter, local stability of the dc-link variables was analyzed using Nyquist plot of Z_o/Z_{in} (output impedance of the supply/input impedance of the load). Then, a general method giving the analytical expression of the input impedance of an inverter-PMSM drive system was presented. This modeling is evidently based on small signal variations because of local nature of this study. However, all dynamics are taken into account except those of the inverter ones which can be often neglected in practical applications. A stabilization block, containing a band-pass filter and a proportional compensator, was proposed and added to the conventional control structure of the system. It allows stabilizing the dc-link voltage when small dc-link capacitances are employed. Therefore, this stabilization block is useful in aerospace applications where the dc-link capacitance should be small because of mechanical constraints. Simulation and experimental results confirm the validity and the efficiency of the proposed approach.

The stability analysis in this chapter has a local nature because of small signal modeling of the system. In the next chapter, we present a large signal stability analysis.

CHAPTER 3

NONLINEAR STABILIZATION OF DC-BUS SUPPLYING A CONSTANT POWER LOAD

Chapter 3

3.1 INTRODUCTION:

In this chapter we present a nonlinear stabilization technique for the electrical system comprised of a DC power supply, LC filter and an actuator (Inverter – Permanent Magnet Synchronous Motor or Induction Motor). In the previous chapter Local stability of the same electrical system was studied and here we will study the global stability of this inverter-PMSM system by using circle criterion.

In many studies, the design of the dc-Link capacitance is based on the first order modeling of the system and is realized to ensure only the asymptotic stability around the operating point. Nevertheless the behavior of the system in case of large disturbance is unknown. In fact the state trajectory goes away from the operating point and behavior of the state trajectory is not foreseen by the modeling. If the state trajectory stays in its attraction region, then it will converge towards the operating point.

Although linear models can be successfully employed to locally describe the behavior of a physical system, they often fail to provide a satisfactory global characterization [Nij 90]. An important class of nonlinear models is given by the feedback interconnection of a SISO linear time-invariant system G(s) and a nonlinear, possibly time-varying, static block N as represented in Fig. 3.9.

Models of this kind are known in literature as Lur'e Systems [Khalil] and their properties have been extensively studied in the last few decades. They reveal to be a very "expressive" class of models, since they can exhibit a wide variety of behaviours that linear systems cannot show (for example the presence of isolate equilibria, limit cycles, quasi-periodic and chaotic attractors [Gen 95].

From this perspective (and considering also their relative simplicity), Lur'e systems can be considered a very attractive class to try to give a more accurate and complete description of a physical system [Bas 97]. Such a consideration shows the importance of having some analytical tools allowing us to investigate qualitatively and quantitatively their properties. One of the significant results for Lur'e systems is the Circle Criterion [Khalil], [Vid 98] which may be employed to estabilish global asymptotical stability of the origin when the nonlinear feedback block satisfies a sector condition.

Two methods of stabilization are presented in this chapter. The first method is based on using the circle criterion to establish global stability of the electrical system [Awa 09]. The second method

creates a virtual resistance in parallel with the dc-bus capacitor [Awa 09a]. Impedance Z is equal to $1/K$ where K is the desired virtual conductance.

3.2 INVERTER MOTOR DRIVE SYSTEM MODEL:

The Inverter-Motor drive system is shown in Figure 1.

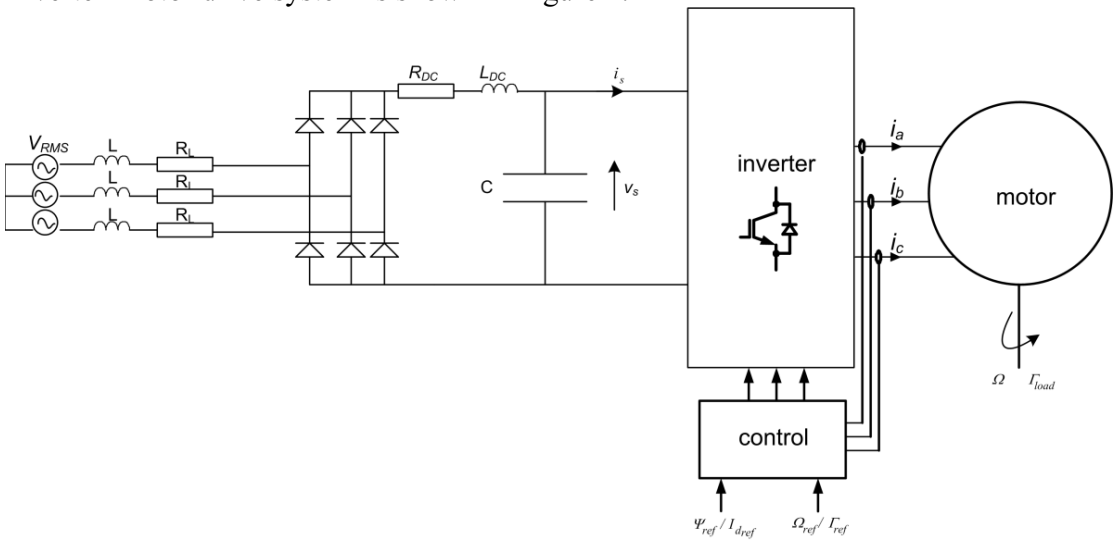

Fig. 3.1- The Inverter-Motor drive system connected to the grid through LC filter and rectifier.

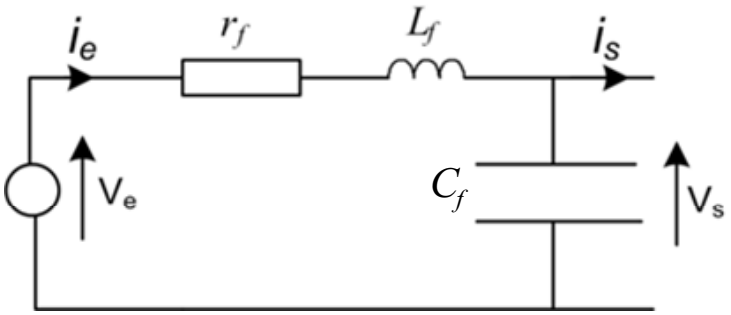

Fig. 3.2- DC model of the voltage source.

Chapter 2 talks about the Inverter-Motor drive system of Fig. 3.1 in detail but here we rewrite the three equations of the DC model of the AC voltage source and rectifier (Fig. 3.2)

$$V_e = \frac{3\sqrt{2}}{\pi} V_{RMS} \tag{3.1}$$

$$L_f = 2L + L_{DC} \tag{3.2}$$

$$r_f = 2R_L + R_{DC} + \frac{3}{\pi} L\omega \tag{3.3}$$

where V_{RMS} represents the *rms* value of the line voltage; L and R_L are respectively the line inductance and serial resistance of the three phase power supply; L_{DC} and R_{DC} represent respectively the dc-link equivalent inductance and resistance and the term $3L\omega/\pi$ is due to the commutation voltage drop. This leads to the following model of the drive supply (Fig. 3.2):

$$L_f \frac{d}{dt} i_e = -r_f i_e - v_s + V_e \tag{3.4}$$

$$C_f \frac{d}{dt} v_s = i_e - i_s \tag{3.5}$$

On the other hand, supposing that the PWM switching frequency is very high, the average model of the VSI – PMSM is the following:

$$\begin{cases} L_d \frac{d}{dt} i_d = -R_s i_d + P L_q i_q \Omega + G_{VSI} v_d \\ L_q \frac{d}{dt} i_q = -R_s i_q - P L_d i_d \Omega - P \Psi_f \Omega + G_{VSI} v_q \\ J \frac{d}{dt} \Omega = P\left(\Psi_f - \left(L_q - L_d\right) i_d\right) i_q - f\Omega - \Gamma_{load} \end{cases} \tag{3.6}$$

where the inverter is modeled by a simple gain:

$$G_{VSI} = k_c v_s = \frac{v_s}{2V_c} \tag{3.7}$$

with V_c as the amplitude of the PWM carrier signal.

It is known that for controlling the power flow in an ac drive, the stator *dq*-currents should be controlled. There are a big number of current controllers in the literature providing good static and dynamic behaviors. Some of these controllers present the advantage of not only controlling the stator currents, but also minimizing the dc-link voltage variations during transitions. In [Dél 95], the authors propose a LQG control for induction motors which minimizes a quadratic criterion taking into account the variations of the dc-link voltage. In [Nah 00], an intelligent controller is used for controlling a PMSM. Another approach based on a feedback linearization combined with a linear *H*∞-controller is used in [Luc 06] to control the stator *dq*currents of an induction motor. We consider the same current controller as that proposed in [Liu 04] based on I/O linearization technique coupled to a sliding-mode controller for the control of the *dq*-currents of our PMSM. Thanks to this control, the state trajectory is forced to move on the sliding surface defined as follow:

$$s = \begin{bmatrix} s_d \\ s_q \end{bmatrix} = \begin{bmatrix} k_{d1} \cdot \left(i_d - i_{dref}\right) + k_{d2} \cdot e_d \\ k_{q1} \cdot \left(i_q - i_{qref}\right) + k_{q2} \cdot e_q \end{bmatrix} \tag{3.8}$$

Where e_d and e_q correspond to integral terms used by the control to ensure a zero steady state error. We have:

$$\begin{cases} \frac{d}{dt} e_d = i_d - i_{dref} \\ \frac{d}{dt} e_q = i_q - i_{qref} \end{cases} \tag{3.9}$$

On the other hand, it is known that in the sliding mode, the system dynamics depends only on the control parameters. Thus, dc-link voltage variations will be rejected quickly by the control and their influence on the dq-currents, and consequently on the motor torque, is negligible. This will be verified by experimentation in the sections 3.4.4 and 3.5.2. Therefore, in the mechanical steady state, the inverter motor drive system can be considered as constant power load device for the DC supply. This leads to the following model for studying the stability of the dc-link voltage (Fig. 3.3):

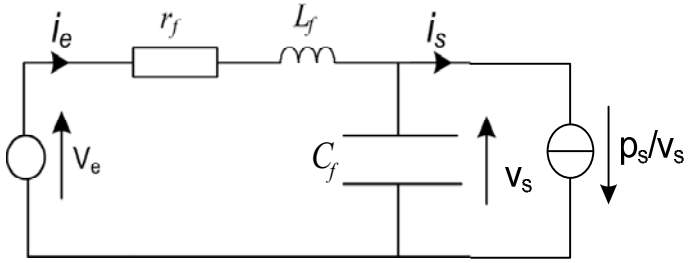

Fig. 3.3- Reduced model of the dc-bus and constant power load.

$$\begin{cases} L_f \frac{d}{dt} i_e = -r_f i_e - v_s + V_e \\ C_f \frac{d}{dt} v_s = i_e - \frac{p_s}{v_s} \end{cases} \tag{3.10}$$

where p_s is the VSI – PMSM input power which is supposed to be constant in the mechanical steady state. As we saw it in Chapter 2, this case corresponds often to the worst case from the stability point of view. In addition, this assumption allows simplifying the model for the stability analysis. In this case, the dc-link voltage v_s is locally asymptotically stable if the Jacobian matrix at the operating point is negative definite; this yields

$$p_s < p_{smax} = \frac{r_f C_f}{L_f} V_e^2 \tag{3.11}$$

In the next section we will study the instability of dc-link variables of the electrical system (Fig. 3.1) when the power consumed by the load does not satisfy the condition (3.11).

3.3 INSTABILITY OF DC-LINK VARIABLES:

3.3.1 *Simulation results:*

In order to study the stability of electrical system presented in Fig. 3.1. A simulink model is developed and its parameters are given in Table 3.I.

TABLE 3.I. Experimental System Parameters

DC-link input voltage	$200\ V$
DC-link inductance	$39.5\ mH$
DC-link resistance	$1.1\ \Omega$

DC-link capacitance	$500\ \mu F$
Switching frequency	$10\ kHz$
No. of pole pairs	4
Stator resistance	$0.5\ \Omega$
Stator inductance	$3.1\ mH$
Torque constant	$124 \times 10^{-3}\ Nm/A$
Friction constant	$24 \times 10^{-3}\ Kg.m^2/s$
Inertia constant	$3.1 \times 10^{-3}\ Kg.m^2$

Simulation results shown in Fig. 3.4 are obtained without nonlinear stabilization structure. The dc-link voltage (v_s) and dc-link current (i_e)are not stable when a *q-current* step is applied. It can be seen in the Fig. 3.4 that the dc-link variables oscillate after the *q-current* step.

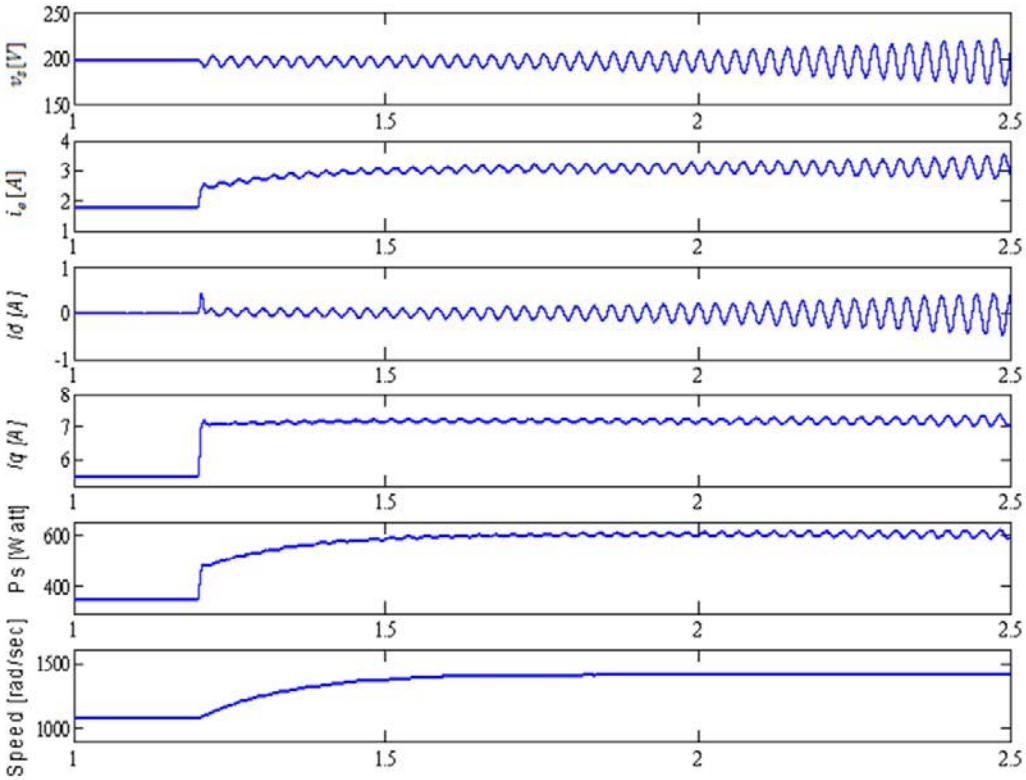

Fig. 3.4- Instability of dc-link variables after a q-current step.

The simulation results shown in Fig. 3.5 are obtained without nonlinear stabilization structure when a speed step is applied $i.e.$ the speed is increased from 1000*rpm* to 1500*rpm*. The dc-link voltage (v_s) is not stable after the speed step because the power consumed by the load does not satisfy (3.11).

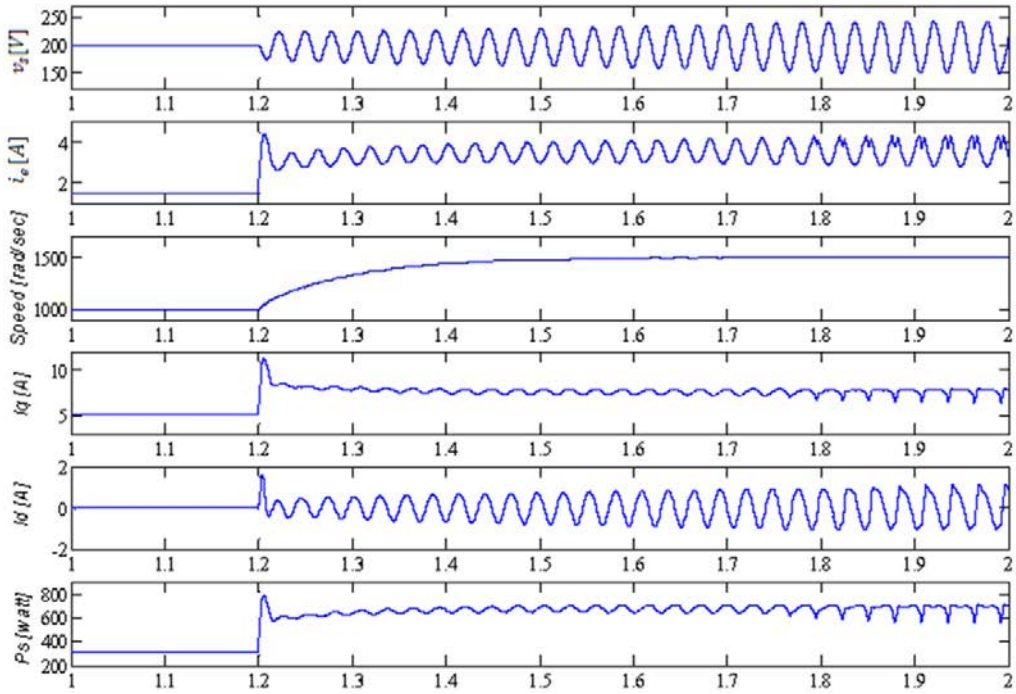

Fig. 3.5- Instability of dc-link variables after a speed step.

3.3.2 *Experimental results:*

To study the stability of dc-link variables of the electrical system (Fig. 3.1), several tests were performed on our experimental bench. In the first test, no stabilization block is provided and the results are shown in Fig. 3.6 which illustrates that the dc-link voltage variations and the dc-link input current are not stable when a q-current step is applied. In the second test, the stability of the dc-link variables is studied when the speed reference step is applied to push the operating point into the unstable region ($p_s > p_{smax}$). Fig. 3.7 shows that the dc-link voltage variations and the dc-link input current become unstable when the speed step is applied.

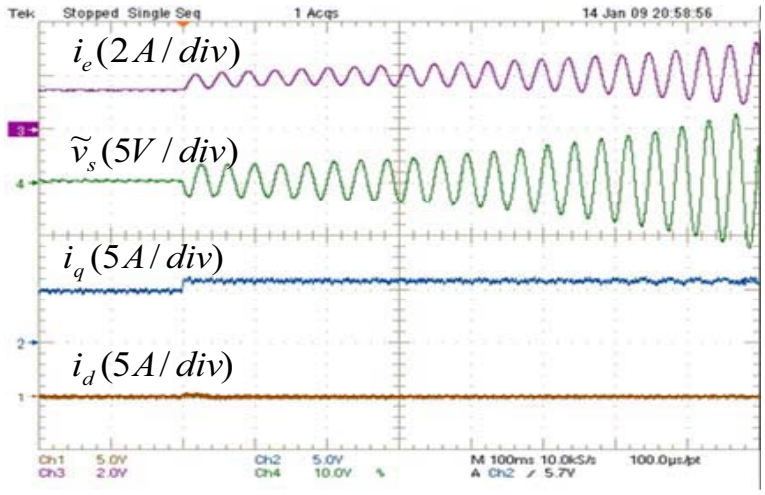

Fig. 3.6-Stator currents (Ch1 and Ch2), dc-link voltage variations (Ch4) and dc-link current (Ch3) after a q-current step without stabilization (C_f=500µF, t_f =1ms, K=0).

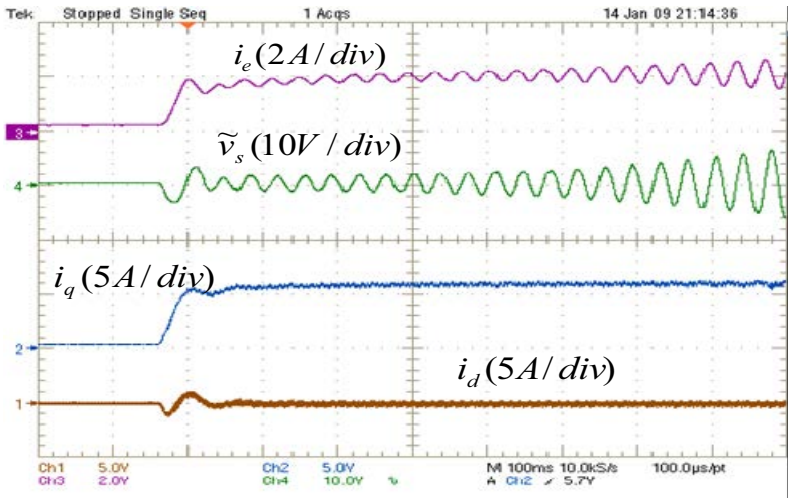

Fig. 3.7-Stator currents (Ch1 and Ch2), dc-link voltage variations (Ch4) and dc-link current (Ch3) after a speed step without stabilization (C_f=500µF, t_f =1ms, K=0).

Fig. 3.8 shows the dc-link voltage variations ($\tilde{\boldsymbol{v}}_{\boldsymbol{s}}$) and the dc-link input current ($\boldsymbol{i}_{\boldsymbol{e}}$) after a mechanical load step is applied. This test indicates that the dc-link variables are not stable after the mechanical load step because this leads to a power consumption unsatisfying the condition (3.11).

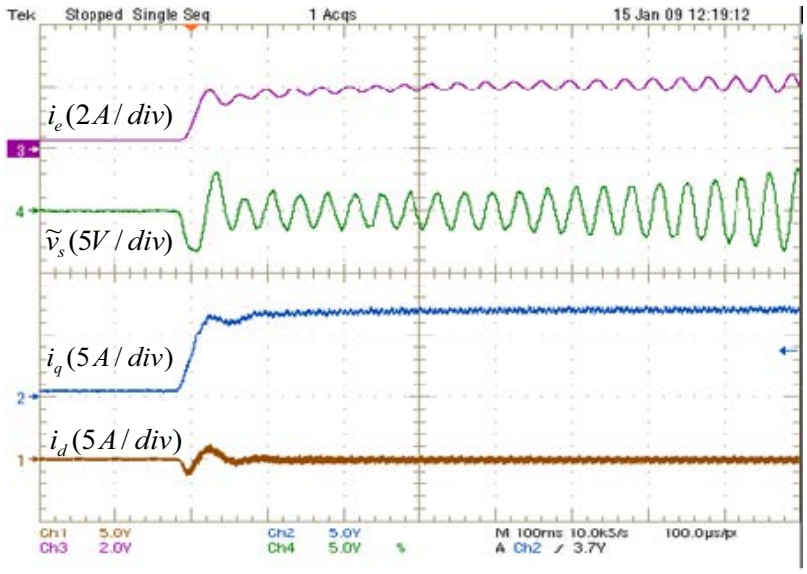

Fig. 3.8-Stator currents (Ch1 and Ch2), dc-link voltage variations (Ch4) and dc-link current (Ch3) after a load power step without stabilization (C_f=500µF, t_f=1ms, K=0).

In the following, we propose two nonlinear stabilization methods for the global stability of the electrical system and we present the stability conditions.

3.4 FIRST METHOD OF STABILIZATION:

Many nonlinear physical systems can be represented as feedback connection of a linear dynamical system $G(s)$ and a nonlinear element as shown in Fig. 3.9.

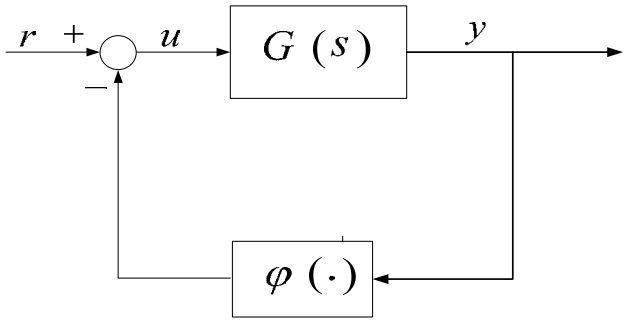

Fig. 3.9- Nonlinear feedback connection

The process of representing a system in this form depends on the particular system involved. For instance, in the case in which a control system's only nonlinearity is in the form of a relay or actuator/sensor nonlinearity, there is no difficulty in representing the system in this feedback form. In other cases, the representation may be less obvious. We assume that the extern input $r = 0$ and study the behavior of the unforced system. The stability of the system is studied by classical control tools like the Nyquist plot and the Nyquist criterion. We study the absolute stability of our system. The system is said to be absolutely stable if it has a globally uniformly

asymptotically stable equilibrium point at the origin for all nonlinearities in a given sector. The circle criterion gives frequency-domain sufficient conditions for absolute stability.

Considering $r = 0$, the system can be represented by:

$$\dot{x} = Ax + Bu \tag{3.12}$$

$$y = Cx + Du \tag{3.13}$$

$$u = -\psi(t, y) \tag{3.14}$$

where $x \in R^n$, $u, y \in R^p$, (A, B) is controllable, (A, C) is observable, and $\psi : [0, \infty) \times R^p \rightarrow R^p$ is a memoryless, possibly time-varying, nonlinearity, which is piecewise continuous in t and locally Lipschitz in y. We assume that the feedback connection has a well-defined state model, which is the case when

$$u = -\psi(t, Cx + Du) \tag{3.15}$$

has a unique solution u for every (t, x) in the domain of interest. This is always the case when $D = 0$. The transfer function matrix of the linear system

$$G(s) = C(sI - A)^{-1}B + D \tag{3.16}$$

is square and proper or strictly proper if $D = 0$. The controllability and observability assumptions ensure that $\{A, B, C, D\}$ is a minimal realization of $G(s)$. From linear system theory, we know that for any rational proper $G(s)$, a minimal realization always exists.

The stability of the nonlinear system in Fig. 3.9 can be proved by the circle criterion.

Circle Criterion:

The nonlinear system in Fig 3.9 has a special structure. If the feedback path simply contains a constant gain $i.e.$, if $\varphi(y) = \alpha y$ then the stability of the system, a linear feedback system, can be simply determine by examining the eigenvalues of the closed-loop system matrix. However, the stability analysis of the whole system with an arbitrary nonlinear feedback function φ is much more difficult. In analyzing this kind of system, we usually require the nonlinearity to satisfy circle criterion. The circle criterion has the two conditions which are defined below.

***Condition I**: The nonlinear feedback function φ belongs to the sector $[\alpha, \beta]$.*

A continuous function φ is said to belong to the sector [α, β], if there exist two constant numbers α and β ($\alpha < \beta$) such that

$$\alpha \cdot y^2 \leq y \cdot \varphi(y) \leq \beta \cdot y^2 \tag{3.17}$$

Geometrically, condition (3.17) implies that the nonlinear function always lies between the two straight lines αy and βy as shown in Fig. 3.10a.

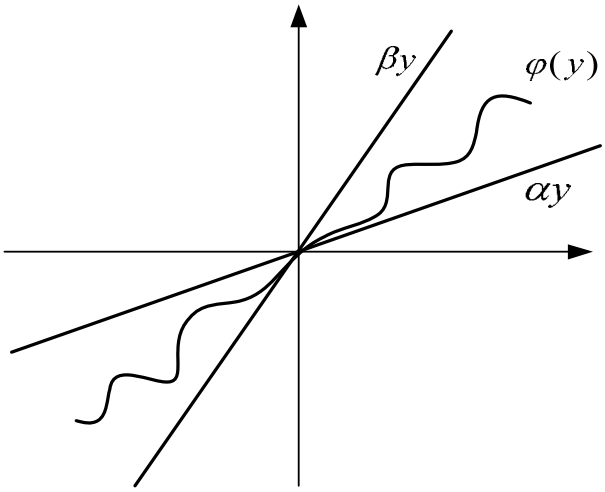

Fig. 3.10a- The sector condition (3.17)

Assume that the nonlinearity φ(y) is a function belonging to the sector$[\alpha, \beta]$, and that the A matrix of the linear subsystem in the forward path is stable$(i.e., Hurwitz)$. What additional constraints are needed to guarantee the stability of the whole system? In view of the fact that the nonlinearity in Fig. 3.10a is bounded by the two straight lines, which correspond to constant gain feedbacks, it may be plausible that the stability of the whole system may have some relation to the stability of constant gain feedback systems.

***Condition II**: The system is absolutely stable if one of the following conditions is satisfied, as appropriate [Khalil]:*

- *If 0< $\alpha < \beta$, the Nyquist plot of the linear system $G(j\omega)$ does not enter the disk $D(\alpha, \beta)$ and encircles it m times in the counterclockwise direction, where m is the number of poles of $G(s)$ with positive real parts.*

- *If 0= $\alpha < \beta, G(s)$ is Hurwitz and the Nyquist plot of the linear system $G(j\omega)$ lies to the right of the vertical line defined by $Re[s] = -1/\beta$.*

- *If $\alpha < 0 < \beta, G(s)$ is Hurwitz and the Nyquist plot of the linear system $G(j\omega)$ lies in the interior of the disk $D(\alpha, \beta)$.*

- *If $\alpha < \beta < 0$, the Nyquist plot of $-G(j\omega)$ does not enter the disk $D(-\alpha, -\beta)$ and encircles it m times in the counterclockwise direction.*

If the sector condition is satisfied only in the interval $[a, b]$ (Fig. 3.10c), then the foregoing conditions ensure that the system is absolutely stable with a finite domain.

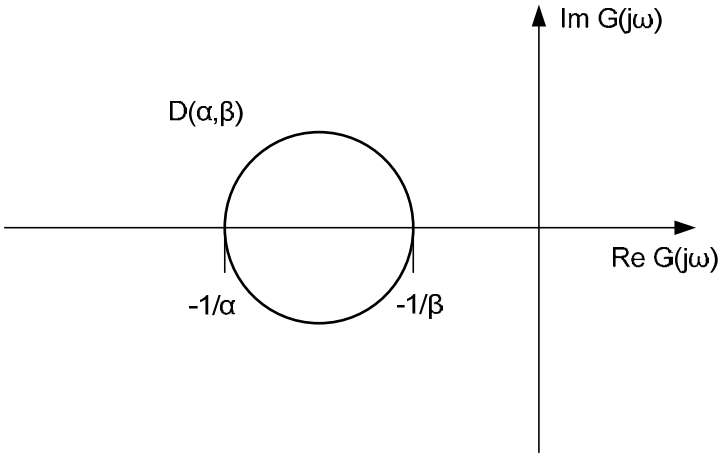

Fig. 3.10b- Disk $D(\alpha, \beta)$

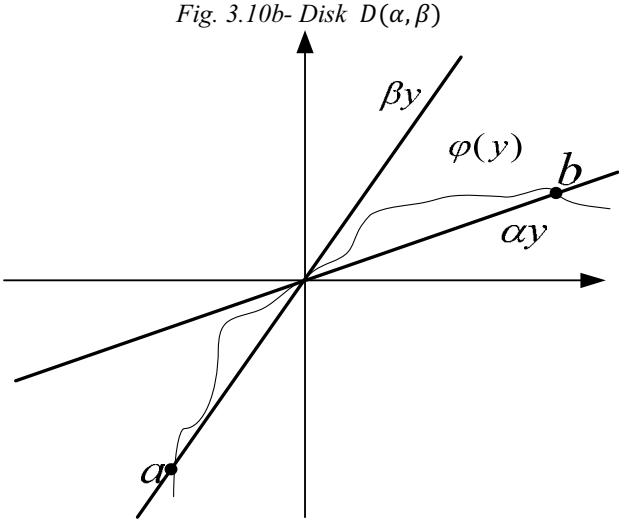

Fig. 3.10c- The sector condition satisfied in the interval [a, b](3.17)

The circle criterion allows investigating absolute stability by using only the Nyquist plot of $G(j\omega)$. This is important because the Nyquist plot can be determined directly from experimental data. Given the Nyquist plot of $G(j\omega)$, we can determine permissible sectors for which the system is absolutely stable.

3.4.1 Stabilization of dc-link variables:

In this section a method for the global stability study of an electrical system containing a DC power supply, an LC Filter and a constant power load is presented. The circle criterion is used to study the absolute stability of the system. In order to stabilize the electrical system, a nonlinear stabilization structure is presented. In the proposed approach, the control structure of the electrical system is slightly modified to implement the nonlinear stabilization structure for improving large signal stability of the system and thus allows reducing the dc-link capacitance value. The efficiency of the proposed nonlinear stabilization structure is evaluated by experimentation on a dc-link supplying an inverter-motor drive load. This inverter-motor drive is

supposed to be tightly controlled in such a manner that the load is simply modeled by a constant power (Fig. 3.3).

The reduced model of the system shown in Fig. 3.3 can be represented as feedback system whose forward path is a linear time-invariant system and the feedback path contains nonlinearity as illustrated in Fig. 3.11. This representation helps us to analyze large signal stability of the whole system (LC Filter and stabilization) using the circle criterion [Khalil]**.** The stabilization approach will be presented later, but here, we should know that it consists of a nonlinear processing of band-pass filtered dc-link voltage.

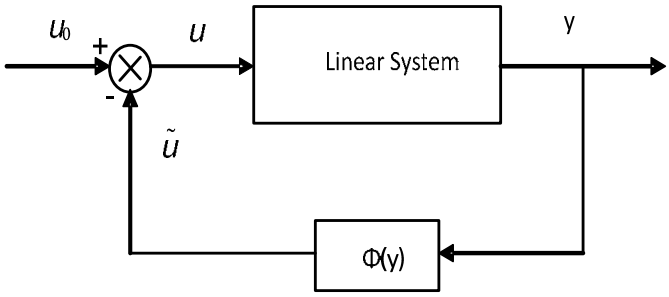

Fig.3.11 System Model.

To study the stability of the model (3.10) around its operating point($\boldsymbol{i_{e0}, v_{s0}}$), it is frequent to move this operating point to the origin by:

$$\begin{cases} \tilde{\imath}_e = i_e - i_{e0} \\ \tilde{v}_s = v_s - v_{s0} \end{cases} \tag{3.18}$$

with:

$$\begin{cases} i_{e0} = \dfrac{V_e - v_{s0}}{r_f} = \dfrac{p_{s0}}{v_{s0}} \\ v_{s0} = \dfrac{V_e + \sqrt{V_e^2 - 4p_{s0}r_f}}{2} \end{cases} \tag{3.19}$$

where p_{s0} is the load power at the operating point ($p_{s0} = v_{s0} \cdot i_{e0}$). The state equations of the linear system are:

$$\frac{d}{dt}\tilde{\imath}_e = -\frac{r_f}{L_f}\tilde{\imath}_e - \frac{1}{L_f}\tilde{v}_s \tag{3.20}$$

$$\frac{d}{dt}\tilde{v}_s = -\frac{1}{C_f}\tilde{\imath}_e + \frac{1}{C_f}u \tag{3.21}$$

$$\frac{d}{dt}x_1 = \omega_{p2}\tilde{v}_s - \omega_{p2}x_1 \tag{3.22}$$

$$\frac{d}{dt}x_2 = \omega_{p1}x_1 - \omega_{p1}x_2 \tag{3.23}$$

$$y = x_1 - x_2 \tag{3.24}$$

Where z_0 corresponds to the value of the variable z in steady state, and ω_{p1} and ω_{p2} are the cut-off frequencies of the band-pass filter. Without loss of generality, the value of the control u_0 is set to 0. The proposed control consists in designing a non linear function $\psi(y)$ so that the linear system in Fig. 3.11 with the control $u = -\psi(y)$ is absolutely stable. Then it is possible to deduce the additional power $\tilde{p}$ which has to be consumed by the load to stabilize the dc-link voltage. This reference power verifies the following relation:

$$u = i_{e0} - \frac{P_0 + \tilde{p}}{v_{s0} + \tilde{v}_s} = -\psi(y)$$
$$\Rightarrow \tilde{p} = v_s.i_{e0} - P_0 + v_s.\psi(y) \tag{3.25}$$

where $P_0 = p_s = cte$ is the absorbed power by the load at its operating point. For the system shown in Fig. 3.11 to be absolutely stable, the system must satisfy the following two conditions:

III. The nonlinearity $\psi(y)$ belongs to the sector [α , β].

IV. One of the following is true.

- *0 < α < β, the Nyquist plot of Linear System does not enter the circle D(α , β).*
- *0 = α < β, the Nyquist plot of Linear System stays in the half plane Re(s) > -1/β.*
- *α < 0 < β, the Nyquist plot of Linear System stays in the interior of the circle D(α , β).*
- *α < β < 0, the Nyquist plot of Linear System does not enter the circle D(α , β).*

The nonlinearity $\psi(y)$ belongs to the sector *[α , β]* if it satisfies the following equation

$$(\psi(y) - \alpha.y).(\psi(y) - \beta.y) \leq 0 \tag{3.26}$$

The above equation implies that our nonlinear function $\psi(y)$ lies between the two straight lines *αy* and *βy* and we have to choose our two slops *α* and *β* such that $\psi(y)$ remains between them. Here, we propose the following equation for $\psi(y)$:

$$\psi(y) = \begin{cases} K \cdot \left(1 - \frac{\delta}{y}\right) \; if \; y > \delta \\ 0 \; if \; |y| \leq \delta \\ K \cdot \left(-1 - \frac{\delta}{y}\right) \; if \; y > -\delta \end{cases} \tag{3.27}$$

By changing the nonlinearity $\psi(y)$, we can actually obtain the additional power $\tilde{p}$ which has to be consumed by the load (3.25). When $|y| \leq \delta$, the nonlinear function $\psi(y) = 0$, which means we are not adding damping for very small variations of v_s (noise, measurement) around the operating point.

The plot of the nonlinear function $\psi(y)$ depends on the value of the gain *K*. Now in order to check the stability of the system, the nonlinear function $\psi(y)$ must satisfy the two conditions of the circle criterion. It should be noted that *K* is to be determined according to the system parameters and the stability requirements, but as we will see, there is always a limitation for the maximum value of *K*. In the following, let us check the stability conditions for different nonlinear functions $\psi(y)$ for different values of *K*.

The plot of the nonlinear function $\psi(y)$ for *K*=3 is shown in Fig 3.12a. For this nonlinear function $\psi(y)$, we have $\alpha = 0$ and a minimum value of β is selected so that the first condition of the circle criterion is satisfied $i.e.$ *"The nonlinearity* $\psi(y)$ *belongs to te sector [*α *,* β*]"*. The value of β for which this nonlinearity $\psi(y)$ respects the sector limits *[*α *,* β*]* and stays between the two straight lines αy and βy is $\beta = 7.5$. Fig 3.12b shows the nonlinear function $\psi(y)$ and slopes α and β.

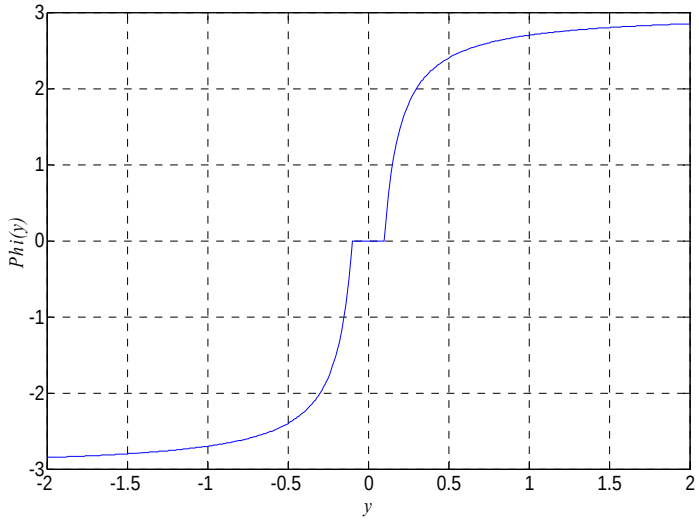

Fig. 3.12a- Nonlinearity $\psi(y)$ *plot for K = 3.*

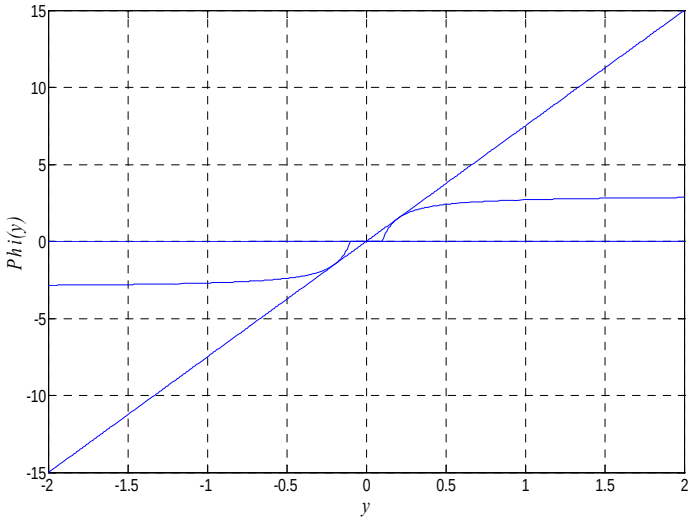

Fig. 3.12b- Nonlinearity $\psi(y)$ plot for K = 3 with sector limits.

In order to avoid the dc-bus voltage oscillation and hence to stabilize the dc-link, the system must satisfy the second condition as $\alpha = 0$; *i.e.* the Nyquist plot of the linear system (3.20)-(3.24) stays in the half plan *Re(s)* > -1/*β*=-1/7.5. The Nyquit plot of the linear system is shown in Fig. 3.13a. The zoomed version of the Nyquist plot is shown in Fig. 3.13b. It is shown in Fig. 3.13b that the Nyquist plot crosses the line *Re(s)*=-1/*β*=*-1/7.5*, which does not prove the stability.

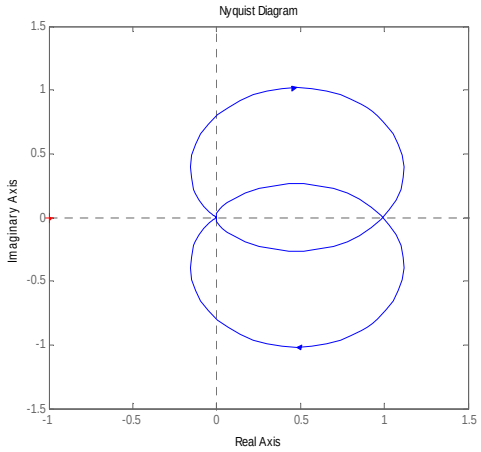

Fig. 3.13a- Nyquist plot of linear system (3.8)-(3.12) with parameters in Table I

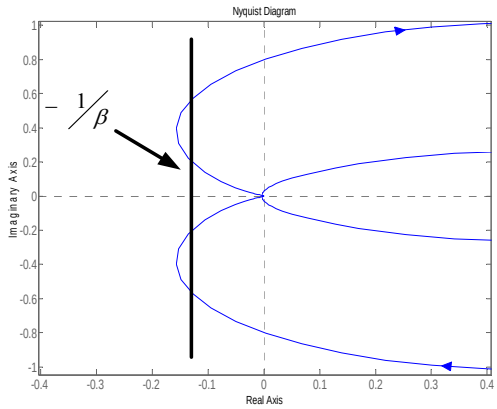

Fig. 3.13b- Nyquist plot of linear system and stability limit with K =3.

Now if we go reverse and first find the maximum value of β_{max} for which the system satisfies the second condition *i.e.* the Nyquist plot of the linear system (3.20) - (3.24) stays in the half plan $Re(s) > -1/\beta_{max}$. The Nyquist plot of the linear system is shown in Fig 3.14. From this figure, the maximum value of β_{max} for which the Nyquist plot of the linear system (3.20)-(3.24) stays

in the half plan $Re(s) > -1/\beta_{max}$ is $\beta_{max} = 6.25$. Fig 3.15 shows that for this value of β_{max}, the plot of nonlinear function $\psi(y)$ for $K = 3$ does not satisfy the first condition of circle criterion and it crosses the limit $\beta_{max} y$ which means our system is not stable.

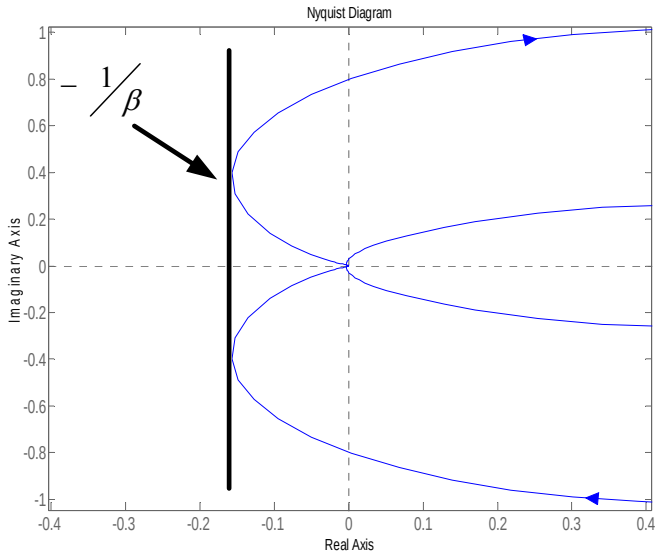

Fig. 3.14- Nyquist plot with maximum value of β to satisfy 2nd condition of circle criterion

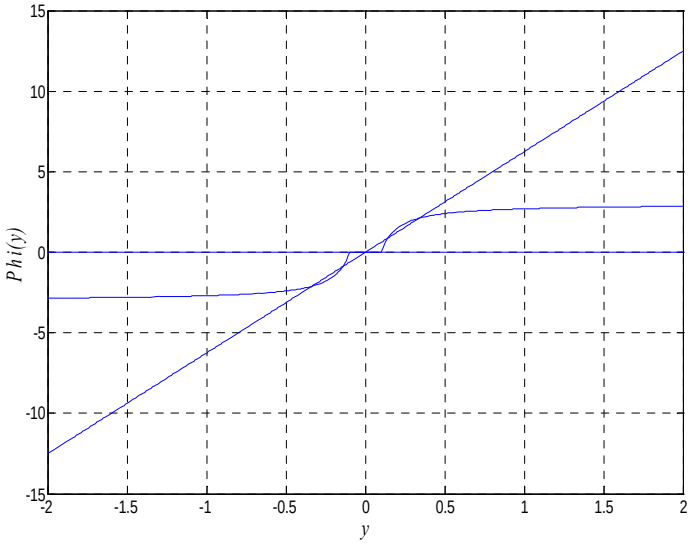

Fig. 3.15- Nonlinearity $\psi(y)$ plot for K = 3 and $\beta_{max} = 6.25$.

So, we have to limit K to $K_{max} = 4\delta\beta_{max}$ which is equal to 2.5 in our system. Now we modify our nonlinearity by changing the value of K to 1. The plot of nonlinearity $\psi(y)$ for K=1 is shown in Fig. 3.16. For this nonlinear function the sector limits are: α = 0 and β = 3. By changing the

nonlinearity $\psi(y)$, we are actually changing the additional power $\tilde{p}$ which has to be consumed by the load (3.25). Fig. 3.17 shows that the Nyquist plot of the linear system does not cross the line *Re(s)* = -1/β = -1/3. So both the conditions for the circle criterion are satisfied *i.e. The nonlinearity* $\psi(y)$ *belongs to the sector [*α *,* β*] with 0 =* α *<* β*, and the Nyquist plot of the linear system stays in the half plane Re(s) > -1/*β*.* So our system is stable.

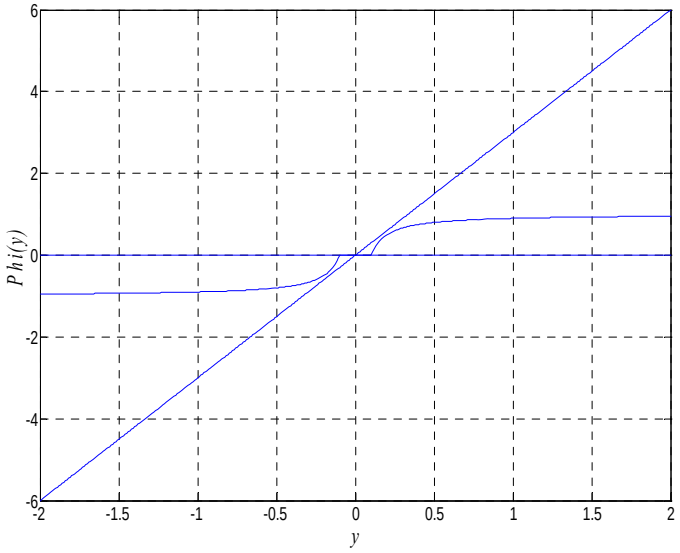

Fig. 3.16- Nonlinearity Φ(y) plot for K =1.

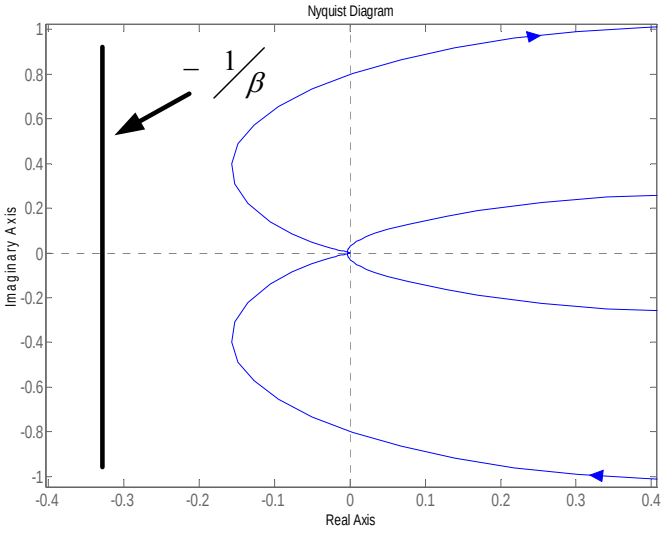

Fig. 3.17- Nyquist plot of linear system and stability limit with K =1

Maximum value of K:

From (3.27) for $y > \delta$

$$\psi(y) = K\left(1 - \frac{\delta}{y}\right)$$

As we know that in order to prove stability the nonlinearity $\psi(y)$ must respect the sector limits and must remain between two straight lines αy and βy.

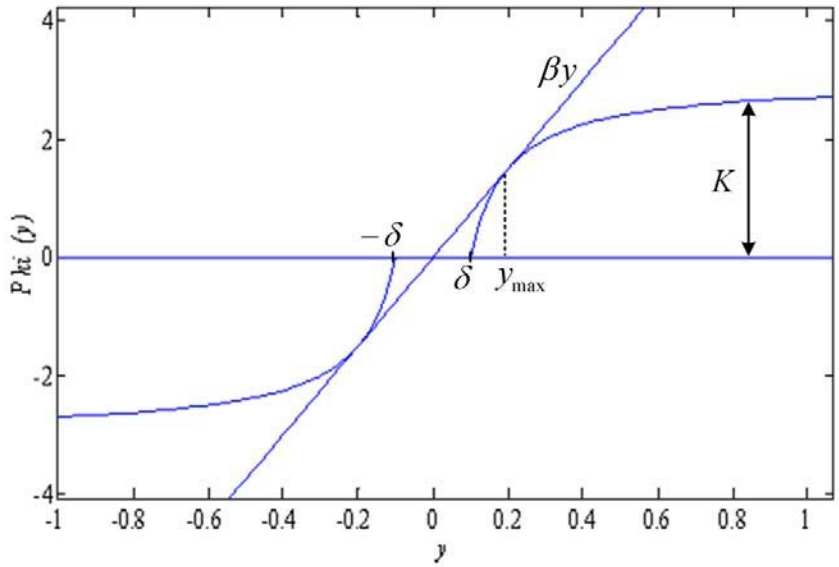

Fig. 3.18- Nonlinearity $\psi(y)$ plot for K_{max}

Let us define a function $x(y)$

$$x(y) = K\left(1 - \frac{\delta}{y}\right) - \beta y \tag{3.28}$$

$x(y) = 0$ at the point where slop βy and nonlinearity $\psi(y)$ have the same value. This is the maximum point up till where the nonlinearity $\psi(y)$ can grow before crossing the sector limit.

$$\left(\frac{dx(y)}{dy}\right)_{max} = 0$$

From (3.28)

$$\frac{K\delta}{{y_{max}}^2} - \beta = 0$$

$$y_{max} = \sqrt{K\delta/\beta}$$

$$x(y_{max}) = 0$$

As y_{max} is the point where the nonlinear function $\psi(y)$ has the maximum value before crossing the sector limit (violating the circle criterion condition) and as our nonlinear function $\psi(y)$ is directly proportional to gain K, so, K_{max} is the maximum value of gain for this method of stability. From (3.28)

$$K\left(1-\frac{\delta}{y_{max}}\right)-\beta y_{max}=0$$

$$\Rightarrow \qquad K_{max}=4\delta\beta_{max} \tag{3.29}$$

3.4.1.1 *Stabilization Block:*

Fig. 3.19 illustrates the block diagram of the proposed dc-link stabilization technique (see equation (3.25)). The proposed approach is applied to an inverter-PMSM drive system.

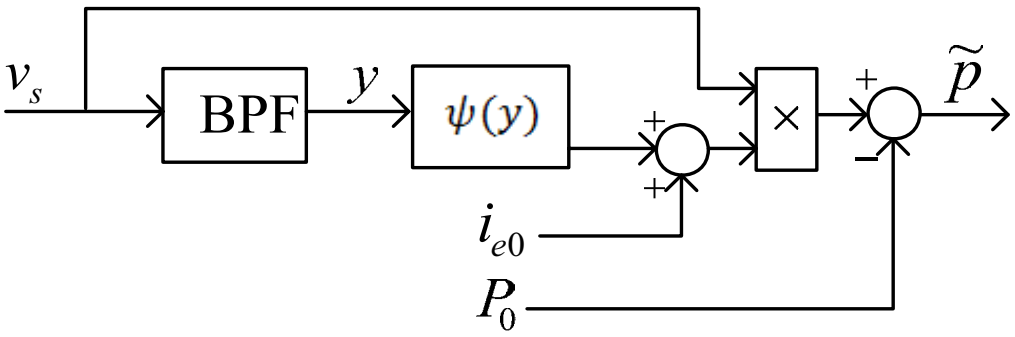

Fig. 3.19- DC-link voltage oscillation compensation structure.

The absorbed drive power (P_0) is calculated from *dq* currents (i_d and i_q) and reference voltages (v_d and v_q). The dc-link current at the operating point (i_{e0}) is obtained as follows:

$$i_{e0}=\frac{P_0}{v_{s0}} \tag{3.30}$$

And finally, the voltage operating point dc-link voltage (v_{s0}) is obtained by filtering the dc-link voltage (v_s) by a narrow band low-pass filter. Then, to realize the power compensation signal ($\tilde{p}$), we transformed it to a torque reference. Then, the latter is added to the usual motor torque reference (output of the speed controller or the torque controller) for obtaining the actual motor torque reference. This allows us to properly modify the absorbed power and to stabilize the dc-link. This stabilization technique improves the stability of the system and thus, it permits to decrease the size of the dc-link capacitance.

For efficient damping of the dc-link oscillations, the first cut-off frequency (ω_{p1}) of the band-pass filter should be sufficiently smaller than the LC-filter resonance frequency:

$$\omega_{p1} << \omega_0 = \frac{1}{\sqrt{L_f C}} \tag{3.31}$$

The second cut-off frequency (ω_{p2}) has to be chosen according to the measurement noises and unmodeled fast dynamics. It is usually much higher than (ω_{p1}).

3.4.1.2 *Simulation Results:*

The effect of this oscillation compensation technique can be verified by simulation. By choosing optimal gain *K* for the nonlinear function $\psi(y)$, the stabilization structure gives the maximum stability margin/minimizes the dc-link capacitance size. A Simulink model, based on (3.20)-(3.24) and (3.27), is developed. Its parameters are given in Table 4.I.

Fig. 3.20 shows the simulation results for a *q-current* step under the same conditions as in the previous test (Fig. 3.4) but after activating the nonlinear compensation structure (see Fig. 3.19). The results confirm the efficiency of our stabilization technique. Indeed, it can be seen that the dc-link voltage (v_s) is no more unstable when the same *q-current* step is applied.

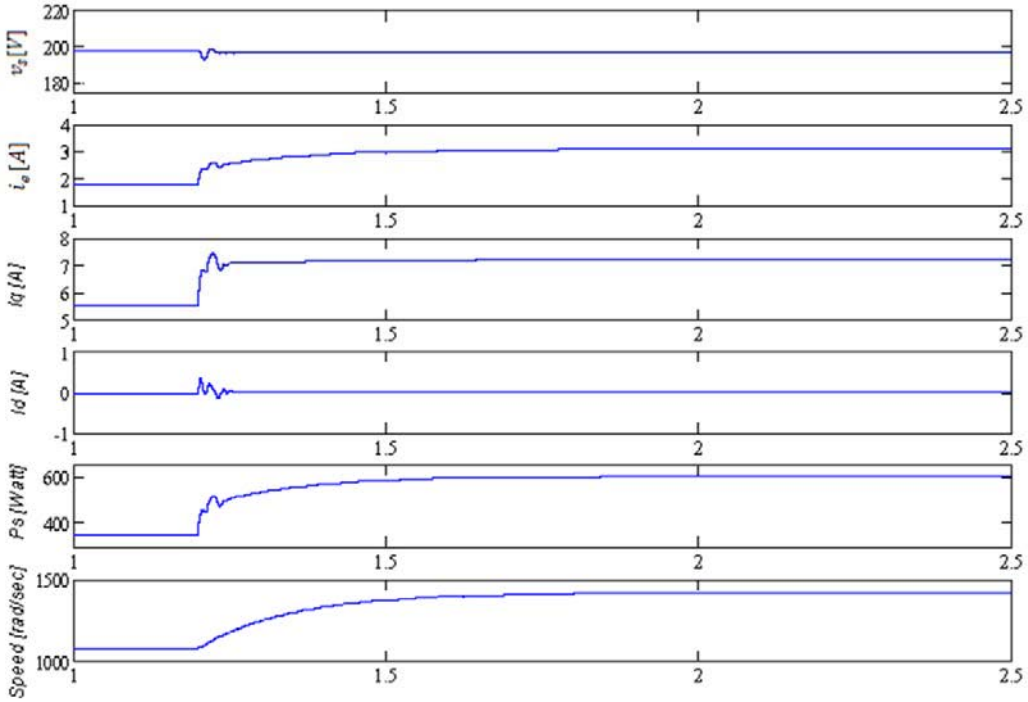

Fig. 3.20- Stabilization of dc-link voltage variations for K=1 after a q-current step.

Fig. 3.21 shows the simulation results for the same speed step test as in Fig. 3.5 after activation of our nonlinear oscillation compensation structure (Fig. 3.19). The results confirm the efficiency of the proposed stabilization technique.

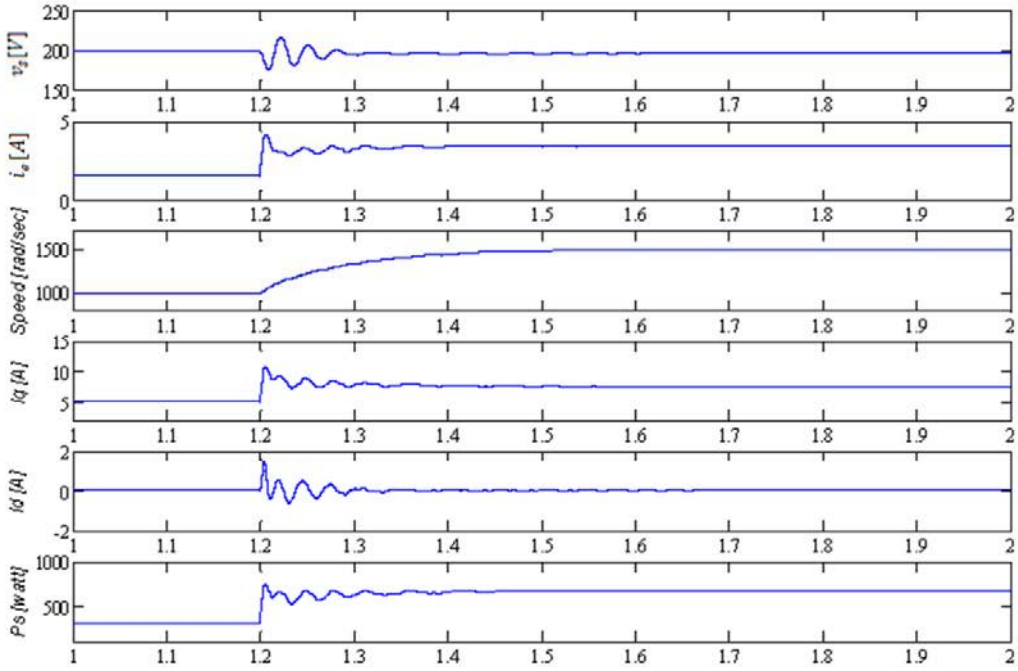

Fig. 3.21- Stabilization of dc-link voltage variations for K= 1 after a speed step.

Fig. 3.22 shows the simulation result for the case when oscillation compensation structure is activated in the binning but it is turned off later on. It is evident from Fig. 3.22 that the dc-link variables are stable after a *q*-current step when the oscillation compensation structure is active and these dc-link variables oscillate and become unstable as soon as the oscillation compensation block is turned off which proves the efficacy of the proposed stabilization approach.

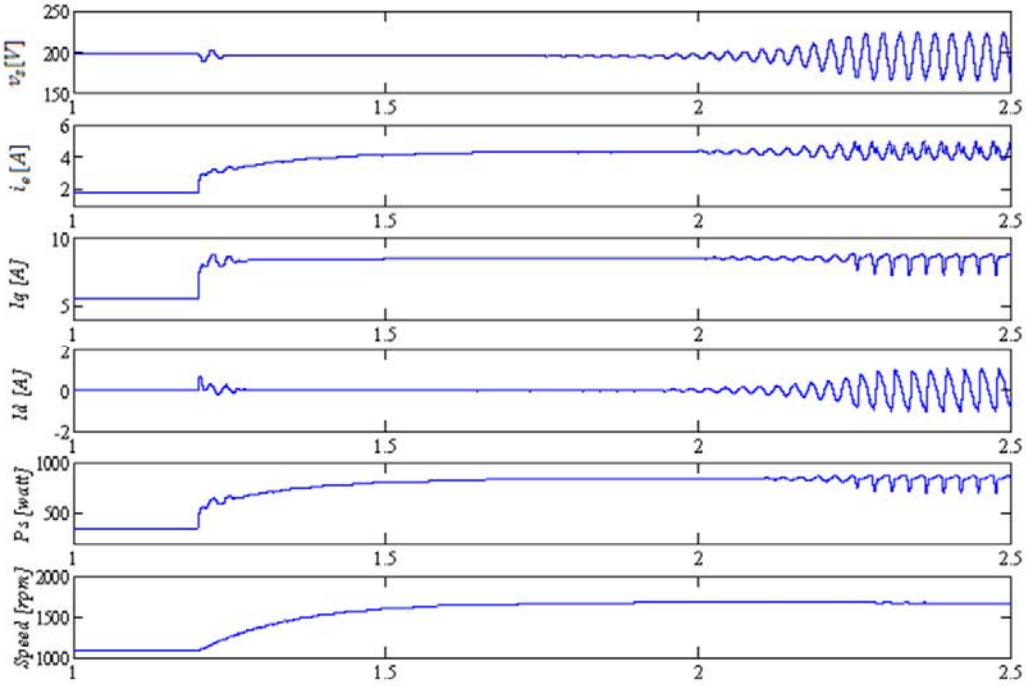

Fig. 3.22- Stabilization block switch on to switch off test.

Now in order to show the effect of the gain K on the stabilization effort and to verify the maximum limit of K, we present some simulation results with a constant power load. A simulation model based on (3.20) to (3.24) and (3.27) is developed and its perameters are given in Table 4.I.

Fig. 3.23 shows the simulation results without oscillation compensation block. It can be seen that the dc-link voltage variations ($\tilde{v}_s$) and the dc-link current variations ($\tilde{\imath}_e$) are no more stable when a power step from $400W$ to $600W$ is applied. The stabilizing power *Ptilt* ($\tilde{p}$) is zero. After activating the oscillation compensation block with gain $K = 1$, we obtain the simulation results shown in Fig. 3.24. From this figure, it is evident that when the power step is applied the stabilization block comes into action and provides an additional power *Ptilit* ($\tilde{p}$) which has to be consumed by the load to stabilize the system. So, the dc-link variables are stable before and after the load power step. Fig. 3.25 shows the simulation results for oscillation compensation gain $K = 2$. Some high frequency oscillations are quit visible around the transition point but they become stable. Fig. 3.26 shows the simulation results for oscillation compensation gain $K = 2.5$, which is the maximum value of oscillation compensation gain K after that the stability of the system is no more ensured.

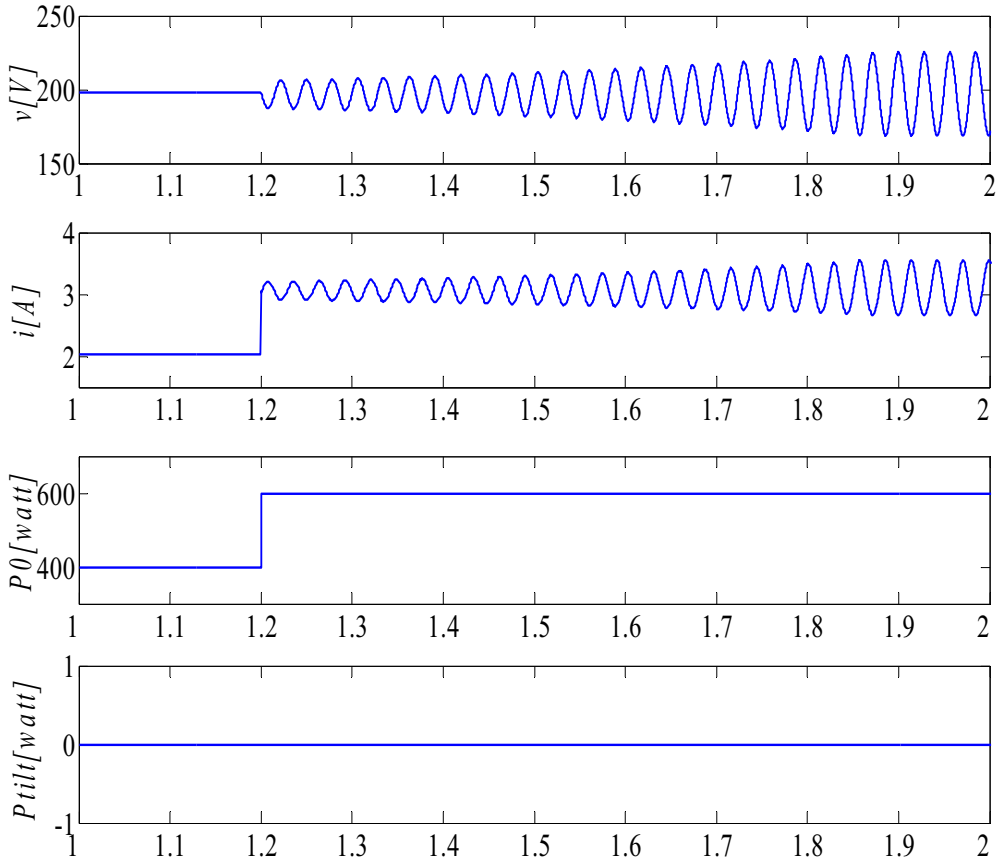

Fig. 3.23- Simulation results with a constant power load after a power step without stabilization block.

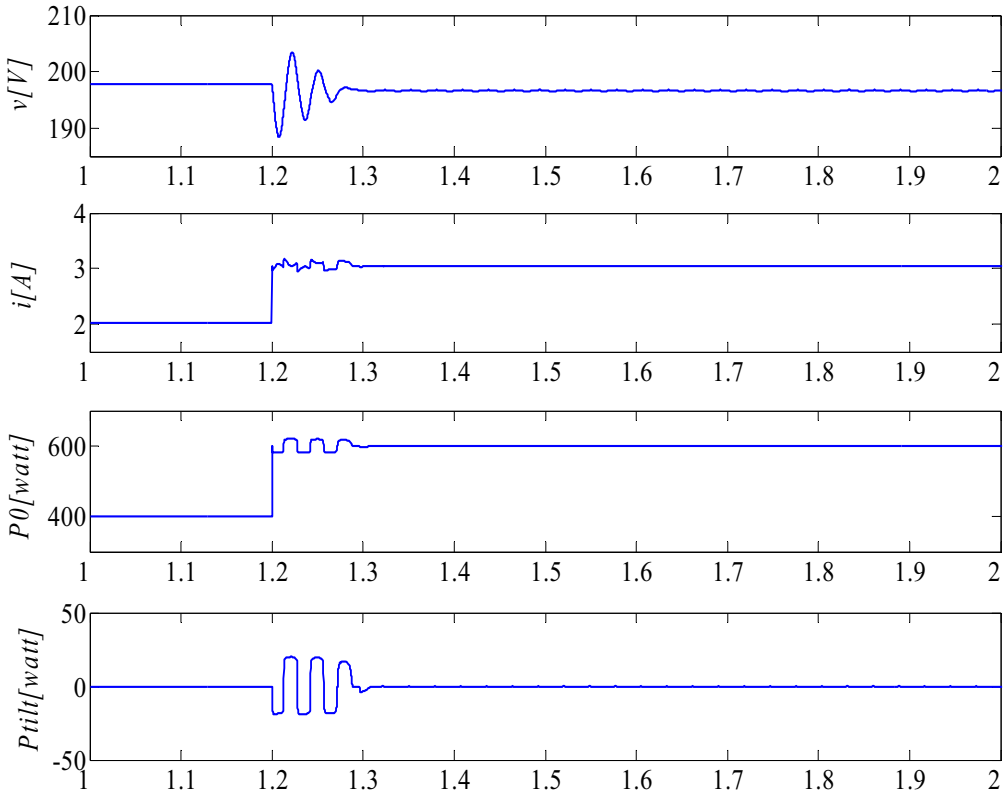

Fig. 3.24- Simulation results with a constant power load after a power step with stabilization block (K=1).

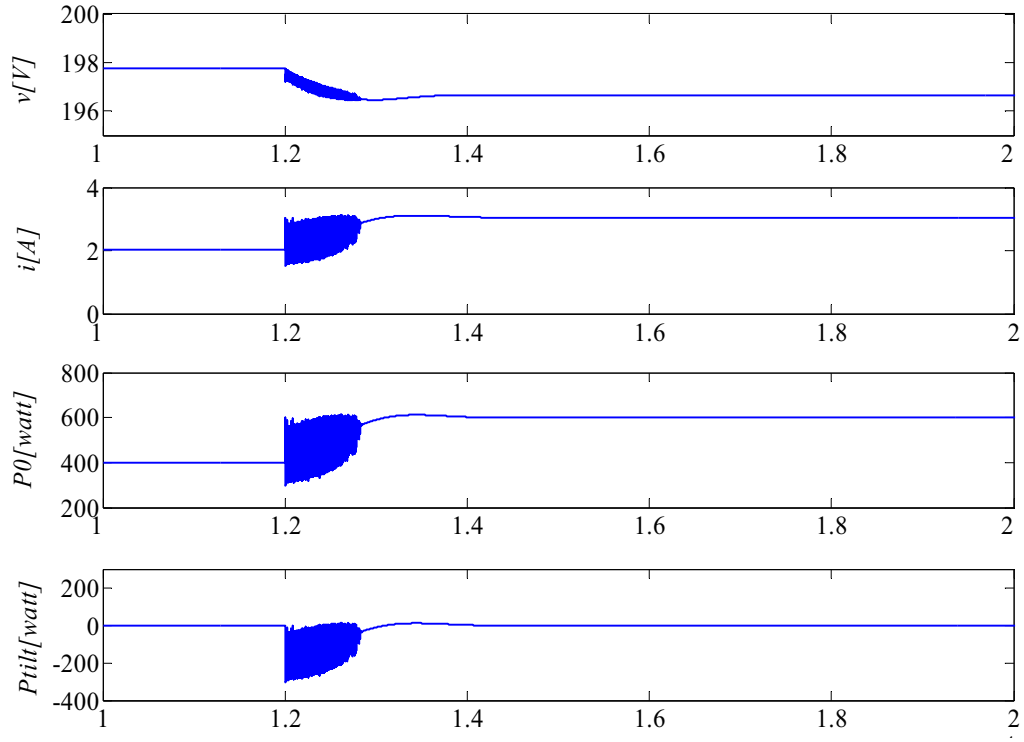

Fig. 3.25- Simulation results with a constant power load after a power step with stabilization block (K=2).

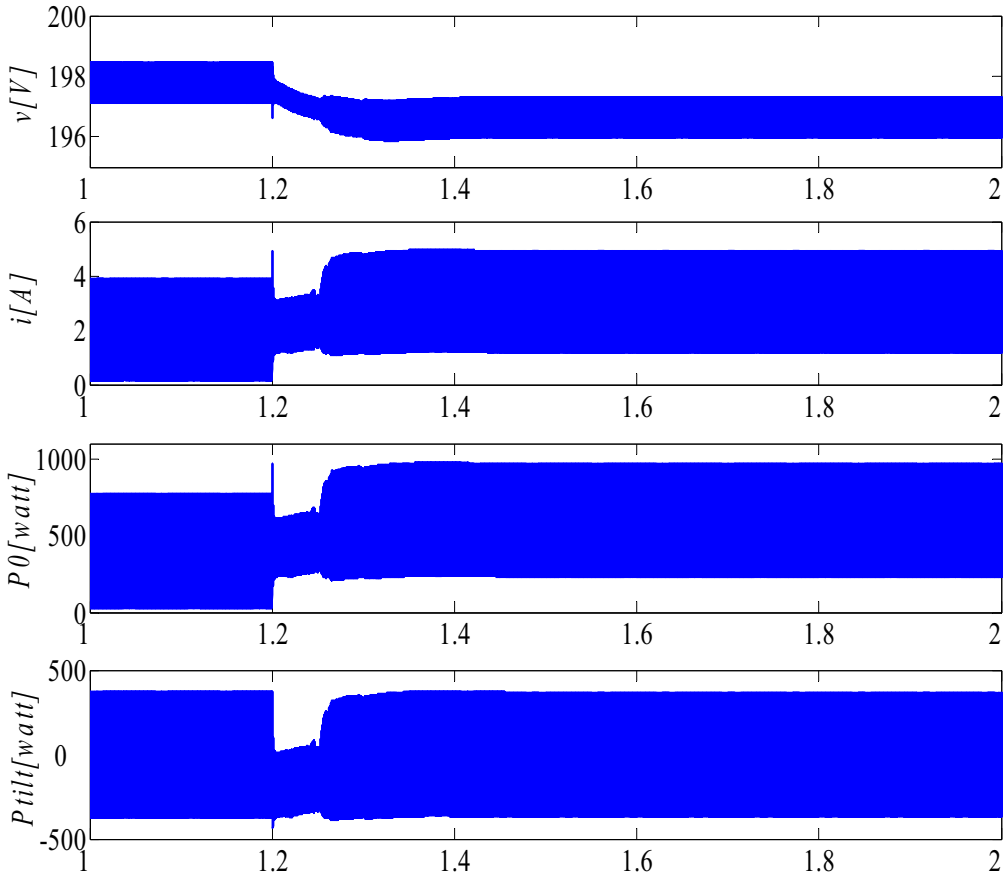

Fig. 3.26- Simulation results with a constant power load after a power step with stabilization block (K=2.5).

3.4.2 Another Example of Nonlinear feedback function $\psi(y)$:

For the nonlinear feedback function $\psi(y)$ described in section 3.4.1 (3.27), there is a dead zone around $y = 0$; *i.e.* $\psi(y) = 0$ when $|y| \leq \delta$. Consequently, the stabilizer does not compensate the dc-link voltage small variations (noise, measurement). However, one may try to damp these variations. To do that, we propose in this section another nonlinear function $\psi(y)$ for which $\psi(y) \neq 0$ when $|y| \leq \delta$. The objective is to make the dc-link variables smoother and more stable. Let us call this nonlinear function as $\psi 1(y)$. Here, we propose the following equation for $\psi 1(y)$:

$$\psi 1(y) = \begin{cases} K \cdot \left(1 - \frac{\delta}{y}\right) + c \quad if\ y > \delta \\ ay\ if\ |y| \leq \delta \\ K \cdot \left(-1 - \frac{\delta}{y}\right) - c\ \ if\ y > -\delta \end{cases} \tag{3.32}$$

With $c = a\,\delta$

Where we put arbitrarily $a = 0.1 \cdot \frac{K}{\delta}$. It is obvious that other choices for a are possible.

The plot of the nonlinear function $\psi 1(y)$ for *K*=1 is shown in Fig 3.27. This figure shows that the minimum value of the sector limits for this nonlinear function may be fixed to $\alpha = 0$ and $\beta = 3$.

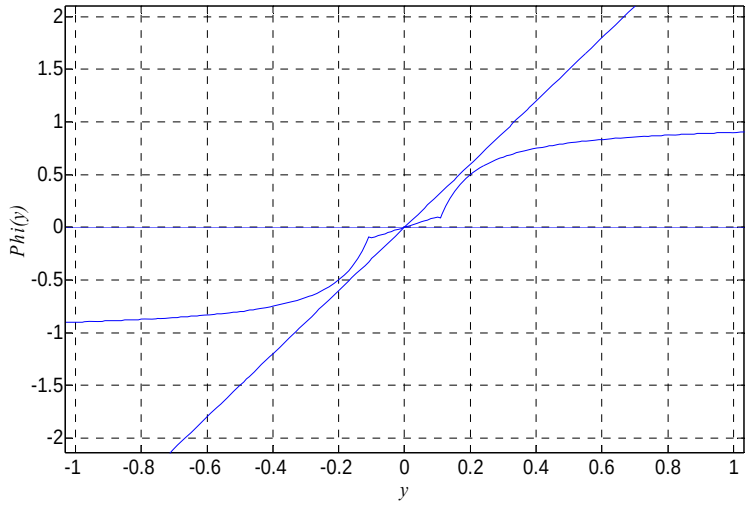

Fig. 3.27- Nonlinearity $\psi 1(y)$ plot for K = 1 with sector limits.

Maximum value of K:

From (3.32) for $y > \delta$

$$\psi 1(y) = K\left(1 - \frac{\delta}{y}\right) + c$$

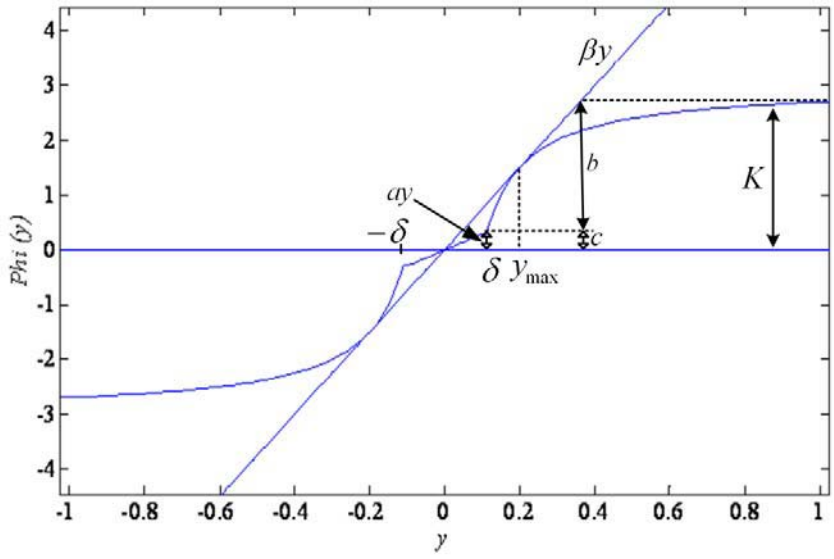

Fig. 3.28- Nonlinearity $\psi 1(y)$ plot for K_{max}

Let us define a function $x(y)$

$$x(y) = \psi 1(y) - \beta y = K\left(1 - \frac{\delta}{y}\right) + c - \beta y$$

$x(y) = 0$ at the point where the line βy and the nonlinearity $\psi 1(y)$ have the same value. This is the maximum point up till where our nonlinearity $\psi 1(y)$ can grow before crossing the sector limit.

$$\left(\frac{dx(y)}{dy}\right)_{max} = 0$$

$$\Rightarrow \quad \frac{K\delta}{{y_{max}}^2} - \beta = 0$$

$$y_{max} = \sqrt{K \cdot \delta / \beta}$$

As y_{max} is the point where the nonlinear function $\psi(y)$ has the maximum value before crossing the sector limit (violating the circle criterion condition) and as our nonlinear function depends on the gain K, so this is a maximum value of gain K_{max} which can be obtained with the relation:

$$K_{max}\left(1 - \frac{\delta}{y_{max}}\right) + \mathrm{a}\,\delta - \beta y_{max} = 0 \qquad (3.33)$$

3.4.3 Comparison between two nonlinear feedback functions $\psi(y)$ and $\psi 1(y)$:

Fig. 3.29 shows a comparison between the dc-link voltage variations for the two nonlinear functions $\psi(y)$ and $\psi 1(y)$. As expected, the simulation results show that for $\psi(y)$ we are not adding daming for the small variations around operating point and there is a dead zone around the operating point, so there are some ripples which apper after the load power step. But with the second nonlinear function $\psi 1(y)$, a damping is added even for the small variations around the operating point, so the dc-link voltage is very smooth after the load power step. In the case of the second nonlinear function $\psi 1(y)$, we are always modifying the I_q current and the load power. Therefore, the second nonlinear function $\psi 1(y)$ makes the dc-link voltage more stable but increases the stabilization efforts. Another advantage of this function lies in the fact that its behavior around the operating point is linear. Therefore, the function $\psi 1(y)$ can be replaced by a linear function around $y = 0$ ($\psi 1(\tilde{y}) \cong a\tilde{y}$) for a small signal analysis. When designing the oscillation compensation block, the choice between the two nonlinear functions $\psi(y)$ and $\psi 1(y)$ depends on the trade-off between more stable dc-link voltage or less stabilizing power delivered by the load.

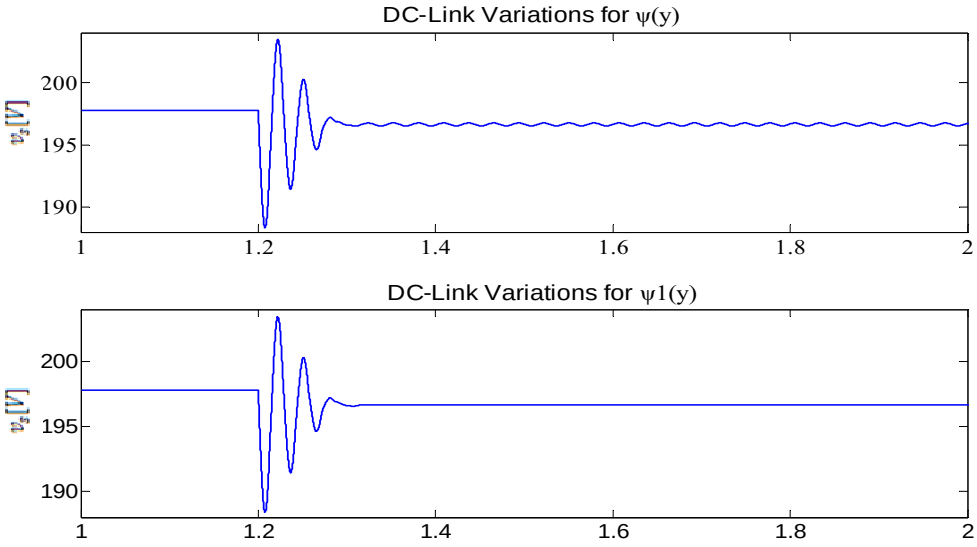

Fig. 3.29- Comparison of two feedback nonlinear functions

3.4.4 Experimental Validation:

The performance and the efficiency of the proposed stabilizer is validated by different tests performed on our experimental bench. In the first test, the oscillation compensation block is activated with K = 0.1. The oscillation compensation block cut-off frequencies are fixed to $\omega_{p1} = 100rad/s$ and $\omega_{p2} = 600rad/s$. Other parameters are kept constant (C=500μF, t_f =1ms). Results in Fig. 3.30 show that the dc-link voltage variations and dc-link input current (which were unstable (Fig. 3.6)) are no more unstable when the *q-current* step is applied.

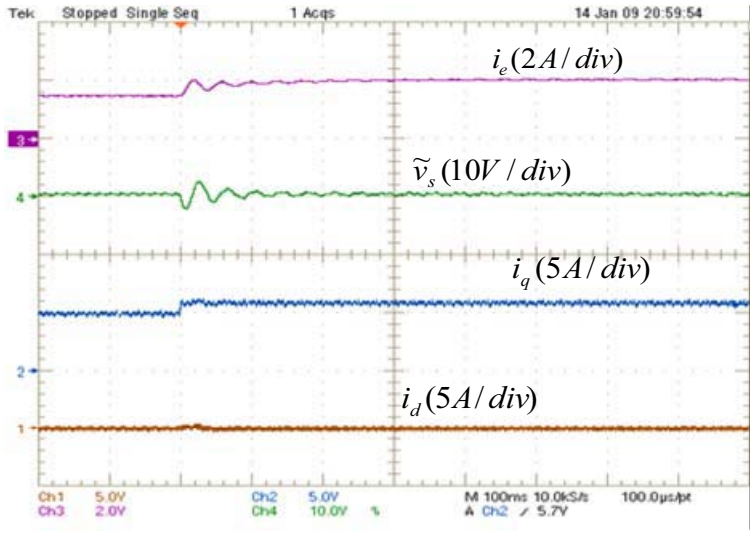

Fig. 3.30- Stabilization of dc-link voltage variations ($\tilde{v}_s$) and dc-link current (i_e) with a q-current step (C_f =500μF, t_f =1ms, K=0.1).

In the second test, the effect of the oscillation compensation technique is studied when the speed step is applied. In this test, the oscillation compensation block is activated with K=0.1 (Fig 3.31).The results in Fig 3.31 show that the system which was unstable without oscillation compensation block (Fig. 3.7) becomes stable by adding a nonlinear oscillation compensation block.

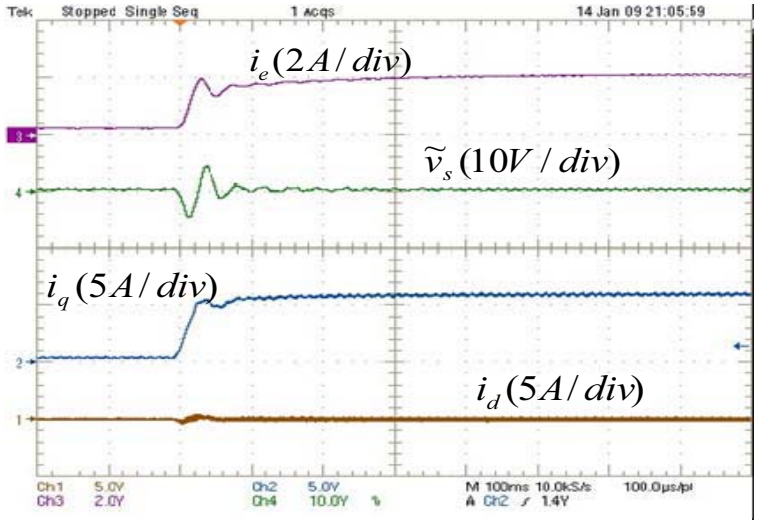

Fig. 3.31- Stabilization of dc-link voltage variations ($\tilde{v}_s$) and dc-link current (i_e) after a speed step (C_f =500µF, t_f =1ms, K=0.1).

3.5 SECOND METHOD OF STABILIZATION BASED ON VIRTUAL RESISTANCE:

This section addresses the global stability study of an electrical system shown in Fig. 3.1. Here, we suppose that the drive control performances are satisfactory. Particularly, it is assumed that the current loop dynamics is sufficiently high. As it was claimed earlier in this chapter, this assumption allows modelling the inverter-motor drive system in its worst case from the stability point of view, *i.e.* a constant power load.

3.5.1 DC-Link Voltage Stabilization:

At first, we remind that

$$\begin{cases} \tilde{\imath}_e = i_e - i_{e0} \\ \tilde{v}_s = v_s - v_{s0} \end{cases} \tag{3.34}$$

Then, from (3.34) and (3.18), the model of the system can be written as follows:

$$\begin{cases} \frac{d}{dt}\tilde{\imath}_e = \dfrac{-r_f}{L_f}\cdot\tilde{\imath}_e - \dfrac{1}{L_f}\cdot\tilde{v}_s \\ \frac{d}{dt}\tilde{v}_s = \dfrac{1}{C}\cdot\tilde{\imath}_e + \dfrac{p_{s0}}{Cv_{s0}}\cdot\dfrac{\tilde{v}_s}{\tilde{v}_s + v_{s0}} - \dfrac{1}{C}\cdot\dfrac{u}{\tilde{v}_s + v_{s0}} \end{cases} \tag{3.35}$$

In this model, the load power p_s is replaced by the following:

$$p_s = p_{s0} + u \tag{3.36}$$

where u is the stabilizing power coming from the stabilization block. To stabilize the dc-link variables, we propose that the stabilizing power u is deduced from U defined by the following stabilization law:

$$U = K \cdot v_s^2 \tag{3.37}$$

in which K is the design parameter to be defined for stabilizing the system (3.35). Indeed, this stabilization law injects damping into the system and makes undamped oscillations disappear. This method creates a virtual resistance in parallel with the dc-bus capacitor (see Fig. 3.32). Impedance Z is equal to $1/K$ where K is the desired virtual conductance. Kv_s^2 corresponds to a dissipative power. Knowing that this damping is only necessary around the operating point, it should be followed by a high-pass filter for removing its dc component due to the dc-link voltage. In practice, it is preferable to put a band-pass filter for rejecting high frequency noises. This leads to:

$$\begin{cases} \frac{d}{dt}x_1 = 2Kv_{s0}\omega_1\cdot\tilde{v}_s - \omega_1\cdot\ x_1 + K\omega_1\cdot{\tilde{v}_s}^2 \\ u = 2Kv_{s0}\cdot\tilde{v}_s - x_1 + K\cdot{\tilde{v}_s}^2 \end{cases} \tag{3.38}$$

for a first-order high-pass filter and to :

$$\begin{cases} \frac{d}{dt}x_1 = 2Kv_{s0}\omega_1\cdot\tilde{v}_s - \omega_1\cdot\ x_1 + K\omega_1\cdot{\tilde{v}_s}^2 \\ \frac{d}{dt}x_2 = 2Kv_{s0}\omega_2\cdot\tilde{v}_s - \omega_2\cdot\ x_1 - \omega_2\cdot\ x_2 + K\omega_2\cdot{\tilde{v}_s}^2 \\ u = x_2 \end{cases} \tag{3.39}$$

for a band-pass filter.

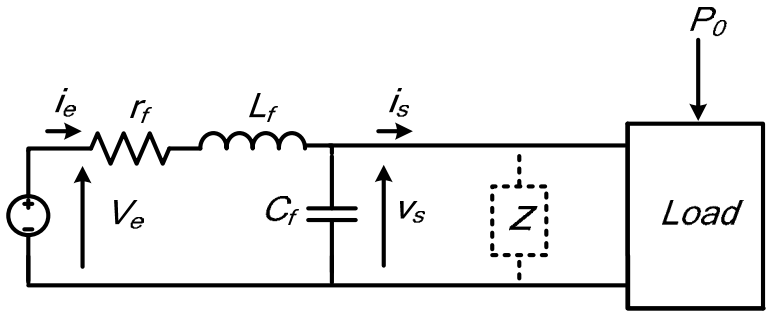

Fig. 3.32: Introduction of the parallel impedance on the DC bus.

The proposed stabilization block is shown in Fig. 3.33. It should be noted that an additional low-pass filter may be added to the stabilization block for improving noise rejection and avoiding the excitation of unmodeled fast dynamics if necessary.

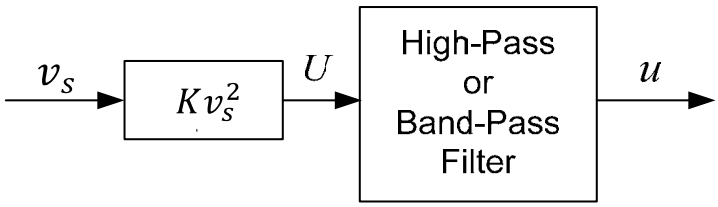

Fig. 3.33- DC-link stabilization law.

It is supposed here that the load power at the operating point p_{s0} does not satisfy the (3.11).

$$p_{s0} > p_{smax} = \frac{r_f C}{L_f} v_{s0}^2 \tag{3.40}$$

This implies that the uncompensated system ($u = 0$) is unstable at the operating point. To illustrate it, Fig. 3.34 shows the phase plane of the system (3.35) without compensation ($u = 0$). The parameters of the system are the same as those of the experimental bench and given in Table 4.I. The initial state is close to the operating point and it is fixed at the following according to the given parameters:

$$\begin{cases} i_{e0} = 4.1\ A \\ v_{s0} = 195.5\ V \end{cases} \tag{3.41}$$

Here, we have:

$$p_{s0} = 800\ W > p_{smax} \cong 540\ W$$

It can be seen in the Fig. 3.34 that the system trajectories do not converge to the operation point, which means the uncompensated system is unstable.

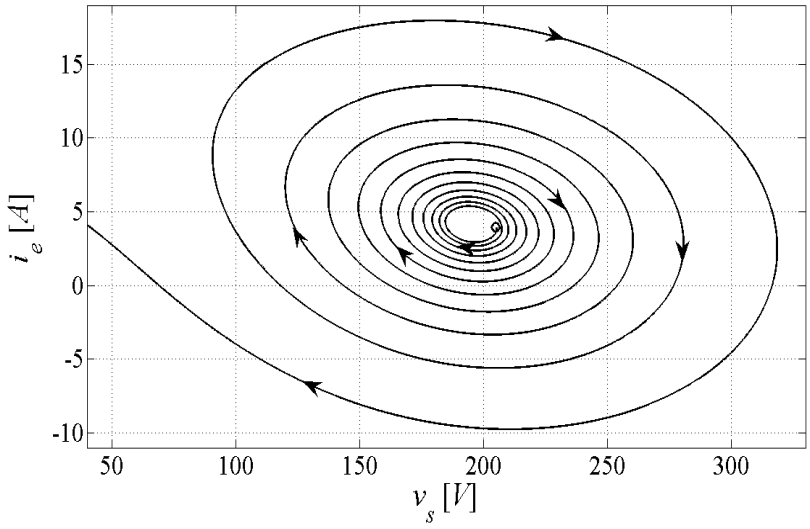

Fig. 3.34- Phase plane of the model (3.35) without compensation ($u = 0$)

It should be noted that in practice, the source current $\boldsymbol{i_e}$ is often nonnegative because of the diode bridge (Fig. 1). Consequently, the system trajectories converge to a limit cycle as shown in Fig. 3.35. Any case, the operating point is not stable and the state variables oscillate.

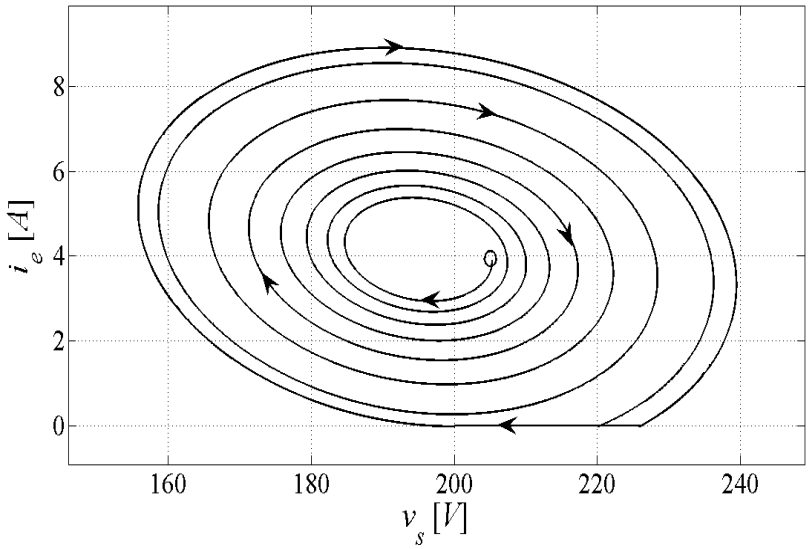

Fig. 3.35- Phase plane of the model (3.35) with $i_e \geq 0$ (without compensation).

To determine the stabilization gain K, a Lyapunov based stability analysis is made. The model of the closed-loop system (model (3.35) + compensator (3.38)) can be written as follows:

$$\frac{d}{dt}x = A_c \cdot x + f(x) \qquad (3.42a)$$

with: $x = [\tilde{\imath}_e \quad \tilde{v}_s \quad x_1]^T$

$$A_c = \begin{bmatrix} \frac{-r_f}{L_f} & \frac{-1}{L_f} & 0 \\ \frac{1}{C} & \frac{-K}{C} & 0 \\ 0 & 2Kv_{s0}\omega_1 & -\omega_1 \end{bmatrix} \tag{3.42b}$$

$$f(x) = \begin{bmatrix} 0 \\ \frac{p_{s0} - Kv_{s0}^2}{Cv_{s0}} \cdot \frac{\tilde{v}_s}{\tilde{v}_s + v_{s0}} + \frac{1}{C} \cdot \frac{x_1}{\tilde{v}_s + v_{s0}} \\ K\omega_1 \cdot {\tilde{v}_s}^2 \end{bmatrix} \tag{3.42c}$$

The stability analysis shows that the origin ($\tilde{\imath}_e = \tilde{v}_s = x_1 = 0$) is a globally asymptotically stable equilibrium point for the system (3.42) if the first cut-off frequency $\omega_1 \ll \omega_0 = \frac{1}{\sqrt{L_f C}}$ and:

$$K > K_{min} > 0 \tag{3.43}$$

The mathematical proof of stability and the expression of K_{min} are given in Appendix II. Fig. 3.36 illustrates the system trajectories on $v_s - i_e$ plane with:

$$K = 0.1 > K_{min} \cong 0.023$$

Obviously, all of the trajectories converge asymptotically to the desired operating point given in (3.41).

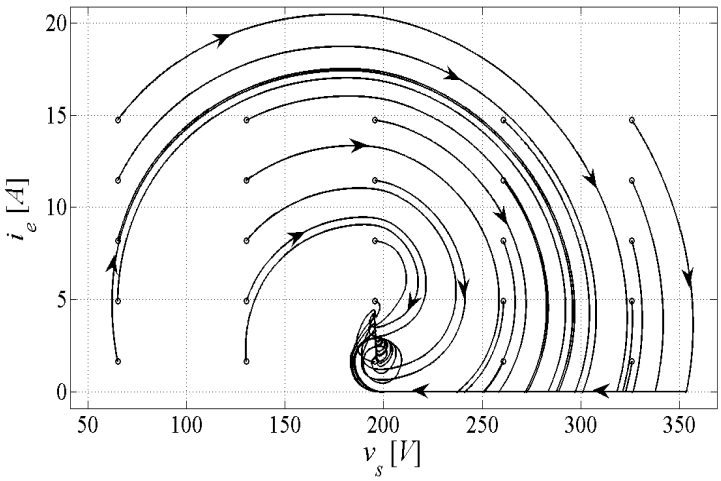

Fig. 3.36- State trajectories of the model (3.35) with the proposed compensation in (3.38) with $K = 0.1$ *and* $\omega_1 = \omega_0/10$ *(o: ini0tial point).*

It should be noted that in the above analysis, the dc-link variables are not limited to positive values. But in practice, as mentioned earlier, the source current i_e is often positive. Taking into account this fact, a small region will be created around the point ($v_s = 0, i_e = 0$) in which

beginning trajectories don't converge to the desired operating point. But in this case, there is no power delivered to the load and so the hypothesis on the constant load power is no more valuable. In addition, the dc-link voltage v_s in this region is likely insufficient for ensuring the controllability of the load and so, the load cannot be considered as constant power.

Figs. 3.37 and 3.38 show the system trajectories on $v_s - i_e$ plane with $K = 1$, $\omega_1 = \omega_0/10$ (Fig. 3.37) and $\omega_1 = \omega_0/2$ (Fig. 3.38). It can be seen that the desired operating point stays asymptotically stable in both cases. In Fig. 3.37, the slow components of the compensation signal u make the current response slow. This effect is less important in Fig. 3.38 because of suppressing the slowest components of u by increasing ω_1. It is obvious that if one continues to increase ω_1, the desired operating point becomes unstable.

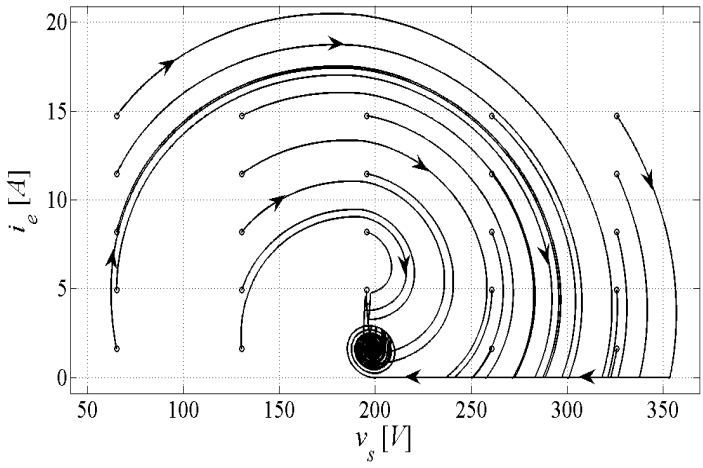

Fig. 3.37- State trajectories of the model (3.35) with the proposed compensation in (3.38) with $K = 1$ and $\omega_1 = \omega_0/10$ (o: initial point).

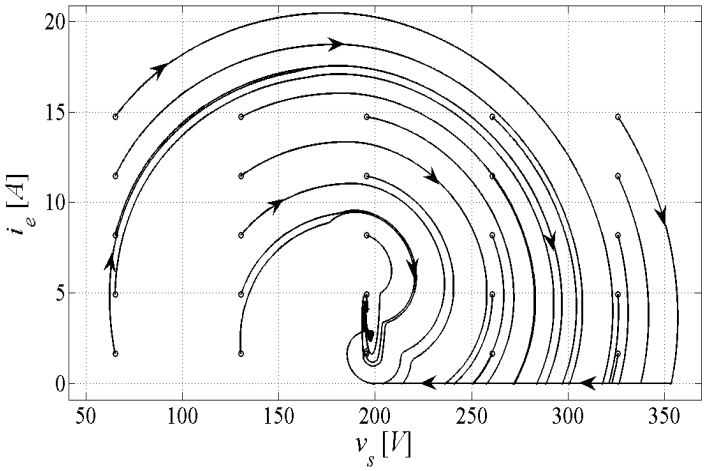

Fig. 3.38- State trajectories of the model (3.35) with the proposed compensation in (3.38) with $K = 1$ and $\omega_1 = \omega_0/2$ (o: initial point).

3.5.2 *Simulation Results:*

Fig. 3.39 shows the simulation results after a q-current step with oscillation compensation block activated. It can be seen in the Fig. 3.39 that the dc-link variables which were oscillating in Fig. 3.4 are no more oscillating after the q-current step.

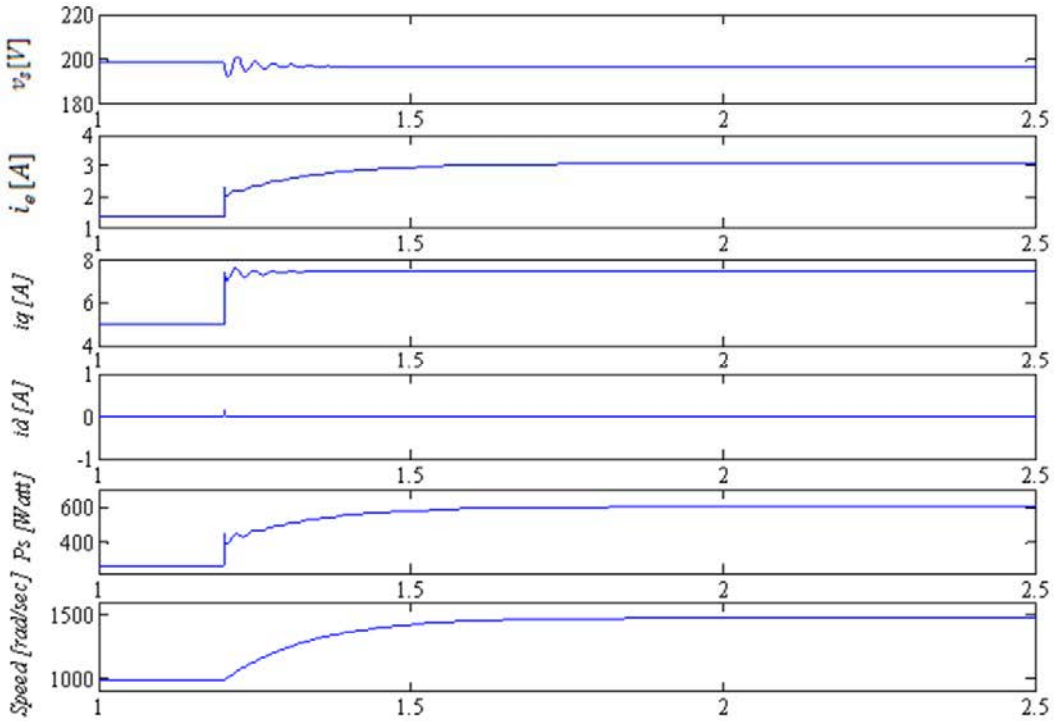

Fig. 3.39- Stabilization dc-link voltage after a q-current step for K=1.

Fig. 3.40 shows the stabilization of the dc-link variables with the help of the proposed oscillation compensation block after the speed step from 1000rpm to 1500rpm. Fig. 3.41 shows the simulation results for a q-current step when the stabilization block is turned off at $t = 1.8s$. The system was stable and achieved its steady state before disabling the proposed stabilizer ($t < 1.8s$). Unstable oscillations come back after turning off the oscillation compensation block. This means that the stabilization is necessary even in steady state.

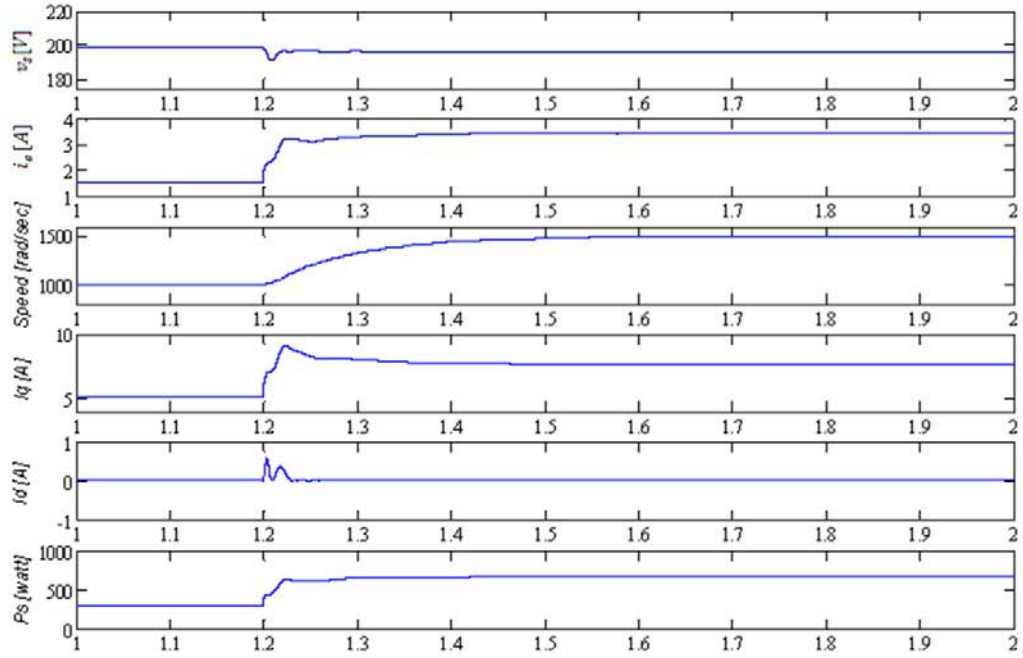

Fig. 3.40- Stabilization dc-link voltage variations after speed step for K=1.

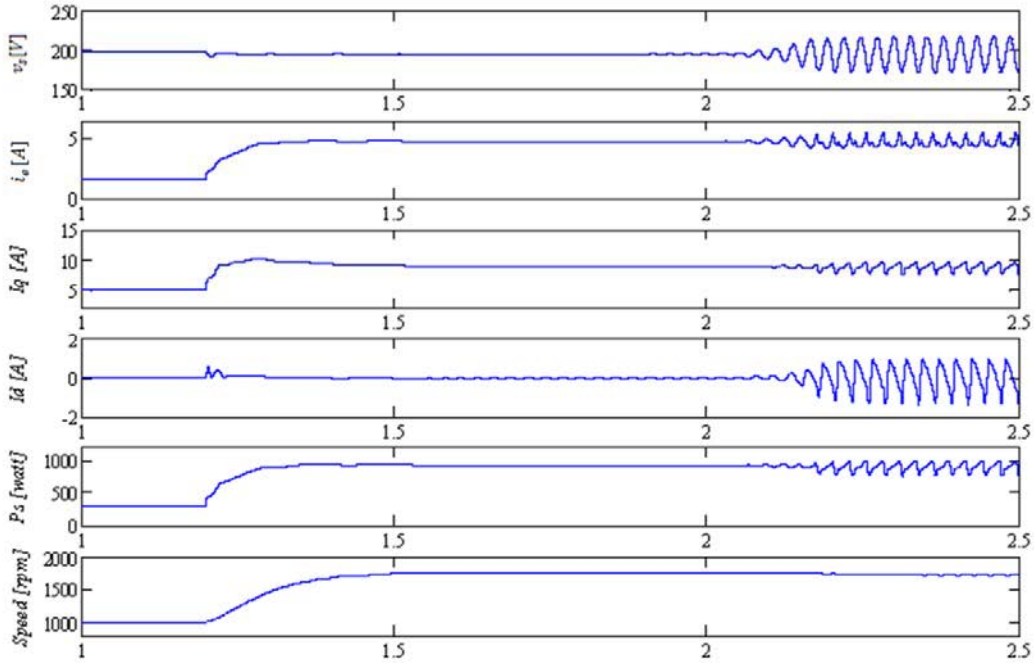

Fig. 3.41- Stabilization block switch on to switch off test after speed step.

3.5.3 *Experimental Validation*

To verify the validity of the proposed stabilization technique, several tests were performed on our experimental bench. The parameters of this bench are those given in Table 4.I.

In the first test, stabilization block is activated and results are shown in Fig. 3.42. This figure illustrates that the dc-link voltage variations ($\tilde{v}_S = v_s - v_{s0}$) and the dc-link input current (i_e) are stable when a q-current step is applied. It should be noted that the drive power consumption after this current step does not satisfy (3.11). Unstable dc-link variables when a speed reference step is applied (Fig. 3.7) becomes stable when the oscillation compensation block is activated (Fig. 3.43). Fig. 3.44 shows that the dc-link variables are stable after a mechanical load step is applied.

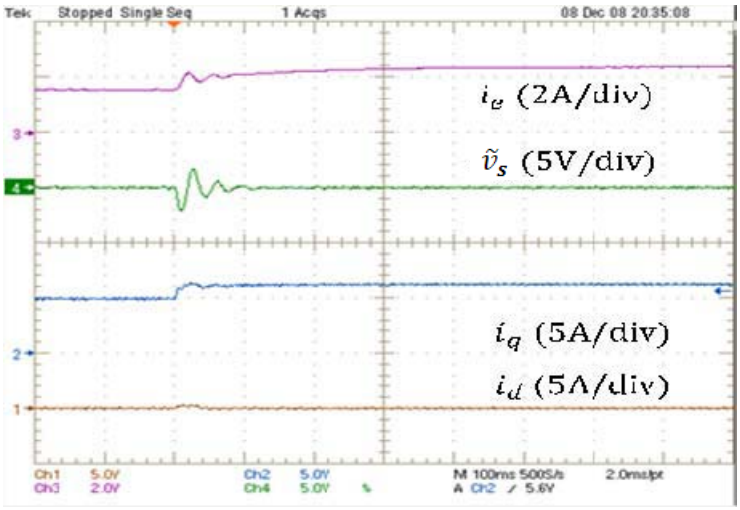

Fig. 3.42- Stator dq-currents, dc-link current and voltage deviation after a load q-current step with the proposed stabilization law with $K = 1$ (measurements).

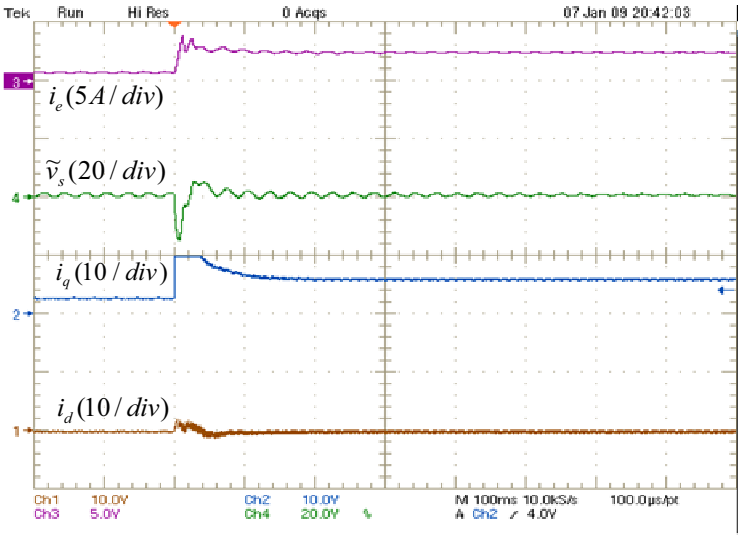

Fig. 3.43- Stator dq-currents, dc-link current and voltage deviation after a speed reference tracking step with the proposed stabilization law with $K = 1$ (measurements).

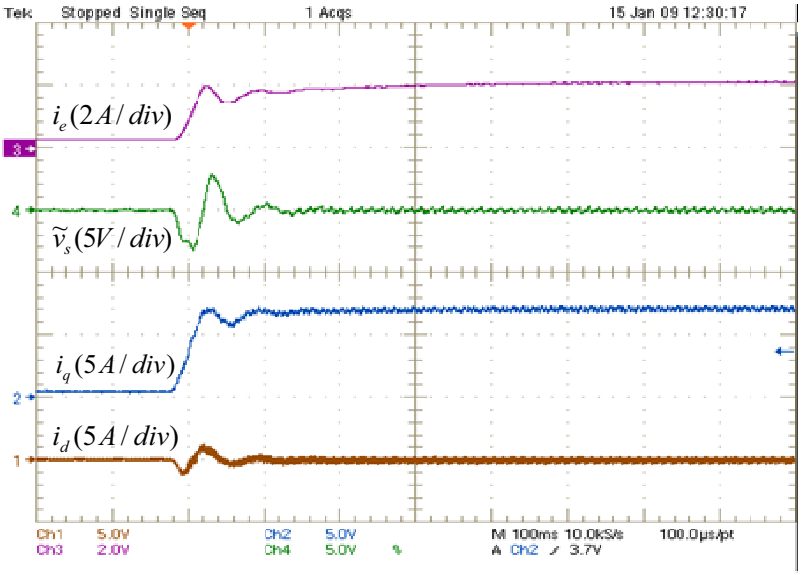

Fig. 3.44- Stator dq-currents, dc-link current and voltage deviation after a load power step with the proposed stabilization law with $K = 1$ (measurements).

This deviation may be reduced if K is greater. To show that, another test was performed with a speed tracking scenario when K is fixed to 10. Fig. 3.45 illustrates the measurements which to be compared with those in Fig. 3.43. Obviously, the dc-link voltage is more stable, but the q-current and thus the speed dynamic are more affected by the stabilization block.

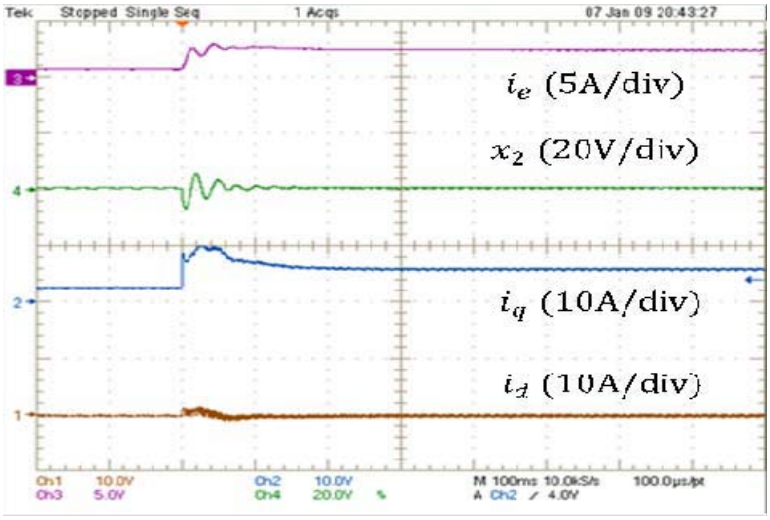

Fig. 3.45- Stator dq-currents, dc-link current and voltage deviation after a speed reference tracking step with the proposed stabilization law with $K = 10$ (measurements).

3.6 CONCLUSION:

The proposed stabilization technique is used to improve the stability of the system and/or to reduce the size of the dc-link capacitance without modifying the structure of the current control loops. The dc-link voltage stability improvement depends on the design requirements: maximum voltage deviation and its response time for a given load power disturbance and the impact of the voltage stabilization on the drive dynamic. When designing the oscillation compensation block, a good designer knows that more stable dc-link voltage leads generally to worse drive torque dynamic. To find a good trade-off, the designer should adjust the stabilization block parameters. In this chapter, we applied this approach to a drive used in aerospace applications.

CHAPTER 4

AN ENERGETIC APPROACH TO INVESTIGATE THE STABILITY OF CASCADED SYSTEMS

Chapter 4

4.1 INTRODUCTION:

Stability analysis of cascaded system and more generally of distributed system is a well known issue. To investigate the intersection between DC-DC power supplies and their input filter the concept of impedance specification was introduced in [Mid 76], [Mid 78]. Other authors [Ema 99], [Wil 95], [Sud 98] have then improved the concept and proposed a large family of impedance constraints that the different elements connected to the same DC bus have to respect to ensure asymptotic stability around an operating point. The most used constraints are deduced from phase margin or gain margin constraints that a transfer function which is the ratio between the output impedance of the source and the input impedance of the load has to verify [Ema 99], [Wil 95], [Sud 98]. The main drawback of this approach is to be dependent on the operating point and to be sensitive to system parameters. In fact, for an electric device, the analytic expressions or the values (in case of experimental measurements) of characteristic impedances are efficient around a given operating point and for a given set of system parameters. To investigate stability properties of the system in case of parameters variations, some authors have introduced first order methods based on μ analysis or modal approach to ensure the stability for bounded variations of parameters [Via 10], [Bar 05]. Nevertheless with these approaches, the behavior of the system for large magnitude perturbations is yet unknown. Some authors have then introduced large signal stability tools to investigate the behavior of distributed DC bus with constant power loads for large external perturbations. In [Gri 08], the authors used a Brayton-Moser's Potential function [Wei 98] to investigate stability of an actuator connected to a DC bus through a second order input filter. This method leads to good results for low order system but cannot take into consideration the inner dynamics of the loads which are modeled by a CPL (**C**onstant **P**ower **L**oad) system. This assumption allows exhibiting sufficient stability conditions and allows optimizing parameters of the filter. Other authors proposed a multi model approach based on the use of a Takagi-Sugeno model to analyze large signal stability properties of **D**istributed **P**ower **S**ystem (DPS) including CPL [Mar 09]. The approach allows taking into account, if necessary, the inner dynamics of the loads but leads to LMI formulations for which the resolution can become difficult when the number of loads or nonlinearities increases.

In recent years, necessity of compactness of DPS leads researchers to find solutions to achieve stability of the system when the values of the passive elements of the DPS are small and can generate stability issues. Active stabilization techniques linear or non linear have been proposed ([Liu 10], [Rah 10]). Most often, the approaches are developed around an operating point and the stability properties of the stabilized system are a function of the operating point.

In this chapter, a new method based on dynamic specifications, is proposed to study the stability of a cascaded electric system. To apply this method, a new modeling based on energetic variables, is introduced to investigate the stability of cascaded systems. Contrary to classical approach for which voltages and currents are the state variables, we propose to use electrostatic

energies and powers as state variables. We will prove that with this approach the stability study, subject to some assumptions, can be few dependent of the operating point. Thus stability of large scale distributed system can be simplified if all the components of the system verify such properties.

The chapter is organized as fallow: Model of electric device is presented in section 4.2. Control strategy for DC/DC converters and PMSM is detailed in section 4.3. Section 4.4 details the improvement of the controlled strategy and in the section 4.5 and 4.6, the proposed control strategy is verified with help of simulation results and experimental validation.

4.2 MODEL OF AN ELECTRIC DEVICE:

In this section we present the model of an electrical system with a new modeling based on energetic variables like electrostatic energy and power. Let us consider the electric system presented in Fig. 4.1. The subscripts *i* and *o* are associated respectively to the input and output variables of the system. P_i et P_o represent respectively the input and output power of the system; y_i and y_o correspond to the electrostatic energies stored in the input and output capacitances.

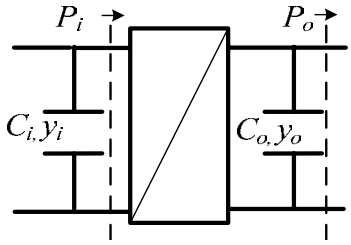

Figure 4.1: presentation of notations used for modeling an electric device.

Now in order to prove the stability around an operating point, let us consider small variations of the electrostatic energies and power around a given operating point X_0. The variations of the system output variables (y_o, P_i) are bound to the variations of the inputs (y_i, P_o) according to the following relationship:

$$\begin{bmatrix} \tilde{y}_o \\ \tilde{P}_i \end{bmatrix} = \begin{bmatrix} H_y(s) & T(s) \\ Y(s) & -H_p(s) \end{bmatrix}_{X_0} \cdot \begin{bmatrix} \tilde{y}_i \\ -\tilde{P}_o \end{bmatrix} \tag{4.1}$$

where H_y represents the electrostatic energy transfer function,
H_P represents the power transfer function,
T represents the energetic output impedance,
Y represents the energetic input Admittance.

The energetic input admittance and output impedance of the electric system are defined by the following relation:

$$Y(s) = \left(\frac{\tilde{P}_i}{\tilde{y}_i}\right)_{\substack{\tilde{P}_{load}=0 \\ \tilde{y}_{oref}=0}} \qquad and \qquad T(s) = \left(\frac{\tilde{y}_o}{-\tilde{P}_{load}}\right)_{\substack{\tilde{y}_i=0 \\ \tilde{y}_{oref}=0}}$$

Let us consider now the cascaded system presented in Fig.2.

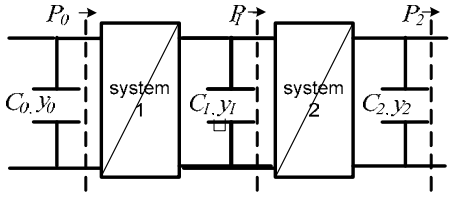

Figure 4.2: Two electric devices connected in cascade.

Thus a relationship between the variations of electrostatic energy can be obtained. It comes:

$$\left(\frac{\tilde{y}_2}{\tilde{y}_0}\right)_{\tilde{P}_2=0} = \frac{H_{y1}(s) \cdot H_{y2}(s)}{1 + T_1(s) \cdot Y_2(s)} \qquad \left(\frac{\tilde{y}_1}{\tilde{y}_0}\right)_{\tilde{P}_2=0} = \frac{H_{y1}(s}{1 + T_1(s) \cdot Y_2(s)} \qquad (4.2)$$

These relations are similar to those obtained with the classical methods based on characteristic impedances of the electric systems [Mid 76], [Mid 78], [Ema 99], [Wil 95]. If the transfer functions H_{y1} and H_{y2} are supposed stable for any operating point then the stability of the cascaded system depends on the transfer function $T_1(s)$. $Y_2(s)$ and a sufficient condition to achieve stability of the cascaded system is that the Nyquist plot of the transfer function $T_1(s)$. $Y_2(s)$ doesn't encircle the point (-1,0).

At this step, stability of the system is bound to the operating point because each transfer function which appears in (4.2) is calculated around an operating point. It is nevertheless possible to modify the control strategy of the electric device to obtain transfer functions less dependent on the operating point.

4.3 PROPOSED CONTROL STRATEGY OF AN ACTIVE ELECTRIC DEVICE:

In this part, we propose to modify control strategy of actuators or DC to DC converters which are connected to the DC bus in such a way that the transfer functions which appear in (2) is less dependent on the operating mode. In this chapter we consider two kind of electric devices, actuators with Permanent Magnet Synchronous Motor (PMSM) and DC to DC converter (boost converter) which operates in continuous conduction mode.

4.3.1 Control of DC/DC converter:

4.3.1.1 Control Strategy:

Without loss of generality, we will explain the control strategy in the case of Boost converter but the approach can be extended easily to others DC to DC converter (Buck, Sepic, Cuk, isolated full bridge fed in current converter,…). For a DC/DC converter, it has been shown in [Sha 10] that the whole losses can be modeled by two nonlinear resistances. The first one is connected in series with the inductive component of the converter and the second one is connected in parallel of the output capacitor. The equivalent model of the system including losses for a Boost converter is presented in Fig. 4.3.

The control strategy we propose to use for DC to DC converter is shown in Fig. 4.4. This strategy uses two control loops. The inner loop is a high bandwidth power loop. Its main function is to ensure that the controlled power follows perfectly its respective reference P_{ref} which leads to the use of any high dynamic controller (for example sliding or flatness based controller can be used [Sha 10a], [Pay 08].

As depicted in Fig.4.4, the power reference P_{ref} is composed of two components $P_{yo,ref}$ and $P_{yi,ref}$. The first one is generated by the energy controller which ensures that the electrostatic energy stored in the output capacitance y_o follows its reference y_{oref}. The trajectory planning transfer function $H_{yo}(s)$ allows setting the dynamic properties of the converter for load perturbations.

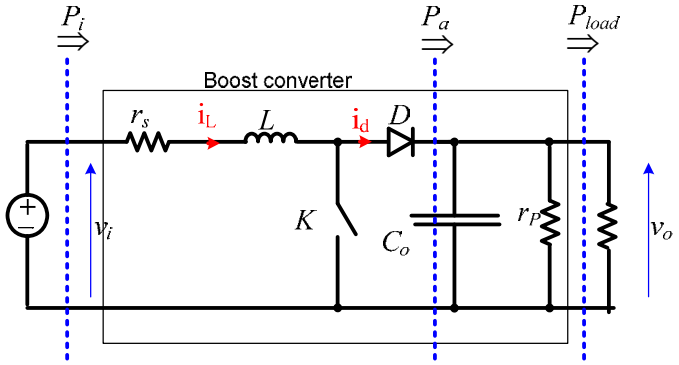

Figure 4.3. Equivalent model of a Boost converter.

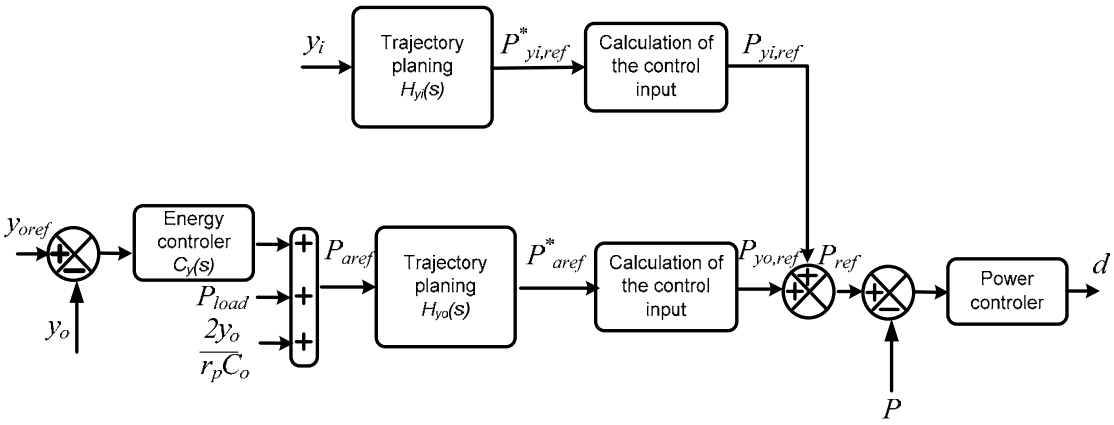

Figure 4.4: Proposed control strategy of DC to DC converter used for DPS.

The measure of the load power is not a requirement to achieve the control of the energy to its reference. The trajectory planning transfer function $H_{yi}(s)$ allows setting the dynamic behavior of the converter for energy variations of the input capacitance. With the help of this control strategy we can remove the variations in the electrostatic energy of the input capacitance, which will make the system stable.

The two others blocks labeled *calculation of the control input* allows calculating the effective power reference P_{ref} which is effectively controlled in the converter. This power has to be a continuous signal for proper operation. In the case of a Boost converter, this power corresponds to the input power P_i. In the case of a Buck converter, it corresponds to the power provided to the output capacitor. For the controller design, we suppose that the additional power due to the variations of the magnetic energy in inductor is small in comparison of the power provided to the load. Then for a Boost converter, the reference powers $P_{yo,ref}$ and $P_{yi,ref}$ can be calculated as follows:

$$P_{yo,ref} = \frac{r_s}{v_i^2} P_{yo,ref}^2 + P_{aref}^*$$

$$\Rightarrow \qquad P_{y_{o,ref}} = 2\frac{v_i^2}{4 \cdot r_s} \cdot \left(1 - \sqrt{1 - \frac{P_{aref}^*}{\frac{v_i^2}{4 \cdot r_s}}} \right) \tag{4.3}$$

$$P_{y_{i,ref}} = P_{y_{i,ref}}^* \tag{4.4}$$

4.3.1.2 Small signal model of DC-DC converter with the proposed control approach: application to the Boost converter:

To analyze the stability of two systems in interaction, the four transfer functions of the matrix given by (4.1) have to be determined. For this study, we suppose that the controlled power follows perfectly its reference ($P = P_i = P_{ref}$). For any structure of converter, it is always possible

to write relations between input and output powers of the converter. In the case of the Boost converter with the control described in Fig. 4.4, it comes:

$$P_a = P_i - \frac{r_s \cdot C_i}{2} \cdot \frac{P_i^2}{y_i} - \frac{LP_i}{\sqrt{2y_i/C_i}} \cdot \frac{d}{dt}\left(\frac{P_i}{\sqrt{2y_i/C_i}}\right) = \Psi_{P_a}\left(P_i, \frac{dP_i}{dt}, y_i, \frac{dy_i}{dt}, y_o\right) \quad (4.5)$$

$$P_i = P_{ref} = P_{yo,ref} + P_{yi,ref} = \frac{y_i}{r_s \cdot C_i} \cdot \left(1 - \sqrt{1 - \frac{P^*_{aref}}{\frac{y_i}{2 \cdot r_s \cdot C_i}}}\right) + P^*_{yi,ref}$$

$$= \Psi_{P_i}\left(P^*_{aref}, y_i, P^*_{yi,ref}\right) \quad (4.6)$$

NB: The derivative term in (4.5) corresponds to the power necessary to store magnetic energy in the inductor element.

Calculation of transfer functions $H_y(s)$ and $Y(s)$:

Calculation of the Electrostatic Energy Transfer Function $H_y(s)$:

The output electrostatic energy verifies:

$$\dot{y}_o = \Psi_{P_a}\left(P_i, \frac{dP_i}{dt}, y_i, \frac{dy_i}{dt}, y_o\right) - \frac{2 \cdot y_o}{r_P \cdot C_o} - P_{load} \quad (4.7)$$

Small variations of (4.5), (4.6) and (4.7) around a given operating point noted X_o leads to:

$$s \cdot \tilde{y}_o = \left(\left(\frac{\partial \Psi_{P_a}}{\partial P_i}\right)_{X_o} + \left(\frac{\partial \Psi_{P_a}}{\partial \frac{dP_i}{dt}}\right)_{X_o} s\right)\tilde{P}_i + \left(\left(\frac{\partial \Psi_{P_a}}{\partial y_i}\right)_{X_o} + \left(\frac{\partial \Psi_{P_a}}{\partial \frac{dy_i}{dt}}\right)_{X_o} s\right)\tilde{y}_i + \left(\frac{\partial \Psi_{P_a}}{\partial y_o}\right)_{X_o} \tilde{y}_o$$

$$- \frac{2 \cdot \tilde{y}_o}{r_P \cdot C_o} - \tilde{P}_{load} \quad (4.8)$$

$$\tilde{P}_i = \left(\frac{\partial \Psi_{P_i}}{\partial P^*_{aref}}\right)_{X_o} \cdot \tilde{P}^*_{aref} + \left(\frac{\partial \Psi_{P_i}}{\partial y_i}\right)_{X_o} \cdot \tilde{y}_i + \left(\frac{\partial \Psi_{P_i}}{\partial P^*_{yi,ref}}\right)_{X_o} \cdot \tilde{P}^*_{yi,ref} \quad (4.9)$$

From (4.8) and (4.9):

$$s\cdot\tilde{y}_o=\left(\left(\frac{\partial\Psi_{P_a}}{\partial P_i}\right)_{X_o}+\left(\frac{\partial\Psi_{P_a}}{\partial\dfrac{dP_i}{dt}}\right)_{X_o}s\right)\cdot\left(\left(\frac{\partial\Psi_{P_i}}{\partial P^*_{aref}}\right)_{X_o}\cdot\tilde{P}^*_{aref}+\left(\frac{\partial\Psi_{P_i}}{\partial y_i}\right)_{X_o}\cdot\tilde{y}_i+\left(\frac{\partial\Psi_{P_i}}{\partial P^*_{yi,ref}}\right)_{X_o}\cdot\tilde{P}^*_{yi,ref}\right)+\left(\left(\frac{\partial\Psi_{P_a}}{\partial y_i}\right)_{X_o}+\left(\frac{\partial\Psi_{P_a}}{\partial\dfrac{dy_i}{dt}}\right)_{X_o}s\right)\tilde{y}_i+\left(\frac{\partial\Psi_{P_a}}{\partial y_o}\right)_{X_o}\tilde{y}_o-\frac{2\cdot\tilde{y}_o}{r_P\cdot C_o}-\tilde{P}_{load}\qquad(4.10)$$

With

$$\left(\tilde{P}^*_{aref}\right)_{\substack{\tilde{P}_{load}=0\\ \tilde{y}_{oref}=0}}=H_{yo}(s)\cdot\left(-C_y(s)+\frac{2}{r_P\cdot C_o}\right)\cdot\tilde{y}_o\qquad(4.11)$$

$$\left(\tilde{P}^*_{yi,ref}\right)_{\substack{\tilde{P}_{load}=0\\ \tilde{y}_{oref}=0}}=H_{yi}(s)\cdot\tilde{y}_i\qquad(4.12)$$

Thus with $\tilde{P}_{load}=0$ and $\tilde{y}_{oref=0}$, equation (4.10) gives:

$$s\cdot\tilde{y}_o=\left(\left(\frac{\partial\Psi_{P_a}}{\partial P_i}\right)_{X_o}+\left(\frac{\partial\Psi_{P_a}}{\partial\dfrac{dP_i}{dt}}\right)_{X_o}s\right)\cdot\left[\left(\frac{\partial\Psi_{P_i}}{\partial P^*_{aref}}\right)_{X_o}\cdot H_{yo}(s)\cdot\left(-C_y(s)+\frac{2}{r_P\cdot C_o}\right)\cdot\tilde{y}_o+\left(\frac{\partial\Psi_{P_i}}{\partial y_i}\right)_{X_o}\cdot\tilde{y}_i+\left(\frac{\partial\Psi_{P_i}}{\partial P^*_{yi,ref}}\right)_{X_o}\cdot H_{yi}(s)\cdot\tilde{y}_i\right]+\left(\left(\frac{\partial\Psi_{P_a}}{\partial y_i}\right)_{X_o}+\left(\frac{\partial\Psi_{P_a}}{\partial\dfrac{dy_i}{dt}}\right)_{X_o}s\right)\tilde{y}_i+\left(\frac{\partial\Psi_{P_a}}{\partial y_o}\right)_{X_o}\tilde{y}_o-\frac{2\cdot\tilde{y}_o}{r_P\cdot C_o}\qquad(4.13)$$

From Equation (4.13), the energy transfer function H_y can be deduced:

$$H_y(s) = \left(\frac{\tilde{y}_o}{\tilde{y}_i}\right)_{\substack{\tilde{P}_{load}=0 \\ \tilde{y}_{oref}=0}}$$

$$= \frac{\left(\frac{\partial \Psi_{P_a}}{\partial y_i}\right)_{X_o} + \left(\frac{\partial \Psi_{P_a}}{\partial \frac{dy_i}{dt}}\right)_{X_o} s + \left(\left(\frac{\partial \Psi_{P_a}}{\partial P_i}\right)_{X_o} + \left(\frac{\partial \Psi_{P_a}}{\partial \frac{dP_i}{dt}}\right)_{X_o} s\right) \cdot \left[\left(\frac{\partial \Psi_{P_i}}{\partial y_i}\right)_{X_o} + \left(\frac{\partial \Psi_{P_i}}{\partial P^*_{yi,ref}}\right)_{X_o} \cdot H_{yi}(s)\right]}{s + \left(\left(\frac{\partial \Psi_{P_a}}{\partial P_i}\right)_{X_o} + \left(\frac{\partial \Psi_{P_a}}{\partial \frac{dP_i}{dt}}\right)_{X_o} s\right) \cdot \left(\frac{\partial \Psi_{P_i}}{\partial P^*_{aref}}\right)_{X_o} \cdot H_{yo}(s) \cdot \left(C_y(s) - \frac{2}{r_P \cdot C_o}\right) - \left(\frac{\partial \Psi_{P_a}}{\partial y_o}\right)_{X_o} + \frac{2}{r_P \cdot C_o}}$$

(4.14)

Calculation of the Energetic Input Admittance Y(s):

From equations (4.9), (4.11) and (4.12), and with $\tilde{P}_{load} = 0$ and $\tilde{y}_{oref=0}$:

$$\tilde{P}_i = \left(\frac{\partial \Psi_{P_i}}{\partial P^*_{aref}}\right)_{X_o} \cdot H_{yo}(s) \cdot \left(-C_y(s) + \frac{2}{r_P \cdot C_o}\right) \cdot \tilde{y}_o + \left(\frac{\partial \Psi_{P_i}}{\partial y_i}\right)_{X_o} \cdot \tilde{y}_i + \left(\frac{\partial \Psi_{P_i}}{\partial P^*_{yi,ref}}\right)_{X_o} \cdot H_{yi}(s) \cdot \tilde{y}_i$$

(4.15)

From (4.14) $\tilde{y}_o = H_y(s) \cdot \tilde{y}_i$

Thus the transfer function $Y(s)$ can be expressed as follows:

$$Y(s) = \left(\frac{\tilde{P}_i}{\tilde{y}_i}\right)_{\substack{\tilde{P}_{load}=0 \\ \tilde{y}_{oref}=0}} = \left(\frac{\partial \Psi_{P_i}}{\partial P^*_{aref}}\right)_{X_o} \cdot H_{yo}(s) \cdot \left(-C_y(s) + \frac{2}{r_P \cdot C_o}\right) \cdot H_y(s) + \left(\frac{\partial \Psi_{P_i}}{\partial y_i}\right)_{X_o}$$

$$+ \left(\frac{\partial \Psi_{P_i}}{\partial P^*_{yi,ref}}\right)_{X_o} \cdot H_{yi}(s) \qquad (4.16)$$

Calculation of transfer functions $T(s)$ and $H_p(s)$:

Calculation of the Energetic Output Impedance $T(s)$:

By definition, the transfer function $T(s)$ is defined as follows:

$$T(s) = \left(\frac{\tilde{y}_o}{-\tilde{P}_{load}}\right)_{\substack{\tilde{y}_i=0 \\ \tilde{y}_{oref}=0}}$$

With $\tilde{y}_i = 0 \; and \; \tilde{y}_{oref} = 0$, equation (4.13) gives the following expression:

$$s \cdot \tilde{y}_o = \left(\left(\frac{\partial \Psi_{P_a}}{\partial P_i}\right)_{X_o} + \left(\frac{\partial \Psi_{P_a}}{\partial \frac{dP_i}{dt}}\right)_{X_o} s\right) \cdot \left(\frac{\partial \Psi_{P_i}}{\partial P^*_{aref}}\right)_{X_o} \cdot H_{yo}(s) \cdot \left(-C_y(s) + \frac{2}{r_P \cdot C_o}\right) \cdot \tilde{y}_o + \left(\frac{\partial \Psi_{P_a}}{\partial y_o}\right)_{X_o} \tilde{y}_o - \frac{2 \cdot \tilde{y}_o}{r_P \cdot C_o} - \tilde{P}_{load}$$

$$T(s) = \left(\frac{\tilde{y}_o}{-\tilde{P}_{load}}\right)_{\substack{\tilde{y}_i=0 \\ \tilde{y}_{oref}=0}} = \frac{1}{s + \left(\left(\frac{\partial \Psi_{P_a}}{\partial P_i}\right)_{X_o} + \left(\frac{\partial \Psi_{P_a}}{\partial \frac{dP_i}{dt}}\right)_{X_o} s\right) \cdot \left(\frac{\partial \Psi_{P_i}}{\partial P^*_{aref}}\right)_{X_o} \cdot H_{yo}(s) \cdot \left(C_y(s) - \frac{2}{r_P \cdot C_o}\right) - \left(\frac{\partial \Psi_{P_a}}{\partial y_o}\right)_{X_o} + \frac{2}{r_P \cdot C_o}} \quad (4.17)$$

Calculation of the Power Transfer Function $H_p(s)$:

The power transfer function $H_p(s)$ is defined as:

$$H_p(s) = \left(\frac{\tilde{P}_i}{-\tilde{P}_{load}}\right)_{\substack{\tilde{y}_i=0 \\ \tilde{y}_{oref}=0}}$$

From (4.15) with $\tilde{y}_i = 0 \; and \; \tilde{y}_{oref} = 0$,:

$$\tilde{P}_i = \left(\frac{\partial \Psi_{P_i}}{\partial P^*_{aref}}\right)_{X_o} \cdot H_{yo}(s) \cdot \left(-C_y(s) + \frac{2}{r_P \cdot C_o}\right) \cdot \tilde{y}_o$$

From (4.17):

$$\tilde{y}_o = T(s) \cdot \left(-\tilde{P}_{load}\right)$$

$$\Rightarrow \quad H_p(s) = \left(\frac{\tilde{P}_i}{-\tilde{P}_{load}}\right)_{\substack{\tilde{y}_i=0 \\ \tilde{y}_{oref}=0}} = \left(\frac{\partial \Psi_{P_i}}{\partial P^*_{aref}}\right)_{X_o} \cdot H_{yo}(s) \cdot \left(-C_y(s) + \frac{2}{r_P \cdot C_o}\right) \cdot T(s) \qquad (4.18)$$

Correct design of the converter controllers leads to stable transfer functions $H_p(s)$ and $H_y(s)$ for any operating point. Thus transfer functions $Y(s)$ and $T(s)$ allows investigating stability of the cascaded system.

Expressions (4.14) to (4.18) are dependent on the operating point. Nevertheless if we suppose that the serial resistances r_s is small enough to ensure that

$$\frac{y_i}{2 \cdot r_s \cdot C_i} \gg P^*_{aref} \qquad (4.19)$$

Then (4.3) and (4.6) lead respectively to $P_{y_{o,ref}} \approx P^*_{aref}$ and $P_i = P^*_{aref} + P^*_{yi,ref}$.

Then the following terms becomes:

$$\left(\frac{\partial \Psi_{P_a}}{\partial P_i}\right)_{X_o} = 1, \qquad \left(\frac{\partial \Psi_{P_a}}{\partial \frac{dP_i}{dt}}\right)_{X_o} = -\frac{L \cdot P_i}{2 \cdot y_i / C_i} = -\frac{L \cdot P_i}{{V_i}^2}$$

$$\left(\frac{\partial \Psi_{P_a}}{\partial y_i}\right)_{X_o} = 0, \qquad \left(\frac{\partial \Psi_{P_a}}{\partial \frac{dy_i}{dt}}\right)_{X_o} = \frac{L \cdot {P_i}^2}{\sqrt{2 \cdot C_i} \cdot {V_i}^3}$$

$$\left(\frac{\partial \Psi_{P_i}}{\partial P^*_{aref}}\right)_{X_o} = 1, \qquad \left(\frac{\partial \Psi_{P_i}}{\partial P^*_{yi,ref}}\right)_{X_o} = 1$$

$$\left(\frac{\partial \Psi_{P_i}}{\partial y_i}\right)_{X_o} = 0, \qquad \left(\frac{\partial \Psi_{P_a}}{\partial y_o}\right)_{X_o} = 0$$

Let us consider the plot of energetic output impedance of a Boost converter operated in continuous conduction mode.

The nominal values of the parameters are given in table I.

$v_i = 48V$	*Input voltage*
$v_o = 200V$	*Output voltage*
K=10	*Stabilization constant*
$r_s = 0.01\Omega$	*Series resistance*
$r_p = 2000\Omega$	*Resistance in parallel with output capacitor*

$L = 10^{-3}$	*Inductance*
$C_o = 1100\mu F$	*Output capacitance*
$T_s = 10^{-4}s$	*Switching period* $((F = 1/T_s))$

Table I: System Parameters

The theoretical energetic output impedance plot stays in the neighborhood of the plot obtained with numerical simulations (Fig. 4.5). Fig. 4.6 shows the energetic output impedance for different values the operating points. The studied boost converter is presented in Fig. 4.3 and its associated control is shown in Fig. 4.4. As shown in the Fig. 4.6, the plots of the energetic output impedance for various operating points are close to each other which concludes that the energetic output impedance is few dependent on the operating point.

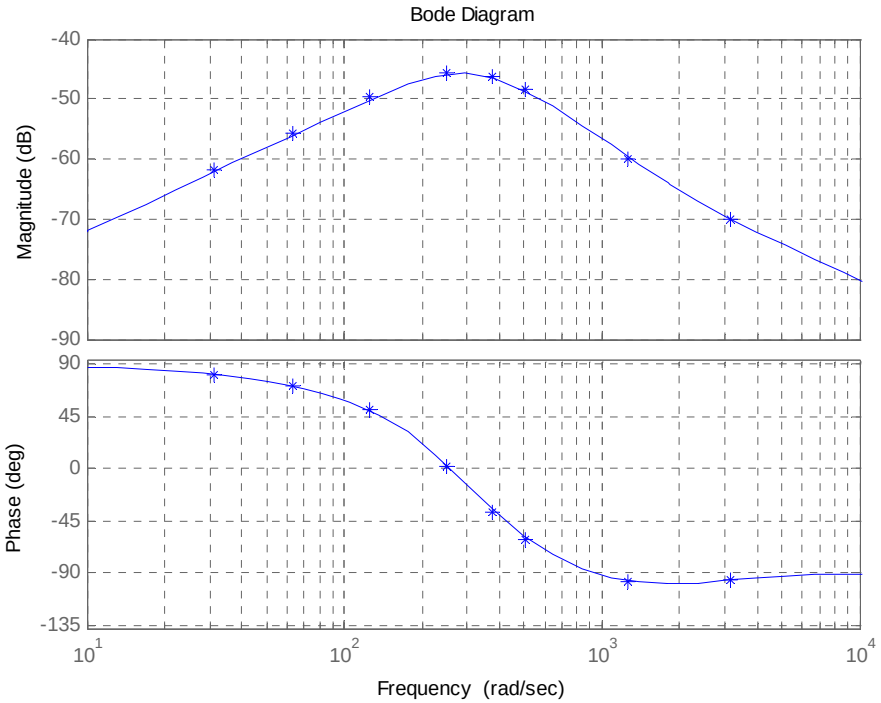

Figure 4.5: Plot of the energetic output impedance, $K = 10, P_{Load} = 2000\ W$ *(all the others parameters given in table I).*

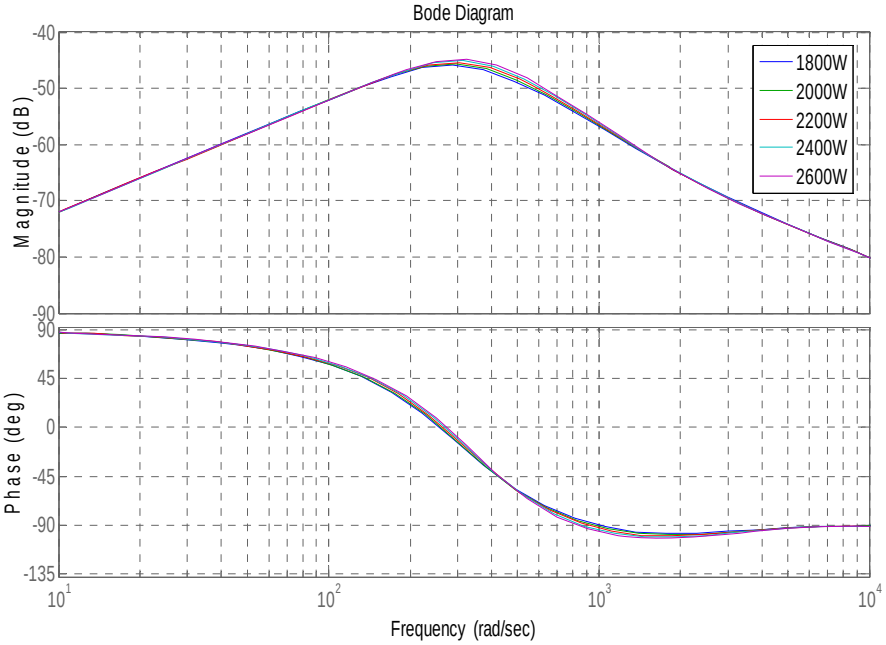

Figure 4.6: Evaluation of energetic output impedance for different values of Pload *(all the others parameters given in table I).*

4.3.2 Control of PMSM actuators:

4.3.2.1 Control strategy:

It is possible to extend this strategy for control of actuators. The scheme describing the control strategy for PMSM actuators is presented in Fig. 4.7.

The equivalent model of the actuator is shown in Fig. 4.7a. The Whole losses are modelled by two resistances. The first one, r_s, is connected in series with 3-phases of the PMSM. The second one, noted R_p, is connected in parallel across the input capacitance C_i. The mechanical power load is noted P_{load}.

Fig 4.7b presents the control strategy of the PMSM actuator. y_c and y_{cref} represent respectively the kinetic energy and its reference, P_{aref} represents the mechanical power reference and, like for DC/DC converter, $P_{yi,ref}$ represents a mechanical stabilizing power generated by variations of the input electrostatic energy. Two possibilities exist for the choice of the controlled power. It can be the electrical input power or the mechanical power. In this chapter, we decide to use the mechanical power as the controlled power. Thus P_{aref} represents the total mechanical power reference. Like previously, all kinds of high bandwidth controllers can be used to ensure the control of the power and the flux to their respective references.

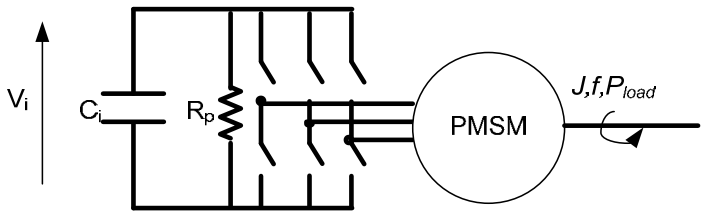

Figure 4.7a: Equivalent model of PMSM actuator.

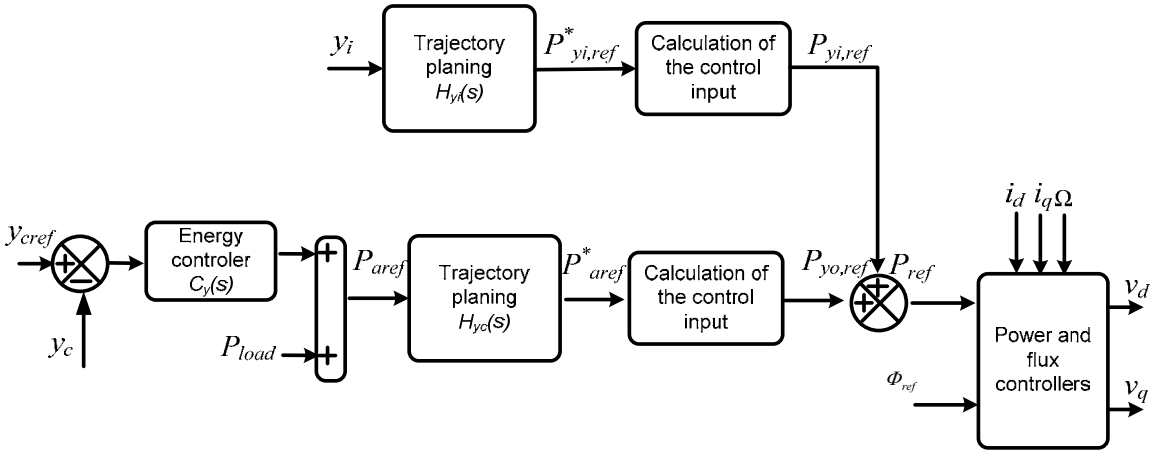

Figure 4.7b: Proposed control strategy for PMSM actuators.

4.3.2.2 Small Signal Model of PMSM Actuator:

We suppose that the mechanical power and the flux follow their respective references. For mechanical loads, only the transfers function *Y(s)* has to be found to investigate the stability of a cascaded system. The equation (4.5) and (4.6) in case of PMSM with a control of the mechanical power P_a can be rewritten as follows:

$$P_i = \frac{2 \cdot y_i}{R_p \cdot C_i} + P_a + r_s \cdot \left(\left(\frac{\Phi_{ref} - \Psi_f}{L_d} \right)^2 + \left(\frac{P_a}{p \cdot \Psi_f \cdot \Omega} \right)^2 \right) + L_q \cdot \left(\frac{P_a}{\left(p \cdot \Psi_f \right)^2 \cdot \sqrt{2 \cdot y_c / J}} \right) \cdot \frac{d}{dt} \left(\frac{P_a}{\sqrt{2 \cdot y_c / J}} \right)$$

$$= \Psi_{Pi} \left(y_i, P_a, \Phi_{ref}, \frac{dP_a}{dt}, y_c, \frac{dy_c}{dt} \right) \tag{4.20}$$

$$P_a = P_{yo,ref} + P_{yi,ref} = P^*_{aref} + F\left(P^*_{aref}, P^*_{yi,ref}\right) = \Psi_{Pa}\left(P^*_{aref}, P^*_{yi,ref}, y_c\right) \tag{4.21}$$

The Function *F* allows taking into account, if necessary, the losses in the PMSM. It can be chosen as follows:

$$F\left(P^*_{aref}, P^*_{yi,ref}\right) = \frac{\left(p\cdot\Psi_f\cdot\Omega\right)^2}{2\cdot r_s} \cdot\left(-\left(1+2\cdot r_s\cdot\frac{P^*_{aref}}{\left(p\cdot\Psi_f\cdot\Omega\right)^2}\right)+\sqrt{\left(1+2\cdot r_s\cdot\frac{P^*_{aref}}{\left(p\cdot\Psi_f\cdot\Omega\right)^2}\right)^2+4\cdot r_s\cdot\frac{P^*_{yi,ref}}{\left(p\cdot\Psi_f\cdot\Omega\right)^2}}\right) \quad (4.22)$$

Remarks:

-In this study the flux controller ensures that the flux follows perfectly its reference Φ_{ref} which is supposed to be constant. Thus the variations of power due to the variations of d-axis magnetic energy have been taken equal to zero.

-The relation (4.22) allows taking into account non linear behaviour due to losses generated by serial resistances in the PMSM. If we suppose that the condition

$$\frac{\left(p\cdot\Psi_f\cdot\Omega\right)^2}{4\cdot r_s} \gg max\left(P^*_{yi,ref}, P^*_{aref}\right)$$

is verified, then a first order development of (4.22) leads to :

$$F\left(P^*_{yi,ref}, P^*_{aref}\right) = P^*_{yi,ref}$$

Calculation of the transfer functions $H_y(s)$ and $Y(s)$:

Calculation of the Electrostatic Energy Transfer Function $H_y(s)$:

The dynamical equation verified by the kinetic energy verifies:

$$\dot{y}_c = P_a - \frac{2\cdot f}{J}y_c - P_{load}$$

A first order development of this equation with $\tilde{P}_{load} = 0$, $\tilde{y}_{cref} = 0$ and $\tilde{\Phi}_{ref} = 0$ leads to:

$$s\cdot\tilde{y}_c = \left(\frac{\partial\Psi_{P_a}}{\partial P^*_{aref}}\right)_{X_o}\cdot H_{yo}(s)\cdot\left(-C_y(s)\right)\cdot\tilde{y}_c + \left(\frac{\partial\Psi_{P_a}}{\partial P^*_{yi,ref}}\right)_{X_o}\cdot H_{yi}(s)\cdot\tilde{y}_i + \left(\frac{\partial\Psi_{P_a}}{\partial y_c}\right)_{X_o}\cdot(\tilde{y}_c) - \frac{2\cdot f}{J}\cdot\tilde{y}_c$$

Thus:

$$H_y(s) = \left(\frac{\tilde{y}_c}{\tilde{y}_i}\right)_{\substack{\tilde{P}_{load}=0 \\ \tilde{y}_{cref}=0 \\ \tilde{\Phi}_{ref}=0}} = \frac{\left(\frac{\partial \Psi_{P_a}}{\partial P^*_{yi,ref}}\right)_{X_o} \cdot H_{yi}(s)}{s + \frac{2 \cdot f}{J} + \left(\frac{\partial \Psi_{P_a}}{\partial P^*_{aref}}\right)_{X_o} \cdot H_{yo}(s) \cdot C_y(s) - \left(\frac{\partial \Psi_{P_a}}{\partial y_c}\right)_{X_o}} \tag{4.23}$$

Calculation of the Energetic Input Impedance Transfer Function $Y(s)$:

By definition, the energetic input impedance is defined by the relation:

$$Y(s) = \left(\frac{\tilde{P}_i}{\tilde{y}_i}\right)_{\substack{\tilde{P}_{load}=0 \\ \tilde{y}_{cref}=0 \\ \tilde{\Phi}_{ref}=0}}$$

From equation (4.20) and (4.21), we deduce:

$$\tilde{P}_i = \left(\left(\frac{\partial \Psi_{P_i}}{\partial P_a}\right)_{X_o} + \left(\frac{\partial \Psi_{P_i}}{\partial \frac{dP_a}{dt}}\right)_{X_o} \cdot s \right) \cdot \tilde{P}_a + \left(\frac{\partial \Psi_{P_i}}{\partial \Phi_{ref}}\right)_{X_o} \cdot \tilde{\Phi}_{ref} + \left(\left(\frac{\partial \Psi_{P_i}}{\partial y_c}\right)_{X_o} + \left(\frac{\partial \Psi_{P_i}}{\partial \frac{dy_c}{dt}}\right)_{X_o} \cdot s \right) \cdot \tilde{y}_c + \frac{2}{R_p \cdot C_i} \cdot \tilde{y}_i$$

From equation (4.21) and with $\tilde{P}_{load} = 0$, $\tilde{y}_{cref} = 0$ and $\tilde{\Phi}_{ref} = 0$:

$$\tilde{P}_i = \left(\left(\frac{\partial \Psi_{P_i}}{\partial P_a}\right)_{X_o} + \left(\frac{\partial \Psi_{P_i}}{\partial \frac{dP_a}{dt}}\right)_{X_o} \cdot s \right) \cdot \left[\left(\frac{\partial \Psi_{P_a}}{\partial P^*_{aref}}\right)_{X_o} \cdot H_{yo}(s) \cdot \left(-C_y(s)\right) \cdot \tilde{y}_c + \left(\frac{\partial \Psi_{P_a}}{\partial P^*_{yi,ref}}\right)_{X_o} \cdot H_{yi}(s) \cdot \tilde{y}_i + \left(\frac{\partial \Psi_{P_a}}{\partial y_c}\right)_{X_o} \cdot (\tilde{y}_c) \right] + \left(\left(\frac{\partial \Psi_{P_i}}{\partial y_c}\right)_{X_o} + \left(\frac{\partial \Psi_{P_i}}{\partial \frac{dy_c}{dt}}\right)_{X_o} \cdot s \right) \cdot \tilde{y}_c + \frac{2}{R_p \cdot C_i} \cdot \tilde{y}_i$$

From equation (4.23):

$$\tilde{y}_c = H_y(s) \cdot \tilde{y}_i$$

$\Rightarrow$

$$Y(s) = \left(\frac{\tilde{P}_i}{\tilde{y}_i}\right)_{\substack{\tilde{P}_{load}=0 \\ \tilde{y}_{cref}=0 \\ \tilde{\Phi}_{ref}=0}} = \left(\left(\frac{\partial \Psi_{P_i}}{\partial P_a}\right)_{X_o} + \left(\frac{\partial \Psi_{P_i}}{\partial \frac{dP_a}{dt}}\right)_{X_o} \cdot s\right) \cdot \left[\left(\frac{\partial \Psi_{P_a}}{\partial P^*_{aref}}\right)_{X_o} \cdot H_{yo}(s) \cdot \left(-C_y(s)\right) \cdot H_y(s) + \left(\frac{\partial \Psi_{P_a}}{\partial P^*_{yi,ref}}\right)_{X_o} \cdot H_{yi}(s) + \left(\frac{\partial \Psi_{P_a}}{\partial y_c}\right)_{X_o} \cdot H_y(s)\right] + \left(\left(\frac{\partial \Psi_{P_i}}{\partial y_c}\right)_{X_o} + \left(\frac{\partial \Psi_{P_i}}{\partial \frac{dy_c}{dt}}\right)_{X_o} \cdot s\right) \cdot H_y(s) + \frac{2}{R_p \cdot C_i} \tag{4.24}$$

4.3.3 Example of application:

Let us consider the cascaded system constituted of an actuator supplied by a dc power source as presented in Fig. 4.8. The different transfer functions presented in Fig. 4.5 are expressed below:

$$H_{yc}(s) = \frac{1}{\frac{s^2}{\omega_{meca}^2} + \frac{2\zeta_{mecas} s}{\omega_{meca}} + 1}, \quad H_{yi}(s) = K \frac{s/\omega_{p1}}{s/\omega_{p1} + 1}, \quad C_y(s) = 2\zeta_{yc}\omega_{yc} + \frac{\omega_{yc}^2}{s}$$

The inner power loop has a bandwidth set to 2000 rad/s. We make the assumption that the power follows perfectly its reference. The others parameter values are given below:

$\zeta_{mecas} = 0.9$	$\omega_{meca} = 500 rad.s^{-1}$	$\zeta_{yc} = 1$	$\omega_{yc} = 20 rad.s^{-1}$	$\omega_{p1} = 22 rad.s^{-1}$

Table II: Control parameters values.

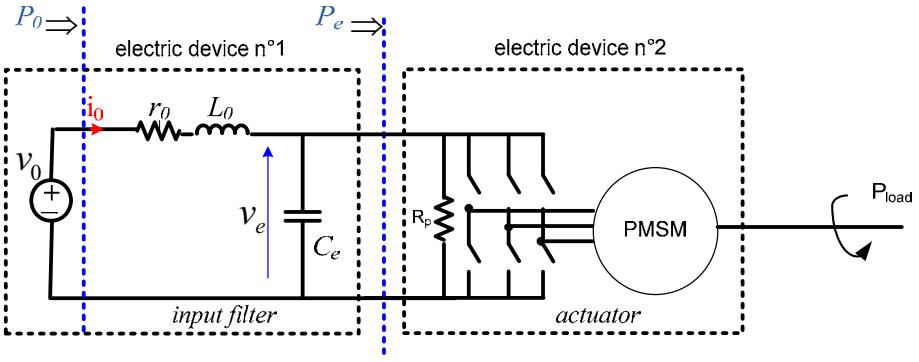

Figure 4.8: DC bus supplying a PMSM with its input filter.

To study the system stability with the proposed approach, it is necessary to identify all the transfer functions introduced in (4.1). In case of ideal voltage source, there is no input capacitance so it is not possible to define an input electrostatic energy. In this particular case, we introduce a fictive large size input capacitance C_0 which has no effect on stability properties of the system. The subscript 1 and 2 will be used respectively for the input filter and actuator.

Calculation of the transfer function $T_1(s)$:

By definition, for the input filter, this impedance is defined by:

$$T_1(s) = \left(-\frac{\tilde{y}_e(s)}{\tilde{P}_e(s)} \right)_{\tilde{y}_0=0} \tag{4.25}$$

With $y_e = \frac{1}{2} C_e \cdot {v_e}^2$

The dynamical equations of the filter verify:

$$C_e \cdot \frac{dv_e}{dt} = i_0 - \frac{P_e}{v_e}\, v \tag{4.26a}$$

$$L_0 \frac{di_0}{dt} = v_0 - r_0 \cdot i_0 - v_e \tag{4.26b}$$

We define $y_e = \frac{1}{2} C_e \cdot v_e$

Thus

$$\dot{y}_e = C_e \cdot v_e \cdot \frac{dv_e}{dt} = v_e \cdot i_0 - P_e \tag{4.27}$$

$$\tilde{y}_e = C_e \cdot V_e \cdot \tilde{v}_e$$

From equations (4.26) and (4.27), with $\tilde{y}_0 = 0 \rightarrow \tilde{v}_0 = 0$, it comes:

$$\Rightarrow \qquad \tilde{\imath}_0 = \frac{-1}{(L_0 \cdot s + r_0)} \cdot \frac{\tilde{y}_e}{C_e \cdot V_e}$$

$$s \cdot \tilde{y}_e = -\widetilde{P_e}(s) + V_e \cdot \tilde{\imath}_0 + I_0 \cdot \tilde{v}_e = -\tilde{P}_e(s) - \frac{V_e}{(L_0 \cdot s + r_0)} \cdot \frac{\tilde{y}_e}{C_e \cdot V_e} + I_0 \cdot \frac{\tilde{y}_e}{C_e \cdot V_e}$$

We deduce:

$$T_1(s) = \left(-\frac{\tilde{y}_e(s)}{\tilde{P}_e(s)}\right)_{\tilde{y}_0=0} = \frac{1}{s + \frac{1}{C_e(L_0 \cdot s + r_0)} - \frac{I_0}{C_e \cdot V_e}}$$

$$= \frac{\left(1 + \frac{L_0}{r_0} \cdot s\right) \cdot r_0 \cdot C_e}{L_0 \cdot C_e \cdot s^2 + \left(r_0 \cdot C_e - {L_0 \cdot P_e}/{V_e^2}\right) \cdot s + 1 - {r_0 \cdot I_0}/{V_e}} \tag{4.28}$$

Calculation of the transfer function $H_{y1}(s)$:

By definition

$$H_{y1}(s) = \left(\frac{\tilde{y}_e(s)}{\tilde{y}_0(s)}\right)_{\tilde{P}_e=0} \tag{4.29}$$

We set: $\tilde{y}_0 = C_0 \cdot V_0 \cdot \tilde{v}_0$

From (4.27) and with $\tilde{P}_e = 0$:

$$\Rightarrow \quad s \cdot \tilde{y}_e = V_e \cdot \tilde{\imath}_0 + I_0 \cdot \tilde{v}_e$$

From (4.26):

$$\tilde{\imath}_0 = \frac{1}{(L_0 \cdot s + r_0)} \cdot \left(\frac{\tilde{y}_0}{C_0 \cdot V_0} - \frac{\tilde{y}_e}{C_e \cdot V_e}\right)$$

$$\Rightarrow \quad s \cdot \tilde{y}_e = V_e \cdot \frac{1}{(L_0 \cdot s + r_0)} \cdot \left(\frac{\tilde{y}_0}{C_0 \cdot V_0} - \frac{\tilde{y}_e}{C_e \cdot V_e}\right) + I_0 \cdot \frac{\tilde{y}_e}{C_e \cdot V_e}$$

$$\frac{\tilde{y}_e(s)}{\tilde{y}_0(s)} = \frac{V_e/C_0 \cdot V_0 \cdot (L_0 \cdot s + r_0)}{s + 1/C_e \cdot (L_0 \cdot s + r_0) - \frac{I_0}{C_e \cdot V_e}}$$

$$\Rightarrow \quad H_{y1}(s) = \left(\frac{\tilde{y}_e(s)}{\tilde{y}_0(s)}\right)_{\tilde{P}_e=0} = \frac{1}{L_0 \cdot C_e \cdot s^2 + \left(r_0 \cdot C_e - {L_0 \cdot P_e}/{V_e^2}\right) \cdot s + 1 - {r_0 \cdot I_0}/{V_e}} \cdot \frac{C_e \cdot V_e}{C_0 \cdot V_0} \tag{4.30}$$

The stability of the transfer function H_{y1} is not guaranteed. If the power consumed by the load P_e becomes greater than $\frac{r_0 \cdot C_e V_e^2}{L_0}$, the coefficient $1 - \frac{r_0 \cdot I_0}{V_e}$ being positive (value of r_o supposed to be very small), the transfer function H_{y1} becomes unstable.

Then the stability analysis of the cascaded system has to be realized with the study of the transfer function:

$$\left(\frac{\tilde{y}_e(s)}{\tilde{y}_0(s)}\right) = \frac{H_{y1}(s)}{1 + T_1(s) \cdot Y_2(s)} \tag{4.31}$$

Where energetic input impedance $Y_2(s)$ is given by (4.24).

Study of the transfer function $Y_2(s)$:

The nominal values of system parameters are given in Table III.

$\Omega_{ref} = 1300rpm$	*Mechanical reference speed*	$p = 4$	*Number of poles*
$V_0 = 200V$	*Dc link voltage*	$\Psi_f = 0.124\ Wb$	*Permanent magnet rotor flux*
$T_s = 10^{-4}s$	*Switching period ($F_s = 1/T_s$)*	$r_s = 0.5\Omega$	*Statoric resistance*
$K = 10$	*Stabilization coefficient*	$L_q = L_d = 3.1e^{-3}$	*dq-axis inductance*
$J = 0.0031\ Kg.m^2$	*Mechanical inertia*	$f = 0.0293N.s^{-1}$	Viscous coefficient
$P = f\Omega^2 = 543\ W\ (P_{load} = 0)$	*Mechanical Nominal power*	$L_0 = 39.56e^{-3}$	*DC-link inductance*
$R_0 = 1.08\ \Omega$	*DC-link resistance*	$C_e = 501\ \mu F$	*DC capacitance*

Table III: System parameters

As depicted in Fig. 4.9, the theoretical energetic input impedance plot when losses are neglected stays in the neighborhood of the plot obtained with numerical simulations (parameters given in table III). Fig 4.10 allows investigating the effect of variations of magnetic energy on the input impedance of the actuator. This figure shows that the plot of $Y_2(s)$ transfer function when the value of the q-axis inductance L_q changes from 0 (variation of magnetic energy neglected) to its nominal value L_{qn}. As shown in this figure, the term due to variations of magnetic energy has a significant influence on the dynamic behavior of the actuators. Fig. 4.10 represents the energetic input impedance for various operating point. As it can be observed, the energetic input impedance is dependent on the operating point.

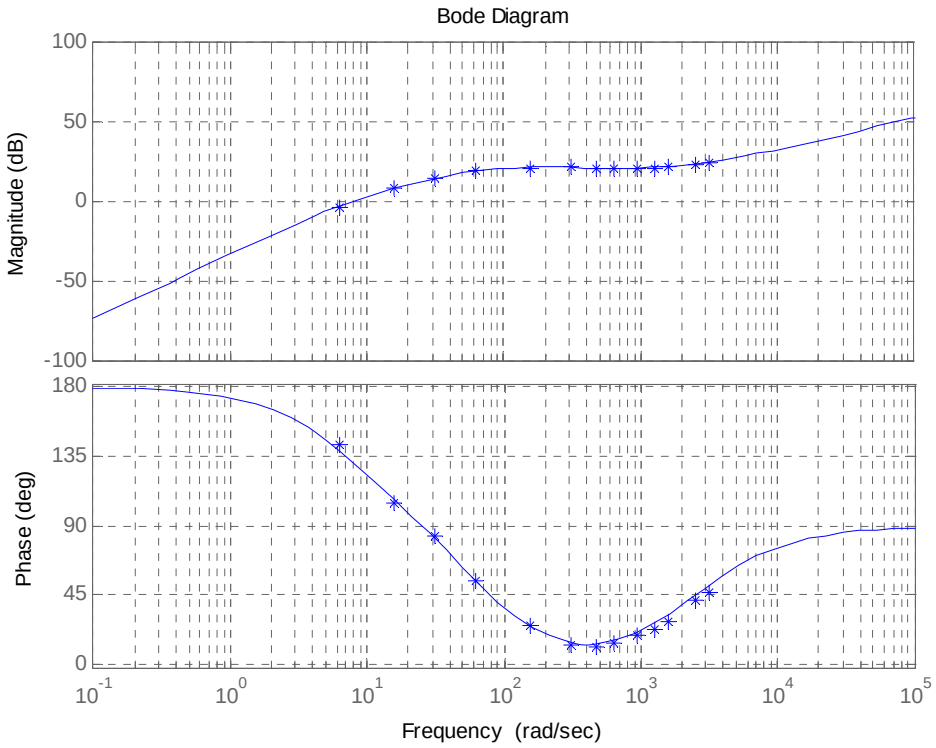

Figure 4.9: Plot of the energetic input impedance, K=10, $\Omega_{ref} = 1300rpm$, P= 543 W (all the others parameters given in table III).

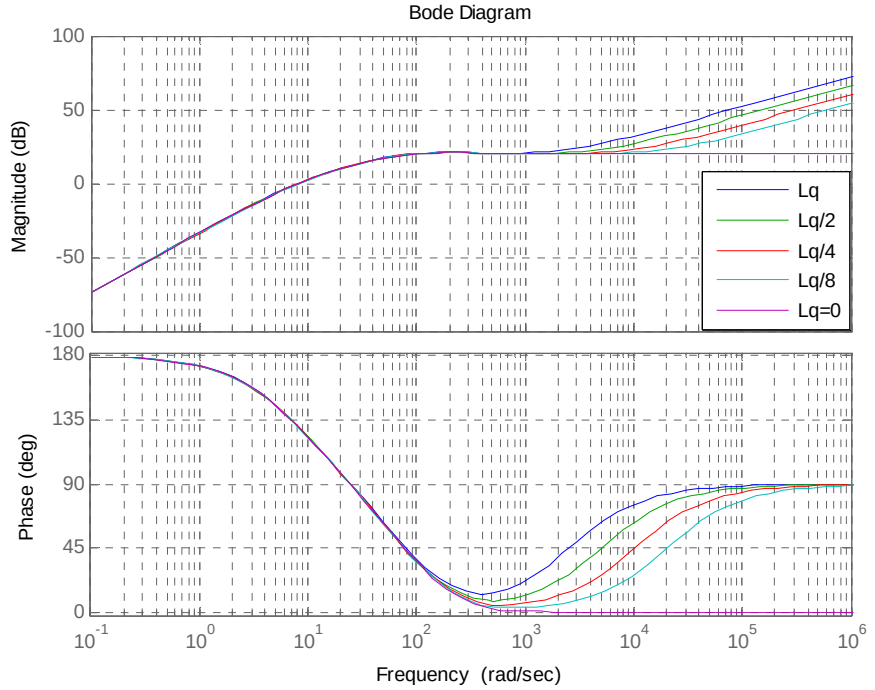

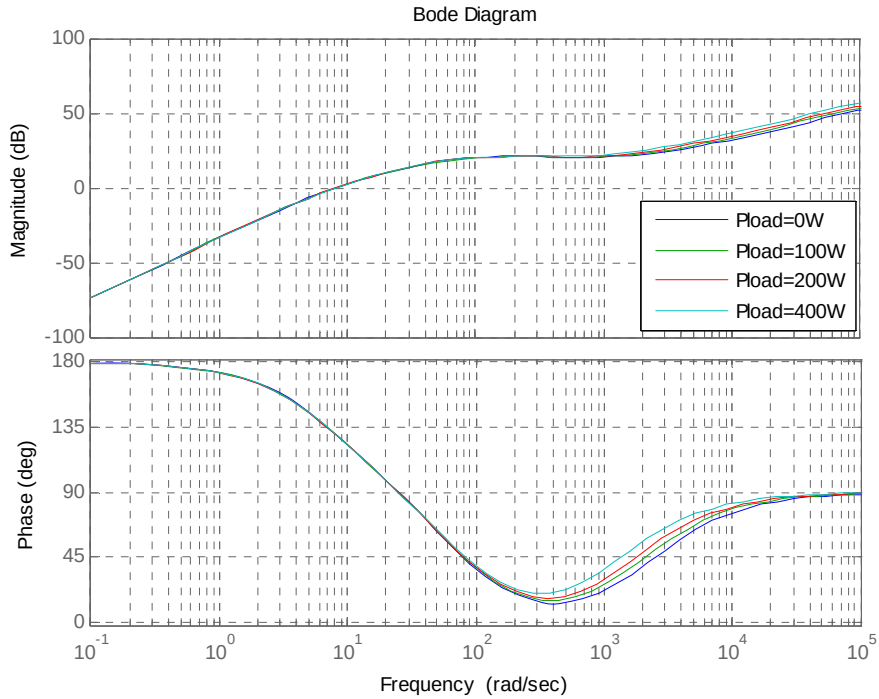

Figure 4.10: Top: Evaluation of transfer function $Y_2(s)$ for different values of L_q, K=10, $\Omega_{ref} = 1300rpm$, P=543W, (all the others parameters given in table III),
Bottom: Evaluation of transfer function $Y_2(s)$for different values of Pload, P= Pload+543 W, K=10, $\Omega_{ref} = 1300\mathrm{rpm}$ (all the others parameters given in table III).

Analysis of the stability:

The analysis of the transfer function (4.31) allows ensuring the stability of the system for values of coefficient *K* greater than $K_c = 2.7$ for the nominal values given in Table III.

4.4 IMPROVEMENT OF THE CONTROL ARCHITECTURE.

4.4.1 Principle:

For some power electronic devices (for example buck converter, PMSM actuators), it is possible to take into account the variations of the magnetic energy with the control law. To explain the proposed improvement of the control, let consider the previous example corresponding to a PMSM actuators. The reference power P_{ref} shown in Fig. 4.5 corresponds to the sum of a mechanical reference power and a stabilizing electrical power. If we want to control energetic input impedance, it is important to ensure that at the input stage of the inverter, the stabilizing power follows correctly its reference $P_{yi,ref}$ without phase shift. To do this, we need to take into account the variations of the magnetic energy. We will now consider that the power P_{ref} is no more a reference mechanical power but corresponds to a reference of the inverter input power. $P_{ref,m}$ being the desired mechanical power. Thus it comes:

$$P_{ref} = P_{ref,m} + r_s\left(\frac{P_{ref,m}}{p.\Psi_f\Omega}\right)^2 + L_q \cdot \left(\frac{P_{ref,m}}{\left(p \cdot \Psi_f\right)^2 \cdot \Omega}\right) \cdot \frac{d}{dt}\frac{P_{ref,m}}{\Omega} \text{ with } \Omega \neq 0$$
$$= P_{yo,ref} + P_{yi,ref} \qquad (4.32)$$

In this expression, like previously, the d-axis current is supposed to be constant and equal to zero. It can be noted that serial losses are taken into account in (4.32). The integration of this relation in the control architecture is achieved as depicted in Fig. 4.11 and is possible because the system does not own unstable dynamical zeroes.

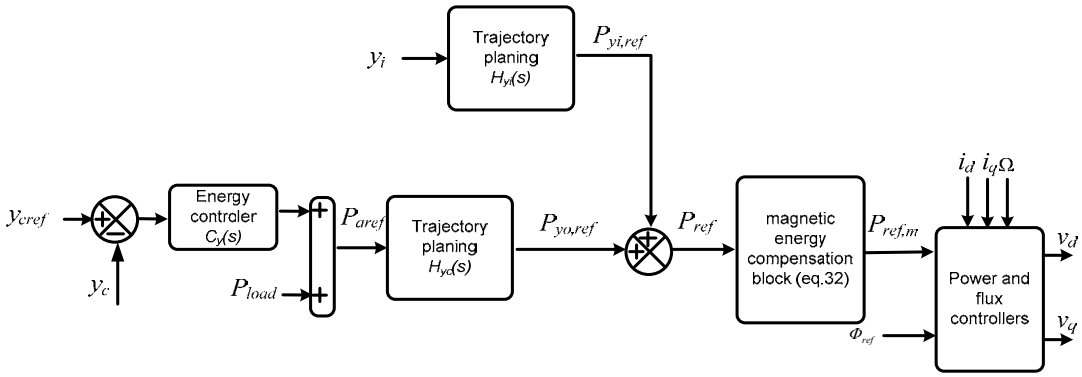

Figure 4.11: Scheme of the control with compensation of the magnetic energy variations.

4.4.2 New expression of the input energetic impedance:

With the control architecture presented in Fig. 4.11, the energetic input impedance can be computed as follows:

We suppose that the mechanical power P_a follows perfectly its reference$P_{ref,m}$. The relation (4.32) can be written into the implicit form:

$$\Psi_{P_a}\left(P_{yo,ref}, P_{yi,ref}, y_c, \frac{dy_c}{dt}, P_{ref,m}, \frac{dP_{ref,m}}{dt}\right) = 0$$
$$= P_{ref,m} + r_s\left(\frac{P_{ref,m}}{p.\Psi_f\Omega}\right)^2 + L_q \cdot \left(\frac{P_{ref,m}}{\left(p \cdot \Psi_f\right)^2 \cdot \Omega}\right) \cdot \frac{d}{dt}\frac{P_{ref,m}}{\Omega} - P_{yo,ref} - P_{yi,ref} \quad (4.33)$$

A first development of the implicit equation (4.33) around an operating point X_0 leads to:

$$\left(\left(\frac{\partial \Psi_{P_a}}{\partial P_{ref,m}}\right)_{X_o} + \left(\frac{\partial \Psi_{P_a}}{\partial \frac{dP_{ref,m}}{dt}}\right)_{X_o} s\right) \cdot \tilde{P}_{ref,m} + \left(\left(\frac{\partial \Psi_{P_a}}{\partial y_c}\right)_{X_o} + \left(\frac{\partial \Psi_{P_a}}{\partial \frac{dy_c}{dt}}\right)_{X_o} s\right) \cdot \tilde{y}_c +$$
$$\left(\frac{\partial \Psi_{P_a}}{\partial P_{yo,ref}}\right)_{X_o} \cdot \tilde{P}_{yo,ref} + \left(\frac{\partial \Psi_{P_a}}{\partial P_{yi,ref}}\right)_{X_o} \cdot \tilde{P}_{yi,ref} = 0$$

Thus, for the reference mechanical power, with $\widetilde{P}_{load} = 0$, $\tilde{y}_{cref} = 0$ and $\widetilde{\Phi}_{ref} = 0$ it comes:

$$\tilde{P}_{ref,m} = \left(\left(\frac{\partial \Psi_{P_a}}{\partial P_{ref,m}}\right)_{X_o} + \left(\frac{\partial \Psi_{P_a}}{\partial \frac{dP_{ref,m}}{dt}}\right)_{X_o} s\right)^{-1} \cdot$$

$$\left[-\left(\left(\frac{\partial \Psi_{P_a}}{\partial y_c}\right)_{X_o} + \left(\frac{\partial \Psi_{P_a}}{\partial \frac{dy_c}{dt}}\right)_{X_o} s\right) \cdot \tilde{y}_c + \left(\frac{\partial \Psi_{P_a}}{\partial P_{yo,ref}}\right)_{X_o} \cdot H_{yc}(s) C_y(s) \cdot \tilde{y}_c - \left(\frac{\partial \Psi_{P_a}}{\partial P_{yi,ref}}\right)_{X_o} \cdot H_{yi}(s) \cdot \tilde{y}_i\right] \quad (4.34)$$

From the dynamical equation verified by the kinetic energy y_c and with the assumption that the load power P_{load} is constant, it comes:

$$\left(s + \frac{2f}{J}\right) \cdot \tilde{y}_c = \tilde{P}_a = \tilde{P}_{ref,m}$$

Then relation (4.34) leads to:

$$\left(\frac{\tilde{y}_c}{\tilde{y}_i}\right)_{\substack{\tilde{P}_{load}=0 \\ \tilde{y}_{cref}=0 \\ \tilde{\emptyset}_{ref}=0}} = H_y(s)$$

$$= \frac{-\left(\frac{\partial \Psi_{P_a}}{\partial P_{yi,ref}}\right)_{X_o} \cdot H_{yi}(s)}{\left(s+\frac{2f}{J}\right)\cdot\left(\left(\frac{\partial \Psi_{P_a}}{\partial P_{ref,m}}\right)_{X_o} + \left(\frac{\partial \Psi_{P_a}}{\partial \frac{dP_{ref,m}}{dt}}\right)_{X_o} s\right) + \left(\left(\frac{\partial \Psi_{P_a}}{\partial y_c}\right)_{X_o} + \left(\frac{\partial \Psi_{P_a}}{\partial \frac{dy_c}{dt}}\right)_{X_o} s\right) - \left(\frac{\partial \Psi_{P_a}}{\partial P_{yo,ref}}\right)_{X_o} \cdot H_{yc}(s)C_y(s)} \quad (4.35)$$

Remark: For practical point of view, serial losses can be supposed negligible. Then

$$\left(\frac{\partial \Psi_{P_a}}{\partial P_{ref,m}}\right)_{X_o} = 1, \qquad \left(\frac{\partial \Psi_{P_a}}{\partial \frac{dP_{ref,m}}{dt}}\right)_{X_o} = L_q \cdot \left(\frac{P_{ref,m}}{\left(p\cdot\Psi_f\cdot\Omega\right)^2}\right)$$

$$\left(\frac{\partial \Psi_{P_a}}{\partial y_c}\right)_{X_o} = 0, \qquad \left(\frac{\partial \Psi_{P_a}}{\partial \frac{dy_c}{dt}}\right)_{X_o} = L_q \cdot \left(\frac{-{P_{ref,m}}^2}{J.\left(p\cdot\Psi_f\right)^2\cdot\Omega^4}\right)$$

$$\left(\frac{\partial \Psi_{P_a}}{\partial P_{yo,ref}}\right)_{X_o} = -1, \qquad \left(\frac{\partial \Psi_{P_a}}{\partial P_{yi,ref}}\right)_{X_o} = -1$$

$$H_y(s) \approx \frac{H_{yi}(s)}{\left(s+\frac{2f}{J}\right)\cdot\left(1+s\cdot L_q\cdot\left(\frac{P_{ref,m}}{\left(p\cdot\Psi_f\cdot\Omega\right)^2}\right)\right) + s\,L_q\cdot\left(\frac{-{P_{ref,m}}^2}{J\cdot\left(p\cdot\Psi_f\right)^2\cdot\Omega^4}\right) + H_{yc}(s)C_y(s)}$$

The whole input power of the inverter can be put into the form:

$$P_i = \frac{2\cdot y_i}{R_p\cdot C_i} + P_a + r_s\cdot\left(\frac{P_a}{p\cdot\Psi_f\cdot\Omega}\right)^2 + L_q\cdot\left(\frac{P_a}{\left(p\cdot\Psi_f\right)^2\cdot\sqrt{2\cdot y_c/J}}\right)\cdot\frac{d}{dt}\left(\frac{P_a}{\sqrt{2\cdot y_c/J}}\right)$$

$$= \frac{2\cdot y_i}{R_p\cdot C_i} + P_{yo,ref} + P_{yi,ref} \quad (4.36)$$

$$\tilde{P}_i = \frac{2\cdot\tilde{y}_i}{R_p\cdot C_i} + \tilde{P}_{yo,ref} + \tilde{P}_{yi,ref} = \frac{2\cdot\tilde{y}_i}{R_p\cdot C_i} - H_{yc}(s)C_y(s)\cdot\tilde{y}_c + H_{yi}(s)\cdot\tilde{y}_i \quad (4.37)$$

From (4.35) $\tilde{y}_c = H_y(s) \cdot \tilde{y}_i$

Then from (4.37)

$$Y_2(s) = \left(\frac{\tilde{P}_i}{\tilde{y}_i}\right)_{\substack{\tilde{P}_{load=0} \\ \tilde{y}_{cref=0} \\ \tilde{\emptyset}_{ref=0}}} = \frac{2}{R_p \cdot C_i} - H_{yc}(s)C_y(s) \cdot H_y(s) + H_{yi}(s) \tag{4.38}$$

4.4.3 Properties of the input energetic impedance:

The use of this new control scheme allows taking into account the magnetic energy variations and leads to an energetic input impedance less dependent on the operating point as shown in Fig. 4.12 and Fig. 4.13. Fig. 4.12 shows that the plot of the energetic input impedance Y_2, computed when losses are neglected, is closed to the plot deduced from numerical simulation (parameters given in table III). Losses have effectively a negligible effect on the energetic input impedance with the chosen parameters. Fig. 4.13 presents the theoretical energetic input impedance (losses neglected) for different operating points and different values of inductances. As shown in this figure, the influence of the magnetic inductance on the energetic input impedance has been reduced. Moreover the energetic input impedance is less dependent on the operating point.

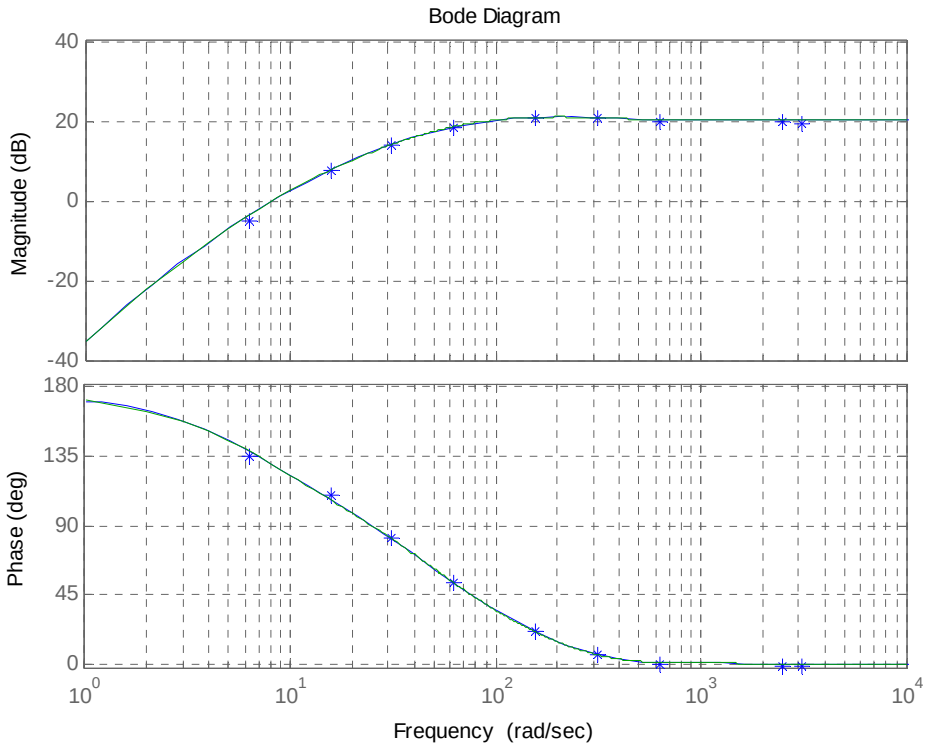

Figure 4.12: Evolution of the theoretical transfer function Y_2 (continuous plot) and values obtained by simulation, K=10; $\Omega_{ref} = 1300rpm$, P= $f\Omega^2$ =543 W.

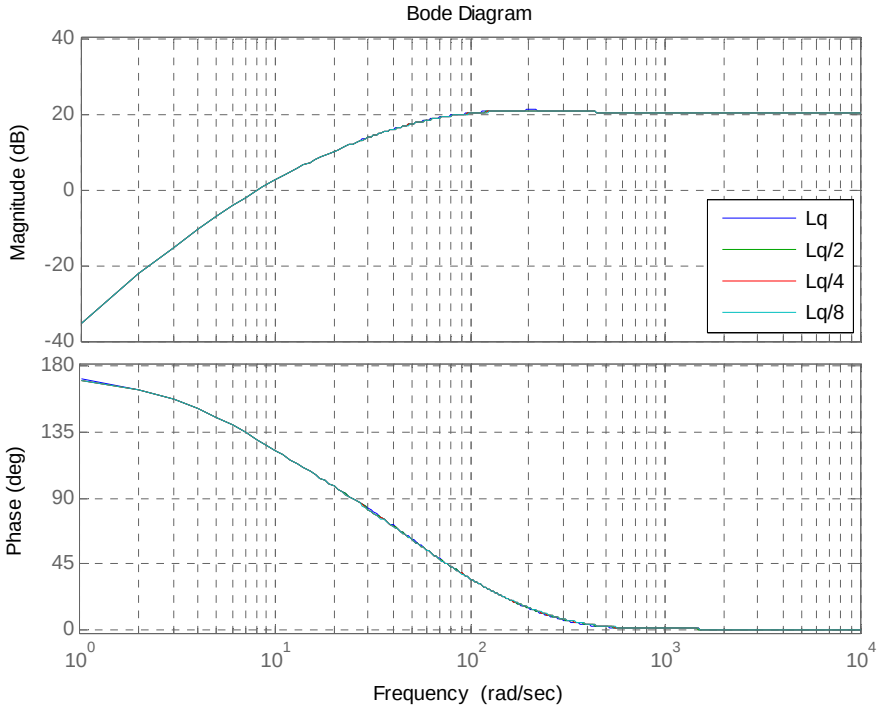

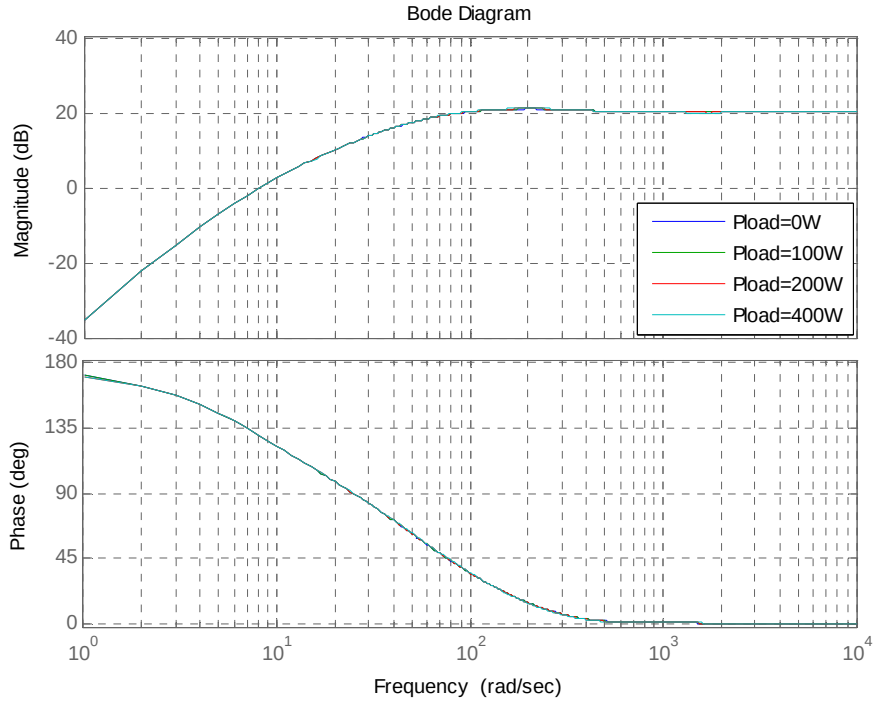

Figure 4.13: Top: Evaluation of transfer function $Y_2(s)$ for different values of L_q, K=10, $\Omega_{ref} = 1300rpm$, P=543W, (all the others parameters given in table III),
Bottom: Evaluation of transfer function $Y_2(s)$for different values of Pload, P= Pload+543 W, K=10, $\Omega_{ref} = 1300rpm$ (all the others parameters given in table III).

4.4.4 Parameter Sensitivity:

As shown in Fig. 4.14, a bad estimation of parameters involves significant changes in the energetic impedance waveform. Fig. 4.14 evaluates the result of bad estimations of the q-axis inductance and mechanical time constant (inertia value error). As depicted in Fig. 4.14, the energetic input impedance is affected by parameters errors. When the operating point changes (results presented in Fig. 4.15), a bad estimation of the inductance value leads to an energetic input impedance dependent of the operating point. Nevertheless a bad estimation of the mechanical time constant has a limited influence on the energetic input impedance waveform, the input impedance being less dependent of the operating point.

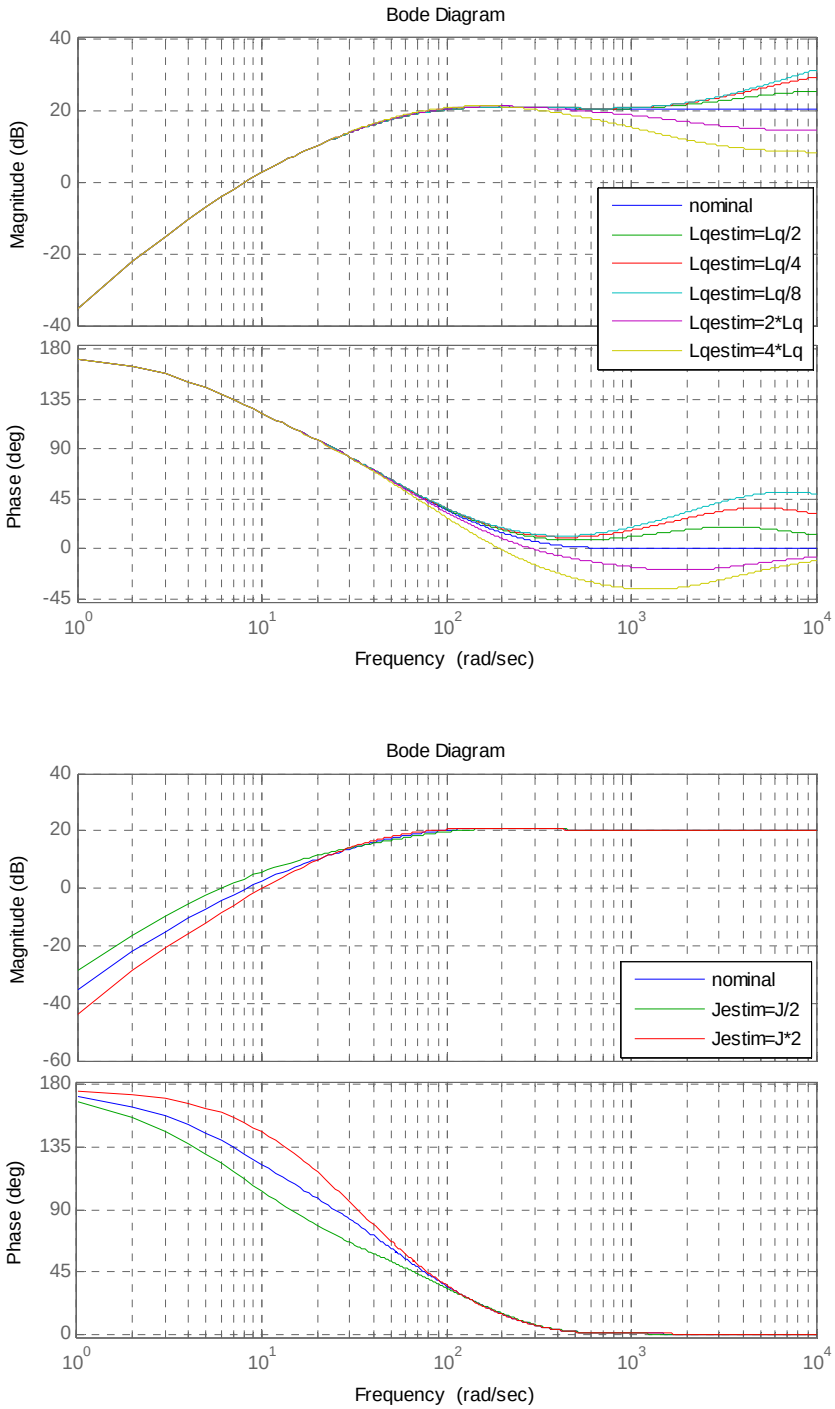

Figure 4.14: Evaluation of sensitivity of the transfer function $Y_2(s)$. K=10, $\Omega_{ref} = 1000rpm$, P=321W, (all the others parameters given in table III)
At top: when value of the q-axis inductance L_{qestim} is bad estimated
At bottom: when value of the inertia J_{estim} is bad estimated

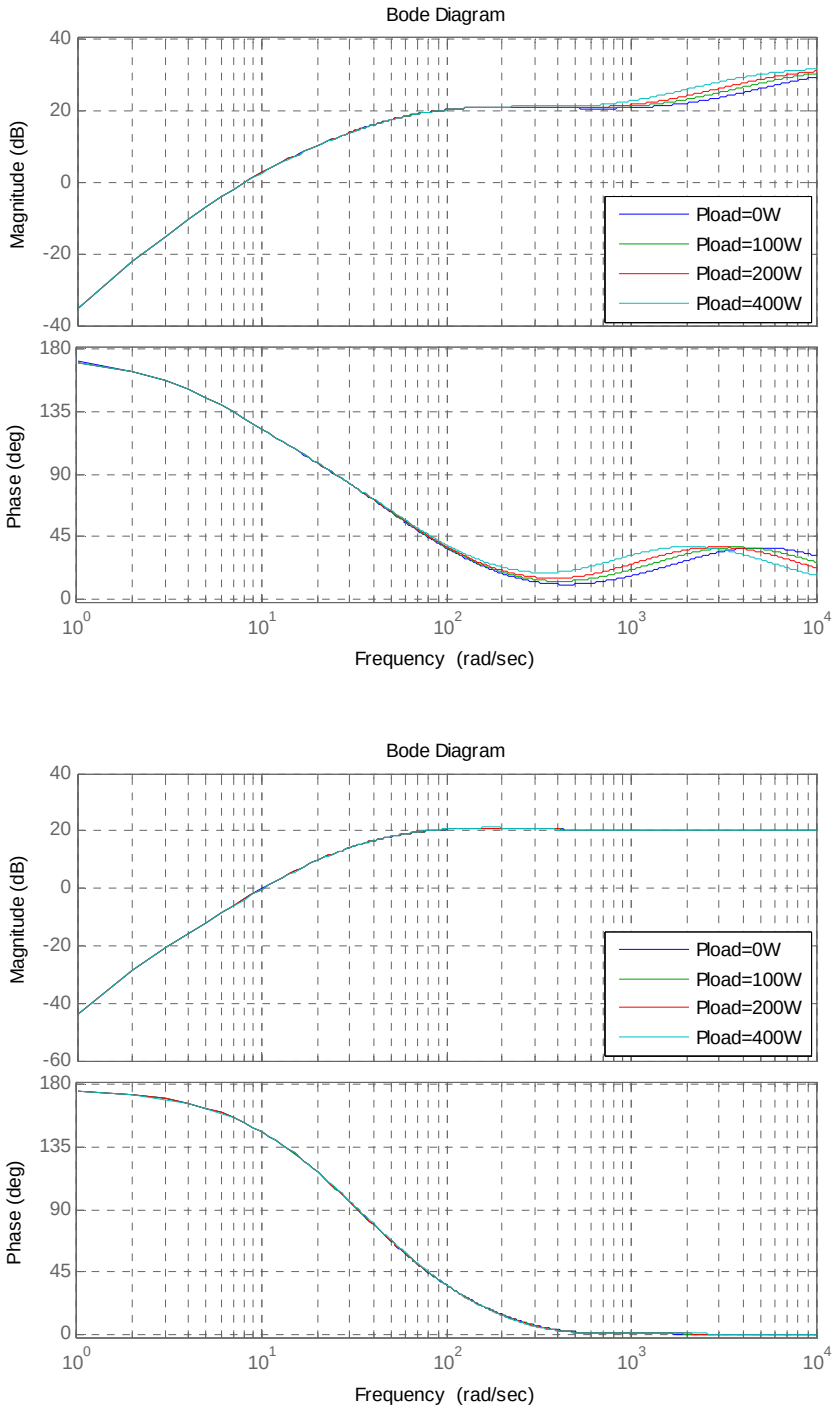

*Figure 4.15: Evaluation the transfer function $Y_2(s)$ when value of the inductance (top:L_{qestim}=L_q/4) and inertia (bottom J_{estim}=J*2) is bad estimated, for different load power, K=10, $\Omega_{ref} = 1000rpm$, (all the others parameters given in table III).*

4.4.5 Linearity properties:

As detailed in the previous paragraph, the energetic input impedance is less dependent on the operating point if the values of parameters are known. Now we want to evaluate if the input power variations are linearly dependent or not on the electrostatic variations. To do this, we realize simulations to measure the transfer function Y_2 for different values of the electrostatic variations.

We set $y_{ik} = y_{i0} + \Delta y_k . sin(\omega t)$ and we measure $P_{ik} = P_{i0} + \Delta P_k(\omega) . sin(\omega t + \emptyset_k(\omega))$ for three values of Δy_k (noted $\Delta y_1, \Delta y_2, \Delta y_3$) and different values of ω. We want to evaluate the magnitude of the three transfer functions Y_{21} Y_{22} Y_{23} defined by $\frac{\Delta P_k(\omega)}{\Delta y_k}, k \in \{1,2,3\}$ and their phases $\emptyset_k(\omega), k \in \{1,2,3\}$. To compare the different results, we define the following relative indicators:

$$\Delta G_k = 100 * max\left(\left|\frac{\frac{\Delta P_k(\omega)}{\Delta y_k} - \frac{\Delta P_1(\omega)}{\Delta y_1}}{\frac{\Delta P_1(\omega)}{\Delta y_1}}\right|\right)_{\omega \in [15,2500]} , k \in \{2,3\}$$

$$\Delta P_k = 100 * max\left(\left|\frac{\emptyset_k(\omega) - \emptyset_1(\omega)}{\emptyset_1(\omega)}\right|\right)_{\omega \in [15,2500]} , k \in \{2,3\}$$

The results are summarized in the table IV. As it can be observed, for the three values of electrostatic energy variations (set respectively to 10%, 20% et 50% of the electrostatic energy value in steady state y_{i0}) in the tested frequency range, the relative variations of gain and phase are small even in case of large variations of the input electrostatic energy.

$\Delta G_2 = 0.6\%$	$\Delta G_3 = 0.9\%$	ΔP_2 =1.5%	ΔP_3 =4%

Table IV: evaluation of linearity

With $\Delta y_1 = \frac{y_{i0}}{10}$, $\Delta y_2 = \frac{y_{i0}}{5}$ et $\Delta y_3 = \frac{y_{i0}}{2}$

4.5 SIMULATION RESULTS:

The effect of this Stabilization technique can be verified by simulation. A Simulink model is developed and its parameters are given in Tables II and III. Fig. 4.16 shows the simulation results of the system after a speed reference step from 1000rpm to 1300rpm without stabilization block. Fig. 4.17 shows the stabilization of the system after the activation of stabilization block. Fig. 4.17a presents the simulation results for K=5 and 15b for K=10 to show the effect of stabilization block gain *K* on stability of the system.

Fig. 4.18 presents the behaviour of the system when the speed is increased from 0 to 1300rpm. This figure shows that the system is unstable without stabilization block and it becomes stable after activation of the stabilization block (K=3). For the results shown in Fig. 4.18 and 4.19 the block which compensates the variations of magnetic energy due to the leakage inductance of the PMSM is added (control scheme presented in Fig. 4.11). The figures 4.18 and 4.19 show that with this additional block, the stabilization block is still efficient.

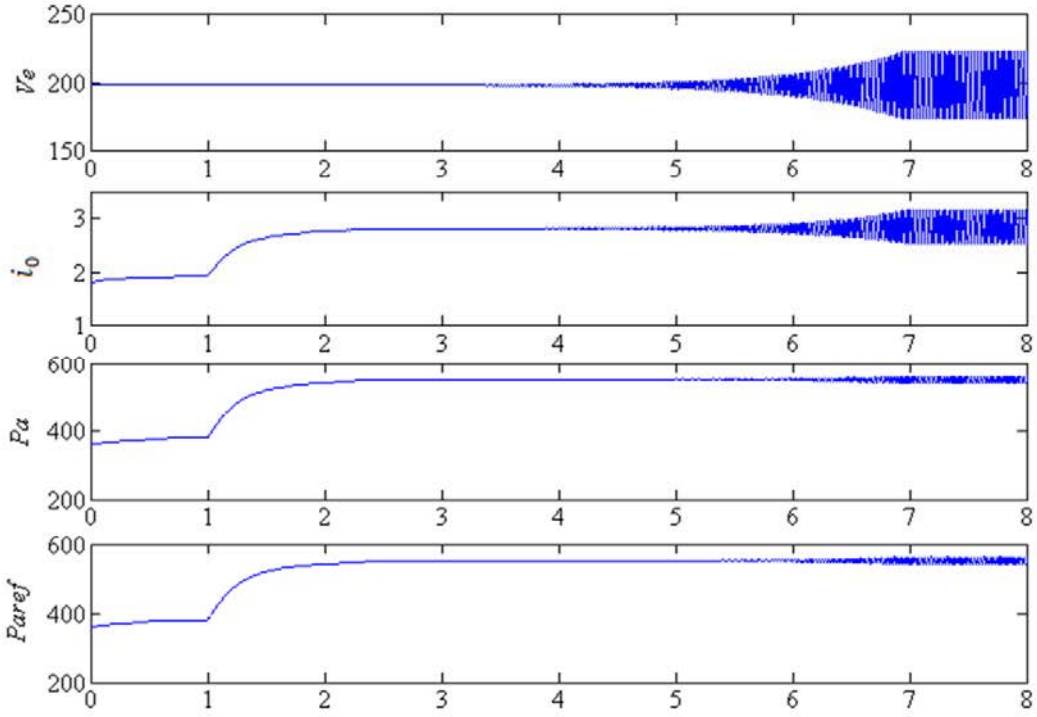

Figure 4.16: Instability of DC-link variables after a speed step from 1000rpm to 1300rpm (K=0)

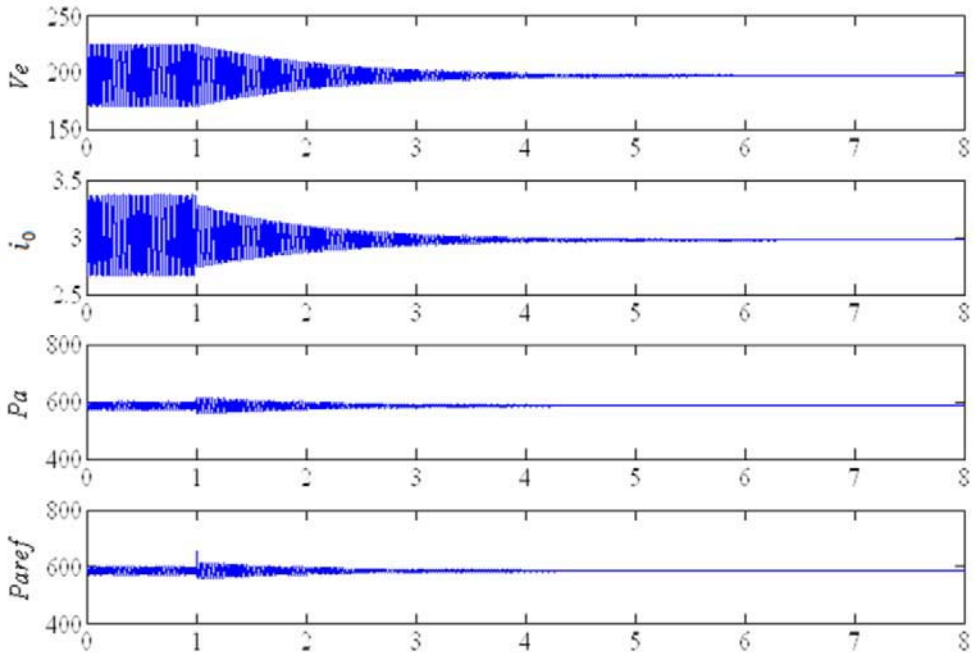

Figure 4.17a: Stabilization of DC-link variables after a speed step from 1000rpm to 1300rpm (with stabilization gain K=5)

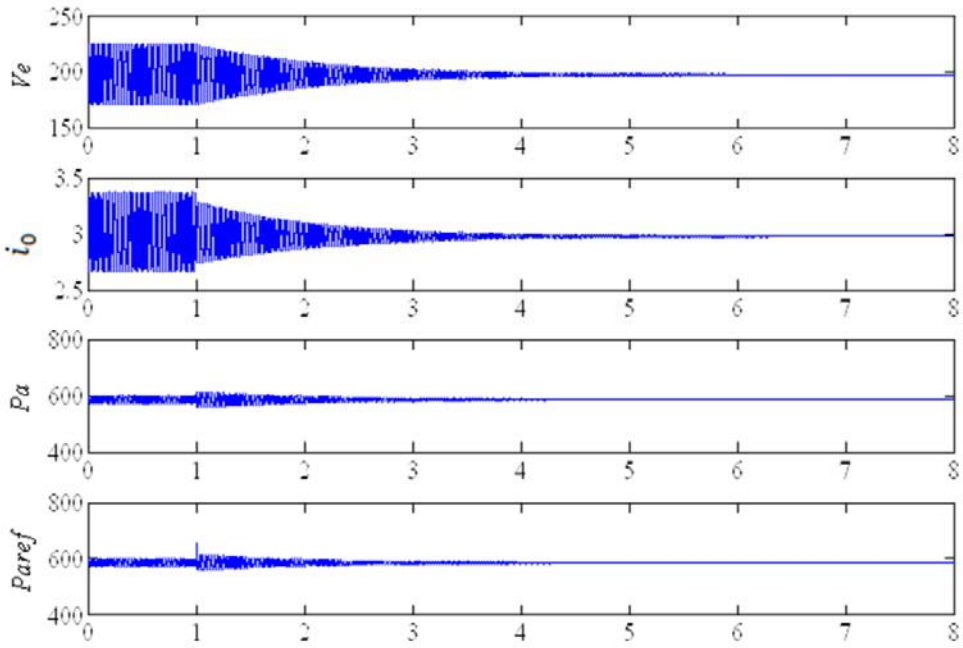

Figure 4.17b: Stabilization of DC-link variables after a speed step from 1000rpm to 1300rpm (with stabilization gain K=10)

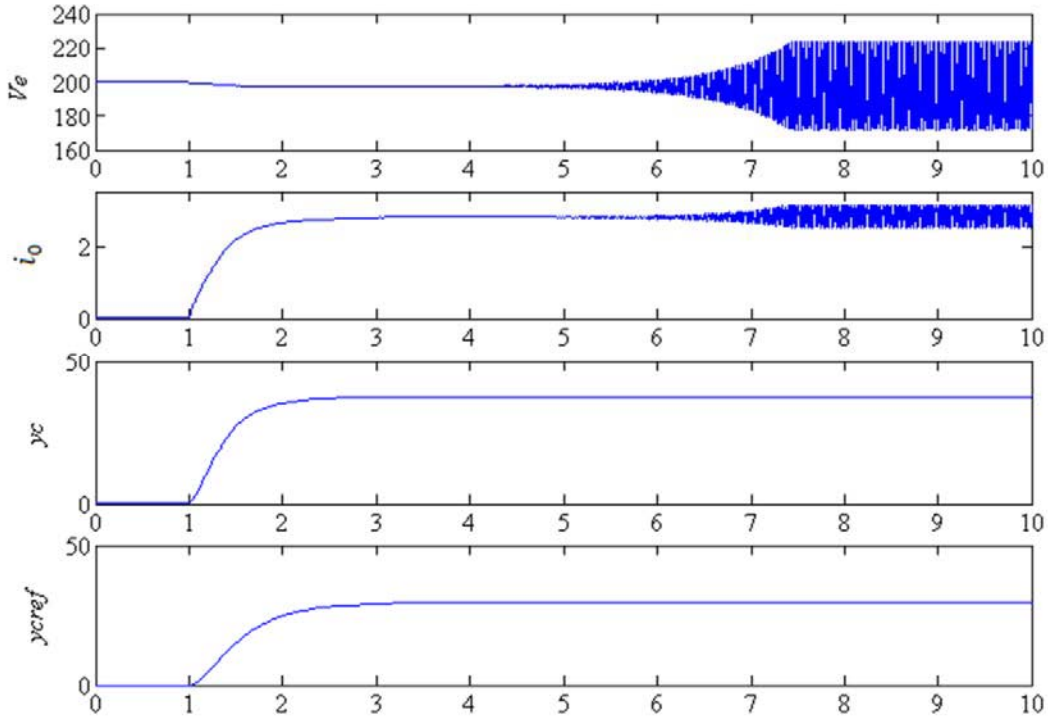

Figure 4.18: behavior of the system after a reference speed variation from 0 to 1300 rpm, K=0 with magnetic compensation block.

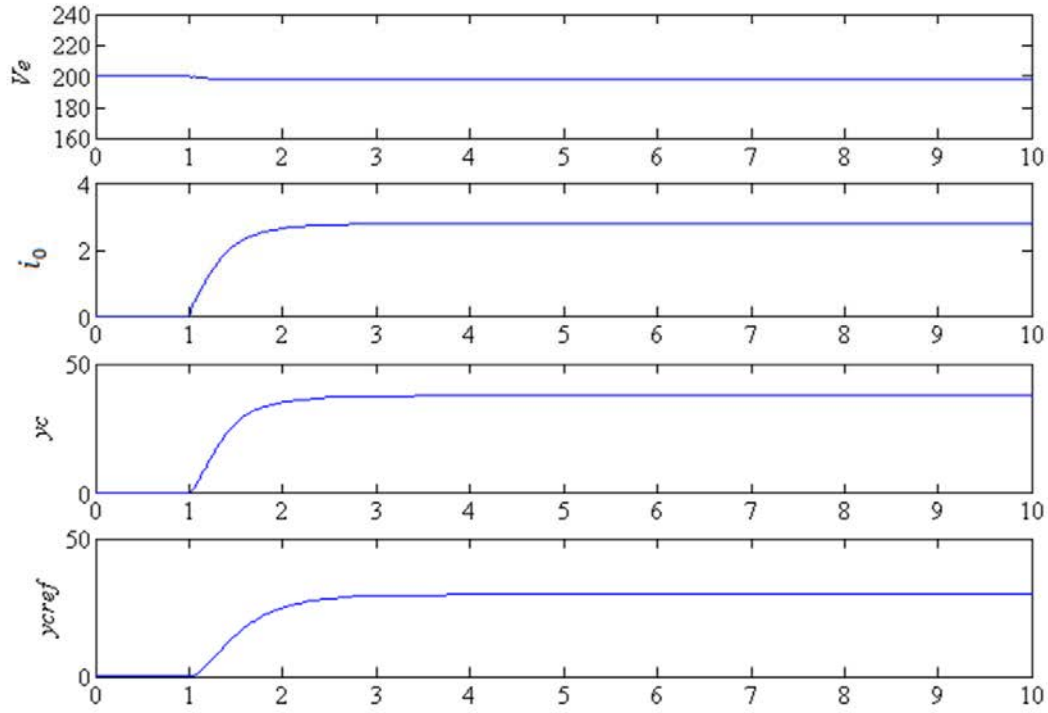

Figure 4.19: behavior of the system after a reference speed variation from 0 to 1300 rpm, K=3 with magnetic compensation block.

4.6 EXPERIMENTAL VALIDATION:

We propose to validate the proposed control with an experimental bench corresponding to the system presented in Fig. 4.8 with the parameters given in Tables II and III.

For practical point of view, the proposed control based on control of kinetic energy is efficient if the speed is different from zero. Thus at low speed (less than 10 rpm), a classical two loop speed-torque controller is used to start the actuator. The algorithm commutation process is not detailed in this manuscript. To achieve tracking of positive or negative speed, the expression of the kinetic energy has been modified as follows: $y_C = 0{,}5J\Omega|\Omega|$. The kinetic controller has been slightly modified to take into account the speed sign. For the first tests, the block which allows taking into account the magnetic energy (eq32) is removed, the control strategy presented in Fig. 4.7 is used. Fig. 4.20 presents the response of the system after a speed reversion from -1000 to 1000 rpm without stabilizing effect (K=0). At this operating point, the system is stable and the proposed control structure is efficient. The kinetic energy and the mechanical power follow their respective references. Fig. 4.21 presents the behavior of the system after a step of the speed reference from 1000 to 1300 rpm without stabilizing effect (K=0). As shown in this figure the new operating point is unstable and large current and voltage undulations appear on the DC bus.

Fig. 4.22 shows the behavior of the system after starting the stabilizing block for two values of the coefficient K. As foreseen by the theoretical study, the value of K being greater than K_c, the system is stable.

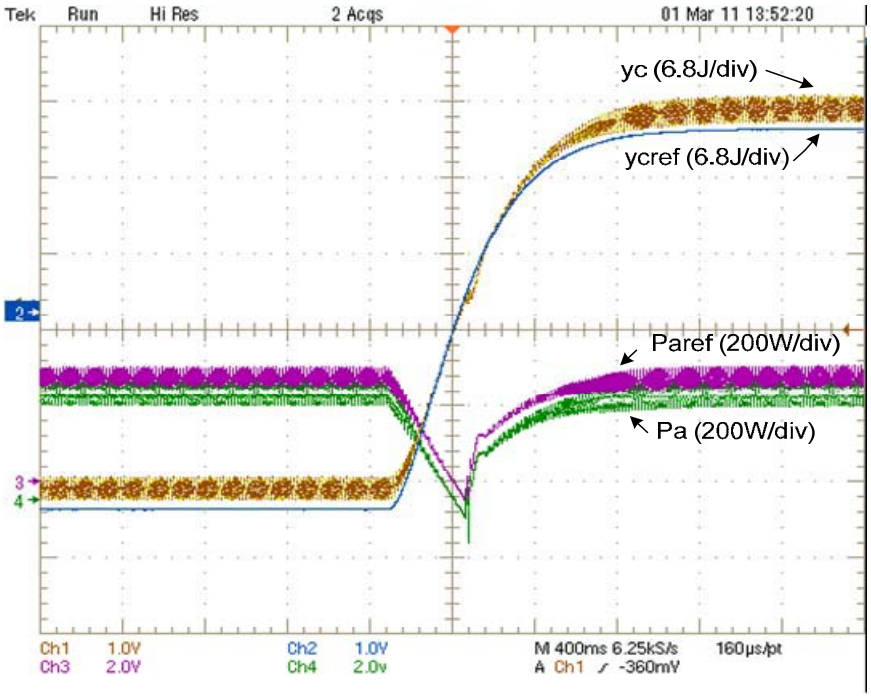

Figure 4.20: behavior of the system after a reference speed reversion from -1000 to 1000 rpm.

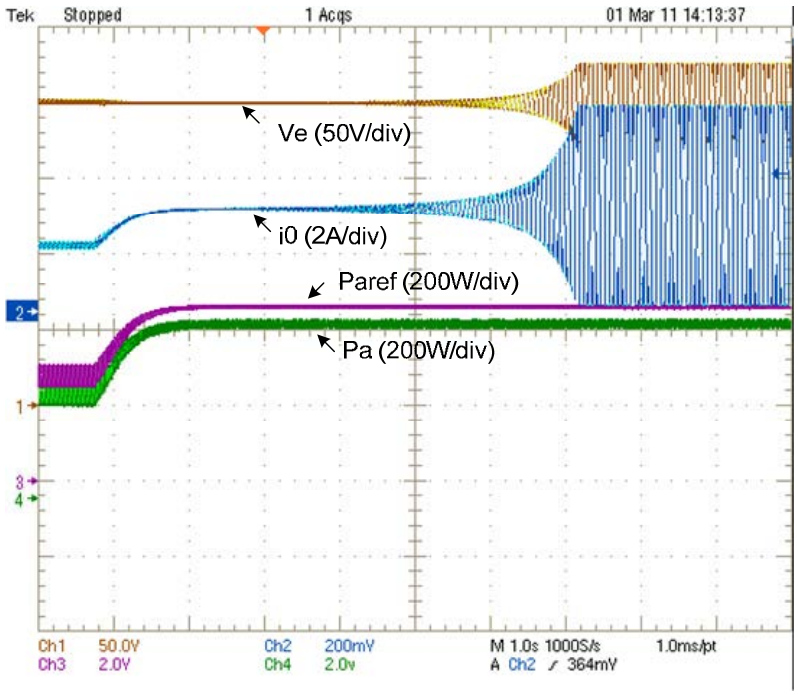

Figure 4.21: behavior of the system after a reference speed variation from 1000 to 1300 rpm, K=0.

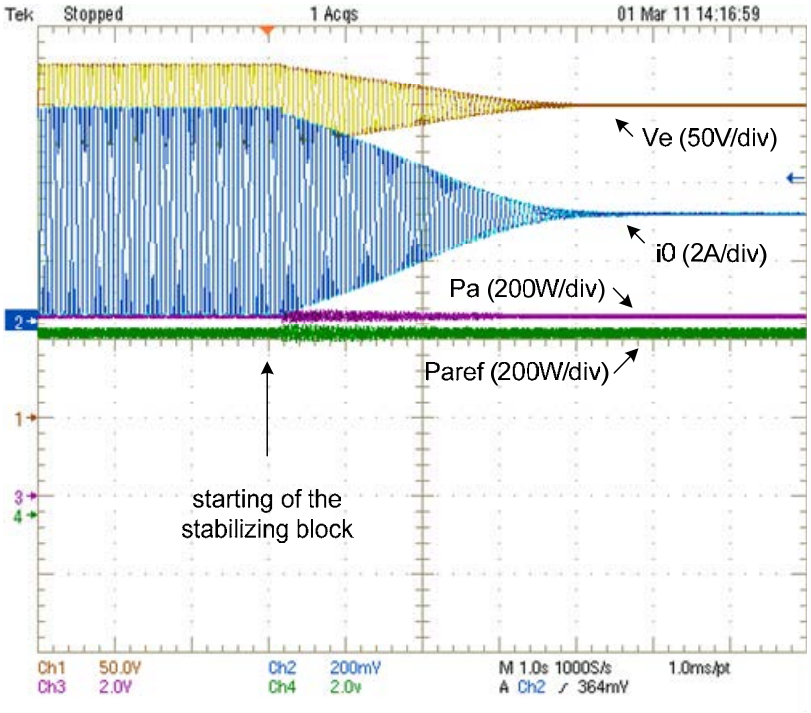

Figure 4.22a: behavior of the system after the starting of the stabilizing block for K=5

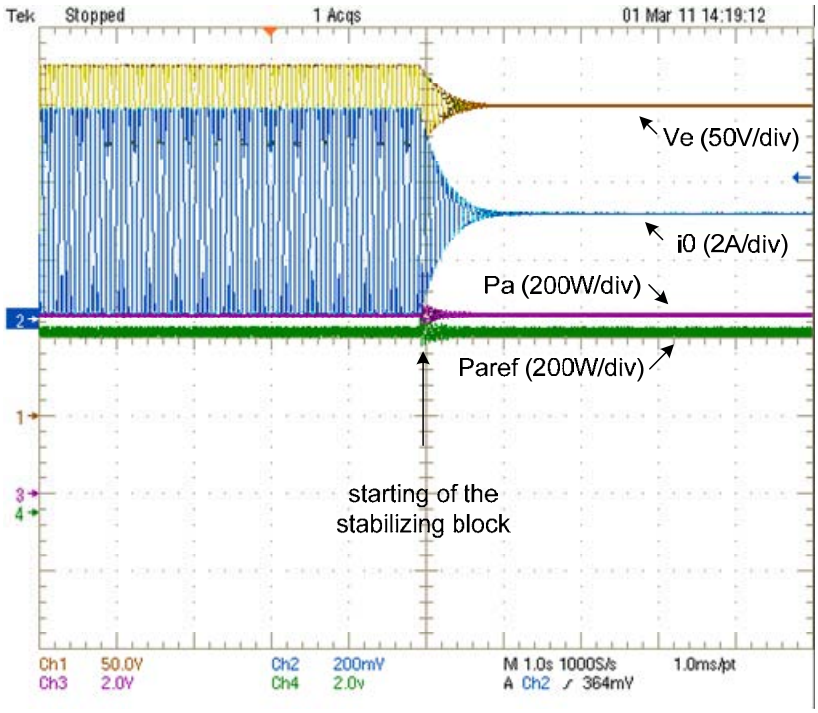

Figure 4.22b: behavior of the system after the starting of the stabilizing block for K=10

For the last tests, the block which compensates the variations of magnetic energy due to the leakage inductance of the PMSM is added (control scheme presented in Fig. 4.11). As shown in figures 4.23 and 4.24, the behavior of the system is similar to those obtained without the block.

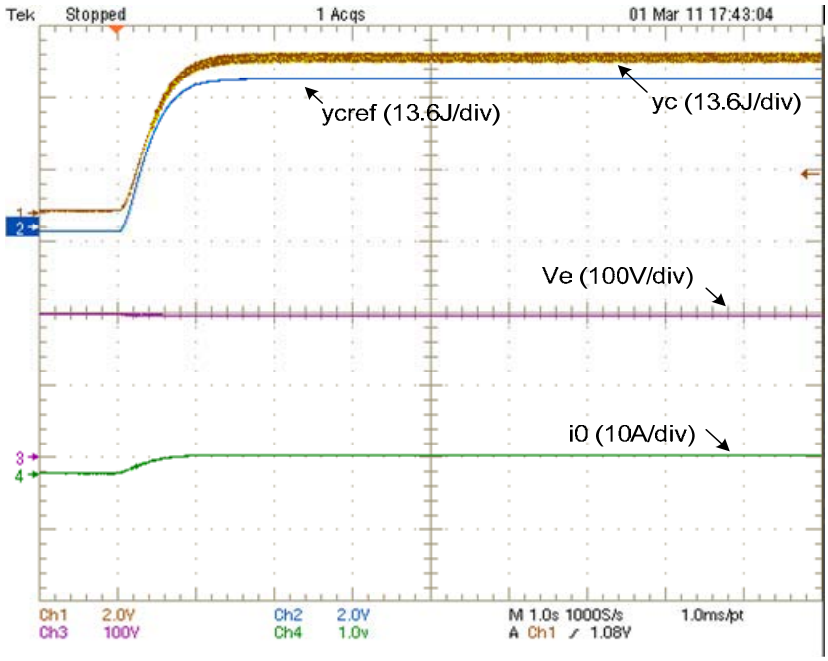

Figure 4.23: behavior of the system after a reference speed variation from 0 to 1300 rpm, K=3 with magnetic compensation block.

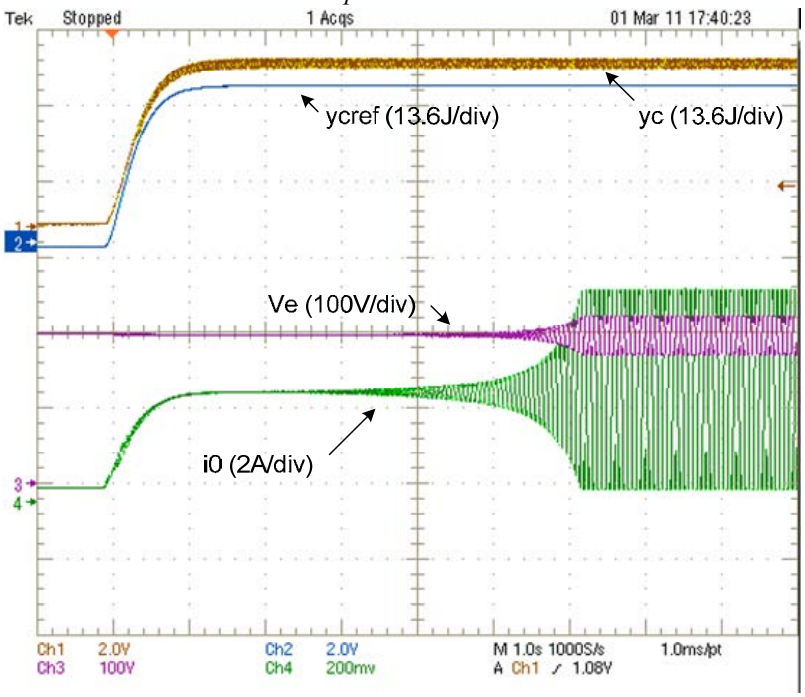

Figure 4.24: behavior of the system after a reference speed variation from 0 to 1300 rpm, K=0 with magnetic compensation block.

4.7 CONCLUSION:

We propose to use a new approach to investigate stability of cascaded system based on energy/power variables rather than the usual voltage/current ones. Like with the classical approach based on input/output impedances, the use of the proposed energetic impedances allows analyzing the stability of cascaded or distributed power system. Nevertheless contrary to classical approaches for which the stability analysis is dependent on the operating point, we have shown that it is possible to design new control architecture which allows obtaining, for some active electric devices, energetic impedances less dependent on the operating point. This property allows simplifying small signal stability analysis of the cascaded system and more generally of large scale distributed system. For some power architectures, the use of this new strategy of control can lead to small signal stability analysis independent of the operating. This last property is closely bound to the knowledge of the system parameters. In the case of PMSM, we have shown that a good knowledge of the q-axis inductance value is required to obtain energetic input impedance few dependent of the operating point.

GENERAL CONCLUSION

The work presented in this thesis deals with the stability of electrical systems where a constant power load (Tightly controlled load) is connected to the common DC-bus through an input LC filter. A stabilization structure was proposed which helps in removing the variations (oscillations) of DC-link variables. Various linear and nonlinear oscillation compensation techniques were presented which can be used for small signal and large signal stability of the electrical system. We have used Circle criterion and Lyapunov criterion to analyze the global stability of the system. In the end a new modeling, based on energetic variables, was introduced to investigate the stability of cascaded systems. Contrary to classical approach for which voltages and currents are the state variables, we proposed to use electrostatic energies and powers as state variables.

In chapter 1, the stability issues of electrical systems with input filter and constant power load connected to a common dc bus are addressed. Chapter 1 discusses that an inverter-motor-drive system connected to the grid through a LC filter and rectifier, when tightly regulated, behaves as constant power load. If the input voltage increases by some factor, the PWM control circuitry cuts back the duty cycle of the controlled switch to maintain a constant output voltage. This, in turn, causes the input current to decrease by the same proportion. An increase/decrease of input voltage results in a decrease/increase of input current, causing the inverter motor-drive-system to look like negative impedance at the input terminal. This negative impedance behavior may lead to the instability of the system. Thus an undamped or lightly damped input filter connected to the input port, can interact with the negative impedance characteristics of the system to form a negative-impedance oscillator. Similarly the problem of instability arises in Distributed Power System (DPS) where multiple sources and loads are connected to a common bus. We have discussed different stability criteria in chapter 1. Impedance based stability criterion is the most practical one which says that a system is stable if the output impedance of the source is less than the input impedance of the load. So for this criterion we only need to study the output impedance of the source subsystems and input impedance of the load subsystems to study the stability of the DPS.

Various existing damping techniques were discussed in the chapter one but these are not practical solutions because of power losses in damping resistances. Similarly stability can be achieved by increasing the size of dc-link capacitance or decreasing the inductance but it is undesirable especially in aerospace application where we have very long cables with natural inductance and also volume and weight are the most important factors. In this thesis we have proposes four methods to stabilize the electrical system which help to gain stability margins even with smaller size of dc-link capacitance which is the premier requirement in aerospace applications.

In order to remove oscillations on the dc-link variables, when small dc-link capacitance and/or large dc-link inductance are used, a drive consists of an LC input filter connected to an inverter-PMSM is treated as illustrative example.

In the first part of this thesis, an oscillation compensation structure was proposed and local stability of the electrical system was achieved (chapter 2). To design the compensator, input impedance of the constant power load and output impedance of the filter were derived. A general method giving the analytical expression of the input impedance of an inverter-PMSM-drive

system was presented. The modeling is evidently based on small signal variations because of the local nature of this study. However, all dynamics are taken into account except those of the inverter ones, which can be often neglected in practical applications. An oscillation compensation block containing a band-pass filter was proposed and added to the conventional control structure of the system. It allows stabilizing the dc-link voltage when small dc-link capacitances are employed. Therefore, this compensation block is useful in aerospace applications, where the dc-link capacitance should be small because of mechanical constraints.

In many studies, the design of the DC-Link capacitance is based on the first order modeling of the system and is realized to ensure only the asymptotic stability around the operating point. Nevertheless the behavior of the system in case of large disturbance is unknown. Although linear models can be successfully employed to locally describe the behavior of a physical system, they often fail to provide a satisfactory global characterization. In chapter 2 we proposed two methods for the global stability study of an electrical system containing DC power supply, an LC filter and a constant power load. These stability techniques can stabilize the system independent of operating point and remove the DC-link variables oscillations even in case of very large disturbances In order to stabilize the electrical system a nonlinear stabilization structure was presented. In the proposed approach the control structure of the electrical system is slightly modified to implement the nonlinear stabilization structure for improving the large signal stability of the system and thus allows reducing the dc-link capacitance value.

In the last part of the thesis we proposed an approach to investigate stability cascaded system based on energy/power variables rather than the usual voltage/current ones. Like with the classical approach based on input/output impedances, the use of the proposed energetic impedances allows analyzing the stability of cascaded or distributed power system. Nevertheless contrary to classical approaches for which the stability analysis is dependent on the operating point, we have shown that it is possible to design new control architecture which allows obtaining, for some active electric devices, energetic impedances less dependent on the operating point. This property allows simplifying small signal stability analysis of the cascaded system and more generally of large scale distributed system. For some power architectures, the use of this new strategy of control can lead to small signal stability analysis of the operating point and sufficient to global asymptotic stability of the system. This subject will be the object of the next work.

BIBLIOGRAPHY

[Abu 04] H. Abu-Rub, J. Guzinski, Z. Krzeminski, and H. A. Toliyat, "Advances control of induction motor based on load angle estimation," *IEEE Trans. Ind. Electron.,* vol. 51, no. 1, pp. 5-14, Feb; 2004.

[Al-f 99] M. Al-Fayyoumi, D. Boroyevich, and A. Nayfeh, "Input filter interactions in DC-DC switching regulators," in *Proc. PESC'99,* pp. 926-932, 1999.

[Art 01] F. Arteche, B. Allongue, F. Szoncso, and C.Rivetta, "EMI filter design and stability assessment of dc voltage distribution based on switching converters," in *Proc. of 7th Workshop on Electronics for LHC Experiments,* pp. 353-357, Stockholm, Sep. 2001.

[Awa 09] A-Bilal Awan, S. Pierfederici, B. Nahid-Mobarakeh (Member IEEE) and F. Meibody-Tabar, "Active stabilization of a poorly damped input filter supplying a constant power load," *IEEE Energy Conversion Congress and Exposition,* pp. 2991-2997, San Jose, USA, 20-24 Spt. 2009.

[Awa 09a] A-Bilal Awan, B. Nahid-Mobarakeh (Member IEEE), S. Pierfederici, and F. Meibody-Tabar, "Nonlinear stabilization of a DC-bus supplying a constant power load," *IEEE Industry Apllication Society Annual Meeting,* Houston, USA, pp. 1-8, Oct. 2009.

[Bae 01] B. H. Bae, B. H. Cho, and S. K. Sul, "damping control strategy for the vector controlled traction drive," in *Proc. EPE'01,* CD-ROM, Austria, 2001.

[Bar 05] F. Barruel, N. Retiere, J. Schanen, and A. Caisley, "Stability approach for vehicules DC power network: Application to aircraft on-board system," *IEEE PESC 2005,* pp. 1163-1169, June, 2005.

[Bas 97] M. Basso, R. Genesio, A. Tesi, and G. Torrini, "*On describing systems with periodic behavior in terms of simple nonlinear models,*" Control of Oscillations and Chaos, St, Petersburg, 1997.

[Bel 95] M. Belkhayat, R. Cooley, and A. Witulski, "Large signal stability criteria for distributed systems with constant power loads," in *Proc. IEEE 26th PowerElectron; Spec. Conf.,* Atlanta, GA, pp. 1333-1338, Jun. 1995.

[Cal 02] J. Calvente, L. M. Salamero, P. Garces, and A. Romero, "Input filter damping design using zero dynamics analysis," in *6th European Space power Conf.,* pp. 6-10, May 2002.

[Che 06] X. Chen and M. Kazerani, "Space vector modulation control of an AC-AC-AC converter with a front-end diode rectifier and reduced DC link capacitor," *IEEE Trans. Power Electronics,* vol. 21, no. 5, pp. 1470-1478, Sept. 2006.

[Cho 95] Byungcho Choi and Bo H. Cho, "Intermediate line filter design to to meed both impedance compatibility and EMI specifications," in *IEEE Trans On Power Electronic.,* vol. 10, no. 5, pp. 583-588, Sep 1995.

[Cho 99] B. Choi, B. Cho, and S; Hong, "Dynamics and control of DC-DC converters driving other converters downstream," in *IEEE Trans. Circuits Syst. I,Reg. Papers,* vol. 46, no. 10, pp. 1240-1247, Oct. 1999.

[Cie 98] J. G. Ciezki and R. W. Ashton, "The design of stabilizing controls for shipboard DC-DC Buck choppers using feedback linearization techniques," in *Proc. of IEEE 29th Power Electron. Spec. Conf.,* Fukuoka, Japan. May 1998, pp. 335-341.

[Dal 85] K. C. Daly, "Comments on "A noval feedforward compensation canceling input filter-regulator interaction"" in *IEEE Trans. Aerosp. Electron. Syst.,* vol. AES-21, no. 4, pp. 584-587, July 1985.

[Dél 95] B. Délémontey, B. Jacquot, C. Iung, B. De Fornel, J. Bavard, "Nonlinear decoupling of an induction motor drive with input filter," in *Proc. IEEE CCA'95,* pp. 1004-1009, 1995.

[Ema 99] A. Emadi, B. Fahimi, and M. Ehsani, "On the concept of negative impedance instability in advance aircraft power systems with constant power loads," *Soc. Automotive Eng. (SAE) J.,* vol. 1, no. 1, 1999. Paper 1999-01-2545.

[Ema 99a] A. Emadi, B. Fahimi, and M. Ehsani, "On the concept of negative impedance instability in advance aircraft power systems with constant power loads," in *Proc. of 34th Inter-Society Energy Convers. Eng. Conf.,* Vancouver, BC, Canada, Aug. 1999, pp. 1-11.

[Ema 00] A. Emadi and M; Ehsani, "Negative impedance stabilizing controls for PWM DC-DC converters using feedback linearizarion techniques," in *Proc. 35th Intersoc. Energy Convers. Eng. Conf,.* Las Vegas, NV, Jul. 2000, pp. 613-620.

[Ema 03] A. Emadi, M. Ehsani, and J. M. Miller, "Vehicular electrical power systems: land, sea, air and space vehicles." New York: Marcel Dekker, Dec 2003.

[Ema 06] A Emadi, A. Khaligh, C. H. Rivetta, and G. A. Williamson, "Constant power loads and negative impedance instability in automotive systems: Definition, Modeling, Stability and Control od power electronic converters motor drives," in *IEEE Trans. Veh. Technol.* vol. 55, no. 4, pp. 1112-1125, July 2006.

[Eri 99] Robert W. Erickson, "Optimal sigle resistor damping of input filter," in *IEEE Applied Power Electronic Conf, APEC'99 Proc,* pp. 1073-1097, 1999.

[Eri 01] R. W. Erickson and D. Maksimovic, *Fundamentals of Power Electronics.* Norwell, MA: Kluwer, 2nd edition, 2001.

[Eri 92] Sandra Y. Erich and William M. Polivka, "Input filter design criteria for current-programmed regulators," in *IEEE Trans. On Power Electronics,* vol. 7, no. 1, pp. 143-151, January 1992.

[Fay 99] Mohammad Al-Fayyoumi, Dushan Boroyevich, and Ali Nayfeh, " Input filter interactions in DC-DC switching regulators," in *Proc. IEEE PESC'99,* pp. 926-932, 1999.

[Fen 99] Xiaogang Feng, Zhihong Ye, Kun Xing, Fred C. Lee, and Dushan Borojevic, "Individual load impedance specification for a stable DC distributed power system," in *IEEE Proc. APEC'99,* pp. 923-929, 1999.

[Fen 02] Xiaogang Feng, Jingjun Liu, and Fred C. Lee, "Impedance specifications for stable DC distributed power systems," in *IEEE Trans. power Electron.,* vol. 17, no. 2, pp. 157-162, March 2002.

[Flo 96] Martin Florez-Lizarraga and Arthur F. Witulski,"Input filter design for multi-module DC power systems," in *IEEE Trans. on Power Electronics.,* vol. 11, no. 3, pp. 472-479, May 1996.

[Gen 95] R. Genesio, A. Tesi, F. Villoresi, "*Models of complex dynamics in nonlinear systems,*" System and Control Letters, vol. 25, no. 11, pp. 185-192, 1995.

[Gir 09] S. Girinon, H. Piquet, N. Roux, and B. Sareni, "Analytical input filter design in DC distributed power systems approach taking stability and quality criteria into account," *13th European conference on Power Electronics and Applications EPE'09,* pp. 1-10, 8-10 Sept. 2009.

[Gir 09a] S. Girinon, C. Baumann, H. Piquet, and N. Roux, "Analytical modeling of the input admittance of an electric drive for stability analysis purpose," *The European Physical Journal Applied Physics,* vol. 47, 2009.

[Glo 98] S. F. Glover and S. D. Sudhoff, "An experimentally validated nonlinear stabilizing control for power electronics based power systems," in *Soc. Automotive Eng. (SAE)J.,* vol. 1, no. 1, Paper No 981255.

[Gri 98] V. Grigore, J. Hatonen, J. Kyyra, and T. Suntio, "Dynamics of a buck converter with constant power load," in *Proc. IEEE 29th Power Electron. Spec. Conf.,*Fukuoka, Japan, pp. 72-78, May 1998.

[Gri 08] A. Griffo, J. Wang and D. Howe, "Large signal stability analysis of DC power systems with constant power loads," *IEEE Vehicle Power and Propulsion Conference (VPPC),* September 3-5, 2008, Harbin, China.

[Har 05] L. Harnefors, K. Pietlainenardier, "Inverter DC-link stabilizing control with improved voltage sag ride-through capability," in *Proc. EPE'05,* Dresden, Germany, CD-Rom, Sept. 2005.

[Hen 04] A. Hentunen, K. Zenger, and T. Suntio, "A systematic approach to analyze the stability of distributed power systems," in *Nordic Workshop on Power and industrial Electronics, NORPIE'04,* 2004.

[Jan 92] Y. Jang and R. W. Erickson, "Physical origins of input filter oscillations in current programmed converters," in *IEEE Trans. On Power Electronics,* vol. 7, no. 4, pp. 725-733, Oct 1992.

[Jos 98] M. Joshi and V. Agarwal, "Generation and propagation of EMI waves in power electronic circuits" in *IEEE Power Electronics Specialists Conf. (PESC 98),* volume 2, pp. 1165-1171, May 1998.

[Kar 03] C. Karimi, D. Sadarnac, and C. Prévot, "On the interaction of the input filter and the converter regulation," in *EPE-Toulouse,* pp. 163-168, Sep. 2003.

[Kel 83] S. S. Kelkar and F. C. Lee, "A novel feedforward compensation canceling input filter – regulator interaction," in *IEEE Trans. Aerosp. Electron. Syst.,* vol. AES-19, no. 2, pp. 258-268, March 1983.

[Kel 84] S. S. Kelkar and F. C. Lee, "Adaptive input filter compensation for switching regulators," in *IEEE Trans. Aerosp. Electron. Syst.,* vol. AES-20, no. 1, pp. 57-66, Jan 1984.

[Kel 84a] S. S. Kelkar and F. C. Lee, "Stability analysis of buck regulator employing input filter compensation," in *IEEE Trans. Aerosp. Electron. Syst.,* vol. AES-20, no. 1, pp. 67-77, Jan. 1984.

[Khalil] H. K. Khalil, "*Nonlinear Systems,*" 3rd Edition, Printice-Hall, Upper Saddle River, New Jersey.

[Kis 83] A. S. Kislovski, "General feedforward input filter compensation method" in *Proc. IEEE PESC'83,* pp. 300-305, 1983.

[Koh 92] Charles R. Kohut, "Input filter design criteria for switching regulators using cruuent-mode programming," in *IEEE Trans. On Power Electronics,* vol. 7, no. 3, pp. 469-479, July 1992.

[Kos 04] Konstantin S. Kostoy, Jukka-Pekka Sjoroos, Jorma J. Kyyra, and Teuvo Suntio, "Selection of power filters for switched mode power supplies," in *Nordic Workshop on Power and Industrial Electronics.* NORPIE'04, 2004.

[Kun 07] Ying-Shieh Kun and Ming-Hung Tsai, "FPGA-based speed control IC for PMSM drive with adaptive fuzzy conrol," *IEEE Trans. Power Electronics,* vol. 22, no. 6, pp. 2476-2486, Nov. 2007.

[Las 04] C. Lascu, I. Boldea, and F. Blaanjerg, "Variable-structure direct torque control−A class of fast and robust controllers for induction machine drives," *IEEE Trans. Ind. Electron.,* vol. 51, no. 4, pp. 785-792, Aug. 2004.

[Liu 04] P. Liutanakul, S. Pierfederici, and F. Meibidy-Tabar, "DC-link capacitor reduction of a controlled rectifier supplying *N* inverter-motor-drive systems by compensating the load variations," in *Proc. PESC'04,* pp. 1398-1303, CD-ROM, 2004.

[Liu 07] X. Liu, A. J. Forsyth, and A. M. Cross, "Negative input-resistance compensator for a constant power load," *IEEE Trans. Industrial Electronics,* vol. 54, no. 6, pp. 3188-3196, Dec. 2007.

[Liu 08] X. Liu, A. J. Forsyth, "Active stabilization of a PMSM drive system for aerospace applications," in *Proc. PESC'08,* pp. 283-289, CD-ROM, June 2008.

[Liu 08a] P. Liutanakul, S. Pierfederice, A. Bilal Awan, B. Nahid-Mobarakeh, and F. Meibody-Tabar, "Stability investigation of inverter-motor-drive system with input filter−Optimization of the DC-link capacitance value," in *Proc. PESC'08,* pp. 3728-3734, CR-ROM, June 2008.

[Liu 08b] P. Liutanakul, S. Pierfederici, F. Meibody-Tabar, "Application of SMC with I/O feedback linearization to the control of the cascade controlled-rectifier/inverter-motor-drive system with small DC-link capacitor," *IEEE Trans. Power Electronics,* vol. 23, no. 5, pp. 2489-2499, Sept. 2008.

[Liu 10] P. Liutanakul, A-Bilal Awan, S. Pierfederici, B. Nahid-Mobarakeh (Member IEEE) and F. Meibody-Tabar, "Linear stabilization of DC bus supplying a constant power load: general design approach," *IEEE Trans. on Power Electronics,* vol. 25, no. 2, pp. 276-284, Feb. 2010.

[Lou 04] Khaled Louati, Daniel Sadarnac, and Sharif Karimi, "Input filter influence on the stability of DC-DC converters" in *Proc. IEEE ISIE'04,* vol. 2, pp. 1165-1171, May 2004.

[Luc 06] A. Lucia, D. Franco, H. Bourlès, E. R. De Pieri, H. Guillard, "Robust nonlinear control associating robust feedback linearization and H control," *IEEE Trans. Automatic Control,* vol. 51, no. 7, July 2006.

[Mar 08] D. Marx, S. Pierfederici, and B. Davat, "Nonlinear control of an inverter-motor-drive system with input filter – Large signal analysis of the DC-link voltage stability," in *Proc. PESC'08,* pp. 498-503, CD-ROM, June 2008.

[Mar 09] D. Marx, S. Pierfederice, B. Nahid-Mobarakeh, and B. Davat, "Contribution to determination of domain of attraction in power systems: Application to drive with input filter," *IEEE IAS 2009,* 4-8 October 2009, Houston , USA.

[Mic 99] Daniel M. Michell. "Power line filter design considerations for DC-DC converters," in *IEEE Industrial Application Magazine,* pp. 16-26, November/December 1999.

[Mid 76] R. D. Middlebrook, "Input filter considerations in design and application of switching regulators," in *Proc.of IAS 76,* pp. 366-382, 1976.

[Mid 78] R. D. Middlebrook, "Design techniques for preventing input-filter oscillations in switched mode regulators," in *Proc. of Powercon 5,* pp. A3-1-A3-16, May 1978.

[Mos 03] H. Mosskull, "DC-link stabilization of an induction machine drive," in *Proc, EPE'03,* Toulouse, France, CD-Rom, sept. 2003.

[Mos 03a] H. Mosskull, B. Wahlberg and J. Galic, "Validation of stability for an induction machine drive using measurements," in *Proc. 13th IFAC Symposium on System Identification,* CD-ROM, Rotterdam, Netherlands, 2003.

[Mos 05] H. Mosskull, "Stabilization of an induction motor drive with resonant input filter," in *Proc. EPE'05,* CD-ROM, Dresden, Germany, 2005.

[Mos 07] H. Mosskull, J. Galic, and B. Wahlberg, "Stabilization of induction motor drives with poorly damped input filters," *IEEE Trans. Inductrial Electronics,* vol. 54, no. 5, Oct. 2007.

[Nah 00] B. .ahid-Mobarakeh, F. Meibody-Tabar, F. M. Sargos, "Self-organizing intelligent controller for speed and torque control of a PMSM," in *Proc. IAS'00,* vol. 2, pp. 1383-1290, Oct. 2000.

[Nah 01] B. Nahid-Mobarakeh, F. Meibody-Tabar, and F. M.Sargos, "On-line Identification of PMSM electrical parameters based on decoupling control," in *Proc. IAS'01,* CD-ROM, Chicago, Oct. 2001.

[Nav 91] M. J. Nave,"Power line filter design for switched-mode power supplies" *Edition Van Nostrand Reinhold,* New York, 1991.

[Nij 90] H. Nijmeijer, A. J. Van Der Schaft, *"Nonlinear Dynamic System,"* Springer-Verlag, New Yark, 1990.

[Pay 08] A. Payman, S. Pierfederici, F; Meibody-Tabar, "Energy control of supercapacitor/fuel cell hybrid power cource," *Journal of Energy Conversion and Management,* vol. 49, 2008, pp. 1637-1644.

[Phe 79] T. Phelps and W. Tate, "Optimizing passive input filter design," in *Proc. of Powercon 6,* pp. G1.1-G1.10, May 1979.

[Pie 04] S. Pierfederici, R. Meuret, F. Meibody-Tabar, B. Davat, Contribution à l'étude de la stabilité des systèmes distribués – Application aux réseaux de bord d'avions, *EDP Science J3EA,* 2004.

[Rah 10] A. M. Rahimi, Member, IEEE, G. A. Williamson, Senior Member, IEEE, and A. Emadi, Senior Member, IEEE, "Loop-Cancellation technique: A novel nonlinear feedback to overcome the destabilizing effect of constant power loads," *IEEE Trans. on Vehicular Technology,* vol. 59, no. 2, Feb. 2010.

[Riv 06] C. H. Riveta, A. Emadi, G. A. Williamson, R. Jayabalan, and B. Fahimi, "Analysis and control od Buck DC-DC converter operating with constant power load in sea and undersea vehicles," in *IEEE Trans. Ind. Applicat.,* vol. 42, no. 2, pp. 559-572, March/April 2006.

[Rou 07] N. Roux, F. Richardeau, "Stability of DC link with reduced energy storage for regenerative synchronous drive – analytical approach," in *Proc. EPE'07*, Aalborg, Denmark, CD-Rom, Sept. 2007.

[Sad 04] D. Sadarnac, C. Karimi, and K. Louati, "Input filter influence on control stability of DC-DC converters," in *IEEE International Symposium on Industrial Electronics,* pp. 1165-1171, May 2004.

[scl] M. Sclocchi,"Input filter design for switching power supplies," in *Application Engineering and National Semiconduction.*

[Sha 10] A. Shahin, J. P. Martin, S. Pierfederici, "Approximate nouvel loss formula estimation for optimization power controller of DC/DC converter," *IEEE IECON,* Phoenix, USA, 7-10 November 2010.

[Sha 10a] A. Shahin, B. Huang, J. P. Martin, S. Pierfederici, B. Davat, "New nonlinear control strategy for non-isolated DC/DC converter with high voltage ratio," *Journal of Energy and Management,* vol. 15, no. 1, pp. 56-63, Jan. 2010.

[Sud 98] S. D. Sudhoff, K. A. Corzine, S. F. Glover, H. J. Hegner, and H. N. Robey, Jr., "DC link stabilized field oriented control of electric propulsion systems, " *IEEE Trans. Energy Conversion,* vol. 13, no. 1, pp. 27-33, March 1998.

[Sud 00] S. D. Sudhoff and S. F. Glover, "Three dimensional stability analysis of DC power electronics based systems," in *IEEE Proc. PESC,00,* pp. 101-106, 2000.

[Sud 00a] S. D. Sudhoff, S. F. Glover, P. T. Lamm, D. H. Schmucker, D. E. Delisle, "Admittance space stability analysis of power electronic systems," in *IEEE Trans. Aerosp. Electron. Syst.,* vol. 36, pp. 965-973, July 2000.

[Tep 04] T. Tepsa and Teuvo Suntio, "Analysis and measurement of load effect on converter dynamics under constant-voltage and constant-current control," in *Nordic Workshop on Power and industrial Electronics, NORPIE'04,* 2004.

[Tsu 00] K. Tsuboi, M. Tsuji, and E. Yamada, "Instability of chopper system with LC input filter and its solution," in *Electrical Engineering in Japan,* vol. 137, no. 4, pp. 49-63, 2001, Translated from D. G. Ronbunshi, vol. 120-D, no. 10, Oct. 2000, pp. 1171-1181.

[Tsu 01] K. Tsubol, M. Tsuji, and E. Yamada, "Instability of a chopper system with input LC filter and its solution," *Electrical Engineering in apan,* 137(4): pp. 49-63, Sep. 2001.

[Usm 06] M. Usman Iftikhar, D. Sadernac, and C. Karimi, "Conducted EMI suppression and stability issues in switch-mode DC-DC converters," in *IEEE International Multitopic Conference (INMIC'06),* pp. 389-394, Dec. 2006.

[Usm 07] M. Usman Iftikhar, D. Sadernac, and C. Karimi, "Input filter design for control loop stability of DC-DC converters," in *IEEE International Symposium on Industrial Electronics (ISIE'07),* pp. 353-358, Jun. 2007.

[Ven] Venable,"Minimizing input filter requirements in military power supply design" in *Venable Technical paper,* no. 4.

[Via 10] R. Vial, D. Riu, N. Retière, "Simulation calculation and optimization design of a new HVDC power supply for light rain system," *IEEE IECON 2010,* Phoenix, USA, 7-10 Nov. 2010.

[Vid 98] M. Vidyasagar, "*Nonlinear System Analysis,*" Prentice-Hall, Engleweed Cliffs, NJ, 1998.

[Wai 05] R. J. Wai and K. M. Lin, "Robust decoupled control of direct fieldoriented induction motor drive," *IEEE Trans. Ind. Electron.,* vol. 52, no. 3, pp. 837-854, Jun 2005.

[Wan 07] J. Wang, A. Griffo, L. Han, D. Howe, "Input admittance characteristics of permanent magnet brushless AC motor dreive systems," in *Proc. IEEE VPPC'07,* CD-Rom, Sept. 2007.

[Wei 98] L. Weiss, W. Mathis, L. Trajkovic, "A generalization of Brayton –Moser's mixed potential function," *IEEE Trans. On Circuits and Systems* vol. 45, no. 4, April 1998.

[Wil 93] C. M. Wildrick, "Stability of distributed power supply system," *Ph.D dissertation, Virginia Polytech. Inst. State Univ.,* Blacksburg, VA, Feb. 1993.

[Wil 95] Carl M. Wildrick, Fred C. Lee, Bo H. Cho, and Byungcho Choi, "A method of defining the load impedance specification for a stable distributed power system," in *IEEE Trans. Power Electron.,* vol. 10, no. 3, pp. 280-285, May 1995.

[Wil 98] P.R. Willcock, J. A. Ferreir and J. D. Van Wyk, "An experimental approach to investigate the generation and propagation of conducted EMI in converters," in *IEEE Power Electronics Specialists Conf. (PESC 98),* volume 2, pp. 1140-1145, May 1998.

[Yu 71] Y. Yu and J. J. Biess, "some design aspects concerning input filters for DC-DC converters," in *IEEE Power Conditioning Specialists Conf.,* pp. 66-76, Record 1971.

APPENDICES

Appendix A: Experimental Bench

The experimental bench includes a regulated DC power supply, an input LC filter, a PWM controlled Voltage-Source Inverter (VSI), a Permanent Magnet Synchronous Machine (PMSM) and a mechanical load. The DC supply provides a constant DC voltage and its output current can be limited. This latter is useful when the bench is unstable, because it helps the DC-bus variables to converge to a limit cycle instead of diverging. The VSI is a conventional three legs IGBT based inverter. The characteristics of the PMSM and the LC filter are the following:

Characteristics	**Values**	**Units**
Rated Power	*2*	*kW*
Rated Current	*11.5*	*A*
Nominal Speed	*2000*	*r/min*
Inertia	3.1×10^{-3}	$kg.m^2$
Stator Resistance	*0.5*	*Ω*
Inductance	*3.1*	*mH*
Rated Torque	*8*	*Nm*
DC-Bus Voltage	*200*	*V*
DC-link Inductance	*39.5*	*mH*
DC-link Resistance	*1.1*	*Ω*
DC-link Capacitance	*500*	*μF*

Table A.1 : Experimental bench parameters.

The control card used for the control of the machine (current and voltage acquisition, control of the inverter and PWM) is a dSpace DS1005 card. Its sampling rate is 100 μs. The switching frequency of the inverter is 10 kHz.

Fig. A.1 shows the experimental bench.

Appendix A:

Figure A.1 : Experimental bench.

Appendix B:

In chapter 3, we proposed the stabilizer shown in Fig. B.1.

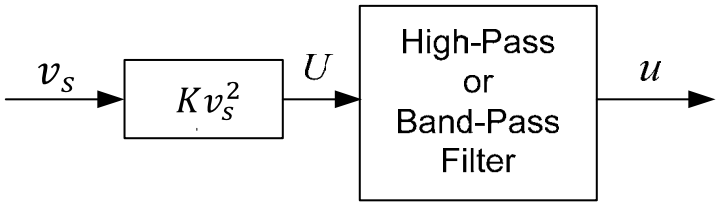

Fig. B.1- DC-link stabilization law.

Here, we develop a Lyapunov based stability analysis to study the asymptotic stability of the operating point with this stabilizer. The model of the closed-loop system (model (3.35) + compensator (3.38)) can be written as follows:

$$\frac{d}{dt}X = A_c \cdot X + F(X) \qquad (B.1a)$$

with:

$$A_c = \begin{bmatrix} \frac{-r}{L} & \frac{-1}{L} & 0 \\ \frac{1}{C} & \frac{-K}{C} & 0 \\ 0 & 2Kv_{s0}\omega_1 & -\omega_1 \end{bmatrix} \qquad (B.1b)$$

$$F(X) = \begin{bmatrix} 0 \\ \frac{p_{s0} - Kv_{s0}^2}{Cv_{s0}} \cdot \frac{\tilde{v}_s}{\tilde{v}_s + v_{s0}} + \frac{1}{C} \cdot \frac{x}{\tilde{v}_s + v_{s0}} \\ K\omega_1 \cdot \tilde{v}_s^2 \end{bmatrix} \qquad (B.1c)$$

$$X = \begin{bmatrix} \tilde{\imath}_e \\ \tilde{v}_s \\ x \end{bmatrix} \qquad (B.1d)$$

The stability analysis shows that the origin ($X = 0$) is a globally asymptotically stable equilibrium point for the system (A.1) if the first cut-off frequency $\omega_1 \ll \omega_0 = \frac{1}{\sqrt{LC}}$ and:

$$K > K_{min} > 0 \qquad (B.2)$$

To prove this condition, we use the theory of singularly perturbed systems motivated by the assumption $\boldsymbol{\omega_1 \ll \omega_0}$ implying a slow dynamic for the filter. Indeed, the third variable ($\boldsymbol{x}$), associated to this filter, can be considered as slowly variable with respect to the dc-link voltage and current variations ($\boldsymbol{\tilde{v}_s}$ and $\boldsymbol{\tilde{\imath}_e}$). Therefore, the state vector can be decomposed in two vectors as follows:

Appendix B:

$$z = \begin{bmatrix} \tilde{\imath}_e \\ \tilde{v}_s \end{bmatrix}, \quad x = x \tag{B.3}$$

This leads to the following model:

$$\begin{cases} \dot{x} = f(x,z) \\ \varepsilon \dot{z} = g(x,z) \end{cases} \tag{B.4a}$$

with

$$f(x,z) = -\omega_1 \cdot x + 2Kv_{s0}\omega_1 \cdot z_2 + K\omega_1 \cdot z_2^2 \tag{B.4b}$$

$$g(x,z) = \varepsilon \cdot \begin{bmatrix} \frac{-r}{L} \cdot z_1 - \frac{1}{L} \cdot z_2 \\ \frac{1}{C} \cdot z_1 - \frac{K}{C} \cdot z_2 + \frac{a_0}{Cv_{s0}} \cdot \frac{z_2}{z_2 + v_{s0}} + \frac{1}{C} \cdot \frac{x}{z_2 + v_{s0}} \end{bmatrix} \tag{B.4c}$$

in which $a_0 = p_{s0} - Kv_{s0}^2$ and ε is a sufficiently small positive number.

It is obvious that $x = 0$ and $z = 0$ is an equilibrium point of the system, because $f(0,0) = 0$ and $g(0,0) = 0$. The asymptotic stability of this point is studied in three steps. At first, we analyze the stability of the reduced system defined by:

$$\dot{x} = f\big(x, h(x)\big) \tag{B.5}$$

where $\bar{z} = h(x)$ is a solution of $g(x,\bar{z}) = 0$ for which $h(0) = 0$. The second step consists in analyzing the stability of the boundary-layer system

$$\frac{d}{d\tau} y = g\big(x, y + h(x)\big) \tag{B.6}$$

where $y = z - \bar{z}$ is the fast component of the vector z and $\tau = t/\varepsilon$ is the fast time scale. Finally, the interconnection conditions should be verified [Khalil]. In the following, this analysis is applied to the system (B.4).

From (B.4), putting $g(x,\bar{z}) = 0$ yields

$$\begin{cases} \bar{z}_1 = \frac{-1}{r} \cdot \bar{z}_2 \\ \bar{z}_2 = \sigma - \sqrt{\sigma^2 + k \cdot x} \end{cases} \tag{B.7}$$

with

$$k = \frac{r}{1 + r \cdot K} \quad \text{and} \quad \sigma = \frac{k \cdot a_0}{2v_{s0}} - \frac{v_{s0}}{2}$$

Appendix B:

Replacing (B.7) to (B.4b), the reduced system in our case is given by the following:

$$\dot{x} = -\alpha_0 \cdot x + \Gamma(x) \tag{B.8}$$

with

$$\alpha_0 = \frac{k \cdot \omega_1}{r}$$

$$\Gamma(x) = K v_{s0} \omega_1 \cdot (k \cdot a_0 + v_{s0}^2) \cdot \left(\sigma - \sqrt{\sigma^2 + k \cdot x}\right)$$

Let $V(x)$ be a Lyapunov function candidate for the reduced system (B.8):

$$V(x) = \frac{1}{2}x^2 \tag{B.9}$$

Then, we have

$$\frac{\partial V}{\partial x} f\big(x, h(x)\big) \leq -\alpha_1 \cdot \psi_1^2(x) \tag{B.10}$$

if $\psi_1(x) = |x|$ and there exists a positive number α_1 such that:

$$x \cdot \Gamma(x) \leq (\alpha_0 - \alpha_1) \cdot x^2 \tag{B.11}$$

Fig. B.2 shows $x \cdot \Gamma(x)$ and $(\alpha_0 - \alpha_1) \cdot x^2$ for $\alpha_1 = 18$ and a given $K > 0$. Other parameters are those given in Appendix I for the experimental bench. It is obvious from this figure that condition (B.11) is verified. So, it can be concluded that the reduced system is stable at $x = 0$ with $V(x) = x^2/2$ as Lyapunov function.

Appendix B:

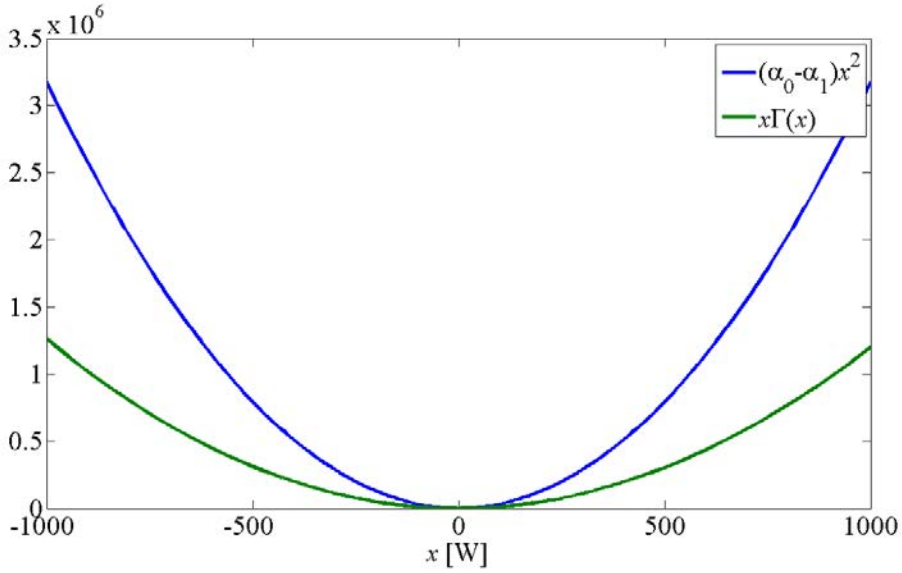

Fig. B.2- Verification of condition (B.11) with $\alpha_1 = 18$.

Now, let's consider the boundary-layer system expressed by

$$\begin{cases} \frac{d}{d\tau}y_1 = \frac{\epsilon}{L}(-r \cdot y_1 - y_2) \\ \frac{d}{d\tau}y_2 = \frac{\epsilon}{C}\left[y_1 - \left(K + \frac{x - a_0}{(\bar{z}_2 + v_{s0}) \cdot (y_2 + \bar{z}_2 + v_{s0})}\right) \cdot y_2\right] \end{cases} \tag{B.12}$$

We propose the following Lyapunov function candidate

$$W(x, y) = \frac{1}{2\epsilon}(L \cdot y_1^2 + C \cdot y_2^2) \tag{B.13}$$

Then, the boundary-layer system is asymptotically stabile at $y = 0$ if there exist a positive number α_2 and a positive function ψ_2 such that:

$$\frac{\partial W}{\partial y} g\big(x, y + h(x)\big) \leq -\alpha_2 \cdot \psi_2^2(y) \tag{B.14}$$

This leads to

$$-r \cdot y_1^2 - \beta \cdot y_2^2 \leq -\alpha_2 \cdot \psi_2^2(y) \tag{B.15}$$

with

Appendix B:

$$\beta = K + \frac{x - a_0}{(\bar{z}_2 + v_{s0}) \cdot (y_2 + \bar{z}_2 + v_{s0})} > 0 \qquad (B.16)$$

Condition (B.14) holds if we choose

$$\begin{cases} 0 < \alpha_2 < min(r, \beta) \\ \psi_2(y) = \|y\| \end{cases} \qquad (B.17)$$

To verify condition (B.16), K should satisfy

$$K > \frac{p_{s0} - x}{v_{s0}^2 + (\bar{z}_2 + v_{s0})^2 + y_2 \cdot (\bar{z}_2 + v_{s0})} = K_0 \qquad (B.18)$$

Knowing that $v_s > 0$, we have $y_2 > -(\bar{z}_2 + v_{s0})$. On the other hand, we can reasonably limit x to the set $[-m \cdot p_{s0},\ m \cdot p_{s0}]$, $m > 0$. It yields

$$K_0 < \frac{p_{s0} - x}{v_{s0}^2} < \frac{(m+1)p_{s0}}{v_{s0}^2} \qquad (B.19)$$

Therefore, to verify (B.16), it is sufficient to choose K as follows

$$K > K_{min} = \frac{(m+1)p_{s0}}{v_{s0}^2} > K_0 \qquad (B.20)$$

It is obvious that this condition is conservative for achieving asymptotic stability and K_{min} may be locally less than that in (B.20) depending to the operating point. In fact, $(m+1)p_{s0}/v_{s0}^2$ is the supremum of K_0 obtained for $\tilde{v}_s \to -v_{s0}$.

The last step consists in verifying the interconnection conditions. It is shown in [Khalil] that these conditions are satisfied if:

$$\begin{cases} \left\| \frac{\partial V}{\partial x} \right\| \le k_1 \cdot \psi_1(x) \\ \left\| f\big(x, h(x)\big) \right\| \le k_2 \cdot \psi_1(x) \\ \left\| \frac{\partial W}{\partial y} \right\| \le k_3 \cdot \psi_2(y) \\ \left\| \frac{\partial W}{\partial x} \right\| \le k_4 \cdot \psi_2(y) \\ \left\| f\big(x, y + h(x)\big) - f\big(x, h(x)\big) \right\| \le k_5 \cdot \psi_2(y) \end{cases} \qquad (B.21)$$

In our case, the first four conditions can be easily verified. To test the fifth one, we develop $\Delta f = f\big(x, y + h(x)\big) - f\big(x, h(x)\big)$ which yields

Appendix B:

$$\Delta f = K\omega_1 \cdot [y_2 + 2(v_{s0} + \bar{z}_2)] \cdot y_2 \qquad (B.22)$$

It is clear that a $k_5 > 0$ exists such that

$$\|\Delta f\| \leq k_5 \cdot \psi_2(y)$$

For example, knowing that $Z_{2min} \leq \bar{z}_2 \leq Z_{2max}$ (from (B.7)), and supposing $v_s < 2v_{s0}$, we can write

$$k_5 = K\omega_1 \cdot (4v_{s0} + Z_{2max} - Z_{2min}) \qquad (B.23)$$

For conclusion, the above analysis showed that the system (B.1) is asymptotically stable in the following domain

$$-m \cdot p_{s0} \leq x \leq -m \cdot p_{s0}, \qquad m > 0$$

$$0 < v_s$$

if

$$K > K_{min} = \frac{(m+1)p_{s0}}{v_{s0}^2}$$

$$\omega_1 \ll \omega_0 = \frac{1}{\sqrt{\boldsymbol{LC}}}$$

Nancy-Université
INPL

AUTORISATION DE SOUTENANCE DE THESE
DU DOCTORAT DE L'INSTITUT NATIONAL
POLYTECHNIQUE DE LORRAINE

o0o

VU LES RAPPORTS ETABLIS PAR :
Monsieur Mohamed-Fouad BENKHORIS, Professeur, IREENA, CRTT, Saint-Nazaire
Monsieur Benoît ROBINS, Professeur, Ecole des Hautes Etudes d'Ingénieur, Lille

Le Président de l'Institut National Polytechnique de Lorraine, autorise :

Monsieur AWAN Ahmed Bilal

à soutenir devant un jury de l'INSTITUT NATIONAL POLYTECHNIQUE DE LORRAINE, une thèse intitulée :

"Contribution à l'étude de la stabilité des systèmes électriques distribués autour d'un bus commun d'alimentation. "

en vue de l'obtention du titre de :

DOCTEUR DE L'INSTITUT NATIONAL POLYTECHNIQUE DE LORRAINE

Intitulé du doctorat : « **Génie Electrique** »

Fait à Vandoeuvre, le 23 novembre 2011
Le Président de l'I.N.P.L.,
F. LAURENT

INSTITUT NATIONAL POLYTECHNIQUE DE LORRAINE - NANCY

Institut National Polytechnique de Lorraine
inpl@inpl-nancy.fr | www.inpl-nancy.fr

2 av. de la Forêt de Haye | BP 3
54501 Vandœuvre-lès-Nancy Cedex
FRANCE
Tél. : +33(0)3 83 59 59 59
Fax : +33(0)3 83 59 59 55

Abstract:

Stability is the first and very important factor in all modes of operation for a Distributed Power System (DPS). In DPS, loads are connected to the DC-bus through an input LC filter. Most of the loads in DPS of aircraft present a constant power load characteristic within a domain of operating in which they are tightly controlled. So they can be modeled as negative resistance. Change of the load in one subsystem may lead a stable system into instability.

A practical solution to decrease the risk of instability presented in this thesis which consists in modifying the control of the converters or inverter-motor drive system connected to the DC-bus. This solution permits to stabilize the system even with a smaller size of capacitor. In the first part of the thesis, a linear method is presented which allows investigating local stability of an inverter-motor-drive system connected to the grid through an LC filter and a rectifier. An oscillation compensation technique is used to improve the stability margin of the system and the size of the dc-link capacitance without modifying structure of the torque or current loops. This technique consists in superposing a stabilizing power on the absorbed power by the drive. Although linear models can be successfully employed to locally describe the behavior of a physical system, they often fail to provide a satisfactory large signal characterization. In the second part, two methods for the large signal stabilization of the electrical system are presented. In the last part, a new method, based on dynamic specifications, is proposed to study the stability of a cascaded electric system.

Key words: *Stability, linear systems, nonlinear systems, dc-link capacitance, ac drives, robustness.*

Résumé:

La stabilité est le facteur très important dans tous les modes de fonctionnement pour un Système à Puissance Distribué (SPD). En SPD, les charges sont connectés au bus DC à travers d'un filtre entrée LC. La plupart des charges de SPD d'avions présents une caractéristique de charge à puissance constante dans un domaine de fonctionnement dans laquelle ils sont étroitement contrôlés. Ainsi, elles peuvent être modélisés comme une résistance négative. Changement de la charge dans un sous-système peut conduire un système stable dans l'instabilité.

Une solution pratique pour diminuer le risque d'instabilité est présentée dans cette thèse qui consiste à modifier le contrôle des convertisseurs ou système onduleur-moteur connecté au bus DC. Cette solution permet de stabiliser le système, même avec un condensateur plus petit. Dans la première partie de la thèse, une méthode linéaire est présentée qui permet étudier la stabilité locale d'un système onduleur-moteur connecté au réseau par un filtre LC et un redresseur. Une technique de compensation d'oscillation est utilisée pour améliorer la marge de stabilité du système et la taille de la capacité dc-link sans modifier la structure de boucles de courant ou du couple. Cette technique consiste à superposer une puissance stabilisatrice sur la puissance absorbée par le lecteur. Bien que les modèles linéaires puissent être employées avec succès pour décrire le comportement d'un système physique au niveau local, ils échouent souvent de fournir une caractérisation satisfaisante de large-signal. Dans la deuxième partie, deux méthodes pour la stabilisation large-signal du système électrique sont présentés. Dans la dernière partie, une nouvelle méthode, basée sur les spécifications dynamiques est proposé pour étudier la stabilité d'un système en cascade électrique.

Mot Clé : *Stabilité, systèmes linéaire, systèmes non linéaire, capacitance dc-link, drives ac, robustesses*